FACULTY OF HEALTH, EDUCATION, MEDICINE, AND SOCIAL CARE

DEVELOPMENT OF LONG CIRCULATION NANO-ENABLED DRUG CARRIERS FOR CANCER TREATMENT

IBRAHIM DUMBUYA

A thesis submitted for the degree of PhD in Anglia Ruskin University

Submitted November 2019

Acknowledgements

ANGLIA RUSKIN UNIVERSITY

ABSTRACT

FACULTY OF HEALTH, EDUCATION, MEDICINE, AND SOCIAL CARE

DOCTOR OF PHILOSOPHY

DEVELOPMENT OF LONG CIRCULATION NANO-ENABLED CARRIERS FOR
CANCER TREATMENT

IBRAHIM DUMBUYA

November 2019

Disulfiram (DSF) is an analogue of the dithiocarbamate family used over half a century ago for the treatment of alcoholism and its Food and Drug Administration (FDA) approved. DSF is a potent anti-cancer agent and Cu^{2+} dependent on mediating growth inhibition and apoptosis against different types of cancer cells. The major biological limitation of DSF against cancer cells is poor solubility and instability in the human body. Repositioning DSF with nano-carriers will improve its half-life, stability and enable long circulation for cancer therapy. Direct nanoprecipitation (D-Nano-Pr) and single emulsion/solvent evaporation (SE) methods were employed to successfully manufactured non-PEGylated and PEGylated nanoparticles (NPs) and including solid lipid nanoparticles (SLNs) of encapsulated DSF. The particle sizes of NPs/SLNs prepared by using the SE method were reduced by probe sonication (PS) or high-pressure homogenization (HPH) techniques. Freshly manufactured DSF NPs/SLNs (including empty NPs/SLNs) were characterized to determine particle sizes, polydispersity index (PDI), zeta potential, thermal degradation using differential scanning calorimetry (DSC), and functional group confirmation of chemical compounds using Fourier transform infrared spectroscopy (FTIR). Percentage encapsulation efficiency, cumulative release, and stability of DSF NPs/SLNs in horse serum media were evaluated by high-performance liquid chromatography (HPLC). This study has also contributed by developing efficient methods used to determine the manufactured NPs/SLNs percentage encapsulation efficiency and stability of DSF in horse serum. The 3-(4,5-dimethylthiazol-2-yl)-2, 5-diphenyl tetrazolium bromide (MTT) cytotoxicity assays *in vitro* experiments of NPS/SLNs was performed against MCF 7, MDA-MB-231, and MDA-MB-231$_{PTX10}$ cancer cell lines, to investigate the inhibition effects of the encapsulated DSF. The MTT cytotoxicity assays of DSF-loaded NPs/SLNs demonstrated increased cytotoxicity and decreased IC_{50} values indicating therapeutic effect against breast cancer cells. PEGylated DSF NPs demonstrated comparable cytotoxic effects over the free drug. PEGylated DSF PLGA NPs demonstrated the potential to be developed as nanomedicine for cancer therapy. Finally, this study showed manufactured nano-size particles of NPs/SLNs to improve DSF biostability and offer efficient protection to DSF in horse serum. Therefore, there is a high potential to enable DSF long circulation for efficient cancer therapy.

Keywords: Disulfiram (DSF), diethydithiocarbamate (DDC), direct nanoprecipitation (D-Nano-Pr) method, single evaporation (SE) method, probe sonication (PS) technique, and high-pressure homogenization (HPH) technique.

Table of Contents

List of Figures

xvi

xvii

List of Tables

List of Abbreviations

1. ATP-binding cassette (ABC)

2. Alcohol dehydrogenase (ADH)

3. Atomic force microscopy (AFM)

4. Aldehyde dehydrogenase (ALDH)

5. Analytical of variance (ANOVA)

6. Adenosine triphosphate (ATP)

7. Bovine serum albumin (BSA)

8. Brunauer-Emmett-Teller (BET)

9. Cis-diaminodichloroplatinum (CDDP)

10. Colorectal cancer (CRC)

11. Diethyldithiocarbamate (DDC)

12. Deoxynucleic acid (DNA)

13. Differential thermal analyser (DTA)

14. Differential scanning calorimeter (DSC)

15. Dynamic light scattering (DLS)

16. Dimethyl sulfoxide (DMSO)

17. Dopamine-beta hydroxylase (DBH)

18. 1,2-distearoyl-sn-glycero-3-phosphoethanolamine (DSPE)

19. Dulbecco's modified eagles' medium (DMEM)

20. Enhanced permeability and retention (EPR)

21. Ethylenediamine-tetraacetic acid (EDTA)

22. European Medicine Agency (EMA)

23. Food and Drug Administration (FDA)

24. Fourier transform infrared spectroscopy (FTIR)

25. Heat capacity (Cp)

26.   High-pressure homogeniser (HPH)

27.   Hot homogenisation (HH)

28.   Hydrogenated phosphatidylcholine from soybean (HPCS)

29.   Human epidermal growth factor receptor 2 (HER_2)

30.   Half maximal inhibitory concentration (IC_{50})

31.   International Agency for Research on Cancer (IARC)

32.   Kilo Hertz (kHz)

33.   Low molecular weight (LMW)

34.   Megapascal (MPa)

35.   Methyl-poly (ethylene glycol) (mPEG)

36.   Micro Littre (µL)

37.   Micro molar (µM)

38.   Michigan Center Foundation (MCF)

39.   Monroe Dunaway Anderson-metastasis breast cancer (MDA-MB)

40.   Millivolt (mV)

41.   Millimeter squared (mm^2)

42.   Molecular weight cut-out (MWCO)

43.   3-(4, 5-dimethylthiazol-2-yl)-2, 5-diphenyl tetrazolium bromide (MTT)

44.   Multidrug resistance (MDR)

45.   Multidrug resistance-associated protein (MRP1)

46.   Nano-meter (nm)

47.   Nano Molar (nM)

48.   Nicotinamide dinucleotide phosphate (NADPH)

49.   Oestrogen receptor (ER)

50.   Oil-in-water (O/W)

51.   Phosphate-buffered saline Tween80 (PBST)

List of Appendices

Appendix A (Chapter 3 supplementary data)

1. DSC thermograms of PLGA NPs by SE method/PS technique

2. DSC thermograms of PLGA NPs by SE method/HPH technique

3. FTIR spectroscopic analysis of PLGA NPs by SE method/PS technique

4. FTIR spectroscopic analysis of PLGA NPs by SE method/HPH technique

Appendix B (Chapter 4 supplementary data)

5. DSC thermograms of PEGylated and non-PEGylated PLGA NPs by D-Nano-Pr method

6. FTIR spectroscopic analysis of PEGylated and non-PEGylated PLGA NPs by D-Nano-Pr method

Appendix C (Chapter 5 supplementary data)

7. DSC thermograms of SLNs by SE method followed by hot homogenization technique

8. DSC thermograms of SLNs by SE method followed by hot homogenization technique

9. DSC thermograms of PLGA NPs by SE method/PS technique

10. DSC thermograms of SLNs by SE method/HPH technique

11. FTIR spectroscopic analysis of PLGA NPs by SE method followed by hot homogenization technique

12. FTIR spectroscopic analysis of PLGA NPs by SE method/PS technique

13. FTIR spectroscopic analysis of PLGA NPs by SE method/HPH technique

Appendix D (Chapter 6 supplementary data)

14. DSC thermograms of DSPE-PEG SLNs by SE method/HPH technique

15. DSC thermograms of DSPE-PEG SLNs by SE method/HPH technique

Declaration

As a registered candidate, I declare this work for the research degree that this submission is made. Since I became a registered candidate or enrolled for the Ph.D. research degree at Anglia Ruskin University, I have not been a registered candidate for any other degree award program from other professional institutions. Therefore, this work or any part hereafter of this thesis has not been previously used to any other University or in any other submission for an academic award.

Chapter 1 Introduction

1.1 Breast cancer

1.1.1 Cancer

Cancer is a generic term used to describe diseases containing abnormal cells transforming from a pre-cancerous lesion to uncontrollable cells, which can invade or spread towards other parts of the body and then destroy normal body tissues (Coussens and Werb, 2002). There were 14.1 million newly diagnosed cases of 27 major cancers worldwide and 8.2 million deaths in 2012 (Ferlay, et al., 2012; Soerjomataram, et al., 2012). The World Health Organisation (WHO), under its cancer research agency of the International Agency for Research on Cancer (IARC), provides below the most commonly diagnosed cancers worldwide. (1) Lung and breast cancer both have 2.09 million diagnosed cases, while (2) colorectal cancer (CRC) had 1.80 million diagnosed cases, and (3) prostate, skin (non-melanoma), and stomach cancer had 1.28 million, 1.04 million and 1.03 million diagnosed cases, respectively, (Bray, et al., 2018). Currently, the following cancers are the most common causes of cancer death, (i) Lung (1.76 million deaths), (ii) colorectal (862,000 deaths), (iii) stomach 783,000 deaths), (iv) liver (782,000 deaths) and (v) breast (627,000 deaths) (Bray, et al., 2018). Moreover, cancer remains the most major public health problem worldwide ranked as the second leading cause of cancer death and accounting for an estimated 9.6 million deaths in 2018 of which 1 in 6 deaths are referred to cancer (Siegel, Miller and Jemal, 2019). Therefore, cancer has a significant economic impact, with an increase in annual economic cost estimated at US $ 1.16 trillion in 2010 (Stewart and Wild, 2014). In this study, the focus will be on breast cancer. Therefore, breast cancer cells were used to investigate the therapeutic effect of manufactured biodegradable DSF-loaded PLGA or phospholipid nano-carrier delivery systems.

1.1.2 Breast cancer and its risk factors

Breast cancer is characterized by a distinct malignant cell causing the metastatic pattern in the mammary epithelial tissue. It is characterized by its uncontrolled growth and the invasion of specific organs in the body, such as regional lymph nodes, bone marrow, pancreas, liver, and lung (Wang, et al., 1998; Dalerba, Cho and Clarke, 2007). Breast cancer is one of the most commonly diagnosed cancers (Bray, et al., 2018), and the fourth most common cause of cancer death globally (Bray, et al., 2018). Lately, breast cancer in the 21st century is no longer considered terminal in public health due to the selection of therapeutic options available. This has helped to cut the mortality to incidence ratio for breast cancer at 0.31 compared to pancreas and liver cancers with increased ratios around 0.98 and 0.85, respectively (Ferlay, et al., 2015). Approximately, 1% of males are diagnosed with breast cancer in the US with less than 0.1% deaths in men is attributed to cancer (Ferzoco and Ruddy, 2016), metastasis which is a process of various sequential steps (Nicolson, 1993). The major risk factors of developing breast cancer can be attributed to the high increase of oestrogens at early menarche and menopause age (Hunter, et al., 1997). Research studies have suggested obesity in postmenopausal women tends to be vulnerable with a high increase of endogenous estradiol described as a risk factor (Kelsey, Gammon and John, 1993; Key, 1999). In addition, the use of oral contraceptive and hormonal therapy for menopause can cause a slight increase in breast cancer risk, and this can be reversed gradually once use stops (Grady, et al., 2000). Furthermore, consumption of alcohol has been linked to increase risk of cancer while daily physical activity is important for human health, and may lower cancer risk (Sellers, et al., 2001). Women are highly affected by breast cancer, and most deaths among women globally are associated with cancer (Murray and Lopez, 1997). The high increase for breast cancer

3

incidence in developing countries has been attributed to rising adaptation of the risk factors linked to the western lifestyle (Lakhani, et al., 2002).

1.1.3 Breast cancer incidence rates

The incidence rates of breast cancer in most developed countries showed a high increase than the under-developed countries (Garcia, et al., 2007). In most developed countries, the early detection of breast cancer is due to population-based screening through mammography imaging which has reduced its mortality rates in developing countries (Shapiro, et al., 1982). Despite the use of advanced technological devices for the improvements of early detection and treatment of breast cancer, in the US only, approximately 192,000 new cases and 40, 000 deaths still occurring in 2009 (Jemal, et al., 2009). Breast cancer incidence increases with age and women who start menstruating at an early age in life or have late menopause are susceptible to a high risk of developing breast cancer (Kelsey, Gammon and John, 1993). Breast cancer incidence increases at younger ages, especially women with natural menopause after the age of 55 than those women with menopause before the age of 45 (Trichopoulos, MacMahon and Cole, 1972; Hughes, et al., 2013).

1.1.4 Breast cancer cell lines of *in vivo* and *in vitro* model

HeLa cell was the first human carcinoma cell population with the ability to self-replicate in the cell culture medium and was established by George Gey in a Baltimore laboratory for over half a century (Gey, 1952). Hela cell development has helped to produce several other classified breast cancer such as BT-20, the first breast cancer established in 1968 (Lasfargues and Ozzello, 1958). Two decades later, the development of breast cancer cells such as Monroe Dunaway Anderson (MDA) metastasis breast (MB) (MDA-MB-231) cancer (Cailleau, Olive and Cruciger, 1978), and Michigan Center Foundation (MCF 7) cell lines were established, as the most

4

commonly used cell lines globally (Soule, et al., 1973; Levenson and Jordan, 1997). The MCF 7 cell line gained popularity due to the existing hormone sensitivity towards the overexpressed oestrogen receptor (ER) (Soule, et al., 1973; Levenson and Jordan, 1997).

Currently, different molecular classifications of breast cancer are introduced to prevent the difficulties in maintaining homogeneous populations of cell culturing without avoiding the high-risk stromal contamination (Brazier and Fovargue, 2006). Several *in vitro* studies have shown that MCF 7 and MDA-MB-231 present high potential for investigating therapeutic drug targeting breast cancer therapy (Neve, et al., 2006). These breast cancer cell lines (MCF 7 and MDA-MB-231) gained interest in examining the pathobiology, screening for therapeutic features of breast cancer, and can be used as a representative of the key genetic and transcriptional features within breast cancer tumours (Kao et al., 2009). The triple-negative phenotypes basal breast carcinoma lacks the expression of ERα, progesterone receptor, (PR) and HER$_2$ and are difficult to treat due to their biological aggressiveness and poor prognosis (Prat, et al., 2010). However, the MCF 7 cells are a good example used to investigate the effect of anti-oestrogens regulatory of tamoxifen-stimulated MCF 7 subtype human breast carcinoma (Osborne, Hobbs and Clark, 1985; Gottardis, Robinson, and Jordan, 1988). This phenomenon of tamoxifen-stimulated MCF 7 led by AstraZeneca to develop and set out subsequent trials of fulvestran, a potential selective ER down-regulator drug recommended for the treatment of recurrent ER+ metastatic breast cancer in postmenopausal women (Gottardis, Robinson and Jordan, 1988; Robertson, et al., 2003). The *in vivo* determination of various molecular classifications of breast cancer has provided invaluable insights into cellular physiology. This development sparked the interest of researchers to develop breast cancer cell lines that are engineered to investigate the molecular profiles observed within the *in vivo* breast carcinomas to

show similar translation compared to the cell line model of breast cancer cell lines (Neve, et al., 2006).

1.1.5 Overcoming drug resistance

The term multidrug resistance (MDR) refers to the resistance of some primary or recurrent tumour cells structurally and mechanically involved in the cytostatic or cytotoxic actions of multiple functionally divergent drugs used in cancer chemotherapy (Gottesman, 1993; Gottesman, Fojo, and Bates, 2002). The molecular mechanism of MDR is mainly intrinsic by which the disease is refractory to chemotherapy agents from the outset. Also, MDR is acquired due to repetitive exposure to chemotherapy upon relapse (Gottesman, 1993). The MDR role is to remove cytotoxic chemotherapy drugs from the exosome environment of the cancer cell. The *MDR1* gene p-glycoprotein (P-gp), gives the MDR phenotype which promote the defensive elements against the toxic chemotherapy drugs (Shen, et al., 1986).

The resistance of tumour cells to most multiple cytotoxic agents can be determined by the human *MDR1* gene, which encodes for high molecular weight membrane glycoprotein (P-glycoprotein) that consist of a polypeptide multiple membranes with hydrophobic domains, and two nucleotides binding sites (Chen, et al., 1986). The mature form of the transmembrane P-gp is well-known as a prototypical MDR protein with a 170 KDa glycoprotein ubiquitous in MDR cells (Riordan, et al., 1985). The P-gp was later found to act as adenosine triphosphate (ATP) energy-dependent export pumps to modulate intracellular levels of chemotherapy drugs (Gerlach, et al., 1986). The binding sites are structurally similar to subunits of active transport pumps found in bacteria, and its energy of ATP is harvested to stimulate efflux within a pore allocated by the transmembrane helices (Chang and Roth, 2001). The overexpressed superfamily of small molecule or ion ATP-binding cassette (ABC) transporters has been elucidated as one of the foremost mechanisms triggering MDR (Gillet and

6

Gottesman, 2010). There are other members of ABC superfamily involved in cancer MDR, such as multidrug resistance-associated protein-1 (MRP1) and its derivatives MRP2-6 have been implicated in transporting glutathione, glucoronate and sulphate-conjugated drugs (Borst, et al., 2000). Most importantly, studies have shown that tumours emerging from cells that are highly expressing P-gp including other MDR related transporters have been identified of intrinsically exhibiting chemotherapy resistance (Loo and Clarke, 1999; Borst, et al., 2000).

Another challenge in cancer therapy is the presence of multiple mechanisms of MDR in tumours with a heterogeneous population of cells causing high increase chemotherapy-resistant cancer (Alves, et al., 2011). Extensive studies have been performed using non-cytotoxic molecule MDR inhibitors, to overcome MDR in tumour cells, drug transport by P-gp and other MDR-associated transporters (Ferry, Traunecker and Kerr, 1996). Therefore, a good number of non-cytotoxic P-gp inhibitors, such as verapamil have been reported to inhibit drug transport, hence sensitized MDR cells to chemotherapeutic drugs (Tsuruo, et al., 1981). The first-generation MDR drugs for MDR inhibition lack specificity and having a low affinity towards MDR transporters (Ferry, Traunecker and Kerr, 1996). During clinical trials, the first-generation MDR drugs failed by exhibiting side effect due to adverse reactions from the MDR drug (Ferry, Traunecker and Kerr, 1996). Subsequently, second-generation MDR drugs were developed as derivatives of first-generation MDR drugs to reduce the side effects and remove their non-MDR pharmacological actions (Höll, et al., 1992). The intricacy and adaptability of cellular MDR mechanisms affected the development of effective clinical anti-cancer chemotherapy (Krishna and Mayer, 2000).

One of the challenges with the mono-encapsulated anti-cancer drug is the developments or the ability to overcome drug resistance from the overexpressed P-gp

pumps having a highly active efflux mechanism against small molecule drugs (Gottesman, 2019). Therefore, the use of nano-carrier delivery systems, such as nanoparticles (NPs) or solid lipid nanoparticles (SLNs), have improved drug circulation, stability and bioavailability in targeting specific tumour sites (Hu, et al., 2016). NPs-based therapeutic systems are rationally designed to circumvent or overcome drug resistance with the aim to neutralizing, targeting, evading or taking advantage of various drug efflux pumps and related resistance mechanisms. In addition, a combination of anti-tumour drugs-loaded NPs or SLNs will enable them to overcome drug resistance and maximized the effect of tumour growth inhibition (Hu, et al., 2016). Anti-cancer drugs are incorporated simultaneously or at different time points using the self-assembled structure of a single drug at a given time. Some polymeric materials are capable of conjugating multiple drugs at the same polymer backbone (Vogus, Krishnan and Mitragotri, 2017).

1.1.6 Costs of developing a new cancer drug

In a 2003 study, the cost of developing the FDA approved pharmacological cancer agent between 1989 and 2002 was estimated at approximately US $ 800 million (Adams and Brantner, 2006). Ten years later, the same authors applied a similar methodology approach and projected a new analysis with an estimated cost at approximately US $ 2.6 billion in 2013, therefore, the new estimate indicated an increased cost of up to 145% compared to the estimated cost in 2003 (Mullard, 2014). For this reason, the interest in anti-cancer drug repurposing or interchangeably drug repositioning has been driven by the costs of developing new potential anti-cancer drugs, and the market for cancer therapeutic effects is extensively expensive. Repurposing existing drugs such as disulfiram will be cost-effective (Ekins, et al., 2011).

One of the advantages of drug repurposing is that the pharmaceutical agent has been known for its clinical use with published articles describing the dosage, pharmacokinetics, bioavailability, and toxicities (Pantziarka, et al., 2014). Drug repurposing provided various advantages over the manufacturing of new drugs, and this can help to lower the risk of failure during preclinical testing. Due to the safety point of view in preclinical models after completion showed drug repurposing to be sufficiently safe, and less likely to fail during trials. Also, drug repurposing can cut production time for drug manufacturing of which formulation development, the preclinical trial, and safety assessments are already completed. Despite the expensive costs in cancer drug development, prevention and treatment of cancer remain a major leading cause of cancer deaths worldwide. Furthermore, the use of new technology such as nanotechnology-based delivery drug carrier system may promote the development of encapsulated anti-cancer agents for enhanced therapy (Zamboni, et al., 2012).

1.1.7 Drug repurposing

Drug repurposing or drug repositioning is a strategy used to identify potential new targets for approved drugs required outside the scope of the original medical requirements or indication (Ashburn, Ted T; Thor, Karl B. 2004). Developing new strategies of therapeutics with FDA approved drugs in treating specific diseases serve as potent anti-cancer agents to overcome drug resistance (Langedijk, et al., 2015). Traditional *de novo* drug discovery tends to be more time-consuming and astronomically expensive compared to the drug repositioning of known safety studies. Drug repositioning of potent anti-cancer agents will give a cost-effective, rapid production and efficient translation from "bench" to "bed" (Langedijk, et al., 2015). Also, drug repositioning can overcome the risks surrounding safety studies from clinical trials to quick, successful access to treatment (Pessetto, et al., 2014). As described in

Figure 1.1, the schematic diagram demonstrates methods and techniques involved in identifying existing drugs to drug-repositioning opportunities.
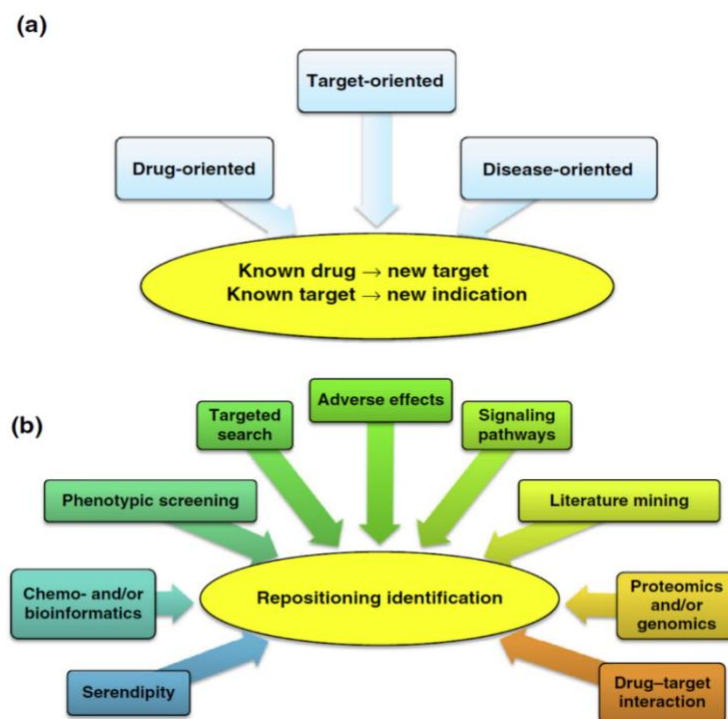
Figure 1.1. Active drug repositioning, (a) Process of identifying new drug target for delivery to exert therapeutic effect, (b) Methods and techniques used to identify existing drugs of known specific disease treatment circumvent for the purpose of drug-repositioning into pathological conditions. It was adapted from (Wuerth, et al., 2016).

1.2 Disulfiram

1.2.1 Overview

Disulfiram, (DSF) or tetraethylthiuram disulphide is a thiuram derivative developed by a German chemist, M. Grodzki in 1881 used as a catalyst to accelerate the vulcanization process in the rubber industry (Christensen, Rønsted and Vaag, 1984). In 1937, DSF was first discovered by an American chemical plant physician, E. E. Williams as a potential agent for the treatment of alcoholism (Williams, 1937; Malcolm, Olive, and Lechner, 2008). In 1945, two Danish researchers, Hald and Jacobsen serendipitously discovered ethanol reaction after ingesting DSF and then alcohol

produces an unpleasant reaction and since then it was used as an anti-alcoholism agent (Hald. and Jacobsen, 1948). However, due to the cytotoxic effects of DSF on cancer cells, it has been repurposed for clinical use in cancer treatments (Ekins, et al., 2011). As shown in Figure 1.2, DSF is a symmetrical molecule bonded by a sulphur-sulphur bridge molecular compound (Liu, et al., 2012a; Najlah, et al., 2017).
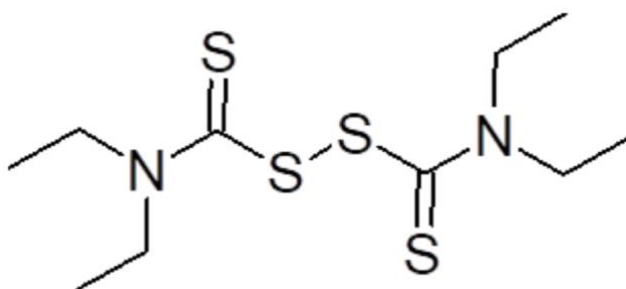
Figure 1.2. Representation of disulfiram stick diagram illustrating its symmetrical chemical structure.

1.2.2 Physicochemical properties of disulfiram

DSF has been identified as an organic compound that involves the combination of a two-electron oxidised dimer of diethyldithiocarbamate acid (DDC) (Fuller, et al., 1986). DSF forms an off-white or light grey, odourless and almost tasteless crystalline powder (Eneanya, et al., 1981). It has the empirical formula $C_{10}H_{20}N_2S_4$ and a molecular weight of 296.54 (Eneanya, et al., 1981). DSF is virtually insoluble in water (0.7% W/V) and practically has varying solubility in certain organic solvents such as ethanol (3.82% W/V) and ether (7.14% W/V) (Eneanya, et al., 1981). DSF clinical use against cancer therapy has been impeded through its poor bioavailability affected by the drug's poor water solubility (4.09 mg/L). DSF poor water solubility reduced the drug absorption rate by increasing its residence time in the stomach, where it is metabolized rapidly (Johansson, 1992). Its melting point and density are approximately 70 °C - 72 °C, and

1.30, respectively (Eneanya, et al., 1981). DSF has the ability to chelate with the non-transition metal zinc (Zn), and the following transition metals, iron (Fe), and copper (Cu) (Eneanya, et al., 1981). In a basic medium of pH 7.0 - 9.0 (pKa, 13.14), DSF and its metabolite DDC are both stable (Eneanya, et al., 1981). Due to their chemical nature, DSF and DDC are both unstable in acidic medium up to pH 7.0 (Eneanya, et al., 1981).

1.2.3 Biological function of disulfiram (anti addiction)

In 1951, DSF with the trade name Antabuse® was the first medication to be approved by the U.S. FDA for the treatment of chronic alcohol dependence and it was distributed in the U.S. by Odyssey Pharmaceuticals, Inc. (Fuller, Richard K; Gordis, Enoch. 2004). Three types of dosages, (i) initial dosage (250 mg/day), (ii) average maintenance dosage (125-500 mg/day), and (iii) maximum dosage (500 mg/day) were recommended for supervised administration by a pharmacist, healthcare providers or if necessary a family member (Fuller, Richard K; Gordis, Enoch. 2004). In the UK, DSF maximum dosage was 200 mg/day recommended by the manufacturer (Brewer, C. 1992).

Addiction is defined as chronic or long-term use of drugs by an individual to relapse disorder causing major problems for both the individual and society (Kosten and Kleber, 1992). Alcohol and drug addiction incur a high burden on social and economic costs. In 2003 to 2004, the UK reported an estimated £15.4 billion spent on policing and medical resources used against harm from the craving of Class A drugs of abuse use in England and Wales (McDonnell and Norris, 2002). The currently available anti-addiction medication such as methadone hardly targets the main underlying causes of addiction (McElroy, et al., 1989). Having alternative strategies for addiction can serve as a significant step in reducing expenses to the most craving of drugs of abuse. Therefore, DSF can be an important anti-addiction drug to help motivating addicts to

remain abstinent from alcohol and the craving for various types of drug abuse such as cocaine. Pilot studies conducted on specific patient population demonstrated DSF to reduce alcohol and cocaine intake (Carroll, Rounsaville, and Bryant, 1993; Carroll, et al., 1998; Carroll, et al., 2000).

Further studies have demonstrated the anti-addiction of DSF on cocaine addicts has been proved effective than the alcohol-and-cocaine dependent addicts (George, et al., 2000; Petrakis, et al., 2000; Carroll, et al., 2004). However, the anti-addiction of DSF in alcoholics has attributed to the negative effects of alcohol aldehyde dehydrogenase (ALDH)-independent mechanism through the inhibition of the liver enzyme to promote alcohol abstinence (Deitrich and Erwin, 1971). The excessive alcohol intake causes a build-up of acetaldehyde, which is a contributor to hangover symptoms such as flushing of the skin, rapid heart rate and vomiting. Oral administration of DSF after excessive alcohol intake effectively induces an immediate hangover state for several hours (van Ieperen, 1984). Intake of cocaine blocks the plasma membrane monoamine transporters, which then increases the extracellular levels of dopamine, norepinephrine, and serotonin in the brain (Goldstein, 1966; Bourdélat-Parks, et al., 2005). Today DSF has shown evidence as a dopamine-beta (β)-hydroxylase (DBH) inhibitor by its metabolite, DDC that blocks the production of norepinephrine (Truitt and Walsh, 1971; Kitson, 1977). The increasing levels of dopamine in the body will eventually lead to the interaction of acetaldehyde to form salsolinol (SAL) (Chen, et al., 2011). The formation of SAL has been linked to cocaine inhibition by competing with the cocaine neuron receptors to enhance abstinence from cocaine addiction (Chen, et al., 2011). DSF is not just a drug for anti-alcoholism but also rather an effective anti-addiction drug that can specifically reduce the craving for cocaine use.

1.2.4 Pharmacokinetics of disulfiram

1.2.4.1 Absorption and biotransformation

After ingesting disulfiram, approximately, 75 - 97% of the drug is absorbed from the human gastrointestinal tract (GI-tract) and rapidly distributed to various tissues and organs, and into the blood (Johansson, 1992). Experimental investigations by (Hald and Jacobsen, 1948), suggested 20 percent of orally administered DSF remain unchanged in faeces. In another study, De Saint Blanquat, et al., (1976), indicated that 70 - 90% of the ingested DSF was absorbed in rats and 2 hours later, they were sacrificed with qualitative analysis showing the presence of DSF and its metabolite, DDC in blood, muscle, liver, and kidney. The ingested DSF is reduced to its monomer, DDC through the endogenous thiols and glutathione reductase system of erythrocytes (Johansson, 1992). DDC is susceptible to extremely acidic condition within the stomach, and most importantly, it is a potent chelator with a strong affinity for Cu to produce Cu complex of bis-(diethyldithiocarbamato) ($Cu(DDC)_2$) (Johansson, 1992a). Clinical analysis has shown how ($Cu(DDC)_2$) is rapidly degraded after DDC chelates Cu to allow the subsequent reformation of DDC (Johansson, 1992). Therefore, DDC is unstable in biological tissues, it is susceptible to degradation into diethylamine (DEA), and carbon disulphide (CS_2) eliminated with no further degradation (Johansson, 1992). DSF can be further oxidised to methyl-diethyldithiomethylcarbamate (Me-DDC) via oxidative desulfurization, which specifically targeted by microsomal cytochrome P450 monooxygenases (Johansson, 1992). Most of the DSF metabolites are formed by further oxidative biotransformation, inorganic sulphate, formaldehyde, and methanethiol (Johansson, 1992).

1.2.4.2 Distribution

DSF is a lipophilic drug. Lipophilicity means the affinity of a drug to dissolve in fats, oils, lipids, and also highly soluble in non-polar solvents. It can accumulate in most lipid or fat environments, such as the brain, thyroid, adrenals, pancreas, stomach, small and large intestine, muscle tissue, liver, testes, kidney, lung, spleen, and heart (Faiman, Dodd and Hanzlik, 1978). The aforementioned shows that DSF and its metabolites are largely distributed simultaneously and uniformly. During the biodistribution process of DSF and its metabolites, DDC and Me-DDC are made inactive through direct interaction by bounding to proteins via protein-free thiol groups, and plasma albumin in the blood, respectively (Johansson, 1992).

1.2.4.3 Metabolism

The metabolism of DSF relatively occurs in different stages and gives various mixed disulphides (Cen, et al., 2002). The first stage of the DSF metabolic process is the reduction of the disulphide bridge-linkage to produce the corresponding thiol, DDC metabolite (Johansson, 1992). Previous studies have shown DSF reduced kinetics reaction rate as first order (Cen, et al., 2002). Glutathione (GSH) reductase system of the erythrocytes plays a big role in reducing DSF (Strömme, 1965), simply to protect the drug from the poisoning of erythrocytes. DSF has been considered to be pharmacologically inactive when bound to protein. Strömme, 1965, demonstrated that up to 50 g of the DSF instantly reduced by the human erythrocyte for 24 hours. It shows how DSF addition into the blood promptly and quantitatively reduced to DDC metabolite within 4 min (Cobby, Mayersohn and Selliah, 1977). DSF metabolite, DDC undergoes further metabolism via four mechanistic pathways, glucuronidation, non-enzymatic degradation, methylation, and oxidation (Figure 1.3) (Johansson, 1992).

1.2.4.4 Elimination

Previous studies have shown the ways at which the metabolites of DSF eliminated from the body through the lungs, faeces (a fraction of the unconverted parent drug, DSF expelled through this route) and kidney (Johansson, 1992). Approximately 20% of ingested DSF is eliminated as the parent drug in the faeces (Eldjarn, 1950). In the kidney, up to 65% of glucuronide bounded DDC is eliminated from the body (Kaslander, 1963; Johansson, 1986). A small number of the DSF metabolites, DDC, Me-DDC, CS_2 and DEA are retrieved in urine (Figure 1.3) (Johansson, 1992). One of the three steps metabolite, Me-DDC and its polar sulphoxide and sulphone derivatives are catalysed by the P450 enzyme (Johansson, 1992). Most of CS_2 is eliminated via the lung (Strömme, 1965).
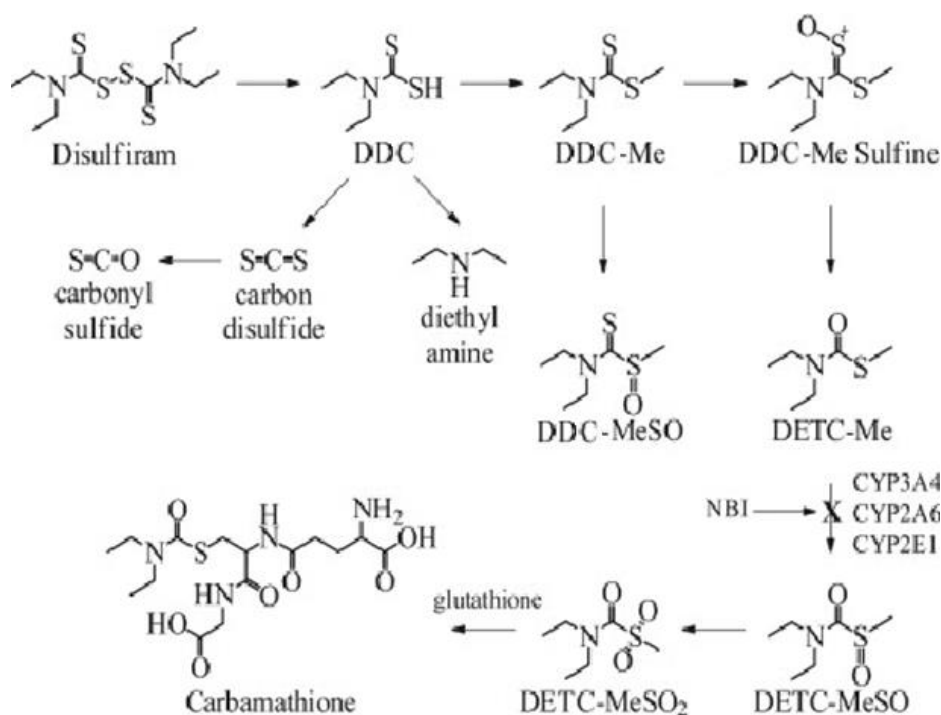
Figure1.3. The bioactivation steps of disulfiram and its metabolites. It was adapted from Faiman, et al., 2013).

1.2.5 Ethanol metabolism

When ethanol is ingested, it is metabolized mostly in the liver mediated through the two enzymes, alcohol dehydrogenase (ADH) and aldehyde dehydrogenase (ALDH) to liberate the ethanol metabolite, ethanal (Edenberg, 2007). As shown in Figure 1.4, the oxidative metabolism of ethanol by ALDH which also takes place in several organs to help break apart the ethanol molecule to its metabolites, acetaldehyde, and acetate (Edenberg, 2007). The higher the blood acetaldehyde concentrations are known to have aversion effect and therefore, identified as the basis for the alcoholism therapy with DSF a potent ALDH inhibitor of acetaldehyde metabolism (Schlesinger, Kakihana and Bennett, 1966). The first ethanol metabolite, acetaldehyde is metabolized by ALDH into acetic acid a highly neurotoxic molecule and a known carcinogen (Smith, Aragon and Amit, 1997; Edenberg, 2007). The second ethanol metabolite, acetate is a less active by-product that is further broken down into carbon dioxide and water ready for elimination from the body (Sarkola, et al., 2002). Evidence has shown ethanol, and peripherally produced acetaldehyde penetrates from blood to brain with difficulty due to metabolic activity by ALDH (Hunt, 1996). The alcohol metabolic pathway, through the isoenzyme of ADH, which is largely responsible for hepatic degradation of ethanol, is not present in the brain (Hunt, 1996). However, research studies conducted in normal and acatalasemic mice (differentially expresses reduced levels of catalase activity within tissue-specific manner) indicated that the first ethanol metabolite, acetaldehyde is formed directly in the brain in part by the help of enzyme catalase (Gill, et al., 1992; Aragon and Amit, 1993).
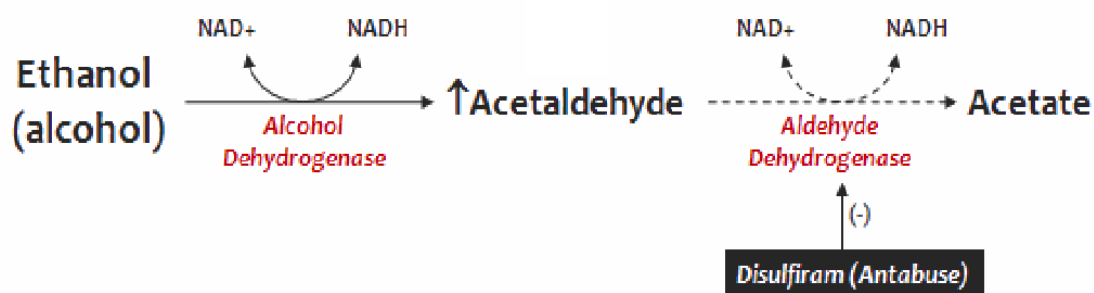
Figure 1.4. Disulfiram-ethanol reaction mechanism of action mediated by the aldehyde dehydrogenase (ALDH) enzyme. It was adapted from (Borja-Oliverira, 2014).

1.2.6 Anti alcoholism

DSF mechanism of action works by specifically inhibiting acetaldehyde dehydrogenase 1 and 2; both are involved in the metabolic oxidation of acetaldehyde in the liver (Marchner and Tottmar, 1978). As described in Figure 1.3, DSF metabolites induce sensitivity to alcohol (Chen, et al., 2006; Wickström, et al., 2007). When DSF is absorbed from the gastrointestinal tract, it causes acetaldehyde build-up through DSF ALDH inhibition mechanism, which triggers the negative effect of the incomplete metabolites alcohol (Johansson, 1992; Najlah, et al., 2017). Approximately, 5 to 15 minutes after ingesting DSF the symptoms of DSF and alcohol reaction commences a few hours after alcohol consumption (Lundwall and Baekeland, 1971). The intensity and time of DSF-alcohol reaction to produce the following symptoms, such as flushing, sweating, palpitation, dyspnea, hyperventilation, accelerated pulse rate, nausea, and vomiting mostly depend on the dosage of DSF (Lundwall, and Baekeland, 1971). Induced DSF-alcohol reaction includes cardiovascular, neurological, gastrointestinal and respiratory reactions ranging from mild to life-threatening reactions (Suh, et al., 2006; Mutschler, Diehl, and Kiefer, 2008). Such psychological deterrent in alcoholic

18

patients makes DSF relevant to its role to curb alcohol abuse (Johnston, 1953). The controlled research study indicated that DSF when used as adjuvant support alcohol abstinence and decreases in days hospitalized patients with alcoholism and severe mental illness (Mueser, et al., 2003). DSF anti-alcoholism primarily based on incompatibility with alcohol and the effective block alcohol-induced reward effects (Soyka, 2014). The subsequent use of DSF for the treatment of alcoholism was found to be an effective new therapeutic compound in treating cocaine addiction (Carroll, et al., 2004). The indirect mechanism pathway was attributed to ALDH-independent, which inhibits dopamine-β-hydroxylase conversion from dopamine to norepinephrine (Chen, et al., 2011). Early studies have suggested that DSF and its metabolite, DDC exhibited anti-tumour activity and when DSF is used as an adjuvant to some anticancer drugs, like cyclophosphamide, thus potentiate effect by augmenting apoptosis in cancer cells (Wang, McLeod and Cassidy, 2003).

As shown in Figure 1.3, DSF is primarily reduced or liberated to diethyldithiocarbamate (DDC), a potent inhibitor of aldehyde dehydrogenase (ALDH) enzyme. DDC was further converted to methyl-diethyldithiocarbamate (Me-DDC) and S-methyl-N, N-diethyldithiocarbamate (DETC) (Figure 1.3). Me-DDC is metabolite to DETC-sulfoxide (SO) while DETC is converted to Me-DDC-SO$_2$ potent inhibitors of mitochondrial ALDH2. The DETC-sulfoxide (DETC-SO) and Me-DDC-sulfoxide (Me-DDC-SO) are further oxidised to DETC-sulfone (DETC-SO$_2$) and Me-DDC-sulfone (Me-DDC-SO$_2$) (Koppaka, et al., 2012).

1.2.7 Anticancer

1.2.7.1 Disulfiram anticancer treatment

Clinical trials have shown that DSF potentially demonstrates efficacy against cancer with no toxicity effects on normal tissues (Johansson, 1992). DSF irreversibly inhibits ALDH enzyme, and the formed DDC-Cu complex is a potent anti-cancer agent (Figure 1.5) (Cen, et al., 2002; Liu, et al., 2012). Recent studies have attributed DSF and DDC-Cu to induce instant cytotoxicity or intrinsically induced anti-proliferation effect in cancer cells (ErebiáTawari and WaiáTsang, 2015). For the past two decades, DSF anti-cancer activity has sparked a high interest in repurposing this drug for cancer treatment. The biological activity of DSF as anticancer is due to its ability to bind Cu (Marikovsky, et al., 2002). The *In vitro* and *in vivo* studies have demonstrated that DSF acts as an anti-cancer agent against various cancer cells with low cytotoxic effects towards normal cells (Wickström, et al., 2007; Liu, et al., 2012). Research data dated from the 1970s to 80s have demonstrated the use of DSF and its metabolites to enhance anti-cancer activity (Yip, et al., 2011). The generated data, therefore, recognised DSF as a potential and useful anti-cancer cytotoxic agent for chemoprevention against cancer cells (Yip, et al., 2011). The successful discovery of DSF as an anti-cancer agent was achieved through the effort of investigating large-scale screening compounds that may show the proteasome for clinical use of non-chemotherapy molecular compounds as novel anti-cancer drugs (Yip, et al., 2011). There are countless articles being published on anti-cancer activity of the old anti-alcoholism drug, DSF. Already, evidence from *in vitro* and *in vivo* studies using animals to preclinical and clinical trials results showed anticancer activity of DSF (Johansson, 1992). As shown in Figure 1.5, two of the single diethyldithiocarbamates can reversely join together sulphur-sulphur bridged DSF, and the bidentate chelating ligands have

the ability to complex quite a good number of transition metal ions such as Cu^{2+} to form

bis(N,N-diethyldithiocarbamato) Cu^{2+}.

Diethyldithiocarbamate   **Disulfiram (DSF)**

bis(N,N-diethyldithiocarbamato) copper(II)
(CuL₂)
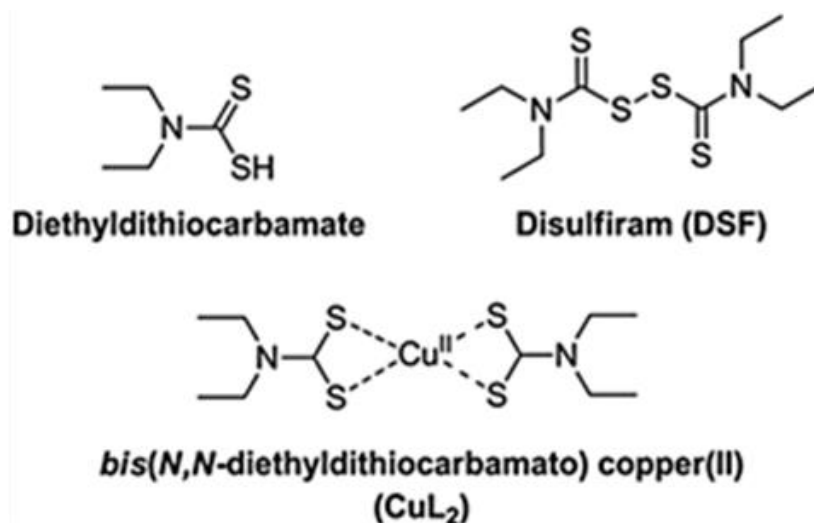
Figure 1.5. Cleaving disulfiram (DSF) (consisting of bidentate chelating ligands) from the sulfur-sulfur linkage gives two separate diethyldithiocarbamate (DDC) ligands. When copper (Cu) is presence, DDC has the ability to bind Cu to form DDC-Cu complex. It was adapted from (Lewis, et al., 2014).

1.2.8 Mechanism of anticancer action

1.2.8.1 Role of reactive oxygen species (ROS)

Reactive oxygen species (ROS) can be defined as a derived group of oxygen-containing chemical species expressing more reactive metabolism generated from the mitochondrial respiratory chain reaction, and involving reactive chemical properties (Mao, et al., 1995; Gupte and Mumper, 2009). Mitochondria and other enzymes, xanthine and nicotinamide adenosine dinucleotide phosphate (NADPH) oxidase generate ROS. Also, cytochrome P450s has been confirmed to generate ROS (Bánfi, et al., 2001; Kumagai, et al., 2002; Zangar, Davydov and Verma, 2004). As shown in Figure 1.6, GSH reductase is used as a source of electron donor to reduce hydrogen peroxides to water (Vaisberg, et al., 2005). In the presence of superoxide dismutase

(SOD) enzyme, a typical example of reduced ROS is superoxide anion radical (O_2^-) formed through the one-electron reduction of molecular oxygen ($O_2 + e^- ==> O_2^-$, superoxide) (Figure 1.6) (Buechter, 1988). Further reduction of oxygen is activated from the dismutation of superoxide ($2O_2^- + 2H^+ ==> H_2O_2 + O_2$) occurring spontaneously under low pH to form hydrogen peroxide (H_2O_2) and singlet oxygen ($^1O_2$) (Buechter, 1988). The Cu, Zn SOD enzyme protects the cell against oxidative damage by removing the superoxide anion radical from generating highly reactive ROS (Getzoff, et al., 1992). Whereas, under physiological condition, SOD can also catalyse highly reactive hydroxyl ($^.$OH) radical, once superoxide anion radical is formed by the deleterious effect of oxygen to liberate hydrogen peroxide (Buechter, 1988). Superoxide anion radical can react with nitric oxide radical ($NO^{-.}$) ($NO^{-.} + O_2^{-.} ==> + OONO^-$, peroxynitrite) to form a relatively reactive molecule called peroxynitrite ($OONO^-$) (Sies, 1997). It is obvious that the superoxide anion radical can trigger a cascade of ROS production.

Increase ROS levels intracellularly can damage DNA, protein and lipid membrane by inducing apoptosis mainly in cancer cells than in normal tissues (Fruehauf and Meyskens, 2007). Previous studies, have suggested that chemical substances generating ROS are more likely to produce high levels of ROS surpassing the threshold compared to the cellular antioxidant levels and then induce apoptosis to produce cell death (López-Lázaro, 2007). DSF nano-carriers have demonstrated how intracellularly Cu chelates with DSF (DSF chelates Cu when released from encapsulated nano-carriers) to form DSF/Cu complex generating ROS to induce an apoptotic response in cancer cells. In addition, studies have indicated DSF/Cu and DDC-Cu complexes as ROS-inducers (Morrison, et al., 2010). Therefore, the DSF cytotoxic effect and ROS-induced apoptotic pathway in cancer cells can be achieved through complexes of DSF/Cu and DDC-Cu nano-carrier delivery systems.
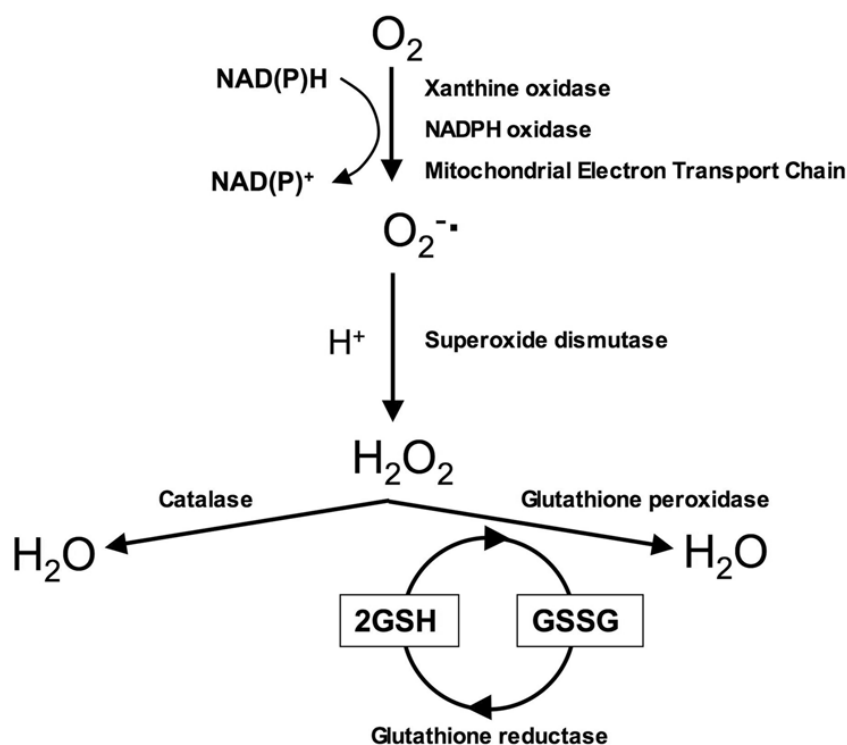
Figure 1.6. The production of reactive oxygen species (ROS) through the biological metabolic mechanism from molecular oxygen (O_2) generated by superoxide dismutase (SOD) enzymes. It was adapted from (Aitken and Roman, 2008).

1.2.8.2 Chemical reaction with disulfiram binding copper to generate reactive oxygen species

As a non-toxic agent to normal tissue cells, DSF anti-cancer activity can be enhanced intracellularly when combining with metal such as copper (Cu) or zinc (Zn) to regulate several pathways in cancer cells, which includes the induction of ROS (Tan et al., 2015). DSF metabolite of DDC has been found to alter the high increase of ROS and exhibiting antioxidant activity. When DDC bind with Cu, a higher ROS concentration generated (Victoriano L.I. 2000). Both DSF and DDC are capable of binding metal Cu to form DSF/DDC-Cu complexes and are ROS-independent inducers through the Fenton reaction, and Haber Weiss reaction (Fenton, H.J.H. 1894; Haber, F; Weiss, J. 1934). These reactions of DSF/DDC metal complexes to produce ROS can take place

23

using any of the following metals (Fe (II), Cu (I), Ti (III), Cr (II), and Co (II)) with the lowest sate of oxidation ready to react with H_2O_2 (this is known as the Fenton reactions) (Fenton, H.J.H. 1894). Hydroxyl radical and the oxidized metal ions were products derived from the DSF/DDC-Cu metal complexes reaction with H_2O_2. These reactions are capable of initiating further reactions (Haber-Weiss reaction), which oxidizes metallic ion that is reduced through the radical anion superoxide (Haber, F; Weiss, J. 1934). The chelated metal can be recycled to restart the Fenton reaction needed to produce toxic hydroxyl species that generate more ROS in cancer cells. It has been reported that DDC is an excellent scavenger of ROS (O_2^{-} and H_2O_2) (Mankhetkon et al., 1994).

The redox-sensitive signalling pathways of mitogen–activated protein kinases (MAPK) and NF-$_k$B are effective in providing defensive response-element against oxidative stress. Therefore, DSF/DDC-Cu complexes use different tumour-associated pathways which included the inhibition of the MAPK pathway that involved in the activation of ERK, PNK, and P38 pathways to allow the production of ROS-induced apoptosis (Tan et al., 2015). The complexation of DSF with a metal such as Cu can produce stable DSF-Cu complex, while DDC-Cu complex stabilizes the metal ion within the complexation resonance formed (Victoriano L.I. 2000). This is a good approach to produce more ROS-induced apoptosis through high uptake of the encapsulated DSF NPs/SLNs to deliver DSF into cancer cells.

Research evidence demonstrated DSF suppressing the anchorage-independent sphere generated in hepatocarcinoma cells via the activation of ROS-p38 MAPK (Chiba et al., 2014). As a Cu-dependent, DSF has the ability to bind with Cu intrinsically to up-regulate ROS through JNK and p38 pathways, and this is done by inhibiting NF-kB so that to prevent any response element that might hinder ROS-induced apoptosis of cancer cells.

1.2.8.3 Disulfiram and diethyldithiocarbamate copper complexes in cancer treatment

Studies have shown that as early as in the stomach, the molecule of DSF is cleaved to form a di-molecule, $(DDC)_2$ which chelates Cu^{2+} transition metal to produce DDC-Cu complex in the body (Johansson, 1992; Jiao, N Hannafon and Ding, 2016). *In vitro* studies involving the use of different cancer cell lines treated with the combination of DSF with Cu (II) ions showed high cytotoxic activity even towards chemo-resistant cancer cells (ErebiáTawari and WaiáTsang, 2015). ErebiáTawari, and WaiáTsang, (2015), reported the anti-cancer activity induced by DSF and its metabolite, DDC when combined with Cu(II) salts: *in vitro* results showed instant apoptosis when treated with DSF/Cu ROS-inducer demonstrates apoptosis in cancer cells. Therefore, the cytotoxic effect of DSF and its metabolite, DDC is reliant on the inclusion of Cu(II) salts which produces ROS (ErebiáTawari, and WaiáTsang, 2015). When exposing cancer cells to DSF and Cu(II) combination the generation of ROS occurs due to the rapid decomposition of DSF to DDC and the redox reaction of Cu(II) ions to Cu(I) ions (Figure 1.7) (Hart and Faiman, 1994; Han, et al., 2013). The current research study indicated the oxidation reaction mechanism of DSF and Cu(II) interaction to form DSF-Cu complex might be responsible for the formation of ROS high cytotoxic effects in cancer cells (ErebiáTawari and WaiáTsang, 2015). The *in vitro* results of earlier research studies showed DSF ability to induce apoptosis for a range of cancer cell lines identified as chemotherapy-resistant such as as*glioblastoma multiforme* (Zhou, et al., 2013; Guo et al., 2010). For the past two decades, recent studies have suggested DSF anti-tumour and chemosensitivity activities in various types of tumours and this including stem cells (Liu, et al., 2012). Up till this date, the mechanism of DSF anti-tumour inhibition profile proved unclear but increased cancer cell death has been found to be induced by ROS through the mediation of DSF/Cu complex (Cen, et al., 2002; Chen and Dou, 2008). Subsequent studies have shown DSF/Cu complex as a tumour

specific through proteasome inhibition mechanism, thereby leading to cancer cell death (Burkitt, et al., 1998; Cen, et al., 2002). Thus, the anti-proliferation effect of DSF in cancer cells was linked to Cu dependent (Cen, et al., 2002). DSF and its metabolite diethyldithiocarbamate (DDC) chelate Cu to form DDC-Cu complex (Figure 1.7). As shown in Figure 1.7, of which intrinsically DSF molecule can reversely reduce to its metabolites (two DDC ionic molecules). Absorbed Cu is highly ubiquitous in the stomach and small intestine, and it is transported to the liver via the portal bound to albumin later distributed towards the peripheral tissues. The two DDC ionic molecules will interact with Cu^{2+} to form DDC-Cu(I) or DDC-Cu (II) complexes. DDC-Cu complexes might be responsible for the DSF inhibition activity of the cellular proteasome *in vivo*.
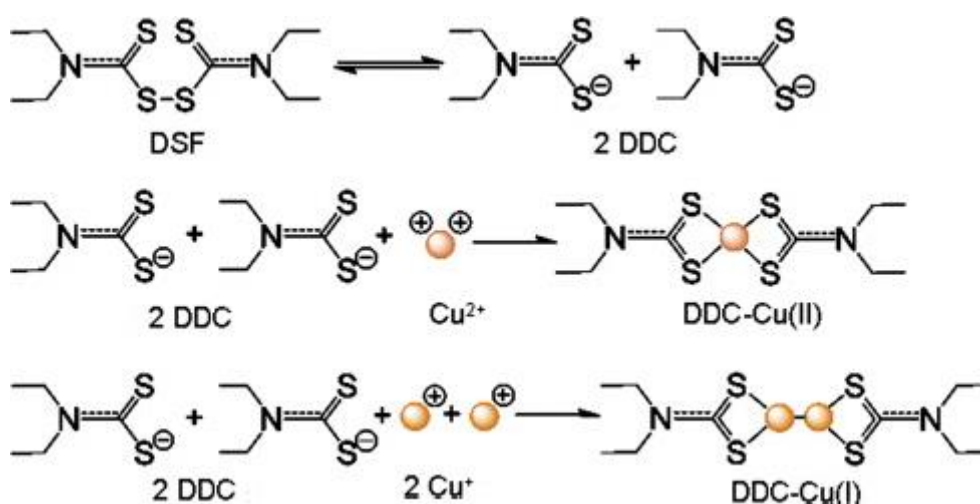
Figure 1.7.The molecular structure of disulfiram (DSF) and its metabolite, diethyldithiocarbamate (DDC) chelating copper (Cu) to form DDC/Cu complex with the potential to induce apoptosis in cancer cells. It was adapted from (Han, et al., 2013).

Nevertheless, DSF efficacy has been hindered by it short half-life (4 min) in the bloodstream and cannot reach cancer cells because of DSF rapid degradation (Chen and Dou, 2008; Najlah, et al., 2017).

To enable the long circulation of DSF and extend its half-life in bloodstream, nano-carriers such as polymeric NPs and SLNs have been developed. The interest in SLNs is increasing due to their wide pharmaceutical applications such as encapsulated hydrophobic compounds for enhanced therapeutic effects (Kumari, Yadav and Yadav, 2010). In a recent study, a lower dose of DSF-loaded PLGANPs was supplemented with oral Cu which inhibited tumour growth and decreased metastasis in a xenograft mouse lung cancer model (Najlah, et al., 2017). Different surface modifiers, such as (Plutonic® 188, polylobate 80, Triton^s) were added in the preparation of DSF-loaded PLGA NPs to enhance drug entrapment properties and hence demonstrated increased cytotoxicity against hepatocellular carcinoma (Hep38) cell lines (Hoda, et al., 2015). Surface modification of dysphonic polymers such as poly (ethylene glycol) (PEG), coated with DSF-loaded PLGA/PEG NPs for long circulation indicated strong cytotoxicity effect and proliferation inhibition against breast cancer MCF7 cell line and solid breast cancer tumour animal model, respectively (Fasehee, et al., 2016).

The formulated DSF-loaded PLGA-PEG-folate NPs demonstrated induced ROS generation leading to induce apoptosis and inhibit cell proliferation in breast cancer cells (Fasehee, et al., 2016). An *in vitro* and *in vivo* anti-tumour therapy with DSF-loaded mPEG-PLGA/polycaprolactone (PCL) mixed NPs showed DSF inhibition of the MCF7 and 4T1 xenograft tumour cell proliferation and tumour growth in Balb/C mice animal model, respectively (Song, et al., 2016). DSF-loaded PLGA supplemented with Cu showed a high inhibition proliferation of the liver cancer stem cell population (Wang, Wang and Xiu-Wu, 2018). Enhanced surface properties of DSF-loaded PLGA/PEG NPs delivery carriers improved dispersion, neutralize the charge, and enable particle diffusion in human cervical mucus (Cu and Saltzman, 2008).

However, more development is still needed in this field, especially for enhanced loading efficiency and extended DSF stability, for example, Najlah et al., (2017) have

found that methods of preparation are critical in terms of producing PLGA nanoparticles of appropriate size. NPs alteration of particle size, shape, and surface chemistry are designed and optimized to meet different requirements with the ability to achieve functionalities such as reaching targeted organs. Optimized nanotherapeutics mostly relied on size to exert effective cellular uptake and tumour permeability. Recent studies indicated larger particles above 200 nm significantly reduce the *in vitro* cytotoxicity, and this might be explained by the effect of particle size cellular uptake (Najlah et al., 2017). In this study, DSF-loaded PLGA, and PEGylated NPs prepared by using the D-Nano-Pr method showed superiority in loading efficiency, provide protection to the encapsulated DSF in horse serum sustained drug release and demonstrated increased cytotoxicity effect on breast cancer cells (this including PTX-resistant MDA-MB-231 cell line). Therefore, it is very important to continue developing nano-formulation of DSF using preparation methods that are efficient, simple, and easy to scale up.

1.3 Nano-carriers (Nanomedicine)

Nanomedicine is the use of nano-scale or nano-structured entities with the ability to cross biological barriers, and achieve therapeutic effects (this can effectively influence medical diagnosis and treatment in the human body) (Royal, 2004). Nanomedicine is an emerging promising synthesis technique for treating dreadful diseases such as cancer and to help avoid some of the shortcomings produced by the conventional chemotherapy agents such as rapid drug clearance, and biodegradation, and limited targeting to tumour sites (Sinha, et al., 2006). Nanomedicines can also minimize the severe side effects caused by the anti-cancer agents due to the properties of nano-carriers such as nanoparticle sizes, high surface to volume ratios, surface charge, targeting modifications to reach tumour tissues and then release the anti-cancer drug

in a stable, controlled mechanism (Wicki, et al., 2015). As shown in Figure 1.8, a variety of entities have now been investigated as nano-carriers for cancer therapy such as polymeric based, lipid-based, inorganic, viral, and drug-conjugated NPs (Wicki, et al., 2015).
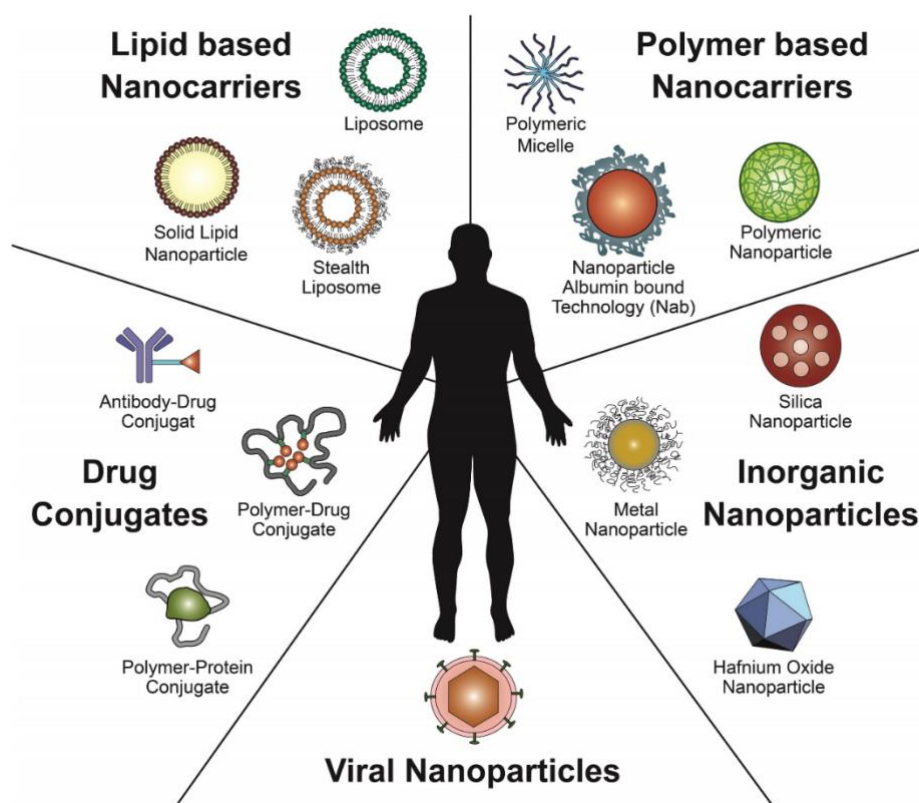
Figure 1.8. Nanomedicines entities currently been investigated, and available in the clinic cancer therapy such has lipid-based nano-carriers, polymer-based nano-carriers, inorganic nanoparticles (NPs), Viral NPs, and drug conjugates. It was adapted from (Wicki, et al., 2015).

Nano-carriers can be defined as sub-micron particulates less than 200 nm in diameter for biomedical application to attain increased drug uptake at the surface of the tumour to achieve high retention effects (Saad, Garbuzenko and Minko, 2008). Recent studies have demonstrated the use of nanotechnologies such as D-Nano-Pr method (Song, et al., 2016) and single emulsion/solvent evaporation (SE) method for the preparation of disulfiram nano-carrier delivery systems through nano-encapsulation (Zhou, et al., 2013; Najlah, et al., 2017). Nano-carriers are designed using lipophilic and hydrophobic molecules encapsulated with the FDA approved polymeric materials, or

phospholipids to enhance efficient drug loading of NPs and SLNs (Narvekar, et al., 2014).

The shape, size, particulate surface area, aggregation, size distribution, surface morphology/topography, a structural type (crystallinity), defect structure and solubility is considered as the main parameters of the physical properties of NPs (Cadden, 1987; Rao and Biswas, 2009).

1.3.1 Size and shape of nanoparticles

The size and shapes are unique parameters used to determine NPs nano-material (Jolivet, et al., 2004). It has been demonstrated that particle size of NPs below 20-30 nm can be thermodynamically unstable due to interfacial tension activity force enabling the instant reduction of the surface area (Slomberg and Schoenfisch, 2012). NPs critical size is within 30 nm of which the nano-size scale properties are exhibited from their bulk material (Slomberg and Schoenfisch, 2012). The size of a nanoparticle has the advantage to significantly influencing the biodistribution of targeted and non-targeted organ-specific tumour sites (Cheng, et al., 2007). Slomberg and Schoenfisch, 2012, suggested that when a nanoparticle decreases in size, the particles surface increases in an exponential trend. Therefore, nanoparticles average size for a formulation might be crucial for not only the stability of the formulation but also for the stability and activity of the loaded drug (Najlah et al 2017).

The NPs surface morphology and surface area are characterized by scanning electron microscopy (SEM) (as described in chapter 2) (Hayat, 1974). The atomic force microscopy (AFM) can be employed to obtain a higher resolution at around 0.2 nm by providing real topographical images of sample surfaces (Honary and Zahir, 2013). In addition, dynamic light scattering (DLS) provides an evaluation of the size distribution of NPs, where, the zeta sizer determines the surface charge of NPs (Honary and Zahir, 2013). NPs with surface charge can determine its effect on cell membrane attachment

(Honary and Zahir, 2013a). At the cell membrane, positively charged NPs are absorbed rapidly than their neutral or negatively charged counterparts (Honary and Zahir, 2013). The surface charge influences the dispersion and aggregation of NPs in aqueous media (Orts-Gil, et al., 2011).

1.3.1.1 Potential for surface engineering

Nanomedicine is a technology design for the application of characterized particle size, shape, and surface chemistry through the invention of molecular tools used for diagnosis and customized for a specific treatment such as cancer (Sinha, et al., 2006; Albanese, Tang and Chan, 2012; Bregoli, et al., 2016). One of the limitations inherent to the majority of the chemotherapy agents is the lack of tumour selectivity. The advantage of nanomedicines to achieve delivery of selective chemotherapeutic drugs design to target solid tumours is by exploiting the tumour's vasculature (hypervascularization and extensive production of vascular permeability) (Fang et al; 2011). NPs based drug delivery systems against cancer mostly rely on the enhanced permeability and retention effect (EPR). EPR effect is known to be the phenomenon that nanomedicines are used to deal with tumour tissues (Mi, Peng et al; 2020). EPR effect and enhanced permeability mechanisms exploited for the accumulation of high molecular weight non-targeted encapsulated drugs and prodrugs in tissues requiring increased vascular permeability (e.g. cancer or site of inflammation) (Maeda and Matsumura, 2011). Abnormalities of tumour vasculature for selective delivery against cancer tissues, thus determine the EPR effect of most macromolecular drugs in solid tumours (Maeda and Matsumura, 2011). This is the reason notably the intravenous (i.v.) administration of large molecular size, and nano-sized macromolecular anticancer drugs escaped renal clearance as they find it hard to penetrate the tight endothelial junctions of normal blood vessels, but extravasate within tumour vasculature where they will be trapped in the tumour environment (Fang et al; 2011). Tumour tissues are

differentiated from normal infected tissues through the dysfunction of the lymphatic tissues, and this caused the EPR un-protective because of rapid lymphatic clearance (Laverman et al., 2001).

The smaller size NPs-based drug delivery allows extravasation in the leaky vascular structure of tumours compared to the larger nano-sized carrier systems are forced out of the blood vessels to the surrounding tissues causing their distribution in the bloodstream to be highly variable (Bregoli, et al., 2016). Also, optimizing the sizes of nano-carriers can improve specific uptake into tumour tissues, and the shape thus has an impact on fluid dynamics to enhance payload, and drug uptake (Truong, et al., 2015). The design of spherical size and shape nano-carriers appears as the most commonly used in nanotechnology compared to non-spherical variety simply because of the challenges in manufacturing and testing (Truong, et al., 2015).

The surface charge of a nano-carrier system is known to affect the stability and distribution of nano-carriers in the blood. In addition, earlier studies have shown positively charged NPs effectively target tumour vessels (Stylianopoulos, et al., 2010). Intracellularly, phagocytic cells preferably interact with negatively charged NPs as they do to ingested negatively charged bacteria (Corpe, 1970). Phagocytes interaction with negatively charged surface structures such as anionic cyanoacrylic NPs are stronger and may have the responsibility to produce higher cytotoxicity compared to cationic NPs (Tomita et al; 2011). The less interactive cationic charged NPs to macrophage uptake and cytotoxicity present PEGylated NPs the advantage for bearded NPs to be shielded with a positive surface charge by producing a minimal effect on cellular uptake, cytotoxicity, and prevent membrane damage in nonphagocytic neuroblastoma cells (Hoskins et al; 2012). Surface modification of nano-carriers such as coating bearded NPs surface with functionalized positively charged cationic PEG ligands is more effective in accumulating tumour tissues than negatively charged anionic NPs

(Chung et al., 2010). PEGylated cationic NPs enhances the encapsulated hydrophobic drug (DSF) half-life and ensure long circulation in the blood by facilitating endocytosis and cellular uptake in cancer (Stylianopoulos, et al., 2010).

Previous studies have indicated the use of PEG on NPs increases solubility and stability of NPs due to its hydrophilicity as a non-ionic polymer (Bregoli, et al., 2016). PEGylated NPs hardly disrupt the function of charged molecules, such as DNA, by masking their hydrophobicity to prevent recognition from the reticuloendothelial system (RES) (Locatelli and Franchini, 2012; Danhier, et al., 2012).

1.3.2 Structural specificity of nanoparticles

NPs purity can be determined by its structural difference as an important factor for various biological applications. For example, the crystal structures are characterized using X-ray diffraction (XRD) (Warren, 1969). The identification of crystal structures provides information about the available crystal structures with more informational analysis for the identified XRD profiles using various structural parameters (Kumar and Yadav, 2009). The structural specificity of NPs thus has an effect based on the type of NPs and nature of biological systems used for a physiological response (Zhang, et al., 2015).

1.3.3 Chemical properties of nanoparticles

The chemical properties of NPs can be dependent on the elemental composition of nonmaterial, especially surface chemistry, including zeta potential and photocatalytic properties (Cadden, 1987; Rao and Biswas, 2009). The electron composition of NPs is an integral part of determining the chemical properties of the material design (Schmid, 2011). NPs are made up of several nanostructures with different chemical properties, such as metals (most flexible nanostructures) (Greulich, et al., 2009), metal oxides (lattice symmetry and effect of size) (Raliya and Tarafdar, 2013), carbon

nanostructure (built from sp2 carbon units based), (Liu, et al., 2007; Prato, Kostarelos and Bianco, 2007) and polymeric nano-spheres and nanocapsules (obtain from synthetic polymers such as PLGA/PCL) (Bilensoy, et al., 2009).

1.3.4 Nanotechnology for disulfiram delivery

Nanotechnology, a technique used to fabricate nanoparticle-based drug delivery systems from polymeric materials, anticipated to exert the efficacy of hydrophobic drugs for systemic delivery (Whitesides, 2003; Shehzad, et al., 2014). The chemical or physical properties and potential biological applications have made biodegradable polymeric NPs of great interest which are widely used (Yurgel, Collares and Seixas, 2013), due to their versatility and compatibility with other polymeric materials (Mora-Huertas, Fessi and Elaissari, 2010). The polymeric materials are highly desirable because of their ability to protect hydrophobic drugs from being rapidly degraded and to enhance intratumorally distribution for sustainable and controlled release (Shieh, et al., 2010).

Formulated NPs are prepared through different approaches including D-Nano-Pr method used to rapidly develop well-defined biodegradable polyesters NPs in water (Song, et al., 2016). Engineered NPs drug-delivery systems of polymeric materials can be tailored to achieve nano-scale particle in the range size between few nm, preferable up to 100 nm suitable size loaded anti-cancer drugs (Lobatto, et al., 2011; Steichen, Caldorera-Moore and Peppas, 2013).

For the past decades, readily fabricated drug-delivery systems using soft organic or polymeric materials or hard inorganic materials have shown great promise in the treatment of cancer (Schubert, Delaney Jr and Schubert, 2011). Therefore, the application of nanotechnology demonstrated great innovation in the development of stable hydrophobic drug formulations, such as DSF-loaded polymeric/phospholipids NPs/SLNs and combinatory therapy with DSF. The manufactured DSF PLGA NPs data

have suggested anti-proliferation against non-small-cell lung cancer, breast cancer, hepatocellular carcinoma, CRC and glioblastoma stem cells (Mosallaei, et al., 2013; Zembko, et al., 2015; Hoda, et al., 2016; Fasehee, et al., 2016; Wang, et al., 2017).

1.3.5 Poly lactic-co-glycolic acid (PLGA) nanoparticles

1.3.5.1 Physicochemical properties of PLGA

Poly lactic-co-glycolic acid (PLGA) can be defined as a biocompatible and biodegradable linear copolymer prepared using different ratios between similar monomers of lactic and glycolic acid (Figure 1.9) (Lü, et al., 2009). PLGA geometry position strongly influences its degradation pattern on the accessibility of water; with an acidic environment, the PLGA degradation accelerates due to autocatalysis (Pamula and Menaszek, 2008). The physicochemical properties of PLGA determine the ultimate performance of biomedical applications (Pamula and Menaszek, 2008). The synthesis of PLGA with low molecular weight (LMW) below 10 KDa can be done by the ring-opening of co-polymerization of lactic and glycolic acid (Figure 1.9) (Lü, et al., 2009). While cyclic dimers or catalysts, can be used as starting materials to get higher molecular weights of PLGA (Lü, et al., 2009).

The PLGA polymer is synthesized by the polymerization process of the ester-linkages of successive monomer units of glycolic or lactic acid to produce linear amorphous aliphatic random polyester PLGA (Dechy-Cabaret, Martin-Vaca and Bourissou, 2004). Sequence PLGA tends to degrade at a slower rate than random PLGA low weight PLGA synthesized by ring-opening polymerization (Stayshich and Meyer, 2010). The synthesis of sequence PLGA demonstrated an advantage over drug delivery applications for control release drug delivery (Stayshich and Meyer, 2010).

The physicochemical properties of PLGA can be determined by the molar ratio between two monomers, lactic or glycolic acid (Miller, Brady and Cutright, 1977).

Previous studies have suggested PLGA mixed with an equal molar ratio of 50:50 between lactic acid/glycolic acid copolymer exhibits the shortest half-life and fastest degradation rates (Miller, Brady and Cutright, 1977; Cohen, Alonso and Langer, 1994; Alexis, 2005). The methyl functional group on the alpha (α) carbon of polylactic acid (PLA) makes the molecule chiral and provided the irregular distribution of different D, L and D/L isomers, therefore, stereochemistry is critical in obtaining the final desired properties of the copolymer (Jalil and Nixon, 1990). D,L-lactic acid has been found to be an amorphous and transparent material containing a random distribution of the D and L units (Jalil and Nixon, 1990).

Most importantly, stereochemistry plays a key role in the PLGA degradation process at which the rate of water, penetration is higher in amorphous D,L regions (i.e. this facilitates the acceleration of PLGA degradation (Wise, et al., 2000). With the lactic acid and glycolic acid, the methyl functional side group from the alpha carbon or PLA is missing making them highly crystalline, whereas, with the PLGA copolymers no crystallinity presents (Gilding and Reed, 1979). PLGA amorphous nature of equal molar ratio (50:50) makes them the most frequently-used copolymers due to their applications in drug delivery providing homogeneous dispersion of the active ingredient in the polymer matrix (Gilding and Reed, 1979).

The PLGA degradation rate is modulated by the free carboxyl end-groups used as chemical modifications (Wu and Wang, 2001). When PLGA is degraded, the lactic and glycolic acid become the end products and are further incorporated into the Krebs cycle and eliminated as carbon dioxide and water (Yoshioka, et al., 2008). To increase the hydrophilicity of PLGA derivatization strategies are developed in order to add hydrophilic moieties such as hydroxyl groups which maintain stronger water absorption capacity compared to the non-functionalized counterparts with an increasing degradation rate as a result (Leemhuis, et al., 2006; Leemhuis, et al., 2007).

Figure 1.9. Schematic representation of the chemical structure of poly (lactic-co-glycolic acid) (PLGA) and its monomers, lactic acid (LA) and glycolic acid (GA). It was adapted from (Gentile, et al., 2014).
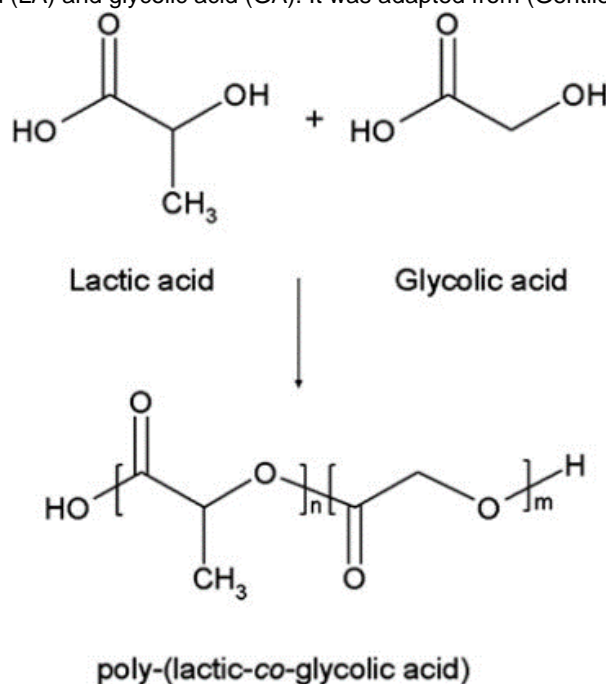
1.3.5.2 PLGA nanoparticles

PLGA based polymeric NPs carrier system has been widely used in the application of pharmaceutical dosage, like, encapsulated hydrophobic compounds, chemotherapy drugs and biological agents (Kumari, Yadav and Yadav, 2010). The synthetic polymers such as PLGA and PCL are of the advantage of having high purity and reproducibility

than the natural polymers (Anderson and Shive, 1997). PLGA is the most successfully used biodegradable synthetic polymer approved by FDA and European Medicine Agency (EMA) as delivery carriers for human therapy (Tice, et al., 1996; Jain, 2000). Also, PLGA is a better option in terms of their physical and chemical properties served as delivery systems by encapsulating hydrophobic drugs to increase chemical stability, enhance solubility, provide better sustainability and endogenously enhances surface area at proximity with biological materials for drug targeting purposes (Danhier, et al., 2012).

From the various nano-particulate carriers, PLGA NPs have improved the conjugation or encapsulation of drugs extended circulation half-life and minimised the unwanted systemic side effects of the therapeutic agents (Sahoo, Dilnawaz and Krishnakumar, 2008). For example, cisplatin-loaded PLGA-mPEG$_{2000}$ NPs demonstrated prolonged drug residence within the systemic blood circulation with satisfactory drug content in both *in vitro* and *in vivo* studies (Avgoustakis, et al., 2002). Similarly, formulated paclitaxel (PTX)-loaded chitosan blended PLGA-mPEG$_{2k}$ NPs were delivered in retinoblastoma, breast cancer and pancreatic cancer cell lines indicated increased *in vitro* cytotoxicity and prolonged *in vivo* blood circulation and reduced macrophage uptake with a tiny amount of NPs sequestered in the liver (Parveen and Sahoo, 2011). The *in vivo* study investigated the biodistribution of bovine serum albumin (BSA)-loaded PLGA-mPEG$_{2k}$ NPs delivery demonstrated a prolonged half-life of BSA from 13.6 min to 4.5 h compared to PLGA NPs (Li, et al., 2001).

To enhance DSF stability and higher drug entrapment efficiency, the FDA approved polycaprolactone polymer has been employed to increase drug stability and bioavailability, sustainable control release of the protected drug into the target tumour sites were obtained (Sun, Radosz and Shen, 2012; Danhier, et al., 2012).

To further protect PLGA NPs from protein adsorption, methyl polyethylene glycol (mPEG) can be employed to change the surface of PLGA NPs to increase cell surface interaction for drug targeting into tumour sites (Danhier, et al., 2012). In this context, the surface functionalized docetaxel-loaded PLGA conjugated soybean lecithin coated with PEG (PLGA-lecithin-PEG) mono shell NPs demonstrated biocompatibility and increased cytotoxicity Hela and HepG2 model human cell lines (Chan, et al., 2009). Similarly, the *in vitro* and *in vivo* co-delivery of cisplatin (cis-diaminodichloroplatinum, CDDP) and PTX-loaded PLGA surface-functionalised PEG conjugated folic acid (CDDP + PTX-encapsulated PLGA-PEG-FA) NPs improved the synergistic effect and increased inhibition of lung cancer cells and high folic acid receptor expression in tumours (He, et al., 2015). The surface functionalised delivery system of daunorubicin (DNR)-loaded PLGA-poly-L-lysine (PLL) PEG combined with gambogic acid (GA) (DAR-PLGA-PLL-PEG-GA) for specific target, demonstrated anti-tumour efficacy and reverse MDR of leukaemia (K562/A02) cancer cells to DNR (Xu, et al., 2015). PTX-loaded PLGA NPs *in vivo* delivery system has also demonstrated high therapeutic improvements survival rate (Xu, et al., 2015). All of these examples support the high-efficiency of using PLGA nanoparticles as a nano-system to overcome problems associated with the delivery of drugs that are MDR substrate, poorly water-soluble or/and instable in the bloodstream.

1.3.6 Solid lipid nanoparticles

Solid lipid nanoparticles (SLNs) are particulates developed from solid lipid matrix with an average diameter in the nanometre range and are stabilised by surfactants (Muller, 1996). Also, SLNs are a new type of colloidal drug carrier systems with biocompatibility and biodegradability for controlled drug delivery into cancer cells (Ekambaram, Sathali and Priyanka, 2012). SLNs are solid lipids at human physiological temperature (37°C) with a diameter of 50-1000 nm. SLNs are produced to replace the liquid lipid (oil) of an

oil-in-water emulsion to a solid lipid (Wong, et al., 2007). SLNs can form a very strong lipophilic matrix incorporating anticancer drugs for subsequent controlled drug release (Müller, MaÈder and Gohla, 2000; Jores, et al., 2005; Mehnert and Mäder, 2012). Biocompatible and biodegradable carrier lipids, such as lipid acids (stearic acid, palmitic acid), triglycerides (tristearin, tripalmitin, trilaurin), and hard fats (glyceryl behenate) are employed in the formulation along with emulsifiers (e.g. Poloxamer 188) (Smith, 1986; Müller, MaÈder and Gohla, 2000).

The introduction of SLNs for the last two decades presents an alternative delivery system to other nano-carrier systems such as polymeric NPs and liposomes (Ekambaram, Sathali and Priyanka, 2012). SLNs-based carrier systems from phospholipids (such as phosphatidylserine, phosphatidyl glycerol and diphosphatidyl glycerol), are FDA approved materials (Ravi, et al., 2014), served as a biocompatible, biodegradable and stable carrier for hydrophobic drugs (Cavalli, et al., 2002; Pilcer and Amighi, 2010). SLNs have shown various advantages such as the ability to incorporate lipophilic and hydrophilic drugs, the natural composition made of physiological lipid and low toxicity with increased bioavailability (Jain, 1997).

In SLNs carrier system, a hydrophobic drug could be incorporated in the solid hydrophobic core of the high melting lipid with a phospholipid monolayer coating (Chandni, Viral and Umesh, 2011). During SLNs formulation, the oil of the lipid emulsion transforms to a solid lipid under room temperature (Chandni, Viral and Umesh, 2011). In a nano-scale range, the carrier system consists of spherical solid lipid particles containing solid lipid core, phospholipid monolayer and the anticancer agent such as DSF or its metabolite, DDC-Cu complex.

1.3.6.1 Physicochemical properties of solid lipid nanoparticles

The physicochemical stability of SLNs nano-carriers is dependent on its chemical and structural composition (Müller, Rühl and Runge, 1996). SLNs physical stability can be

indicated by the mean particle size distribution in the submicron size range (Heurtault, et al., 2003). Therefore, a clear indicator of SLNs physical instability is the increase in particle size above submicron size range (Benoit, et al., 1988; Heurtault, et al., 2003). The concentration of the surfactant or surfactant mixture expressed as surfactant/lipid ratio, used during the preparation can affect particle size production of SLNs (Bunjes, Westesen and Koch, 1996; Bunjes, Koch and Westesen, 2003). To achieve the highest product quality and physical stability of SLNs, there are many parameters to control such as time, temperature, homogenization speed, sterilization and lyophilisation (Mller, et al., 1995). For instance, high-speed stirring homogenization process can reduce particle size and polydispersity index (PDI) values (Schwarz, et al., 1994; Patravale and Ambarkhane, 2003). The chemical stability of SLNs incorporating drugs can be affected due to catalyst residues and molecular non-homogeneity of polymeric NPs in pharmaceutics and cosmetics (Mller, et al., 1995). The storage temperature has also a greater influence on the chemical stability of SLNs, and they are less stable at 40 $^\circ$C compared to that stored at 4 $^\circ$C and room temperature (Dingler, et al., 1999; Meot-Ner, 2005).

As shown in Figure 1.10, SLNs colloidal particulate structure constitutes of rigid external membrane that is composed of phospholipids soft condensed materials with amphipathic property of polar and non-polar tails (Heurtault, et al., 2002).
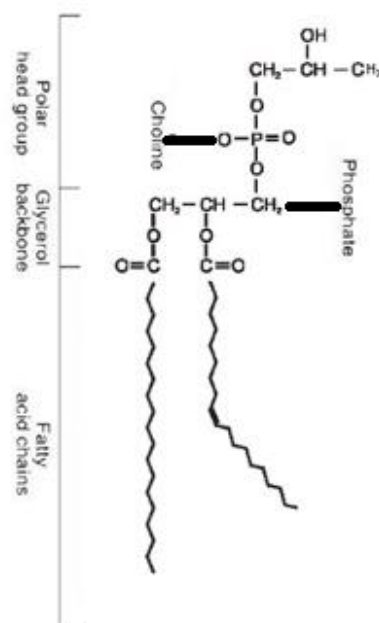
Figure 1.10. The model structure of a phospholipid with an amphipathic property contains a polar head group (choline), glycerol backbone, and fatty acid chains. It was adapted from (Osman, Christof 2011).

1.3.6.2 Solid lipid nanoparticles in cancer treatment

SLNs nano-carriers also referred to as lipospheres or solid lipid nano-spheres have the prospect of improving hydrophobic anticancer cytotoxic drugs in a more efficient, specific and safer anticipated manner (Mehnert and Mäder, 2012). The delivery of lipophilic drugs incorporated into the oil droplets was the start of a new delivery system, such as Diazemuls in the 1970s and Diprivan in the 1980s (Klang and Benita, 1998). Liposomes were the next parenteral carrier systems designed to reduce the toxic side effects and enhance the efficacy of anticancer drugs (Bangham and Horne, 1964); few products were commercially available for clinical use such as Ambisome (1990), DaunoXome (1996), and Doxil (1995) (Lasic, 1998; Al-Jamal and Kostarelos, 2007). The development of SLNs was an innovative approach to protect potent anticancer drugs from degradation, produce effective controlled release and minimise associated side effects (Schwarz, et al., 1994; Müller, MaÈder and Gohla, 2000). In this context,

nano-structured doxorubicin-loaded SLNs-(Dox) formulations demonstrated increased apoptosis of breast cancer cells by overcoming chemo-resistance breast tumour cells (Kang, et al., 2010). The *in vitro* study showed that Dox and PTX-loaded SLNs formulations demonstrated higher anti-proliferative effect on human colorectal cancer (CRC) cells at low concentrations of 1.72 nM and 1.17 nM, respectively (Serpe, et al., 2004).

Formulated transferrin-mediated curcumin (Tf-C)-loaded SLNs indicated increased cytotoxicity in breast cancer cells (Mulik, et al., 2010). Quercetin (QT)-loaded SLNs nano-carriers improved the oral delivery of the encapsulated poorly water-soluble QT with a significantly increased bioavailability (Li, et al., 2009).

In this study, the ability of SLNs to protect DSF from horse serum will be explored. It is essential that this protection is associated with maintained or improve cytotoxicity of DSF toward cancer cells.

1.3.7 Characterisation of nanoparticles

1.3.7.1 Particle size

Engineered NPs are purified by characterisation of particle size, polydispersity index (PDI) and zeta potential to determine the feasibility of delivering loaded chemical agents into the biological environment (Soppimath, et al., 2001; Reis, et al., 2006; Treuel, et al., 2014). Particle size and zeta potential can influence biological reaction, particularly the interaction of cellular uptake (Fröhlich, 2012) and toxicity effects (Bhattacharjee, et al., 2013).

The zeta sizer device used to characterise particle size, and zeta potential requires a small number of samples. In 2011, there has been unifying consensus guidelines provided by the European Union (EU) on how to determine a nano-material, mainly its particle size range with a lower limit suggested at 1 nm and an upper limit within 100

nm (Blanco, Shen and Ferrari, 2015; Rauscher, Rasmussen and Sokull-Klüttgen, 2017). However, nano-encapsulation of drugs consists of drug-loaded nano-carrier known as a solid colloid system with a submicron-sized drug delivery system at a range from 1-1000 nm (Couvreur, 1988; Couvreur, Dubernet and Puisieux, 1995).

There is no scientific data proposed by the EU on particle size limit range of NPs derived from polymeric materials for drug delivery (Bleeker, et al., 2013). The agreed binding definition of particle size dimension with nano-materials provides the ability to regulate NPs characterisation parameters (Rauscher, Rasmussen and Sokull-Klüttgen, 2017).

1.3.7.2 Zeta potential

Zeta potential refers to as the mean average electrostatic potential of colloidal dispersion occurring at the hydrodynamic radius and potential difference existing within the slipping plane of electrophoretically mobile particulates (Figure 1.11) (Rabinovich-Guilatt, et al., 2004; Delgado, et al., 2007; Lim, et al., 2013).

As described in Figure 1.11, zeta potential or electric surface potential is the interfacial double layer of 0.2 nm from the surface of the colloid system. Zeta potential is easily measured to determine the magnitude of electric surface charge value, and zeta potential unit is millivolt (mV) (Huynh, et al., 2009). The zeta potential maximal electric surface charge of NPs in suspension mixture is measured optically to determine physical stability (Mishra, et al., 2009; León-Rodriguez, et al., 2010). Therefore, NPs surface charge is considered highly important for drug delivery target sites, and NPs without electric surface charge faced major obstacle by macrophages ready to remove such NPs in the bloodstream (Kumar, Ravikumar and Domb, 2001).

The liver is a vital organ containing the largest number of fixed tissue macrophages (Kupffer cells), including reticuloendothelial system (RES) that is responsible for reducing efficient targeting of colloidal nano-carriers (Hamazaki et al., 1994). RES is a

network of various cells and tissues present in the mononuclear phagocyte system and polymorphonuclear leukocytes responsible for detecting foreign particles and removed them from blood circulation by macrophages (Saba, 1970). Various studies have investigated the possibilities of decreasing and increasing RES uptake, and nano-carrier systems concentration to achieve target tumour sites, respectively (Patil et al., 2008). To achieve decreased RES uptake will be to produce a reduced particle size that enabled steric stabilization NPs coated with PEG amphiphilic polymer chains (Zahr et al., 2006; Gref, 2012). Attached PEG on the surface of NPs increases the biocompatibility of the NPs with ability to evade RES and extend NPs time in the blood circulation of encapsulated hydrophobic drugs capable of locating the tumour site (Klibanov et al., 1990). Surface charge is essential in determining the efficiency and mechanism of cellular uptake by enhancing the pharmacokinetic properties of the particle in the body (Jabr-Milane, et al., 2008).

Also, the delivery of NPs to reach cancer cells in the liver and spleen can be difficult to reach their target as they are easily removed from the systemic circulation when detected by the RES system (Kumar, Ravikumar and Domb, 2001). Hydrophilic polymers such as PEG attached on the surface of NPs with high zeta potential value is modified to avoid opsonisation and enhanced long-term systemic circulation in the bloodstream (Soppimath, et al., 2001; Reis, et al., 2006).
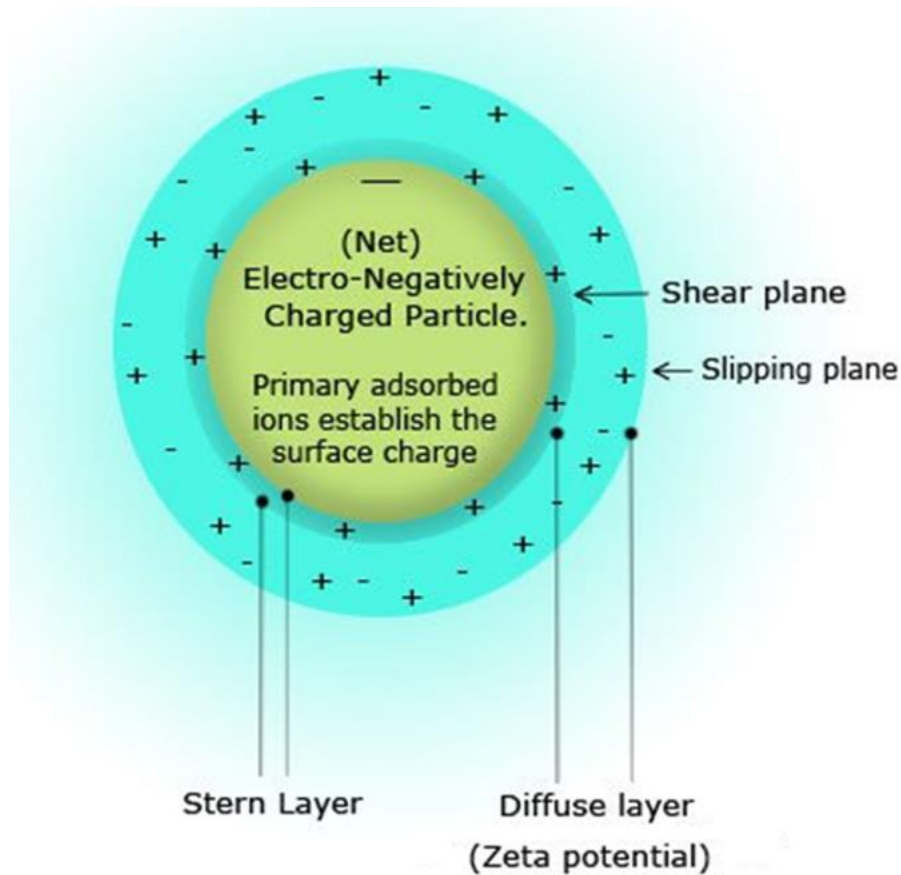
Figure 1.11. The structure of surface charged zeta potential of a nano-material. It was adapted from (Goctsch, 2006).

1.4 Characterization of nanoparticles and solid lipid nanoparticles

1.4.1 Direct Nanoprecipitation Method

Direct nanoprecipitation (D-Nano-Pr), also refers to as the solvent displacement method is a modified process employed in the preparation of nano-size core-shell particulates (Figure 2.12) with increased dispersion stability in aqueous phase medium (Huang, Yu and Ru, 2010). Nano-encapsulation of chemical agents and food ingredients by the D-Nano-Pr method has been rapidly expanding in the pharmaceutical and food industries (Chen, Remondetto and Subirade, 2006; Alexis, et al., 2008). The D-Nano-Pr method is a cost-effect technology used to be entrapped

46

small particles of core materials incorporated or bounded within the polymeric materials to form nano-spheres, or capsules (Fessi, et al., 1989).

The potential application of D-Nano-Pr method is to protect hydrophobic chemical compound such as DSF and enable controlled release at the targeted sites (Alexis, et al., 2008). The D-Nano-Pr method involves the spontaneous interaction of supersaturated solutions of the lipid and aqueous phases to form colloidal systems (Fessi, et al., 1989). When the lipid phase dissolving polymeric materials and the hydrophobic drug is in contact with the polar solvent such as water (aqueous phase), the organic solvent rapidly diffuses allowing the polymeric encapsulation of the drug to form nanoparticle (Fessi, et al., 1989; Shegokar and Müller, 2010). This phenomenon, leading to the formation of nanometric colloidal particles, might be dependent on pH, the molecular weight of the polymers, ionic strength, polymeric concentration and other physiochemical factors related to the loaded drug and both solvents (Govender, et al., 1999; Augustin and Sanguansri, 2009).

The advantages of D-Nano-Pr method are; (i) nanoparticles show high stability against degradation, (ii) increased encapsulation efficiency and (iii) nanoparticles maintain sustained release with increased cellular uptake (Ribeiro, et al., 2008). For instance, the development of PTX-loaded PLGA NPs by using the D-Nano-Pr method exhibited *in vitro* controlled release of PTX. It resulted in a high cytotoxicity effect on human small cell lung cancer (NCI-H69 SCLC) (Fonseca, Simoes and Gaspar, 2002). Likewise, the fabrication of curcumin-loaded PLGA by D-Nano-Pr method resulted in high induced-apoptotic effect in cisplatin-resistant A2780CP ovarian and metastatic MDA-MB-231 breast cancer cells (Yallapu, et al., 2010).
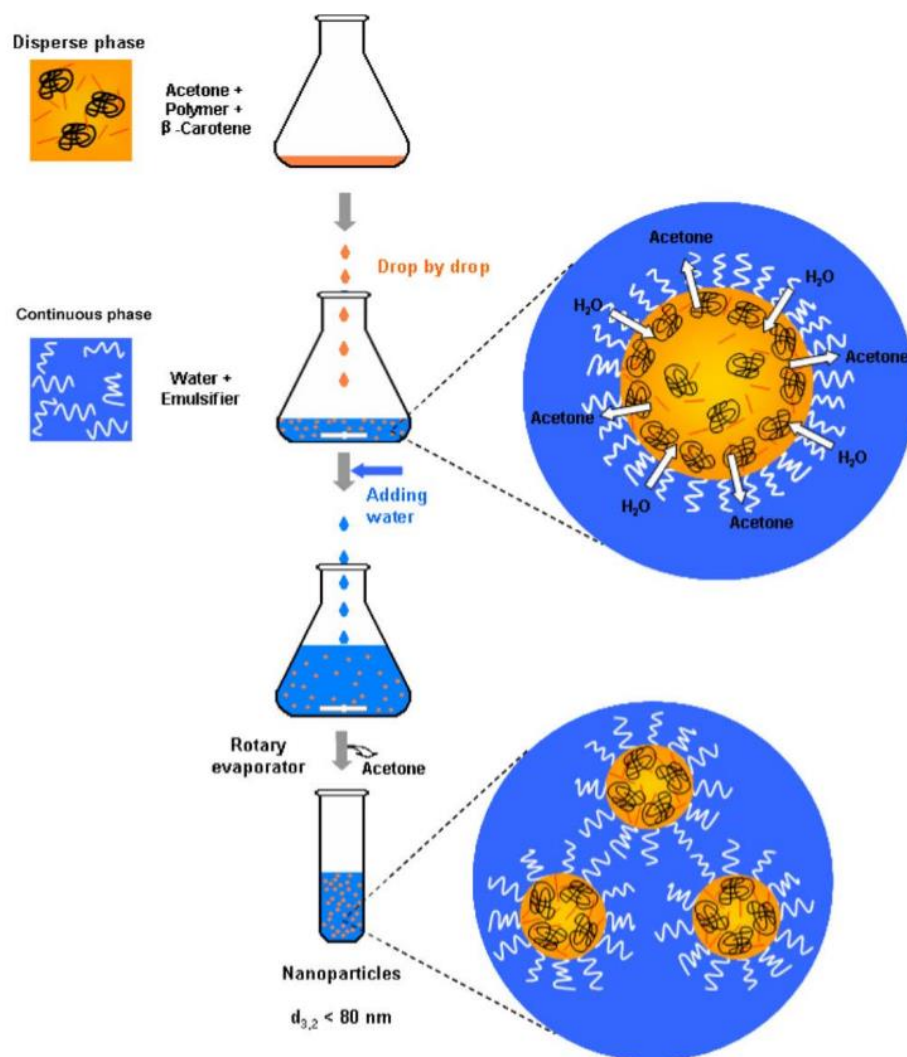
Figure 1.12. The spontaneous formation of a nanoparticle demonstrated by direct nanoprecipitation (D-Nano-Pr) or single emulsion solvent evaporation (SE) methods. It was adapted from (Ribeiro, et al., 2008).

1.4.2 Single emulsion/solvent evaporation method

Single emulsion/solvent evaporation (SE) method is most widely used in the preparation of encapsulated active agents with polymeric materials or phospholipids dissolved in an organic solvent to form nanocapsules, or nano-spheres (Figure 2.13), or solid lipid nanoparticles (Sanguansri and Augustin, 2006). The organic phase droplets are emulsified with the aqueous phase consisting of a stabilizer, such as PVA (Vandervoort and Ludwig, 2002), and after sonication to form nano-sized particles the

suspension is stirred to evaporate the organic solvent leaving nanoparticles in suspension (Moinard-Chécot, et al., 2008).

Furthermore, the SE method proved successful in the preparation of NPs and nanoemulsion (Moinard-Chécot, et al., 2008; Teo, et al., 2017). Due to the high-energy force employed by HPH to form emulsified nano-suspensions, SE method can be used in the preparation and development of nanoemulsion-based delivery systems (Silva, et al., 2011).
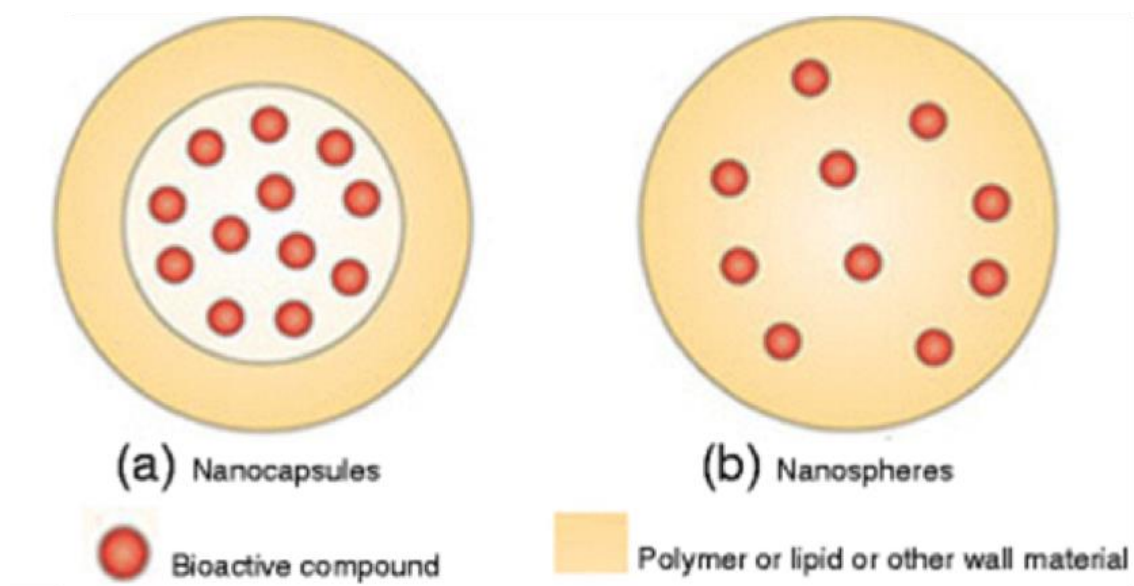
Figure 1.13. A schematic representation of (a) nanocapsules and (b) nano-spheres. It was adapted from (Orive, et al., 2009).

1.4.3 High-pressure homogenisation technique

High-pressure homogenization (HPH) technique is an efficient, non-contaminant process with high energy densities required to produce fine nanoemulsion particles using high-pressure up to 45,000 psi (Fathi, Mozafari and Mohebbi, 2012). The high-pressure energy forces apply high shear stress on the sample after feeding emulsion or suspension through narrow reactors into the collision chamber. Thus, the high-pressure reduces the sizes down to nanometer range emulsion particles collected via

an outlet chamber or container (Figure 2.14) (Fathi, Mozafari and Mohebbi, 2012). Using the HPH technique, particle sizes can be reduced at a higher temperature (hot homogenization) or room temperature (cold homogenization) (Müller, Mäder and Gohla, 2000). Previous studies have shown high physical stability of the nanoemulsions homogenized at homogenization of three to four cycles at a lower temperature (cold homogenization) (Yuan, et al., 2008). Also, the droplet sizes decrease with increased homogenization pressure, cycle and/or temperature less than 50 °C (Yuan, et al., 2008). Published articles have demonstrated that HPH technique can produce smaller droplet sizes compared to high-speed homogenization technique which is an impeller (rotor) and a stator made up of stainless steel driven by a high-voltage motor (Shirgaonkar, Lothe and Pandit, 1998)(Wang, et al., 2008).
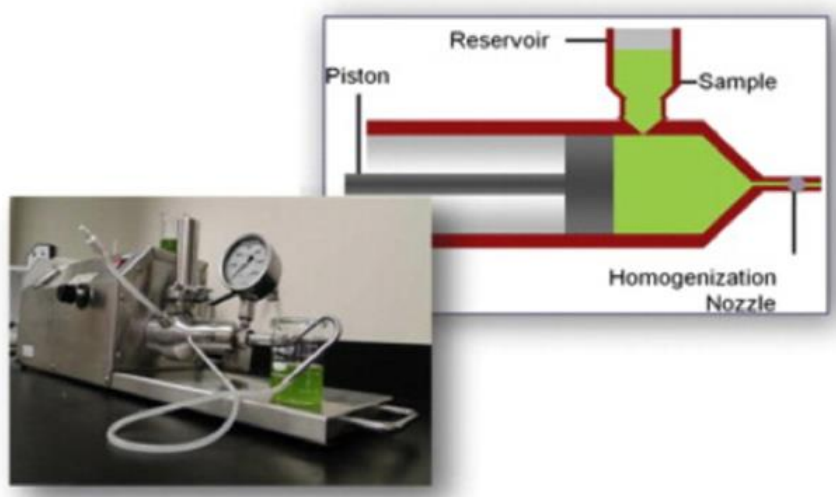
Figure 1.14. High-pressure homogenizer demonstrating sample feeding. It was adapted from (Samarasinghe, et al., 2012).

1.4.4 Probe sonication technique

Probe sonication technique or high power ultrasound referred to as sound waves frequency up to 20 kHz used to disrupt large structural nanoemulsion particles through the high shear forces generated during ultrasonication (Chen, Remondetto and Subirade, 2006). In the year 1927, the first ultrasound device was produced to improve

the production of chemical reaction rates by Richard, (Richards and Loomis, 1927). Presently, the ultrasound technique has been widely used in the production of various fields of chemical engineering, material science, the food industry and the different fields of chemistry (Suslick and Price, 1999; Jambrak, et al., 2008). Ultrasound has been widely used in various areas in the food industry as a non-destructive green technology for food processing (Jambrak, et al., 2008; Awad, et al., 2012). Ultrasonication is the process whereby ultrasound energy is employed to achieve nanoparticle dispersion for various purposes (Bang and Suslick, 2010). Ultrasonication provides sufficient energy to reduce droplet-size of emulsion particles in the presence of surfactant to nanometric-scaled (Figure 2.15) (Behrend, Ax and Schubert, 2000). Therefore, sonication has been considered as the most widely used to manufactured nano-emulsions and nanoparticles in the research field of drug delivery of nano-carrier systems (Samer and Schork, 1999).
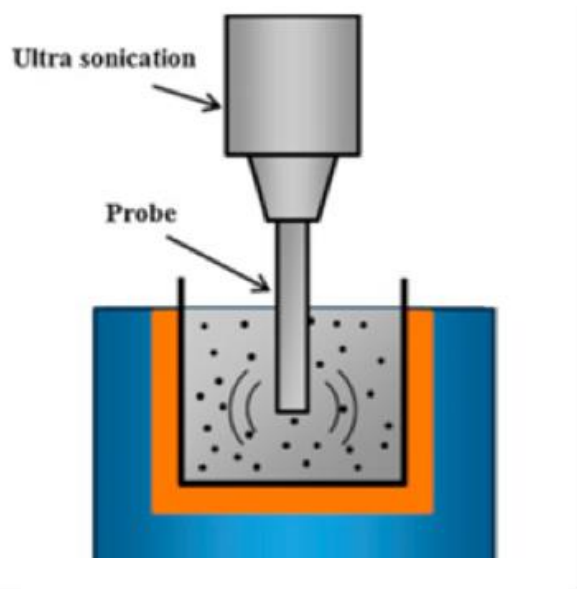
Figure 1.15. A schematic diagram of probe ultrasound. It was adapted from (Park, et al., 2014).

1.4.5 Freeze drying technique

Freeze-drying, also known as lyophilisation, refers to a stepwise process involving the dehydration of the water trapped from the manufactured heat-sensitive materials such as polymers (Anandharamakrishnan, Rielly and Stapley, 2010). Also, freeze-drying is a technique used to separate the encapsulated nanoparticles by removing water from the nanoparticle samples (Anandharamakrishnan, Rielly and Stapley, 2010). The technique is operated by multiple stages for stabilising materials in a stepwise process from solid to sublimation known as the primary drying, then followed by desorption step which is the secondary drying and the last step is storage (Figure 2.16), (Anandharamakrishnan, Rielly and Stapley, 2010).

The freeze-drying technique can produce high quality and stable (have extended shelf lives) products ready to be reconstituted in a suspension or solution (Singh and Heldman, 2001). During the freeze-drying process, pores are formed as the entrapped water that transformed into ice sublimes from solid to vapour. This may cause the nanoparticles to collapsed, allowing the uncontrolled release of the encapsulated active agent (Anandharamakrishnan, Rielly and Stapley, 2010). Therefore, to avoid the deformations the particle surface suitable frozen temperature is selected to maintain the physical stability of the materials before freeze-drying (Anandharamakrishnan, Rielly and Stapley, 2010). Besides, a cryoprotectant such as sucrose or trehalose plays an essential role by stabilizing samples, such as nanosuspensions, during freezing. The cryoprotectant prevents samples from freezing stresses (nanosuspensions concentration may enhance the interaction of particulates leading to aggregation or fusion), such as low freezing temperature which allows proper re-dispersibility (Kesisoglou, Panmai and Wu, 2007). Previous studies have demonstrated sucrose as a better and effective cryoprotectant in the conversion of

liquid containing semisolids samples with poor dissolution to a fast-dissolving solid sample (Van Eerdenbrugh, et al., 2007).
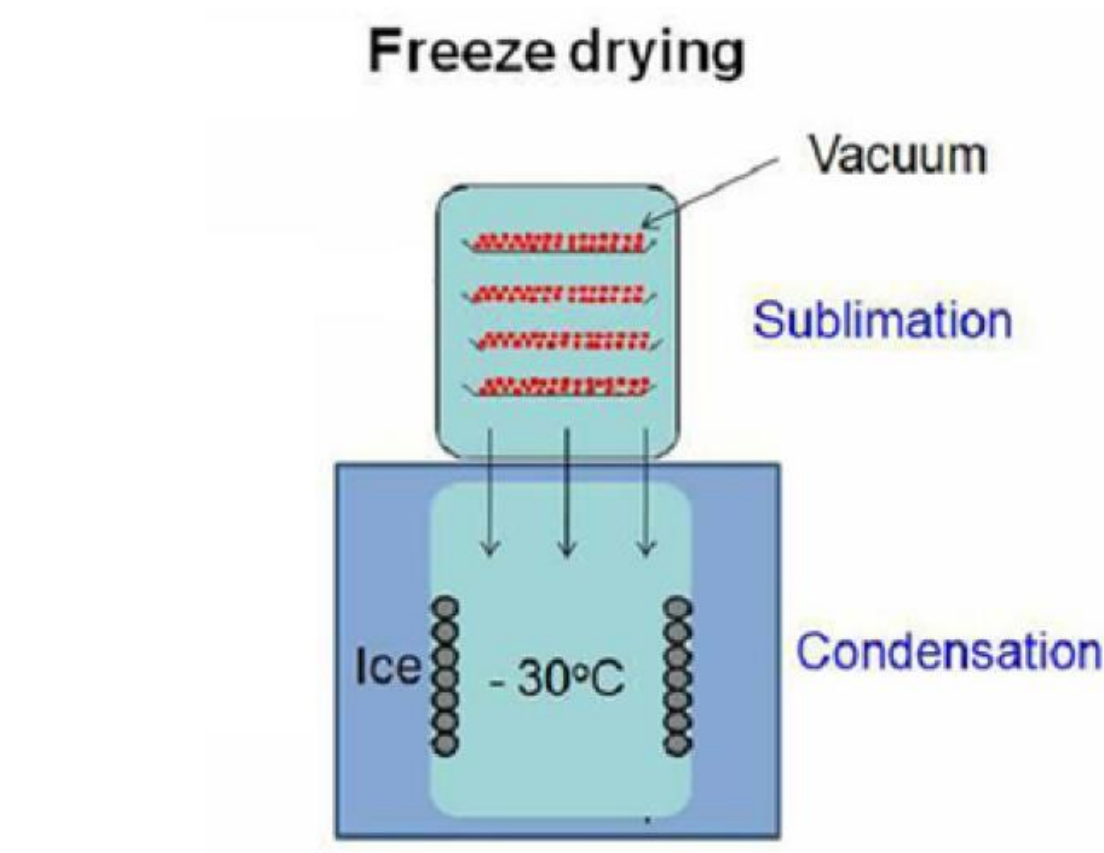
Freeze drying

Figure 1.16. A schematic diagram of a freeze-drying device. It was adapted from (Kasvayee, 2011).

1.4.6 Sucrose cryoprotectant in lyophilization of PLGA nanoparticles and solid lipid nanoparticles

Sucrose cryoprotectant is widely used for the benefit of lyophilization of therapeutic proteins used as drugs for the treatment of specific pathological conditions such as multiple sclerosis, diabetes, and cancer (Danhier et al., 2012). Previous studies have shown the non-use of cryoprotectant resulted to the instability of PLGA NPs stored in an aqueous condition because of the polymeric material containing hydrolytically unstable polyesters group when in water-mediated can activate hydrolysis (Konan et al., 2002; Allison et al.,1999).

The novel approach use of a cryoprotectant such as sucrose for particulates lyophilization process provides benefit for the long-term storage of NPs/SLNs to maintain stabilization while still viable in the treatment of cancer. The lyophilization of NPs/SLNs formulations mostly can be done in an amorphous phase below the cryoprotectant glass transition temperature (T_g) for an effective rate of diffusion-controlled reactions to lower aggregation of particulates by hydrogen bonding formed after the removal of ice or water during the lyophilization step (Allison et al., 1999). Also, the use of surfactants as stabilizers demonstrated the formation of aggregation of NPs in solution during storage (De Jaeghere et al., 1999). Therefore, it is essential to use cryoprotectant such as sucrose as a better approach for the stabilization of loaded NPs/SLNs to maintain the ability of *in vitro* DSF sustained release, stability in horse serum, and while remaining active against the treatment of breast cancer cells.

The externally added amorphous cryoprotectant, such as sorbitol, glucose, fructose, and sucrose have less influence on the particle size and zeta potential of NPs/SLNs. Instead, sucrose cryoprotectant enhanced the lyophilization step for more stable NPs/SLNs, and the SEM images showed successful colloidal particles exhibiting spherical shape and smooth surface.

 As previously reported from kinds of literature, this study used a lower concentration of 1% (w/v) solution sucrose cryoprotectant to lyophilize samples for the stabilization of DSF-loaded and unloaded NPs/SLNs. NPs/SLNs containing sucrose tends to be more stable at −80 °C for three hours storage before lyophilization process. This agrees with Van et al., (2015), results of

cyclohehexanone monooxygenase (CHMO) a model enzyme used to determine suitable freeze-drying conditions to maintain stability for the long-term storage of the isolated CHMO. Their findings suggested that in the presence of a low concentration of sucrose cryoprotectant, CHMO was more stable when stored at −80 °C than 4 °C before lyophilization.

The data confirms the shift in T_g of the NPs/SLNs lyophilized with sucrose cryoprotectant compared with the standards and maintaining drug-polymer interaction by the DSC, and FTIR, respectively, which demonstrates the ability of sucrose to stabilize the PLGA encapsulated DSF during lyophilization. This also indicates that the concentration of sucrose may have played a critical role in the stabilization of NPs/SLNs at 4 °C after the lyophilization step.

1.4.7 Differential scanning calorimetry

Differential scanning calorimetry (DSC) is a technique that has been widely used to investigate the thermal properties of biological macromolecules and chemical substances by undergoing phase transitions and conformational differences (Hinz and Schwarz, 2001). DSC and differential thermal analysers (DTA) are the two types of thermal analysis devices commercially available and both provide quantitative information relating to exothermic, endothermic and heat capacity differences as a function of temperature and time, which include melting, purity and glass transition temperature (Turi, 2012). DTA is used in measuring temperature differences, whereas, DSC is employed to measure energy differences between a sample and a reference material as the function of a pre-programmed temperature cycle (Figure 2.17) (Turi, 2012).

DSC is capable of measuring the excess heat capacity (Cp) of a substance by providing the thermodynamic and kinetic data of the analysed molecule as the function

of temperature peak (Celej, Montich and Fidelio, 2003). The Cp transition can be observed through a sharp endothermic peak where at the height of the temperature midpoint (T_m) is recognised as the maximum in Cp (Robertson and Murphy, 1997). The technique is based on the application of the heating and cooling process to a small amount of sample then simultaneously measures the temperature and enthalpy changes including thermal events of melting and polymorphic transformation (Vitez, et al., 2007). The sample thermocouple is employed to control the furnace temperature using suitable software. As the sample temperature increases linearly to the reference, the thermal peak is plotted between the sample and against reference temperature (Wunderlich, et al., 1998).

The popularity of DSC technique is due to its accuracy, simplicity, rapidity of measurement and the use of low sample size to obtain detailed information of the product stability at an early stage of the development of nano-carriers delivery systems or drug discovery and development (Clas, Dalton and Hancock, 1999; Chiu and Prenner, 2011). Thermal analysis technique considered as one of the established solid states pharmaceutical products for characterisation and determination of polymorphism (Barnes, Hardy and Lever, 1993; Demetzos, 2008).

The basic characteristic feature of the crystalline solid state is commonly described as the relative ordered arrangement of an atom, molecule or ion (Wunderlich, et al., 1998; Lu, Weng and Cao, 2006). While the non-crystalline solid has a very low ordered arrangement composed of complex molecules or ions are cooled rapidly to form a glass (Wunderlich, et al., 1998). Therefore, the transition of a substance from its rigid glassy state to a relaxing flexible state is called glass transition temperature (T_g); it is an important area covered by DSC especially when polymers are involved (Wendlandt, 1986; Wunderlich, et al., 1998).
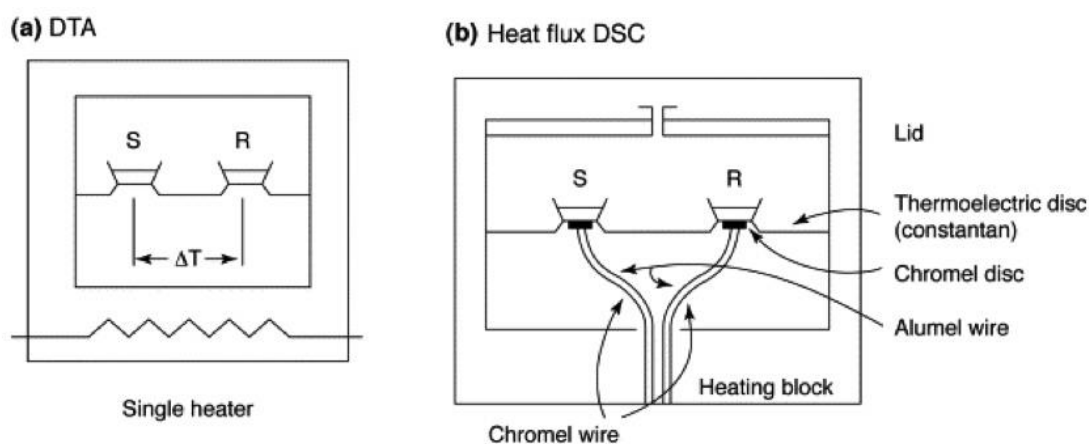
Figure 1.17. Schematic diagrams of (a) differential thermal analysis (DTA), and (b) heat-flux differential scanning calorimetry (DSC). It was adapted from (Wendlandt, 1986).

1.4.8 Fourier transform infrared spectroscopy

Fourier transform infrared spectroscopy (FTIR) is a convenient and less sample preparation technique used to analyse fundamental information of the molecular structure of organic and inorganic components (Parikh and Chorover, 2005; Smith, 2011). FTIR is a widely used analytical technique for chemical characterisation of geological samples (coal, microfossils and minerals) and bio-macromolecules (Lis, et al., 2005; Johnson, 2006; O'Keefe, et al., 2013). For the past four decades, IR spectrometry has changed dramatically from the structural elucidation of organic compounds to a more robust and rapid with reduced measurement times from minutes to less than a microsecond (Wang, et al., 2008). The basic principle of FTIR analytical technique is due to the analysis of the absorption of IR radiation by a molecule excited a photon to a higher quantized vibrational energy state (Figure 2.18) (Griffiths and De Haseth, 2007). During the exciting state transition, the absorbance of molecular vibration is specific to functional groups, e.g. C-H, O-H, S-H and C=O vibrational bands (Griffiths and De Haseth, 2007; Smith, 2011).

57

The number of waves scanned of each IR absorbance peak has been determined by the intrinsic physicochemical properties of the compound of interest, and it is a fingerprint of the vibrational molecular bonds exhibited by stretching, bending, twisting, rocking, wagging and out-of-plane deformation (Smith, 2011).

FTIR with a diamond cell is typical benchtop spectrometer whereby the IR radiation causes to split into two beams, forming the constructive and destructive beam which in turn produces a waveform as the sample selectively absorb radiation at specific wavelengths from 4000 to 400 cm^{-1} (Mukhopadhyay, 2004; Griffiths and De Haseth, 2007). The resulting radiation is received via a detector and channel through a fast FT that generates a characteristic spectrum of the sample of interest (Mukhopadhyay, 2004). IR spectroscopy cannot perform the Fourier transform algorithm on the received data at the detector compared to the FTIR which performs the Fourier transform from the data, and then generate a frequency domain of data obtained (Poletto, Zattera and Santana, 2012).
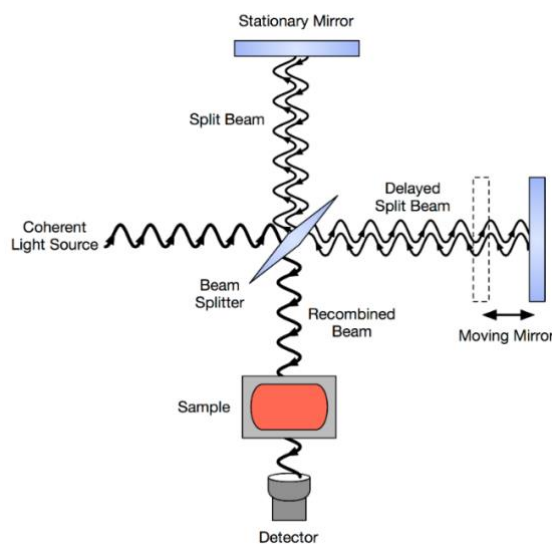
Figure 1.18. A schematic diagram of FTIR. It was adapted from (Wang, et al., 2007; Wang, et al., 2008).

1.5 Aims and objectives

1.5.1 Aims

1- This study aims to develop an *in vitro* evaluate nano-carrier systems to enhance biostability of encapsulated DSF and provide prospective long-time drug circulation without reducing DSF anti-cancer activity.

2- To develop long circulation DSF-loaded NPs/SLNs delivery systems coated with PEGylated polymers and phospholipid materials for efficient cancer therapy. The selection of $mPEG_{2k}$-PLGA and DSPE PEG_{2k} is to compare their ability to maintain sustainable drug release, increase half-life, and long circulation of the encapsulated DSF in the physiological condition of pH 7.4, horse serum, and the *in vitro* testing of breast cancer cells. Besides, selecting a lower PEG that contains PLA long chains (Mw, 2000) and using less PEG contents, thus decrease plasma protein adsorption and enhance cellular uptake of the DSF-loaded PEGylated NPs/SLNs in cancer cells.

3- To investigate encapsulated DSF anticancer activity on resistance paclitaxel (PTX) (an established anticancer drug) breast cancer cell (MDA-MB-231$_{PTX10}$).

1.5.2 Objectives

1- To develop and optimise methods and formulations for PEGylated DSF loaded PLGA NPs and SLNs.

2- To develop and optimise methods required in determining DSF encapsulation efficiency and stability in horse serum.

3- To manufacture formulations of NPs and SLNs prepared by D-Nano-Pr and single evaporation methods.

4- To perform a full characterisation of the formulated NPs and SLNs.

5- To assess the ability of the formulation to protect DSF form degradation in horse serum.

4- To evaluate the anticancer activity of the formulations *in vitro* using MTT cytotoxicity assay.

This study met its aims and objectives, and in support of the hypothesis that developed PEGylated NPs/SLNs can maintain long circulation and provide protection of the DSF to enhance cancer-targeting compared to the conventional chemotherapy. Also, improve the stability for DSF in horse serum. For the first time, this study has established methods to determine DSF encapsulation efficiency and stability of DSF in horse serum.

1.6 Hypothesis

The PEGylated PLGA NPs and PEGylated SLNs will be able to provide protection and long-circulating nano-carrier of DSF. This will enhance cancer targeting and improve drug disposition compared to conventional chemotherapy.

Chapter 2 Materials and Methods

2.1 Materials

2.1.1 Chemicals

2.1.1.1 Reagent grades

Tetraethylthiuram disulfide or disulfiram (DSF) (97% pure), poly ($_{D,L}$-lactide-co-glycolide acid) (PLGA) 50/50 lactide/glycolide polymer (MW 19,000 Da), Poly (ethylene glycol) (PEG$_{2k}$) methyl ether-block-poly (lactide-co-glycolide) polymer (MW 11,500 Da), Tween 80 and Dimethyl sulfoxide (DMSO) (99.7%) were purchased from Acros Organics, UK. Diethyldithiocarbamate-copper (DDC-Cu) (97% pure) was purchased from China. Polycaprolactone (PCL) polymer (molecular weight, 70,000 g/mol) was purchased from Corbiob purac. Hydrogenated Phosphatidylcholine from Soybean (HPCS), purchased from LIPOID GMBH. Poloxamer 188 was purchased from SIGMA, UK. Sucrose, Dialysis tubing (3500 MWCO), Acetone, Methanol, Ethanol, Dichloromethane (DCM), Methanol (HPLC grade) and purewater (HPLC grade) were obtained from Fisher Scientific UK. Horse Serum was purchased from gibco, New Zealand. Compritol 888 ATO (Glycerol Dibehenate), Precirol ATO-5 (Glycerol Distearate-Type I) were purchased from GATTEFOSSE (UK) LTD. 1,2-distearoyl-sn-glycero-3-phosphoethanolamine-N-[Maleimide(polyethylene glycol)-2000] (DSPE-PEG$_{2000}$) was purchased from SIGMA, UK. All other reagents were of pharmaceutical grade and used as received.

2.1.1.2 Cell culture reagents

MDA-MB 231, MDA-MB 231 paclitaxel (PTX) resistance (10 nM), and MCF-7 cell lines were generously provided by Prof. W. Wang (The University of Wolverhampton, Wolverhampton, UK). Growth media for cell culture, Dulbecco's Modified Eagle's Medium (DMEM), high glucose (stored at 4 °C), fatal bovine serum (FBS) heat-inactive, 100 units/ml of penicillin and 100 ug/ml of streptomycin solution with Trypsin

Ethylenediamine-tetraacetic acid 0.25% (EDTA) were purchased from Gibco™ (Fisher Scientific, UK) and stored at -20 °C. 3-(4, 5-dimethylthiazol-2-yl)-2, 5-diphenyl tetrazolium bromide (MTT) was purchased from SIGMA, UK and stored at 4 °C. Phosphate-buffered Saline (PBS) was obtained from Fisher Scientific UK. PBS 10x (10 ml) in sterile water (90 ml) was subsequently autoclaved and stored at room temperature. Sterilised EasyFlasks with polystyrene filter cap (25 and 75 cm^2), 96-well cell culture plate (flat-bottomed) and sterile petri dishes were purchased from Fisher Scientific, UK. All other reagents were of pharmaceutical grade and used as received.

2.2 Methods

2.2.1 Direct-nanoprecipitation method

Two different sets of formulations of (1) PLGA (blank), disulfiram (DSF)-loaded PLGA and DSF-loaded PLGA PEGylated nanoparticles (NPs), and (2) solid lipid nanoparticles (SLNs) (blank) and DSF SLNs were prepared by the direct nanoprecipitation (D-Nano-Pr) method as shown in Figure 2.1.

2.2.1.1 Preparation of non-PEGlated and PEGylated disulfiram-loaded poly lactide-co-glycolide acid nanoparticles by direct nanoprecipitation method

Set (1) NPs were prepared in different organic solvents (acetone and acetone/methanol) and volume (3 and 6ml) using D-Nano-Pr method, Figure 2.1. Table 2.1 shows the mixed ratios of five different loaded PLGA NPs formulations (DNP1-5), including the blank (DNP1E-5E) NPs. The ratio 1:9 between drug and polymer or phospholipid material was selected purposely to investigate the effect of DSF at a lower ratio. As part of the method development using a low ratio of the active ingredient such as DSF worked out the best in this study. In the method development, the 1:9 ratio of DSF to polymer/phospholipid achieved satisfactory results in the determination

of percentage encapsulation efficiency, and stability experiments. The 1:9 ratio of DSF to polymer/phospholipid was used in all formations of NPs and SLNs.

Table 2.1. Different formulation ratios of disulfiram (DSF) loaded PLGA with polycaprolactone (PCL), and PEGylated nanoparticles were manufactured by direct nanoprecipitation (D-Nano-Pr) method.

Ingredient (ratio) / Formulation*	PLGA	PCL	mPEG$_{2k}$-PLGA	DSPE PEG2k	DSF	Total
DNP1E	10	-	-	-	-	10
DNP1	9	-	-	-	1	10
DNP2E	9.5	-	0.5	-	-	10
DNP2	8.5	-	0.5	-	1	10
DNP3E	9.5	-	-	0.5	-	10
DNP3	8.5	-	-	0.5	1	10
DNP4E	4.5	4.5	0.5	-	-	10
DNP4	4.25	4.25	0.5	-	1	10
DNP5E	5	5	-	-	-	10
DNP5	4.5	4.5	-	-	1	10

*DNP represents nanoparticles (NPs) of different formulations prepared by direct nanoprecipitation (D-Nano-Pr) method. E denotes the empty NPs of different formulations.

The ratio used between DSF to polymer/phospholipid material was the 1:9 in a total weight of 300 mg. The polymers (270 mg) and drug (DSF, 30 mg) were dissolved in 6 ml of acetone and methanol in a ratio 3:1(organic phase), respectively. In a fume-hood, the glass vials were heated in a water bath at 60 °C with continuous stirring at 200 rpm for three minutes to dissolve the polymers and drug. Five labelled conical flasks (DNP1-5 or DNP1E-5E) containing 24 ml ultrapure water (aqueous phase) were placed on a magnetic stirring plate at 60 °C to maintain the isothermal temperature with the organic phase. The organic phase of DNP1-5 or DNP1E-5Ewas added dropwise using a syringe (10 ml) and a needle (18G) into the aqueous phase under continuous stirring at 350 rpm for five minutes (Figure 2.1). The resulting suspension containing nano-formulated DSF-loaded PLGA (non-PEGylated) and PEGylated NPs were placed under the fume-hood to stir continuously for five hour to allow the organic solvents to

evaporate. A sample of 0.5 ml was taken from the aqueous suspensions to measure particle size, polydispersity index (PDI) and zeta potential. The aqueous suspensions were centrifuged at 11,952 g for 5 minutes. DSF NPs pellets were resuspended in 2 mL sucrose (1%) for lyophilization. The blanks were manufactured using similar steps as described above. All formulations were repeated three times.
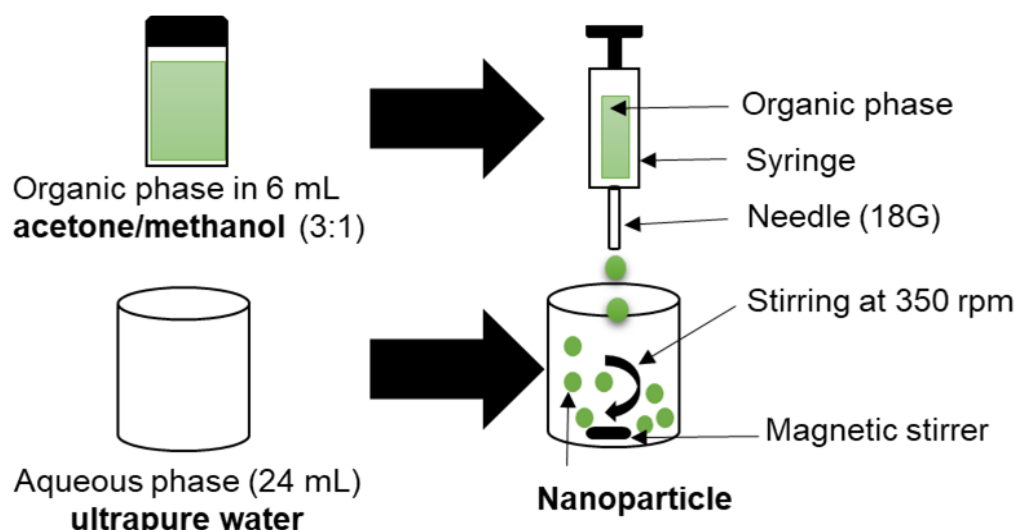
Figure 2.1. Formulations of blanks, DSF-loaded PLGA and PEGylated nanoparticles (NPs) were prepared by using the D-Nano-Pr method.

2.2.1.2 Preparation of disulfiram-loaded solid lipid nanoparticles by direct nanoprecipitation method

Set 2, DSN1 and DSN1E were prepared using the D-Nano-Pr method followed by the hot homogenisation technique (Figure 2.2). Table 2.2 shows adjustable mixed ratios between DSF and phospholipids (1:9). The DSF and phospholipids were dissolved in 6 mL acetone (lipid phase). The aqueous phase consists of 54 ml of ultra-pure water. The lipid and aqueous phase were immersed in a hot water bath (80 °C). At isothermal temperature (80 °C), the lipid phase was added dropwise into the aqueous phase using a syringe (10 mL) and a needle (18G). Simultaneously, the dropwise lipid phase and

65

aqueous phase mixture were homogenised at 20,000 energy force, for 10 minutes using a T18 ULTRA-TURRAX (IKA®) homogenizer (Figure 2.2).

Table 2. 2. Formulation ratios of disulfiram (DSF) loaded solid lipid nanoparticles manufactured by direct nanoprecipitation (D-Nano-Pr) method using high-speed homogenization technique.

Ingredient (ratio) Formulation*	Preciprol	Compritol	Hydrogenated Phosphatidylcholine from soybean (HPCS)	DSF	Total
DSN1E	6.5	2.5	1	-	10
DSN1	5.5	2.5	1	1	10

*DSN represents solid lipid nanoparticles (SLNs) formulations prepared by direct nanoprecipitation (D-Nano-Pr) method using high speed homogenization technique. E denotes the empty SLNs formulation.

Figure 2.2. Formulations of solid lipid nanoparticles (DSNs) were prepared under hot homogenisation by using the
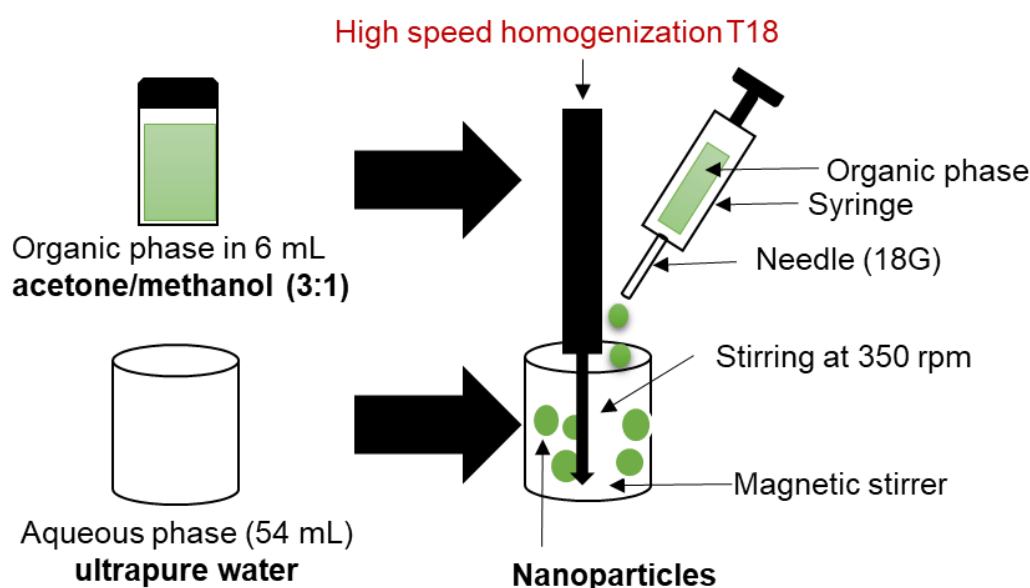
D-Nano-Pr method.

The resulting product of DSN1 and DSN1E SLNs were placed on a magnetic stirrer in a fume-hood to continuously stir at 350 rpm for five hour to allow acetone evaporation from the aqueous suspension solution. A sample of 0.5 ml was taken for characterization, as described in section 2.2.3. The aqueous suspension was centrifuged at 11,952 g for 5 min (1x) and pellets re-suspended in 2 mL sucrose (1%) ready for lyophilisation. All formulations were repeated three times.

2.2.2 Single emulsion/solvent evaporation method

The formulations of two different sets (1) blank and DSF-loaded PLGA NPs, and (2) blanks (DPS1E, DSN1E and PEGylated DSN1aE/DSN1bE) NPs/SLNs, DSF-loaded DPS1, DSN1 and PEGylated DSN1a/DSN1b NPs/SLNs were prepared by single emulsion/solvent evaporation (SE) method. Particle sizes were reduced using two different techniques; probe sonication (PS) and high-pressure homogenisation (HPH).

2.2.2.1 Preparation of disulfiram-loaded poly lactide-co-glycolide acid nanoparticles by single emulsion/solvent evaporation method

Set (1) formulations of NPs were prepared by SE method, and particle size reduction was performed by PS technique for two different periods (to investigate the sonication time between 5 and 8 minutes) (Figure 2.3). Set (2) NPs formulations were prepared by using the SE method and particle sizes were reduced by the PS (Figure 2.3) or HPH (Figure 2.4) techniques. Set (3) SLNs formulations were prepared by the SE method and particle sizes were reduced using the HPH technique (Figure 2.4).
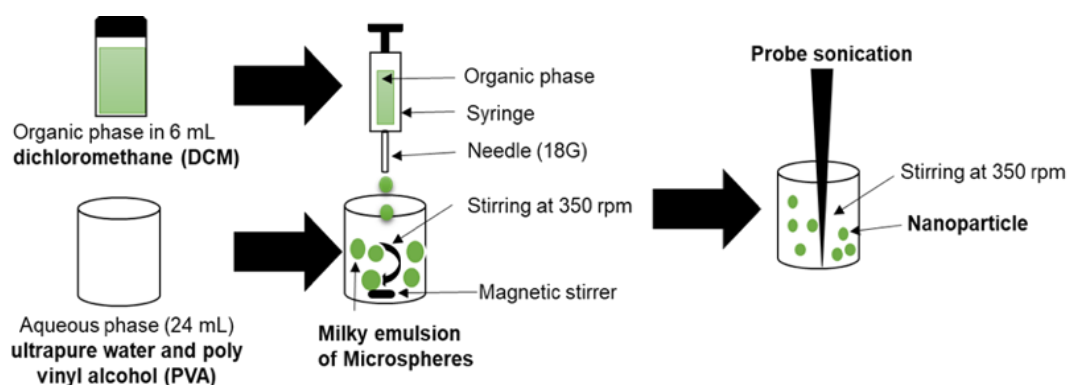
Figure 2.3. Formulations of blanks and DSF-loaded PLGA nanoparticles (NPs) were prepared by single emulsion/solvent evaporation (SE) method, and probe sonication (PS) technique was used to reduce particle size.

Set (1) formulations as described in Table 2.3, DPS1 and DPS1E, with a drug to polymer ratio 1:9, were prepared using oil-in-water (O/W) single emulsion/solvent evaporation (SE) method (Najlah, et al., 2017a). Size of the resulting particles was further reduced using PS technique (Figure 2.3). The labelled glass vials were used to weigh out 30 mg of DSF, and 270 mg of the PLGA were all dissolved in 6 mL dichloromethane (DCM) (organic phase). The aqueous phase consists of 54 mL of ultrapure water containing 100 mg of polyvinyl alcohol (PVA) as a surfactant. The organic phase was heated at 60 °C at a speed of 350 rpm on a magnetic stirring plate to dissolve the polymers and drug. The organic phase was added dropwise to the aqueous phase (Figure 2.3). The resulting formulations were left under fume cupboard for five hours of continuous stirring at 350 rpm to allow organic solvent evaporation. Manufactured samples were subjected to particle size reduction by using the PS technique (section 2.2.2.2) or HPH technique (section 2.2.2.4).

Table 2.3. Formulation ratios of disulfiram (DSF) loaded solid lipid nanoparticles manufactured by using the single emulsion/solvent evaporation (SE) method.

Ingredient (ratio) / Formulation*	PLGA	DSF	Total
DPS1E	10	-	10
DPS1	9	1	10

*DPS represent nanoparticles (NPs) formulations prepared by single emulsion/solvent evaporation (SE) method then particle sizes were reduced using the probe sonication (PS) and high-pressure homogenization techniques. E denotes the empty SLN formulation.

2.2.2.2 Particle size reduction by probe sonication

The NPs/SLNs particulates prepared by using the SE method were subjected to particle size reduction by PS technique or HPH technique, as shown in Figure 2.3 and 2.4, respectively. After been immersed in ice, NPs/SLNs samples were subject to PS (trace of titanium residue after sonication) for 5 min; in a 1-min-on-and-1-min-off cycle. A 0.5 ml of sample was taken from aqueous suspensions for characterizations as described in section 2.2.3. The aqueous suspensions were centrifuged three times at 11,952 for 5 minutes to wash PVA surfactant (or Poloxamer 188 in case of SLNs). NPs and SLNs pellets were re-suspended in 2 mL sucrose (1%) and ready for lyophilisation. All formulations were repeated three times.
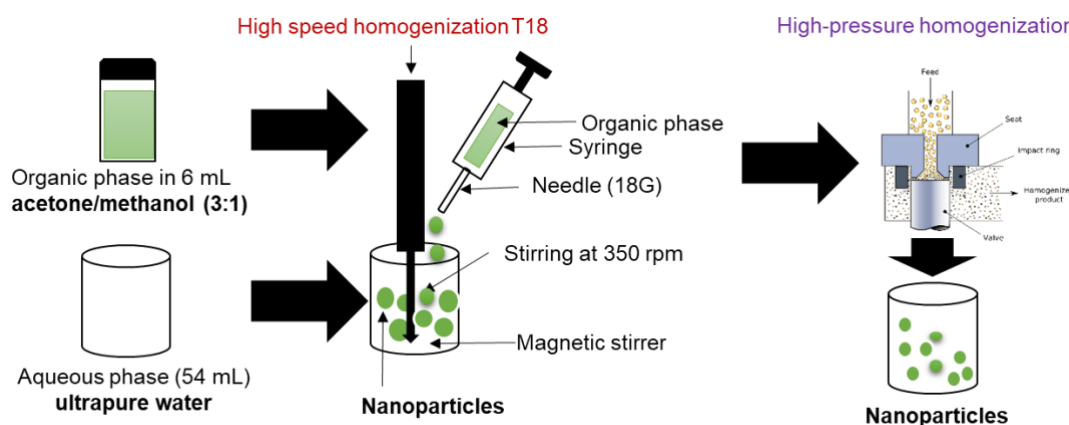
Figure 2.4. Formulations of blanks and DSF-loaded PLGA nanoparticles (NPs) were prepared by single emulsion/solvent evaporation (SE) method, and particle size reduction using high-pressure homogenisation (HPH) technique.

2.2.2.3 Preparation of disulfiram-loaded solid lipid nanoparticles by single emulsion/solvent evaporation method

Set 2, formulations of DSL1E/DSL1 SLNs and DSL2E/DSL2 SLNs nano-carrier systems were prepared by the SE method, as described in section 2.2.2.1 using adjustable ratios, as shown in Table 2.4. The particle size is reduced by the PS technique and HPH technique, respectively.

Table 2. 4. Formulation ratios of disulfiram (DSF) loaded solid lipid nanoparticles manufactured by single emulsion/solvent evaporation (SE) using high-speed homogenization technique.

Ingredient (ratio) Formulation*	PLGA	DSF	Total
DSL1E	10	-	10
DSL1	9	1	10

*DSL represents solid lipid nanoparticles (SLNs) formulations prepared by single emulsion/solvent evaporation (SE) method then particle sizes were reduced using probe sonication (PS) and high-pressure homogenization techniques. E denotes the empty SLN formulation.

Total weight of 300 mg was used to calculate the right amount of phospholipids and DSF. Phospholipids and DSF were dissolved in acetone (lipid phase). The aqueous phase has 5% Poloxamer 188 (surfactant) in 54 ml of ultrapure water (Figure 2.3).

The manufactured SLNs milky emulsions were placed in a fume-hood to cool for two hours. Samples were then stored overnight at 4 °C for next day ready for particle size reduction by the PS technique (as in section 2.2.2.2) or HPH technique(see section 2.2.2.4) as shown in Figure 2.4. All formulations were repeated three times.

2.2.2.4 Particle size reduction using high-pressure homogenization

Particle sizes of milky emulsions of blanks (NPs/SLNs), DSF loaded NPs/SLNs, and PEGylated NPs/SLNs were subjected to four cycles using the HPH (Deebee Nano, USA) technique (Figure 2.4). Particles were forced through a 0.2 mm narrow passage of seven reactors at 20,000-psi. Thereafter, nano-emulsions were placed on a magnetic stirring plate at 350 rpm in a fume-hood to stir for five hour for the organic solvents to evaporate. A sample of the resulting aqueous suspension (0.5 ml) was taken for characterizations of particle size and zeta potential, as described in sections 2.2.3.2 and 2.2.3.3, respectively. The aqueous suspension was centrifuged and washed with pure water three times as described in section 2.2.2.2. NPs and SLNs pellets were re-suspended in sucrose (1%) and ready for lyophilization. All formulations were repeated 3 times.

2.2.2.5 Preparation of disulfiram-loaded PEGylated solid lipid nanoparticles by single emulsion/solvent evaporation method

Set (3) formulations of blank mPEG$_{2k}$-PLGA (DSL1aE) SLNs, DSF-loaded mPEG$_{2k}$-PLGA (DSL1a) SLNs, PEG-DSPE blank (DSL1bE) SLNs and DSF-loaded PEG-DSPE (DSL1b) SLNs (Table 2.5) were prepared by SE method as described in section 2.2.2.2. Particle size in milky emulsions was reduced by the HPH technique (see Figure 2.4).

Table 2.5. Different formulation ratios of disulfiram (DSF) PEGylated loaded solid lipid nanoparticles (SLNs) manufactured by single emulsion/solvent evaporation (SE) method.

Ingredient (ratio) / Formulation*	Preciprol	Compritol	HPCS	mPEG$_{2k}$-PLGA	PEG$_{2k}$-DSPE	DSF	Total
DSL1aE	6.5	2.5	1	-	-	-	10
DSL1a	5	2.5	1	0.5	-	1	10
DSL1bE	6.5	2.5	1	-	-	-	10
DSL1b	5	2.5	1	-	0.5	1	10

*DSL(a & b) represents PEGylated solid lipid nanoparticles (PEG-SLNs) formulations prepared by single emulsion/solvent evaporation (SE) method, then particle sizes were reduced using probe sonication (PS) and high-pressure homogenization techniques. E denotes the empty SLN formulation.

2.2.3 Characterizations of nanoparticles and solid lipid nanoparticles

2.2.3.1 Scanning electron microscopy

Scanning electron microscopy (SEM) images of PLGA and PEGylated PLGA NPs freeze-dried samples were obtained through the Zeiss Evo50 electron microscope (Oxford instrument, UK). A small amount (approximately 10mg) of the freeze-dried powder was suspended in 1 ml purified water. Drops of the suspension were placed on the SEM disc and left to dry for under the fume cupboard for few hours. Before the images were taken, sample suspension surfaces were sputter-coated with gold. An accelerating voltage of 30 kV with the low-vacuum mode of the electron microscope was used to obtain fine SEM images.

2.2.3.2 Measurement of particle size and polydispersity index by zeta sizer

The particle size and polydispersity index (PDI) measurements of NPs and SLNs (including blanks) formulations were performed by applying Photon Correlation Spectrometry using the zeta sizer Nano series (Malvern Instruments Ltd, Malvern, UK.). With a single channel pipette, 10 µL of the aqueous suspension of each formulation was diluted in 990 µL ultrapure water. The zeta sizer software was used to determine the intensity percentage peak of particle size (Figure 2.5) and PDI by taken three readings for each measurement. The mean ± SD values obtained for the particle size and PDI were reported from three different experiments.
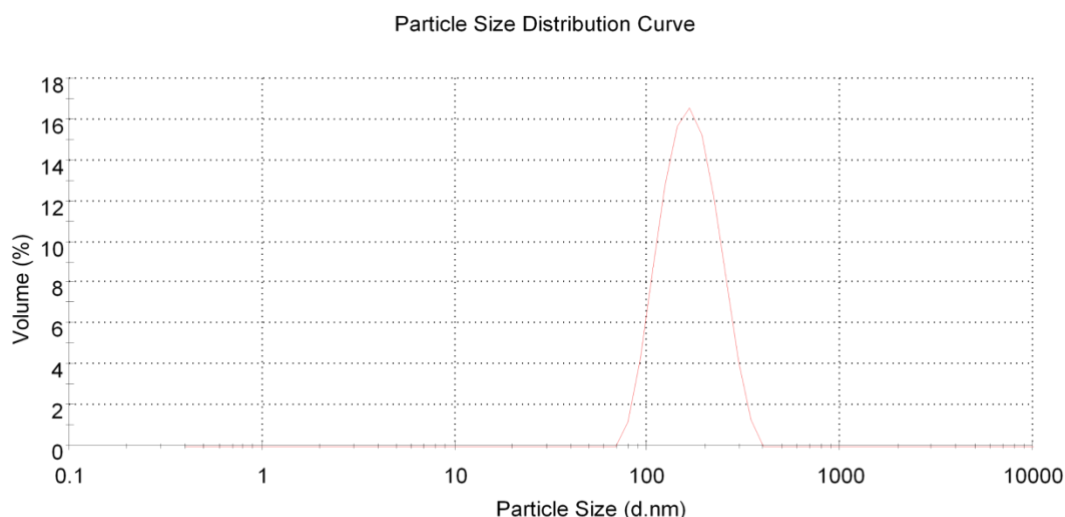
Figure 2.5. A representative diagram used to demonstrate the DSF NP particle size measurement by the zeta sizer software.

2.2.3.3 Zeta potential

Zeta potential measurements of NPs/SLNs and blanks were performed using Zeta sizer Nano series (Malvern Instruments Ltd, Malvern, UK.). A volume of 200 µL of samples in aqueous suspension of each formulation was added in 800-µL ultrapure water. The zeta potential measurement was taken after extracting 700 µL in a capillary

72

cell (Figure 2.6). The mean ± SD values of zeta potential were obtained from three different experiments.
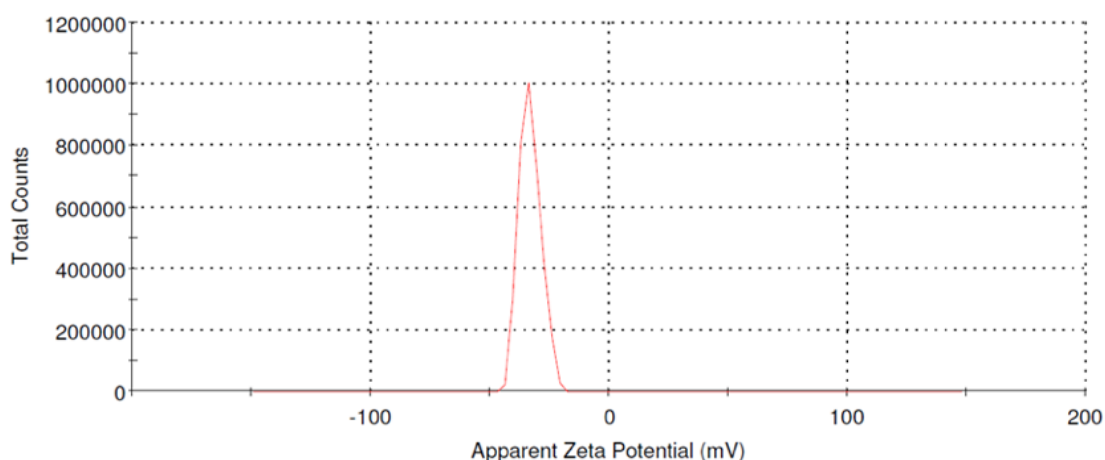
Figure 2.6. A representative diagram demonstrates the DSF-loaded NP zeta potential peak measured by using the zeta sizer software.

2.2.3.4 Freeze-drying

NPs/SLNs and blank pellets were re-suspended in a plastic tube (50 ml) containing 2 ml of 1% sucrose solution. The tube was sealed with a parafilm, and then the parafilm sealing was pierced with a needle, to allow lyophilization. Aqueous suspensions of NPs/SLNs were preconditioned to freeze in -21.0 $^{\circ}$C ± 0.5 $^{\circ}$C for two hours. The frozen NPs/SLNs were placed in -80.0 $^{\circ}$C ± 0.1 $^{\circ}$C overnight. The frozen NPs/SLNs were freeze-dried (LYOTAP, LTE Scientific LTD. UK) for 72 hours at -50 ± 1°C with a pressure 0.05 ± 0.04 millibar. Samples were stored at 4 $^{\circ}$C to maintain the optimum condition and are ready for further characterization.

2.2.3.5 Differential scanning calorimetry

The thermal analysis of freeze-dried NPs/SLNs and blank formulations and standards were performed using DSC. Freeze-dried samples and standards were weighed (3-5 mg) and added to spread the surface area of the aluminium pan. The aluminium pan was sealed using a manual hydraulic press, and the lid was pierced. Both sample and

reference (empty) aluminium pans were placed in the thermal chamber of the DSC. Samples were heated from room temperature to 350 °C (this range of temperature was selected due to PLGA having a higher melting point) at a rate of 10°/min under an atmosphere of nitrogen at a flow rate of 40 ml/min.

2.2.3.6 Fourier transform infrared spectroscopy

FTIR analysis was performed on NPs/SLNs (including empty NPs and SLNs) and standards using a Nicolet IS5, FTIR (FTIR, Thermo Scientific, UK). A small amount of each lyophilized samples and standards powder was placed on the diamond-tipped surface for scanning spectral at 7800-350 cm^{-1}. Each sample was measured up to 16 scans and saved in transmission mode at room temperature.

2.2.3.7 High-performance liquid chromatography

DSF was analysed using the Ultimate High-Performance Liquid Chromatography (UHPLC) (Dionex Ultimate 3000, Thermo Scientific, Germany). Methods were followed as reported by Najlah et al 2017; the UHPLC system equipped with a BetaBasic C-18 4.6 x 150 mm (reverse phase column) of 5-µM particle size. The mobile phase consisted of water-methanol HPLC grade in a ratio 20:80. The injection volume and flow rate used was 20µl and 1.0 mL/min, respectively. The UV detection wavelength of DSF was set at 275 nm. The standard range of detection for the method was from 0.2 mg/L to 20 mg/L. NPs and SLNs formulations data were collected, DSF concentrations were extrapolated using standard calibration curves.

2.2.3.8 Calibration curve of disulfiram using high-performance liquid chromatography method

A stock solution was prepared by dissolving 5 mg of DSF standard (free drug) in 5 ml Methanol (1mg/ml). Several dilutions of DSF were prepared using equation 1 from 0.2 mg/L to 20 mg/L.

$$C1 \ X \ V1 = C2 \ X \ V2 \hspace{4cm} Equation \ 1$$

C1 = Initial concentration

V1 = Initial volume

C2 = Final concentration

V2 = Final volume

DSF calibration standards were carried out as described in section 2.2.3.7 with the calibration curve plotted after the absorbance values obtained, and the R^2 including the calibration curve equation was obtained from the graph (Figure 2.7). DSF demonstrated a retention time of 3.865 minutes, as shown in Figure 2.8. The calibration standards were repeated three times.
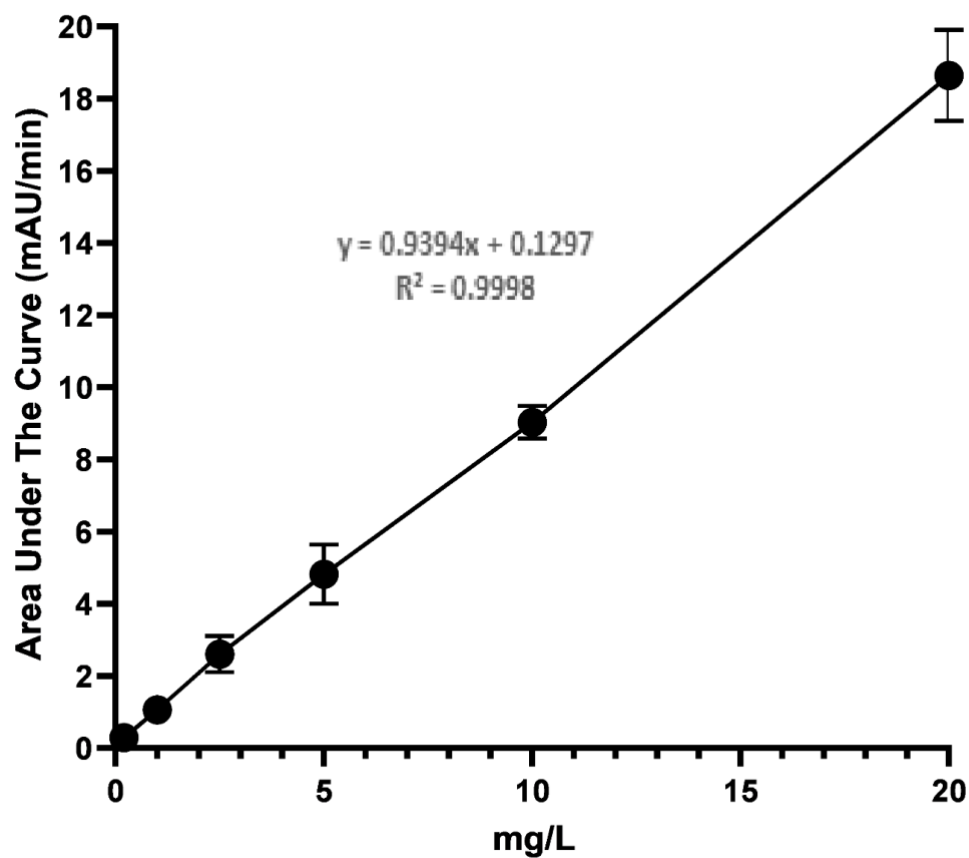
Figure 2.7.The DSF calibration curve indicates the extrapolated equation, mean ± SD (3).
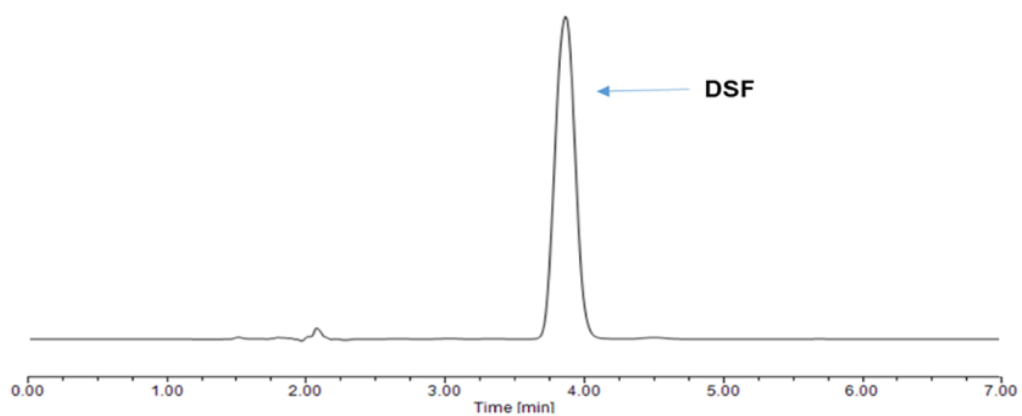
Figure 2.8.The DSF peak demonstrates a retention time of 3.865 minutes ± 0.3.

2.2.3.9 Percentage encapsulation efficiency

The percentage encapsulation efficiency of DSF was determined for each formulation. Samples (10 mg) were added in an Eppendorf tube (1.5 ml) containing 1 mL ice-cold methanol (Methanol-placed at -20 °C for three minutes). Un-encapsulated DSF can freely dissolve in ice-cold methanol. To ensure complete wash samples in ice-cold methanol were agitated gently for 10 seconds and centrifuged at 11,952 g for 1 min using ultracentrifuge (Sorvall MTX 150 Bench Micro-Ultracentrifuge, USA). A volume of 50 µL from the supernatant was added in 950 µL methanol, and DSF was analyzed by HPLC method. Pellets were crushed in 1000 µL DCM and vortexed for 1 min to calculate the amount of encapsulated DSF. Therefore, 50 µL of the supernatant was added into 950 µL methanol, and the resulting solution was analyzed. The total amount of the drug content was confirmed by dissolving 10 mg of the formulation in 1 ml DCM; the resulting solution was vigorously vortexed for 1 min. A volume of 50 µL from the solution was added in 950 µL methanol was analyzed by the HPLC method. The data were collected, and DSF concentration was extrapolated using the DSF standard calibration curve. Percentage encapsulation of NPs/SLNs was calculated using the following equation.

$$\% \, EE \left(\frac{The \; total \; amount \; of \; drug - the \; amount \; of \; free \; drug}{The \; total \; amount \; of \; drug} \right) 100\% \qquad Equation \; 2$$

2.2.3.10 Cumulative release studies

The freeze-dried NPs/SLNs were weighed (10 mg) and re-suspended in a dialysis membrane containing 3.0 mL phosphate buffer saline (PBS) (10x with pH 7.4) solution with 1% Tween80.The PBS solution was prepared by pipetting 100 mL PBS 10x stuck solution in less than 900 mL ultrapure water (1% Tween80 was calculated using the total volume). The dialysis membrane was immersed in a dissolution solution of 22 mL PBS with 1% Tween80. The samples were incubated at 37 °C in a shaking water bath

with a speed of 100 rpm-control, shaking stroke. At different time intervals of 4 min, 10 min, 20 min, 30 min, 1 h, 2 h, 4 h, 6 h, 8 h, and 24 h, 300 µL of the dissolution was taken and added into 300 µL methanol and ready to be analyzed by the HPLC method. After each aliquot, 300 µL of the fresh PBS with 1% Tween80 was added to the release medium. The data were collected, and DSF concentration was extrapolated using the DSF standard calibration curve.

2.2.3.11 Calculation of encapsulated disulfiram cumulative release

The cumulative release of DSF-loaded NPs incubated in physiological pH 7.4 of PBS was determined using the HPLC method described earlier in section 2.2.3.10. Also, as described in section 2.2.3.8, the equation extrapolated from the DSF calibration curve was employed to calculate the amount of DSF release in the PBS. At different time interval, the cumulative percentages of DSF were calculated using the release amount of DSF in the dialysis bag divided by the percentage encapsulated efficiency of DSF content after separating the DSF bounded at the NPs surface in methanol multiplied by hundred.

2.2.4 Stability of disulfiram in horse serum

2.2.4.1 Stability of free disulfiram in horse serum

The stock solution of DSF standard was prepared by dissolving 5 mg of free DSF in 2.5 mL DMSO (2 mg/mL). From the stock solution, 25 µL was pipetted in 975 µL of ethanol (0.05 mg/mL in ethanol of 2.5% DMSO). The solution was vortex for 1 minute. 50 µL of this solution was poured into the HPLC vial of 550 µL ethanol ready for UHPLC analysis.

The same stock (2 mg/mL in DMSO) was used to pipette 25 µL in 975 µL of horse serum (0.05 mg/ml, 2.5% DMSO) and then incubated at 37 °C for 100 rpm-control,

shaking stroke. At specific time intervals, 50 µL was added in an Eppendorf tube of 550 µL ethanol (to stop the reaction between DSF and the horse serum). After 60 s of vortexing, the mixture solution of the denatured plasma protein and the free DSF were separated through centrifugation at 11,952 g for 5 min by using the ultracentrifuge (Sorvall MTX 150 Bench Micro-Ultracentrifuge, USA). The supernatant was collected in HPLC vial to detect DSF content by the HPLC.

2.2.4.2 Stability of encapsulated disulfiram in horse serum

The full content of DSF in the formulations was determined by crushing 5 mg of DSF-loaded NPs/SLNs in 50 µL DCM vortex for 60 seconds (here DCM was used for crushing open NPS/SLNs and released encapsulated DSF), and 4.950 ml ethanol (theoretically, this is equivalent to 0.1 mg DSF per ml). A volume of 30 µL was added in 570 µL ethanol (EtOH) (theoretically, this is equivalent to 0.005 mg DSF per ml) HPLC vial. The solution was vortex for 60 s and ready for HPLC analysis. The stability of encapsulated DSF from NPs/SLNs in horse serum media was determined at different time intervals. A weight of 5 mg from each formulation of DSF NPs/SLNs was weighed in 5 mL horse serum. Samples were incubated at 37 °C for 100 rpm. At specific time intervals, 30 µL of the mixture was poured in 50 µL of ethanol and vortexed for 60 seconds. Ethanol was introduced to stop DSF degradation by denaturing the protein plasma in horse serum. Immediately after vortexing 50 µL, DCM was added to crush NPs and release the drug and then vortex for 60 s. To maintain a similar concentration to the (0.005 mg/mL), 470 µL ethanol was added and then vortex for 60 s. The mixture solution was spun at 10,000 (G) force for 5 min by ultracentrifuge to separate the denatured plasma protein and dissolved the release DSF in ethanol. The supernatant was collected and analyzed by the HPLC.

2.2.5 Maintenance of human adenocarcinoma breast cancer cell lines

2.2.5.1 Cell culture of human adenocarcinoma breast cancer cell lines

The cancer cells were cultured in a sterile class II microbiological safety cabinet (Thermo Fisher Scientific, UK). The monolayer cell cultures were grown at 37 °C humidified environment containing 5% carbon dioxide (CO_2). MDA-MB-231, MDA-MB 231$_{PTX10}$ (resistant to paclitaxel (PTX), 10 nM) and MCF 7 cancer cell lines were sustained in Dulbecco's modified Eagles' medium (DMEM) supplemented with 10% FBS, 100 units/ml of penicillin and 100 μg/ml of streptomycin. Incubated cell tissue cultures in T75 flasks were checked regularly under the microscope at approximately 4-5 times a week for changes in the colour of the growth media and cell density. Cell tissue cultures were sub-cultured when more than 70% confluent. Cells were sub-cultured by trypsinization, and 1 ml of re-suspended cell pellet was then added to the T75 flasks consisting 8-10 ml growth media and grown again at 37 °C humidified environment containing 5% carbon dioxide (CO_2).

2.2.5.2 Cell passaging

At 70-90% confluence, cell cultures were passaged as required for maintenance, growth rates and percentage cell viability experiments. Cells were harvested after removing the media, rinsed with 5 ml PBS, and 0.4 ml of trypsin-EDTA (0.25%) was added to detached adherent cells for 3 minutes at 37 °C humidified environment containing 5% carbon dioxide (CO_2). Cells in T75 flasks were gently tapped and checked under the microscope for detachment. Trypsin was neutralized by adding 5 ml pre-warmed (37 °C) growth media (DMEM) and cell suspension centrifuged at 1006 g for three minutes. Supernatant discarded and the cell pellet resuspended in 5 ml growth media (DMEM). Cells were counted and seeded in a flat-bottomed 96-well culture plate, with an appropriate density in pre-warmed (37 °C) growth media (DMEM).

2.2.5.3 Cell counting

At 70-90% confluence, the number of viable cells per ml solution was determined by manually counting viable cells using the chambers of a haemocytometer (Neubauer, Germany). The haemocytometer was cleaned with isopropanol and distilled water. The cover-slip was placed in a fix position on one chamber of the haemocytometer. Harvested cells were suspended in growth media (DMEM), and 10 µL of the cells were aspirated on to the chamber. Cells were counted using an inverted microscope (magnifying lens 10x) objective and phase contrast to distinguish between the viable and dead cells. The four large central gridded square (1 mm^2) chambers containing cells were counted with the average mean multiply by 10^4 to determine the actual number of viable cells per ml. The number of cells per ml was adjusted by fresh growth media (DMEM) as required per each experiment.

2.2.5.4 Freezing viable cells for cryogenic storage

For each passage, cells were harvested at above 90% confluence. Cells were trypsinised and centrifuged at 1006 g for 3 minutes. The supernatant containing trypsin-EDTA and DMEM solution discarded in an appropriate waste container, while the remaining cell pellet was re-suspended in PBS (10 ml). The resuspended cell pellet was centrifuged at 1006 g for 3 minutes. The supernatant was discarded, while the remaining cell pellet re-suspended in freezing medium of mixed fetal calf serum (90%) and DMSO (10%) then stored at -150 °C until use. Cryovials 1 ml (Thermo Fisher Scientific, UK) was used to aliquot cells re-suspended in a freezing medium. Cryovials containing cancer cells were initially stored at -80 °C for 3 hours. Frozen cells in cryovials were transferred to storage in a freezer (-150 °C).

2.2.5.5 Cell thawing

Frozen cell suspensions were carefully selected from the manual logbook, then removed from storage in -150 $^{\circ}$C freezer and thawed using pre-warmed (37 $^{\circ}$C) growth media (DMEM). After thawing, the cell suspension was centrifuged at 1006 g for three minutes. The supernatant containing DMSO and calf serum was discarded. The cell pellet was re-suspended in T75 cell culture flasks consisting of pre-warmed (37 $^{\circ}$C) growth media (DMEM), and incubated at 37 $^{\circ}$C humidified environment containing 5% carbon dioxide (CO_2).

2.2.6 Characterizing growth of human adenocarcinoma breast cancer cell lines

2.2.6.1 Optimizing seeding densities

Growth curve analysis was conducted for the following cell lines, MDA-MB-231, MDA-MB-231$_{PTX10}$, and MCF 7 to determine the growth rates and select the most appropriate seeding density. Cells were harvested above 70-90% confluent, trypsinised, and viable cells were counted. Cell suspensions were diluted to obtain different densities of 10^3, 10^4 and 10^5 cell/well in 96 well plates (flat bottomed). Cells were incubated for 24 h, 48 h, 72 h, 96 h, and 120 h, at each time 20 µL of 3-(4, 5-dimethylthiazol-2-yl)-2, 5-diphenyltetrazolium bromide (MTT) solution (5mg MTT dissolved per ml of PBS) was added to each well, wrapped with aluminium foil, and then incubated at 37 $^{\circ}$C. Viable cells were able to reduce the MTT to a water-insoluble blue-coloured salt known as formazan after four hours of treatments. MTT solution (in growth media) was removed gently, and DMSO (100 ml) was added and incubated at 37 $^{\circ}$C for 30 min. The multi-plate reader was used to obtain the absorbance values of each well by spectrophotometer at a wavelength of 540 nm. The readings were tabulated, and the growth curves plotted (Figure 2.9-2.11) to determine the appropriate seeding density before cytotoxicity studies.
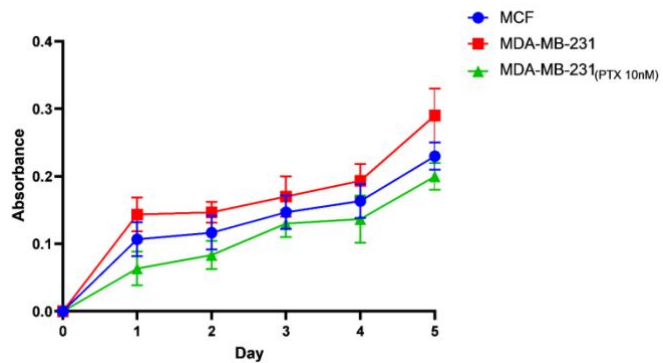
Figure 2.9. Growth curves of the three cell lines at seeding density 10^3 cells/well mean ± SD (3).
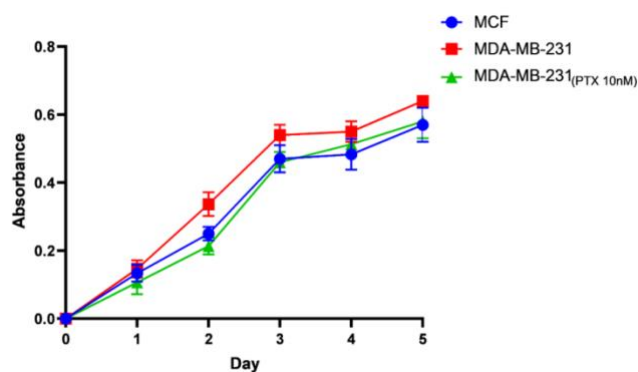
Figure 2.10. Growth curves of the three cell lines at seeding density 10^4 cells/well, mean ± SD (3).
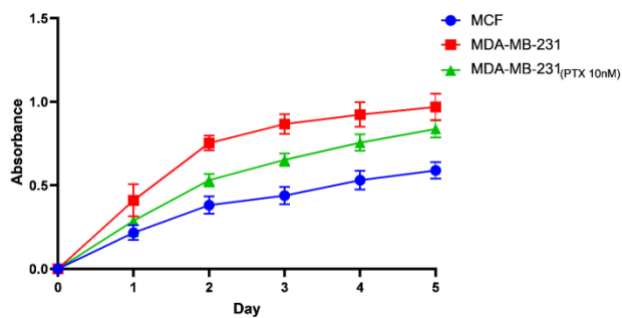
Figure 2.11. Growth curves of the three cell lines at seeding density 10^5 cells/well, mean ± SD (3).

2.2.7 Cytotoxicity assay

2.2.7.1 MTT stock solution

A stock solution of MTT in PBS was prepared by dissolving 2.5 g of 3-(4, 5-dimethylthiazol-2-yl)-2, 5-diphenyltetrazolium bromide in 500 mL of sterile PBS and

this produce a final concentration of 5 mg/mL MTT solution. The MTT solution was wrapped in an aluminium foil to prevent direct light exposure and leave to stir on a magnetic stirrer for three hrs in a fume-cupboard. In a clean bottle, MTT solution was filtered in a dark room, wrapped in an aluminium foil, and then stored at 4 °C ready to use for the evaluation of cells growth rates, and the effect of anti-cancer drugs on cell viability studies.

2.2.7.2 MTT assay

The seeding density of 10^4 cells/well was considered optimal for all three cell lines; MCF 7, MDA-MB-231, and MDA-MB-231$_{PTX10}$ (figure 2.12). Cell lines were seeded in 96 well plates, as described in section 2.2.6.2. Seeded cells were incubated overnight at 37 °C and then exposed to different concentrations of the freshly prepared formulations. The formulations were prepared in serial dilution in growth media (DMEM) at six concentrations ranging from 12 nM to 1000 nM. Cells treated with empty formulations (blanks) were used as the negative control. Whereas, wells treated with DSF standard (free drug) were used as positive controls and cells with DMSO 2.5% in DMEM used as carrier control. All media used in MTT were supplemented by 1 μM CuCl$_2$.

Before treatment, growth media was removed, and 200 μL of pre-warmed growth media (DMEM of 1 μM CuCl$_2$) at 37 °C containing different concentrations of each formulation was added in each well. Cells were incubated at 37 °C for 72 hours. MTT solution of 20 μL per well was added to all wells. MTT assay was performed as described in section 2.2.6.1. The readings were collected, tabulated to calculate percentage viability and the IC$_{50}$ for each cell line was extrapolated using Excel. The IC$_{50}$ value was calculated from the inhibitor concentrations over the percentage activity by inserting the data in a scatter plot using Microsoft Excel. The Y-axis was

transformed to the logarithmic scale. The linear equation (y=mx+n) was used from the plotted graph to calculate IC_{50}. Experiments were performed in triplicates using different formulations and expressed as of the mean ± SD.

2.3 Statistical analysis

All mean values obtained from three different experiments were reported as triplicates of the mean ± SD. The statistical analysis of the results was conducted to compare two groups using paired t-test and one-way analysis of variance (ANOVA) test (GraphPad Prism version 5.0 statistics software for windows). Post-hoc was used for comparisons of the means through Turkey's Kramer Significance Difference test. ANOVA was carried out for more than two groups of results to compare the significance of the difference. The p values < 0.05 were accepted as significant.

Chapter 3. Design and Characterizations of Disulfiram-loaded PLGA nanoparticles

3.1 Introduction

The FDA approved biodegradable and biocompatible poly (lactic-co-glycolic acid) (PLGA) polymers are commonly used for the fabrication of PLGA nanoparticles (NPs) or nano-carrier systems for drug delivery applications (Houchin and Topp, 2008). The formulated NPs are prepared using different approaches by using the D-Nano-Pr and SE methods (Shieh, et al., 2010). These NPs drug-delivery systems are designed to achieve particle sizes in the range between 100-300 nm (Lobatto, et al., 2011; Steichen, Caldorera-Moore and Peppas, 2013). For the past decades, readily fabricated drug-delivery systems, such as PLGA NPs have shown a great promise in the treatment of cancer (Schubert, Delaney Jr and Schubert, 2011).

3.2 Aims

This chapter aims to develop efficient methods to optimise DSF-loaded PLGA NPs. DSF-loaded PLGA NPs were formulated following different methods, D-Nano-Pr and SE methods. The sizes of prepared particles by using the SE method were reduced to nano-size particles using either probe sonication (PS) or high-pressure homogenization (HPH) techniques.

DSF-loaded PLGA NPs were characterised to compare particle size, zeta potential and polydispersity index (PDI). The interaction between drug and Polymers were investigated using FTIR and DSC. Whereas, encapsulation efficiency and release studies of DSF-loaded PLGA NPs were determined by the high-performance liquid chromatography (HPLC).

3.3 Experimental Design

3.3.1 The influence of organic solvent ratio and volume in direct nanoprecipitation method

The D-Nano-Pr method was adapted from Ford, et al., (2015) as described in chapter 2. Different volumes of acetone and mixed acetone/methanol (3:1) organic solvents were used to dissolved DSF and PLGA (1:9) standards. Table 3.1 shows the organic solvents with different ratios and volume used to dissolve PLGA and DSF standards.

Table 3.1. Different weights of PLGA and DSF dissolved in different ratios of organic solvents using different volumes prepared by using the direct nanoprecipitation (D-Nano-Pr) method.

Solvent	*Ratio	*Volume (ml)	*Volume 2 (ml)	*PLGA(mg)	*PLGA/DSF(mg)
Acetone	1	6	-	100	90/10
Acetone/Methanol	3:1	6	-	100	90/10
Acetone/Methanol	3:1	-	3	100	90/10

*PLGA 100 mg was used as blank NPs, while the PLGA/DSF 90/10 mg was used as PLGA-loaded DSF NPs. The different ratio of mixed solvents of acetone/methanol (3:1) and acetone in different volumes (3 and 6 ml) was employed for the above formulations prepared by direct nanoprecipitation (D-Nano-Pr) method.

The data obtained from the characterization of NPs suggested that the mixed acetone/methanol (3:1) organic solvents had superiority over acetone alone in both 6 ml and 3 ml. Therefore, the two water-miscible solvents, acetone/methanol (3:1) were used to manufacture blank and DSF-loaded PLGA NPs. The resulting data after characterization was compared between the D-Nano-Pr method and the SE method of which particle sizes were reduced by the PS and HPH techniques.

3.3.2 The influence of poly (vinyl alcohol) molecular weight and sonication time by the SE method.

An oil-in-water (O/W) single emulsion/solvent evaporation (SE) method was adapted from Najlah, et al., (2017), to prepare DSF-loaded PLGA NPs as described in Chapter 2. Three different molecular weights (MW) of poly (vinyl alcohol) (PVA) surfactants as described in Table 3.2, were used to manufactured PLGA NPs and to investigate the

effect of PVA MW on particle size, PDI, and zeta potential after 5 minutes sonication to reduce particle size.

After selecting the optimal MW of PVA, the next step was to determine the effect of sonication time on particle size, PDI and zeta potential between 5 and 8 minutes.

Table 3.2. Different molecular weights (Mw) of poly(vinyl alcohol) (PVA) were added to the PLGA using similar weights, then dissolved in dichloromethane (DCM) to be prepared by using the single emulsion/solvent evaporation (SE) method.

Poly (vinyl alcohol) (PVA) (KDa)	PVA (mg)	PLGA (mg)	*Sonication (Time)
95	100	100	5
20-30	100	100	5
31-50	100	100	5
31-50	100	100	8

*Different sonication time was used to compare reduced NPs.

3.3.3 The influence of size reducing technique after the NPs preparation by the SE method

The PVA molecular weight (31-50 KDa) and sonication time (5 minutes) exhibited reduced particle size (Figure 3.1), narrow PDI (Figure 3.2), and increased charged particle surface (zeta potential) (Figure 3.3). Once the PVA molecular weight surfactant and sonication time were established, blanks and DSF-loaded PLGA NPs were prepared by using the oil-in-water (O/W) single SE method as described in Chapter 2. Total weight of 100 mg between DSF (10 mg) and PLGA (90 mg) in a ratio 1:9 as shown in Table 3.3 was weighed and dissolved in 6 mL dichloromethane (DCM) (organic phase). The organic phase was added to the aqueous phase containing 24 mL ultrapure water, which consists of 100 mg PVA using a syringe and needle. The milky emulsion microparticles were subjected to PS and HPH techniques, as described in Chapter 2.

Table 3.3. Disulfiram (DSF)-loaded PLGA and blank NPs formulations were prepared by the single emulsion/solvent evaporation (SE) method.

Ingredient (ratio) / Formulation*	PLGA	DSF	Total
BLANK (PS)	10	-	10
Probe Sonication (PS)	9	1	10
BLANK (HPH)	10	-	10
High-pressure homogenization (HPH)	9	1	10

*PLGA-loaded DSF and blank NPs formulations were prepared by the single emulsion/solvent evaporation (SE) method, then particle sizes were reduced using the probe sonication (PS) and high-pressure homogenization techniques.

3.4 Results and discussion

3.4.1 Characterization of DSF-loaded PLGA nanoparticles prepared by the direct nanoprecipitation method

A variety of different delivery strategies have been developed for the manufacturing of DSF-based nano-carriers for cancer treatments in pre-clinical research studies such as breast cancer (metastatic) (Cvek, B. 2011). The development of DSF-based nano-carrier systems, with well establish formulation is critical for DSF delivery as an anticancer agent for clinical use. In this study, to circumvent DSF poor stability in the circulatory system, PLGA nano-carrier systems have been manufactured using the D-Nano-Pr method by Ford, et al., (2015) and SE method by Najlah, et al., (2017).

The first phase of this research experiments was to develop efficient methods applicable to the production of decrease particle size with good loading efficiency using the D-Nano-Pr method (Ford, et al., 2015). The binary mixture of acetone/methanol (3:1) or acetone organic solvents used to prepare both the blanks and DSF-loaded PLGA NPs by the D-Nano-Pr method achieved a smaller size of NPs.

As shown in Figure 3.1a, there is a significant variation in particle size of the blank NPs prepared in 6 ml acetone, than those manufactured in asimilar volume of acetone/methanol (3:1) ratio organic solvents. The blank nanoparticle (NP) prepared

in acetone demonstrated asignificantly ($p < 0.05$) smaller particle size of 226.9 ± 6.26 nm, than the blank NP prepared in acetone/methanol (3:1) with a particle size of 257.0 ± 17.89 nm. Previous studies have indicated that the use ofthe nanoprecipitation method in manufacturing PLGA copolymer typically occurs in methanol. Therefore, the interaction parameter for a binary mixture of acetone/methanol is slightly higherfor the hydrophobic lactic acid (LA) of the PLGA which diffuses into the binary mixture of acetone/methanol (3:1). Besides, when compared to the acetone solvent, the PLGA copolymer is more likely to precipitate to form a smaller particle size. A study conducted by Fonseca et al., (2002), demonstrated asmaller particle size of the blank PLGA NPs prepared in acetone by using the D-Nano-Pr method (also known as the interfacial deposition method). Solvent and polymer interaction to produce smaller size lack the fundamental explanation as to why the decrease in particle size distribution for blank NPs prepared in acetone (aprotic solvent). One of the reasons attributed to the decrease particle size prepared in acetone is the organic solvent/aqueous phase ratio. Preliminary studies were conducted to compare the differences in particle size of blank PLGA NPs preparedin acetone by the D-Nano-Pr method indicated critical of theorganic solvent/aqueous phase ratio. In their findings, the blank PLGA NPs of the organic solvent/aqueous phase (1:2) ratio demonstrated decrease particle size than blank PLGA NPs prepared in organic solvent/aqueous phase (1:1) ratio (Fonseca et al., 2002).

Figure 3.1b showed no significant ($p > 0.05$) change between DSF-loaded PLGA NP with aparticle sizeof 230.8 ± 7.06 nm prepared in 6 ml binary mixture of acetone/methanol (3:1) organic solvents, and DSF-loaded PLGA NP prepared in a similar volume of acetone solvent with particle size 237.4 ± 3.07 nm. Fasehee et al., (2017), prepared DSF/PLGA (1:10) ratio in DMSO to form the diffusing phase, then added to the aqueous phase containing PVA (0.5% in water) by using the

nanoprecipitation method produced a smaller particle size of DSF encapsulated PLGA NPs. Previous studies have demonstrated the use of PVA in aqueous phase enhances drug/polymer interaction to produce smaller particle size, and this might be the reason why the increase in particle size of PLGA NPs prepared in aqueous phase without PVA. This study is the first to prepare blanks and DSF-loaded PLGA NPs using a binary mixture of acetone/methanol (3:1) ratio organic solvents. It has been previously demonstrated that maintaining the rate of diffusion between solvent and non-solvent volume ratio, including polymer concentration increases particle size. Therefore, the higher the rate of diffusion between solvent and non-solvent gives smaller NPs with increased drug encapsulation efficiency (Stainmesse et al., 1992).

However, DSF-loaded PLGA NPs against cancer is the formulation of homogeneous particle size used to circumvent the EPR effect around areas of new blood vessel growth in cancer cells via passive targetting isone of the biological advantages of encapsulated hydrophobic therapeutic drugs (Maeda. H. 2001). A previous study demonstrated high polymer/solvent (PLGA/methanol) interaction produced smaller particle size withincrease drug encapsulation surface area with and regular distribution (Choi et al., 2002). The use of a binary mixture of acetone/methanol (3:1) ratio organic solvents improves the production of smaller particle size.The formulation of smaller particle size PLGA NPs with high drug encapsulation surface area by D-Nano-Pr method deemed inecessaryfor cancer treatment. There are over 20 clinically approved NPs therapeutics, and a small number of engineered novel NPs carrier systems are also in clinical and pre-clinical development (Zhang et al., 2008).
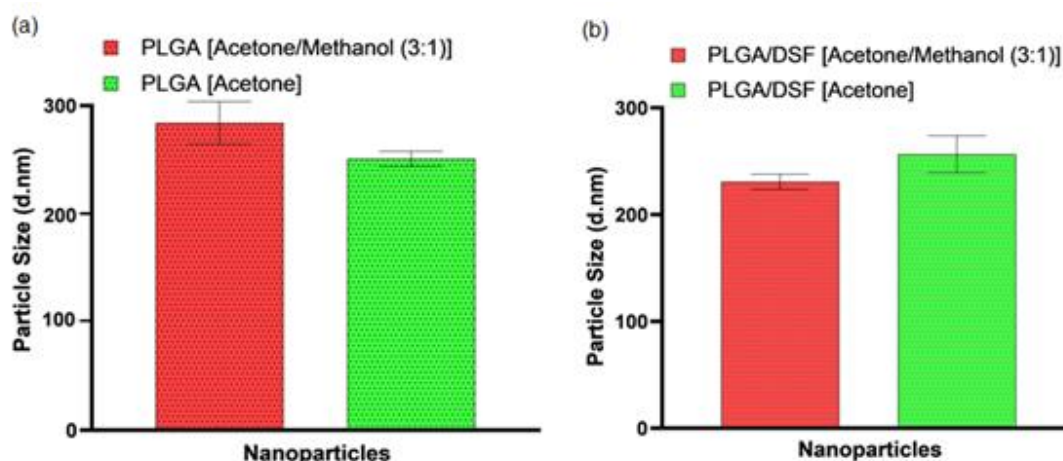
Figure 3.1. Particle sizes of (a) blanks and (b) DSF-loaded PLGA nanoparticles prepared in different organic solvents (acetone and acetone/methanol) by the direct nanoprecipitation (D-Nano-Pr) method. (Mean ± SD, n=3).

Both blank and DSF-loaded PLGA NPs showed low polydispersity(PDI) (< 0.3), and this is irrespective of the binary mixture of acetone/methanol (3:1) organic solvents used (Figure 3.2a and b). The NPs prepared in two batches of organic solvents, acetone/methanol (3:1) ratio and acetone by the D-Nano-Pr method produces narrow PDI. Regardless of the slight changes in the polarity of the organic phase of the binary mixture which may not have affected the NPs formulation of narrow PDI. The blank PLGA NPsare considered not significant ($p > 0.05$) between the two batches of organic solvents (Figure 3.2a). The DSF-loaded PLGA NP prepared in acetone solvent had aconsiderablet effect on PDI compared to DSF-loaded PLGA NPs prepared in a binary mixture of acetone/methanol (3:1) ratio organic solvents (Figure 3.2b). This is an indication that the blank and encapsulated DSF NPs had homogeneous NPs suspensions. As part of the method development, D-Nano-Pr method used in this study improves the spontaneous and reproducibility of NPs below 300 nm and low PDIs. The NPs produced in this study showed a slight difference in terms of particle sizes and PDIs from the published results. Therefore, this isdue to the various parameters (such as polymer/drug concentration and types of solvent) used during the NPs preparation in organic solvent/aqueous phase volume ratios.

93
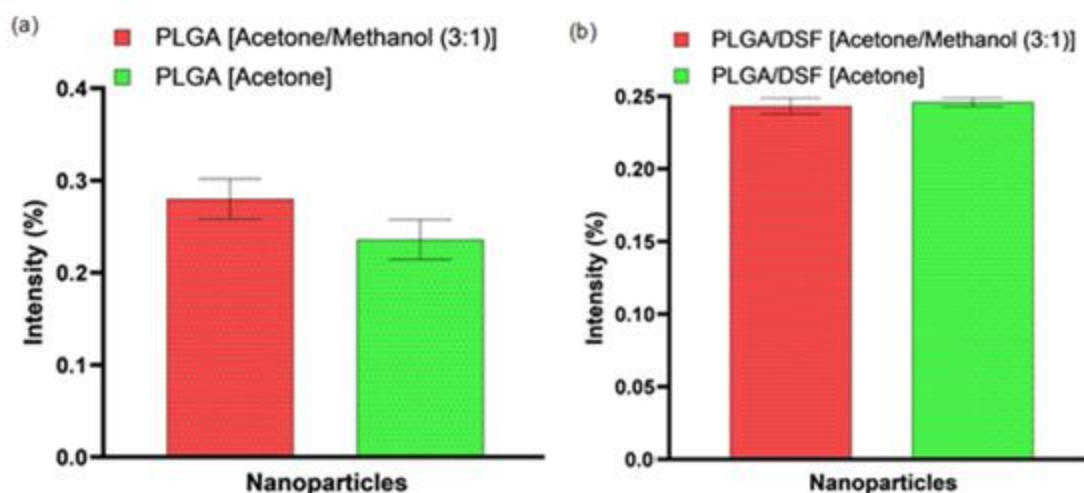
Figure 3.2. Polydispersity index of (a) blank and (b) DSF-loaded PLGA nanoparticles manufactured in different organic solvents of acetone/methanol and acetone by using the D-Nano-Pr method. (Mean ± SD, n=3).

Figure 3.3a and b demonstrated increased zeta potential values of both blank and DSF-loaded PLGA NPs. Regardless of drug loading or solvent ratios, no significant ($p > 0.05$) changes in zeta potential values among all NPs (Figure 3.3a and b).To the two batches of organic solvents (acetone/methanol, 3:1 ratio, and acetone) the results suggested no effect over the PLGA copolymer (50:50, LA/GA ratio) on the surface charge as high values of zeta potential obtained. A previous study demonstrated that PLGA copolymers with different monomers of LA and GA are critical of increased particle size and surface charge NPs (Stolnik et al., 1994). Also, in this study, the absence of surfactant in the preparation of NPs by the D-Nano-Pr method exhibited similar high values surface charge NPs. It is often known that the preparation of NPs using surfactants in the aqueous phase by the D-Nano-Pr method tends to interact with NPs surfaces by causing decrease surface charge (Stolnik et al., 1994; Muller, RH 1993). Sahin et al., 2017, prepared PLGA NPs in acetone solvent with PVA, demonstrated increased particle size, and decreased zeta potential values. This is due to PVA interaction with the PLGA in the organic phase.

94
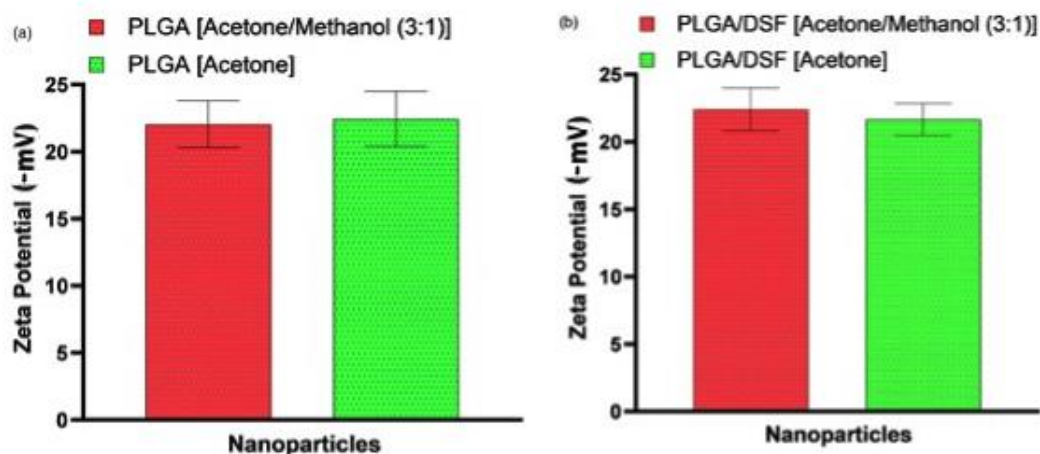
Figure 3.3. Zeta potential of (a) blank and (b) DSF-loaded PLGA nanoparticles prepared by using the D-Nano-Pr method was employed to compare the effect of organic solvents between acetone/methanol and acetone during formulations. (Mean ± SD, n=3).

The choice of using suitable organic solvents might be vital in the determination of small particle size. However, there was no difference between the two baches of solvent ratios in this study. Therefore, the use of binary mixture water-miscible solvents, acetone/methanol with a ratio 3:1 has never been used, and it was selected to enhance drug/polymer interaction without compromising the size, PDI, and zeta potential.

The second phase of the experiments for efficient method development using the D-Nano-Pr method was to determine the volume required for binary mixture organic solvents to produce PLGA NPs. Two volumes of the binary mixture organic phase, 6 ml, and 3 ml were used to dissolve the pure drug and polymer. As shown in Figure 3.4a and b, PLGA NPs prepared in binary mixture of 3 ml acetone/methanol (3:1) showed a significantly ($P < 0.05$) decreased particle size for blank and DSF-loaded PLGA NPs of 126.8 ± 0.96 nm and 145.1 ± 0.40 nm, respectively, than the blank and DSF-loaded PLGA NPs prepared in 6 ml acetone/methanol with particle sizes of 257.0 ± 17.89 nm, and 230.8 ± 7.06 nm, respectively. As previously stated, a similar result from the preparation of PLGA NPs, in 6 ml of organic solvent ratios demonstrated

increase particle sizes (Figure 3.1a and b). Therefore, lowering theorganic solvent with constant drug/polymer concentration will lead to increase diffusion rate with high yield drug loading and decrease particle sizes (Stainmesse, 1992). Reduced volume of organic solvent affects theparticle size of PLGA NPs prepared in a 3 ml binary mixture of acetone/methanol. Lowering the volume of organic solvents might explain the decrease in particle sizes for PLGA NPs prepared in 3 ml compared to the increased particle sizes prepared in a 6 ml binary mixture of acetone/methanol organic solvents. In a recent study, DSF-loaded PLGA NPs were manufactured in 5 ml acetone solvent into30 ml aqueous medium of different surfactants using the D-Nano-Pr method. Their results demonstrated lower particle sizes ranging from 100 to 125 nm (Hoda et al., 2017). In this study, the particle sizes of PLGA NPs obtained in 3 ml acetone/methanol organic solvents are not reflective of the published results as the difference might be the presence of surfactant which causes a decrease in particle size. The surfactant may play a role to produce smaller particle size of NPs as a stabilizer. Still, the drug encapsulation efficiency might be affected because of the surfactant interaction with the PLGA prevents more drug loading.

The PLGA NP prepared in 3 ml binary mixture of acetone/methanol (3:1) organic solvents demonstrated a significantly decreased PDI ($P < 0.05$) of the blank. Also, decreased PDI ($p < 0.05$) of the DSF-loaded PLGA NPs compared to the blank and DSF-loaded PLGA NPs prepared in 6 ml acetone/methanol organic solvents, respectively, Figure 3.5 a and b.
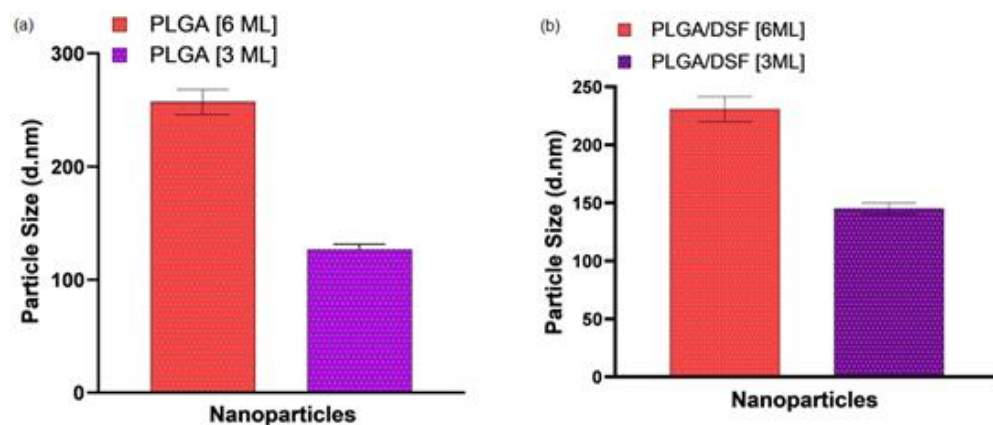
Figure 3.4. Particle sizes of (a) blank, and (b) DSF-loaded PLGA nanoparticles, were prepared in different volumes of organic solvents by using the D-Nano-Pr method. (Mean ± SD, n=3).
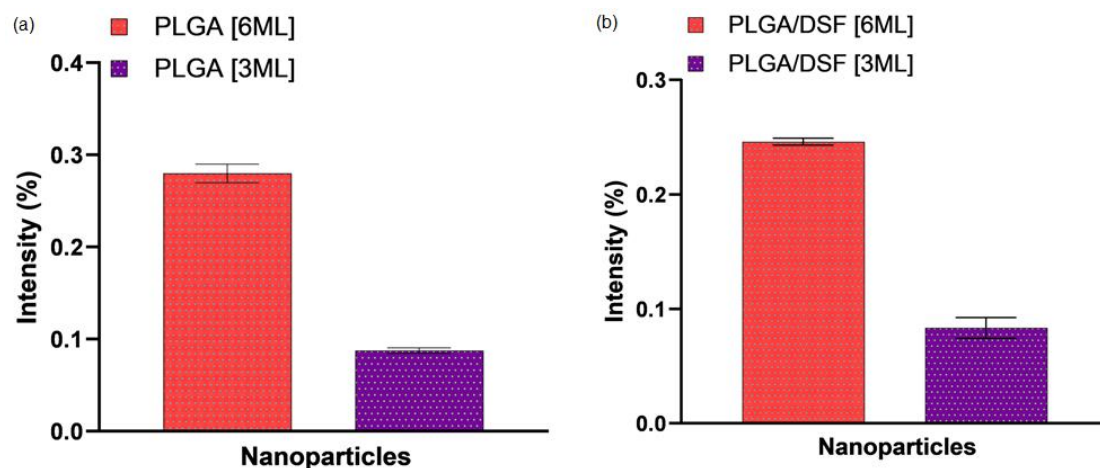
Figure 3.5. Polydispersity index (PDI) of (a) blank and (b) DSF-loaded PLGA nanoparticles were prepared in different volumes of organic solvents by using the D-Nano-Pr method. (Mean ± SD, n=3).
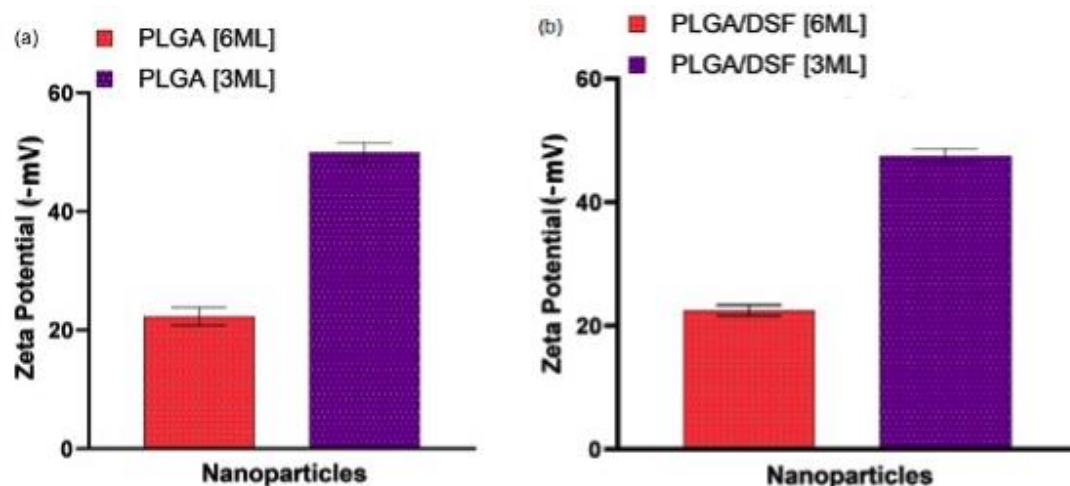
Figure 3.6. The zeta potential of (a) blank and (b) DSF-loaded PLGA nanoparticles were prepared in different volumes of organic solvents by using the D-Nano-Pr method. (Mean ± SD, n=3).

Both the blank and DSF-loaded PLGA NPs produced in 3 ml acetone/methanol (3:1) organic solvents demonstrated a significantly ($p < 0.05$) increased values of zeta potential (Figure 3.6a and b). All formulations prepared in different volumes of a binary mixture, acetone/methanol 3:1 ratio organic solvent exhibited a net surface charge with zeta potential values ranging from -22 to -50 mV. Previous studies have demonstrated the use of surfactants affecting the surface charges by binding to NPs surfaces (Fonseca C 2002; Stolnik et al., 1994). This study can confidently deduce that the use of the D-Nano-Pr method without the use of surfactant prepared in a low volume of solvent/s will lead to decrease particle size, narrow PDI, and increase zeta potential. Irrespective of the effect on particle size exhibited using different volumes and mixed organic solvents (acetone/methanol), there is strong evidence that this study showed all NPs formulations had low PDIs and narrow particle size distribution. The low volume (3 ml) binary mixture of acetone/methanol organic solvents showed increase zeta potential for all NPs formulations, and the significant change in surface charges was not drug loading dependent. In other words, the blank and loaded NPs prepared in low mixed organic solvents demonstrated increased zeta potential values (Figure 3.6a and b). Also, the amount of polymer and drug mixture in low organic solvents significantly affects the zeta potential surface charges. It has been confirmed that increase surface charges produce strong electrostatic repulsion of NPs with less aggregation (Honary and Zahir, 2013). Therefore, NPs prepared in 3 mL acetone/methanol (3:1) organic solvents show strong electrostatic repulsion in suspension solution, thereby, causing less aggregation.

The particle size of PLGA NPs increases when prepared in acetone solvent (Jeon, et al., 2000).This finding is in support of DSF-loaded PLGA NPs prepared in acetone solvent (Figure 3.4a). The increase in particle size with acetone solvent is linked to the rate of diffusion between the organic solvent and aqueous phase ratios, and the

difference in polarity between acetone and water (Jeon, et al., 2000). Methanol might play the role of co-solvent facilitating the miscibility between both phases; hence, this might explain the significant reduction in particle size of NPs prepared by low volume binary mixture organic solvents.

3.4.2 Development of disulfiram-loaded PLGA nanoparticles by using the single emulsion/solvent evaporation method.

3.4.2.1 Effect of molecular weight of poly (vinyl alcohol)

The choice for poly (lactide-co-glycolide acids) (PLGA) was due to its desirable biocompatibility and biodegradability properties (Vandervoort and Ludwig, 2002). Therefore, the first phase of an efficient method development by the SE method was to use various molecular weights of poly (vinyl alcohol) (PVA) stabilizers for the production of PLGA (blank) NPs with desirable particle size, PDI, and zeta potential.
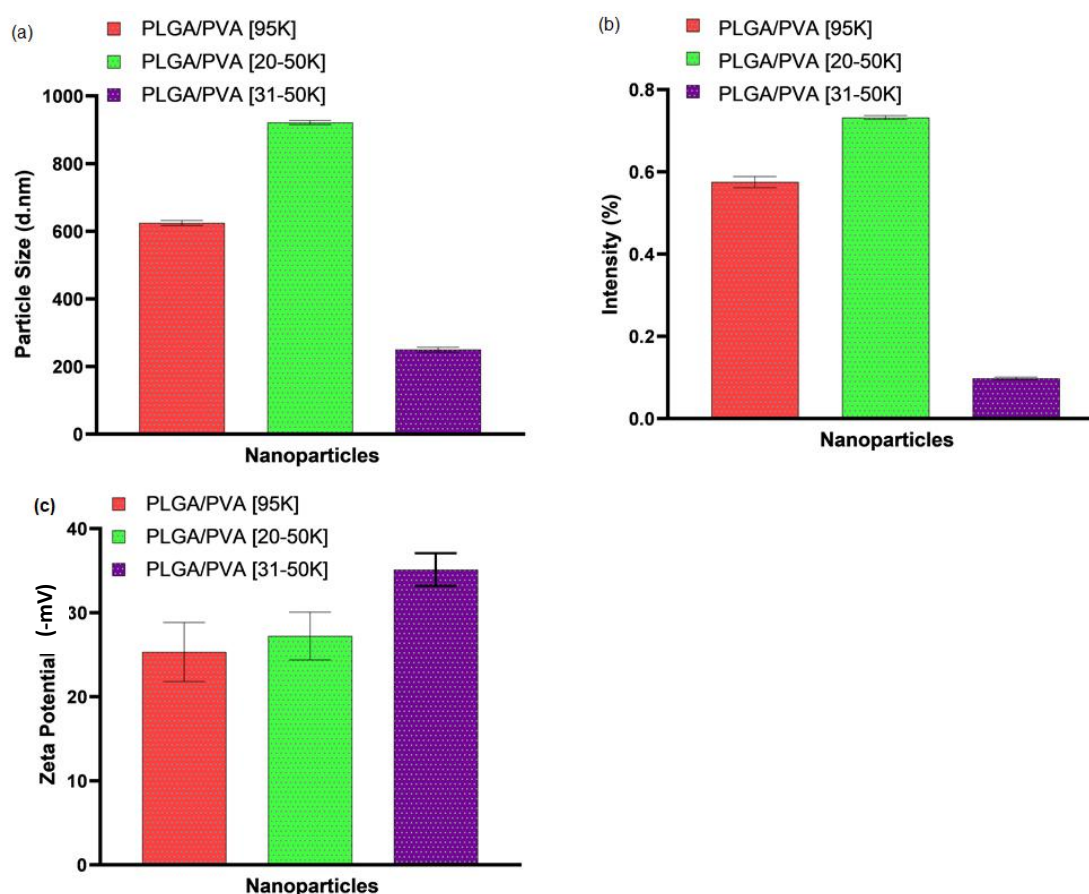
Figure 3.7. PLGA NPs using different molecular weights of PVA (20-30 KDa, 31-50 KDa and 95 KDa) were manufactured by using the SE method were characterized by (a) Particle sizes (b) polydispersity index (PDI), and (C) zeta potential. (Mean ± SD, n=3). As part of the method development this experiment was performed to select the molecular weight of PVA that produces a smaller particle size, PDI, and increased zeta potential when interact with PLGA.

As a stabilizer, PVA of three different molecular weights (Mw), 20-30 KDa, 31-50 KDa, and 95 KDa were used to develop and evaluate the blanks of PLGA NPs formulations. This experiment was performed to select the PVA with molecular weights (Mw) suitable to produce small particle size. As shown in Figure 3.7a, PLGA NP prepared with PVA 95 KDa Mw after five minutes sonication demonstrated a significantly ($P < 0.05$) decreased particle size of 624.0 ± 43.77 nm compared to PVA 20-30 KDs Mw of particle size of 922.0 ± 35.71 nm. Also, PLGA NPs prepared with PVA 95 KDa Mw showed a significantly ($P < 0.05$) increased particle size of 624.0 ± 43.77 nm than the PVA of 31-50 KDa Mw with a particle size of 250.0 ± 6.22 nm. In addition, PLGA NPs

of PVA with 20-30 KDa Mw demonstrated a significantly ($P < 0.05$) increased particle size, compared to PLGA NPs with PVA 31-50 KDa Mw (Figure 3.7a). Figure 3.7b shows that NPs prepared by PVA 95 KDa Mw indicated a significantly ($p < 0.05$) decreased PDI than the PLGA NPs with PVA 20-30 KDa Mw. PLGA NPs prepared with PVA 95 KDa Mw showed a significantly ($P < 0.05$) decreased PDI than the PLGA NPs with PVA 31-50 KDa Mw. While PLGA NPs prepared with PVA 20-30 KDa Mw indicated a significantly ($P < 0.05$) decreased PDI compared to PLGA NPs with PVA 31-50 KDa Mw. All NPs showed high zeta potential surface charges with a slight increase for those prepared with PVA 31-50 KDa Mw, Figure 3.7c.

In a recent study, published results showed higher molecular weight PVA (120 KDa) produced smaller NP than those of 10 KDa and 75 KDa (Najlah, et al., 2017). This indicates different experimental conditions and starting materials (i.e. PLGA of different molecular weight and functional group) are critical of small particle size. Nevertheless, PVA of lower molecular weights is widely used as surfactant stabilizers for the development of PLGA NPs and this support the experimental results obtained (Konan, Gurny and Allémann, 2002).

3.4.2.2 Effect of sonication time

PVA 31-50 KDa Mw produced NPs with smaller particle size and lower PDI than those of 20-30 and 95 KDa Mw; hence, it was selected.

The second phase of this experiment was to determine the best sonication time between 5 and 8 minutes. The particle size of blank PLGA NP reduced by five minutes sonication was considered very significant ($P < 0.05$) with a decreased particles size of 278.8 ± 37.55 nm compared to the corresponding blank PLGA NP sonicated for 8 minutes with the particle size of 318.0 ± 3.7 nm (Figure 3.8a). In this study, the 5 minutes sonication was considered suitable for reduced nano-scale particulates for

which the use of shorter sonication time can decrease droplet breakdown to produce smaller particle sizes due to reducing share stress.

Whereas, DSF-loaded PLGA NP sonicated for 5 minutes showed a significantly ($p <$ 0.05) decreased particle size of 254.6 ± 12.90 nm, than DSF-loaded PLGA NP sonicated for 8 minutes produced a particle size of 283.6 ± 3.7nm (Figure 3.8b).The addition of PVA 31-50 KDa Mw did not affect the particle size. Also, increasing sonication time decreases particle size by increasing shear stress. Therefore, extended sonication time may increase droplet breakdown by reducing particle size (Budhian et al., 2007). The increase in particle size may be caused by particle aggregation when in aqueous suspension due to surface tension or, polarity.
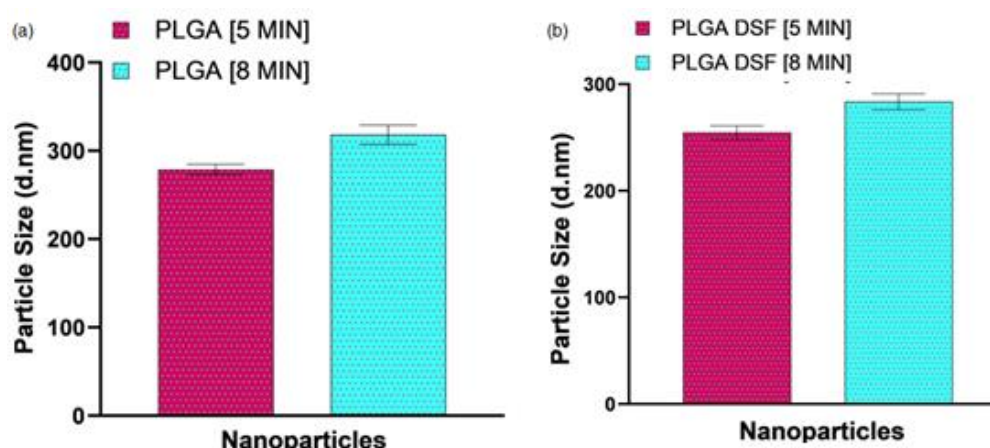
Figure 3.8. Particle sizes of blank and DSF-loaded PLGA nanoparticles reduced by probe sonication for 5 and 8 minutes of (a) blank PLGA nanoparticles, and (b) DSF-loaded PLGA nanoparticles were prepared by using the SE method (mean ± SD, n=3).

Figure 3.9a showed the PLGA (blank) NP produced for 5 minutes sonication had a significant (*P < 0.05*) increased narrow PDI (< 0.1) than the 8 minutes sonication PLGA (blank) NP. Besides, the reduced DSF-loaded PLGA NP for 5 minutes sonication showed a significantly ($p <$ 0.05) decreased narrow PDI compared to the reduced DSF-loaded PLGA NP for 8 minutes sonication (Figure 3.9a).
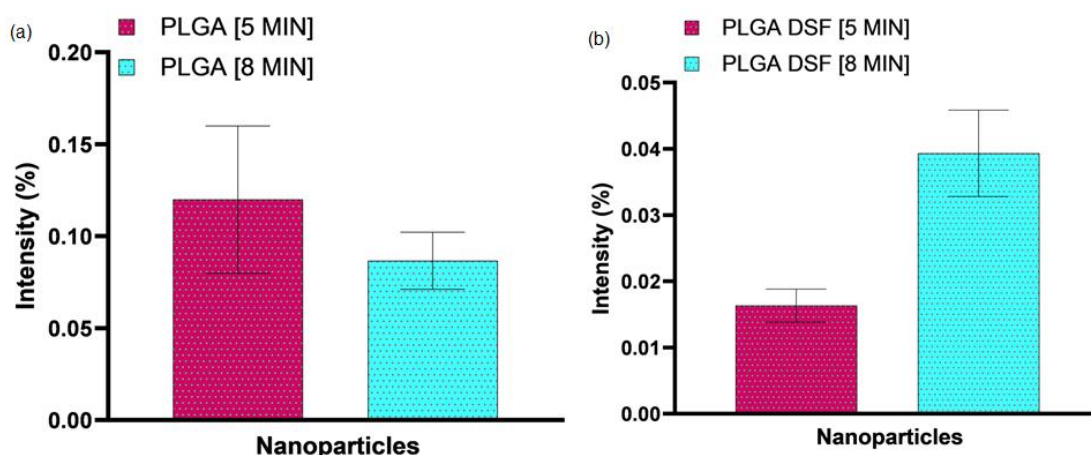
Figure 3.9. Polydispersity index (PDI) of blank and DSF-loaded PLGA nanoparticles reduced by probe sonication for 5 and 8 minutes demonstrated narrow PDIs (a) blank PLGA nanoparticles, and (b) DSF-loaded PLGA nanoparticles prepared by the SE method. (Mean ± SD, n=3).

Irrespective of sonication times, all NPs (blank and loaded) showed similar zeta potential values ranging from -23.8 ± 2.59 mV to -25.7 ± 1.06 mV (Figure 3.10a, and b). Published studies have reported an increase in sonication time thus affects the liposomes bilayer and then alters the electrical potential (zeta potential). Labhasetwar, Mohan and Dorle, (1994) investigated the effect of different sonication time from 0 to 5 minutes, and their results demonstrated an increase in zeta potential as the sonication time increases, which is critical to the high increase NPs dielectric. Also, Shao, et al., (2015) indicated in their studies that increased sonication time increases zeta potential due to the increased surface area of loaded NPs. However, this study aims to investigate and evaluate efficient preparation methods than to examine the impact of sonication. The sonication for five minutes was selected based on size and PDI results.
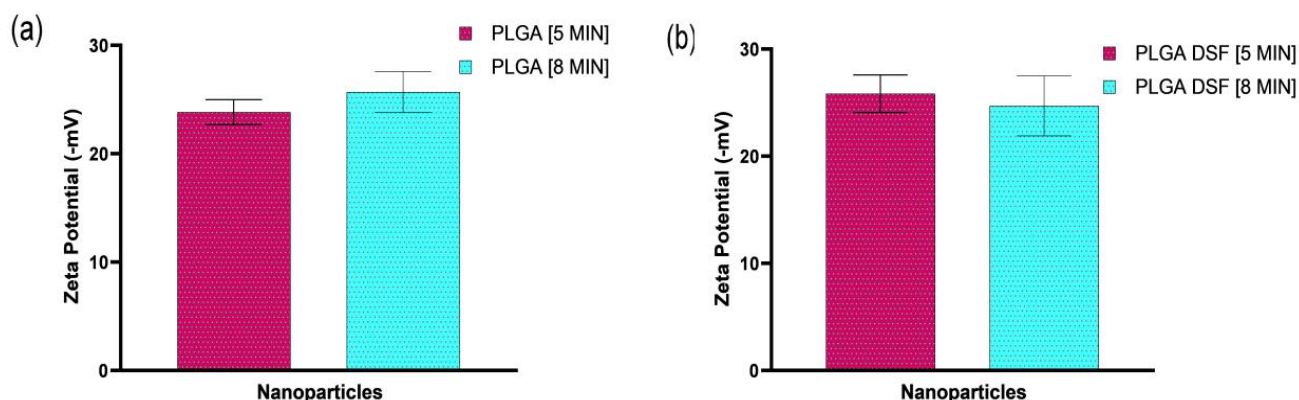
Figure 3.10. Zeta potential of blank and DSF-loaded PLGA nanoparticles (NPs) reduced by probe sonication for 5 and 8 minutes (a) blank PLGA NPs, and (b) DSF-loaded PLGA NPs, were prepared by using the SE method (Mean ± SD, n=3).

3.4.3 Comparison between direct nanoprecipitation and single emulsion/solvent evaporation methods

This study generates acceptable results evaluated during the initial method development of PLGA NPs using the D-Nano-Pr and SE methods. The different ratio and volumes of organic solvents for D-Nano-Pr method, and the different types of PVA molecular weights and sonication time for SE methods exhibited nano-scaled particle sizes, narrow PDIs. The increased zeta potential values are like most published results. All PLGA NPs formulations prepared by the D-Nano-Pr and SE methods were compared to select the materials and parameters used during the manufacturing of NPs. Furthermore, after selecting the sonication time using the PS technique, the HPH technique was also employed to investigate and compare particle size reduction between both techniques after NPs preparation by using the SE method.

Regardless of particle size reduction of blank NPs developed by the HPH and PS techniques, the blank PLGA NP produced by using the D-Nano-Pr method showed no significant ($p > 0.05$) effect in the particle size of 257.0± 17.89 nm, compared to the reduced blank NPs by HPH and PS techniques using the SE method, therefore,

produced particle sizes of 211.9 ± 1.76, nm, and 278.8 ± 37.51 nm, respectively (Figure 3.11a). The increase particle size of DSF-loaded PLGA NP developed by the D-Nano-Pr method can be attributed to the drug/polymer interaction in a binary mixture of acetone/methanol (3:1) ratio organic solvents. The PLGA polymer with more uncapped end groups diffuses much in methanol causes increased particle size of the blank PLGA NPs.

The blank PLGA NP prepared by the SE method then reduced particle size using the HPH technique demonstrated a significantly ($p < 0.05$) decreased particle size of 211.9 ± 1.76 nm, than the blank NP that was reduced by the PS technique which produces a particle size of 278.8 ± 37.51 nm (Figure 3.11a). In addition, after introducing DSF into the formulation of DSF-loaded PLGA NP developed by the D-Nano-Pr method demonstrated a significantly ($p < 0.01$) decreased particle size of151.3 ± 17.7 nm, compared to the reduced DSF-loaded PLGA NPs by the HPH and PS techniques with particle sizes of 237.4 ± 21.42, nm, and 246.9 ±10.96 nm, respectively (Figure 3.11b). DSF and PLGA polymer seem to have high interaction when dissolved in the binary mixture of acetone/methanol 3:1 ratio organic solvents. Also, the high affinity to the corresponding LA backbone tends to incorporate more of the drug into the hydrophobic core might lead to decreased particle size. Mostly, the hydrophobic domains of LA of the PLGA adsorbed the drug in its hydrophobic core. This will enable the binary mixture of organic solvents to diffuse when added in a dropwise manner into the aqueous phase. Thereby, it causes the removal of the organic solvents by evaporation through continuous stirring.The reduced particle size of DSF-loaded PLGA NP by the HPH or PS techniques had no significant ($p > 0.05$) effect between particle sizes (Figure 3.11b).

As shown in Figure 3.14 – 3.16, the three types of DSF-loaded PLGA NPs developed by the D-Nano-Pr and SE methods (NPs were further reduced by HPH and PS

techniques) showed smooth and spherical morphological surface structures. The NPs from the SEM images exhibited homogeneous narrow (PDI, < 0.3) particle size distribution.

The blank PLGA NP developed by the D-Nano-Pr method demonstrated a significantly ($p < 0.05$) decreased narrow PDI compared to the SE/HPH technique (Figure 3.12a). However, no significant effect ($p > 0.05$) was observed between the blank PLGA NP developed by D-Nano-Pr and SE/PS technique methods. There is a significantly ($p < 0.01$) decreased PDI between the blank PLGA NP produced by SE/HPH technique and SE/PS technique (Figure 3.12a). In contrast, DSF-loaded PLGANP developed by the D-Nano-Pr method showed significant ($p < 0.05$) narrow, PDI than DSF-loaded PLGA NP developed by the SE/HPH technique and SE/PS technique (Figure 3.12b). However, no significant ($p > 0.05$) effect on DSF-loaded PLGA NP manufactured by the SE-HPH/technique and SE-PS/technique. As shown in Figure 3.12b, overall, blank, and DSF-loaded PLGA NPs demonstrated narrow particle size distribution (Figure 3.12a and b).
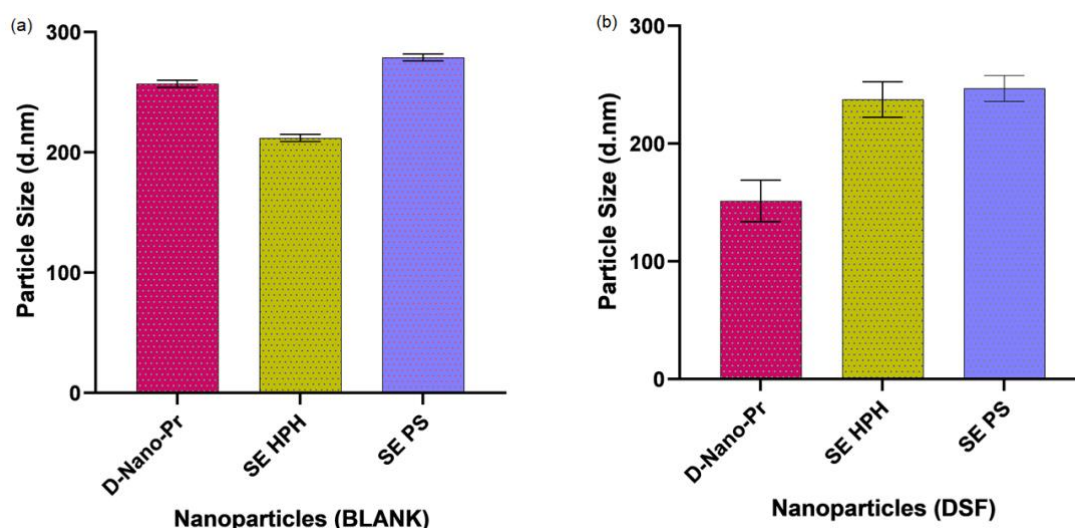
Figure 3.11. Particle sizes of (a) blank, and (b) DSF-loaded PLGA nanoparticles were prepared by using the D-Nano-Pr method, and the SE method followed by particle size reduction using the HPH and PS techniques (Mean ± SD, n=3).
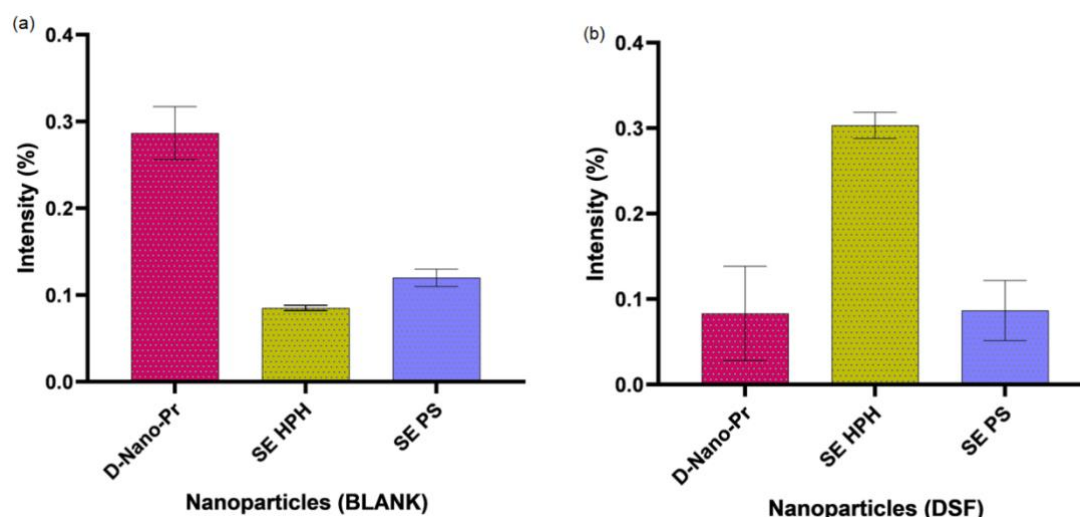
Figure 3.12.The polydispersity index (PDI) of (a) blank, and (b) DSF-loaded PLGA nanoparticles were prepared by using the D-Nano-Pr method, and the SE method followed by particle size reduction using the HPH and PS techniques(Mean ± SD, n=3).

All methods of preparation used to manufacture blank PLGA NPs showed no significant ($p > 0.05$) effect on zeta potential (Figure 3.13a). But, the DSF-loaded NP prepared by the D-Nano-Pr method demonstrated a significantly ($P < 0.05$) higher charged surface zeta potential, than the SE/HPH technique and SE/PS technique (Figure 3.13b). Nevertheless, the size reducing technique for DSF-loaded NP developed by the SE method followed by particle size reduction using the HPH technique had no significant ($p > 0.05$) effect on zeta potential, compared to the DSF-loaded PLGA NP reduced by the PS technique (figure 3.13b).

Due to the non-mechanical intervention to reduce smaller particle size, D-Nano-Pr method demonstrated superiority over the SE method followed by particle reduction using the HPH and PS techniques. All NPs formulations maintained narrow PDI or even monodispersed particles (Figure 3.12a and b). The high energy impact through the HPH and PS techniques to reduce particle size affects the zeta potential of the loaded NPs (Figure 3.13b). This might be because of both techniques apply shear forces that disturb the polymer matrix, which leads to a higher amount of the drug

107

adsorbed on the surface rather than embedded within the NP (Bouaouina, et al., 2006;

Sharma, et al., 2015).
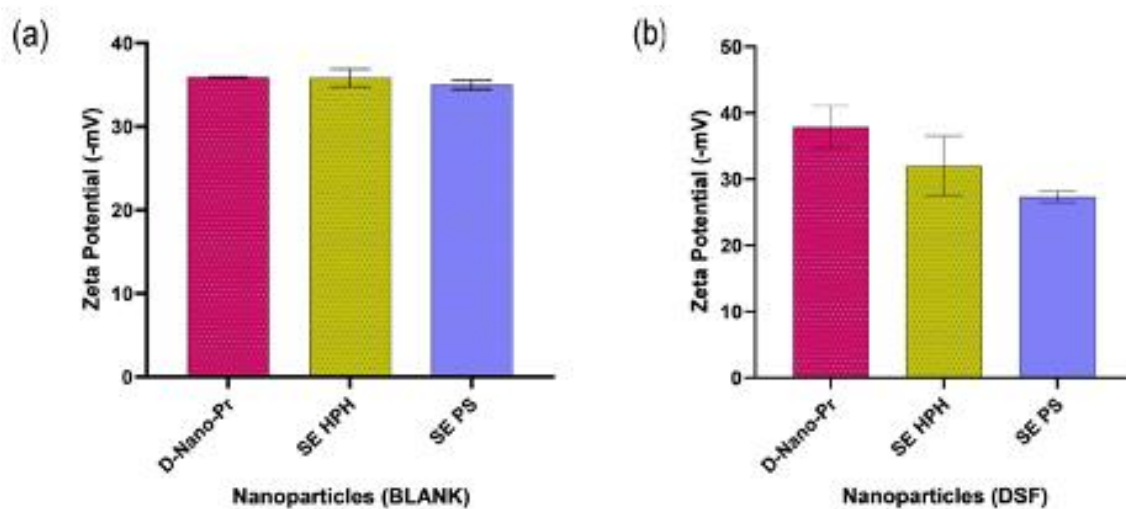
Figure 3.13. Zeta potential of (a) blank and (b) DSF-loaded PLGA nanoparticles were prepared by using the D-Nano-Pr method, and the SE method followed by particle size reduction using the HPH and PS techniques. (Mean ± SD, n=3).
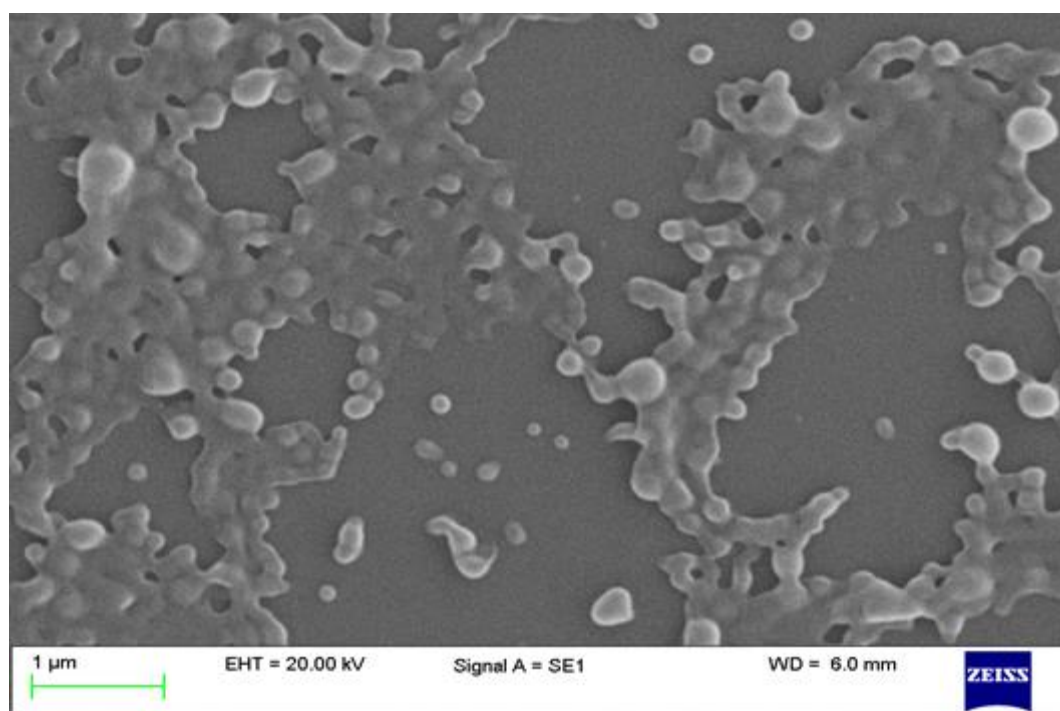
Figure 3.14. Scanning electron microscope (SEM), demonstrating the surface morphological images of disulfiram-loaded PLGA nanoparticles prepared by the D-Nano-Pr method.
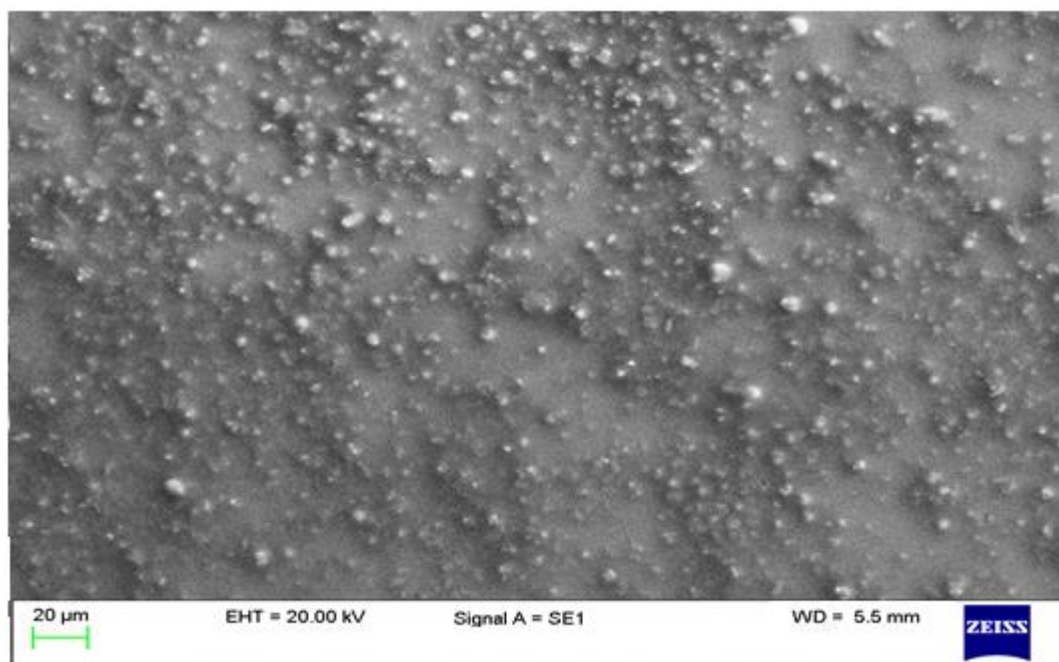
Figure 3.15. Scanning electron microscope (SEM), demonstrating surface morphological images of reduced DSF-loaded PLGA nanoparticles using the high-pressure homogenization (HPH) technique prepared by the SE method.
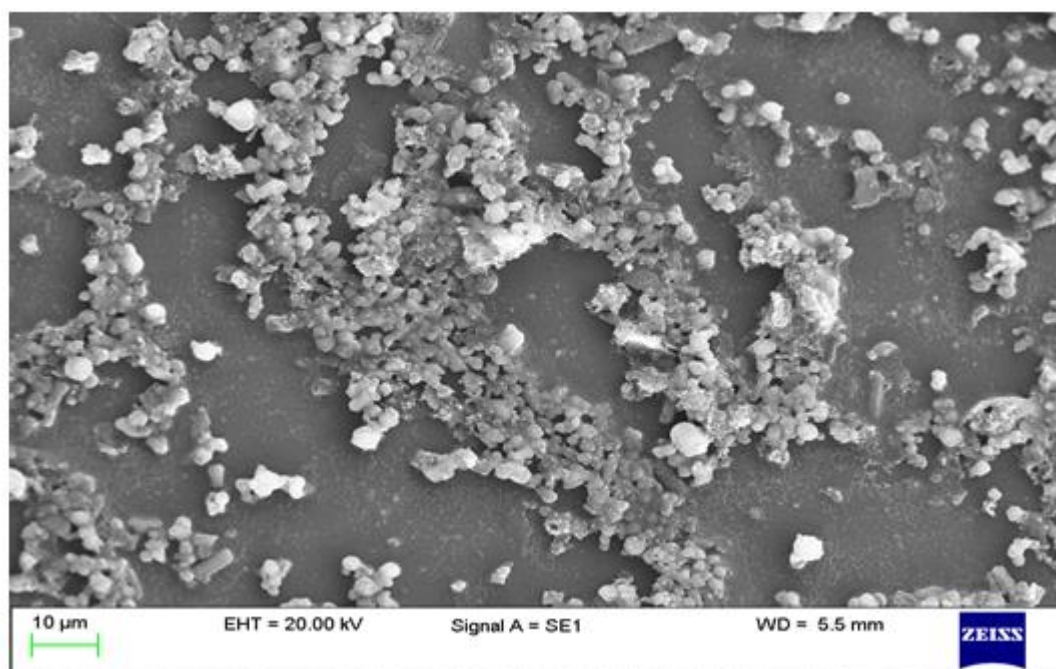
Figure 3.16. Scanning electron microscope (SEM), demonstrating surface morphological images of reduced DSF-loaded PLGA nanoparticles using the probe sonication (PS) technique prepared by the SE method.

3.4.4 Differential scanning calorimetry

As shown in Figure 3.17a-d, DSC thermograms were applied to assess the thermal behaviour in a different state of raw (a) sucrose, (b) PLGA, (c) DSF, and (d) physically mixed standards (pure sucrose, PLGA, and DSF). DSF and physically mixed standards had sharp endothermic peaks of DSF at 70 ^{o}C, and this is simply showing the melting point of pure DSF and its crystalline nature (Figure 3.17c and d).Figure 3.17a-d demonstrated a representative of DSC thermograms employed to compare DSF-loaded PLGA NPs, and blank PLGA NPs formulations (Figure 3.17e and f) and to determine if the PLGA NPs are in the amorphous or crystalline state. Figure 3.17e demonstrated a very short peak at 70 ^{o}C, which indicates the melting point of 10% (w/w) DSF-loaded PLGA NPs in 1% sucrose. The peaks detected from the DSC thermogram of DSF-loaded PLGA NPs formulation indicated the crystalline state of DSF, sucrose, and PLGA (Figure 3.17e). Pure DSF had an intense band compared to the loaded PLGA NPs with a very short band, which indicates DSF encapsulation as there are less un-capsulated DSF bounded on the NPs surface. The unloaded (blank) PLGA NPs formulation was also compared to the DSC thermogram standards and no detection of DSF peak observed, apart from sucrose and PLGA peaks confirming that the blank PLGA NPs were in a crystalline state (Figure 3.17f). As shown in appendix-A, the DSC thermograms of DSF-loaded PLGA NPs developed using the SE method then followed by particle size reduction through the HPH and PS techniques showed similar DSF peak at 70 ^{o}C (Appendix-A, Figure 3.21 and 3.23). Therefore, this indicates a crystalline state. In contrast, appendix-A (Figure 3.22 and 3.24) showed no DSF peaks on the blanks for both NPs reduced by the HPH and PS techniques. The long sharp peak of the DSF standard exhibits the crystalline form of the free drug bounded to the PLGA polymer. The crystalline form of DSF-loaded PLGA NPs was obtained due to the preparation of DSF encapsulated NPs below its melting point. Boyd, et al.,

(2014), developed DSF-loaded vaginal rings at different temperatures to determine the stability of the incorporated DSF using the DSC. Their DSC analysis of DSF-loaded vaginal rings showed a peak at 70 $^{\circ}$C, which indicates a crystalline state, and this was due to the preparation of DSF below its melting point. Figure 3.17b and d demonstrated a typical broad peak of PLGA standard similar to the loaded and unloaded PLGA NPs.
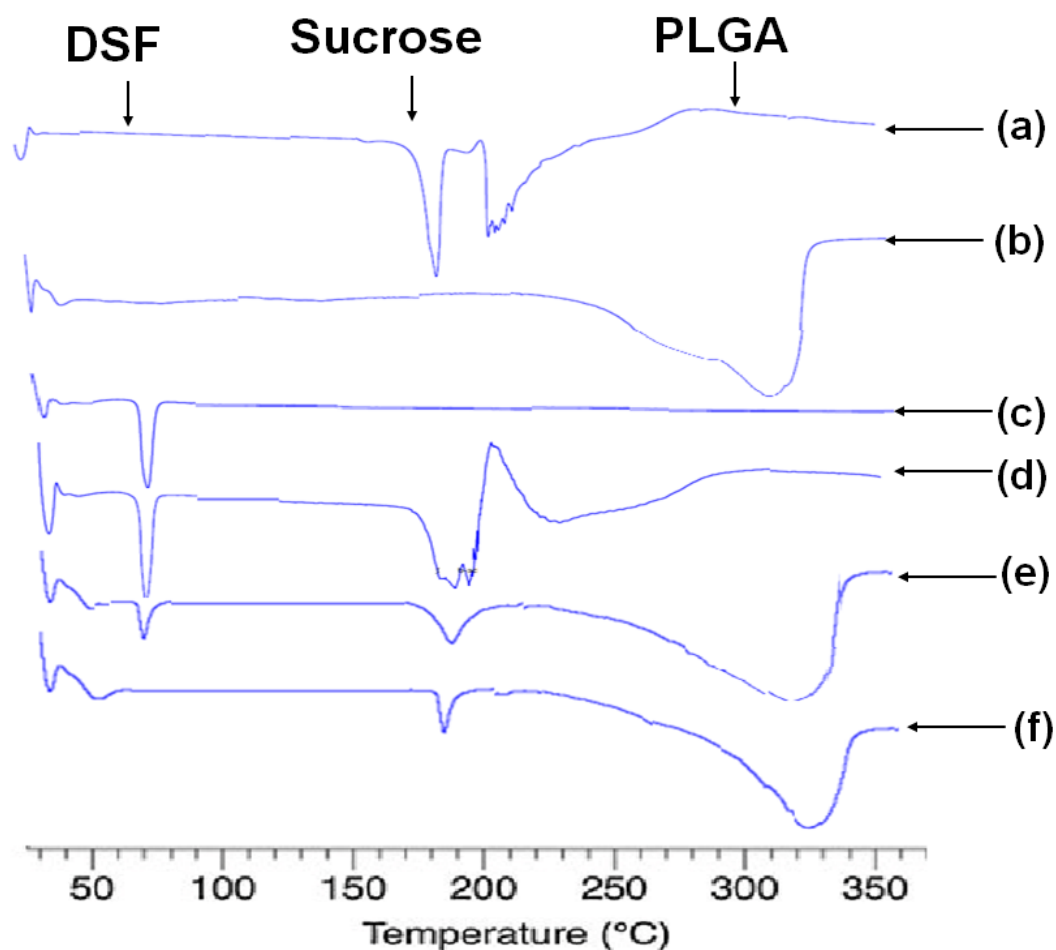
Figure 3.17. A representative of DSC thermal analysis of (a) sucrose standard, (b) PLGA standard, (c) disulfiram (DSF) standard, (d) physically mixed standards of raw DSF, PLGA, and sucrose, (e) DSF-loaded PLGA nanoparticles (NPs), and (f) blank PLGA NPs formulations. Both NPs formulations, and physically mixed standards were prepared in a drug/polymer 1:9 ratio.

3.4.5 Fourier transform infrared spectroscopy

The FTIR spectroscopic analysis of standards, DSF loaded PLGA and unloaded PLGA NPs formulations in 1% sucrose were performed to determine the different molecular

111

interactions (Figure 3.18a-f). As depicted in Figure 3.18c-e, FTIR spectroscopic analysis of DSF standard absorption bands at $2974 cm^{-1}$, $1506 cm^{-1}$, $C-H-CH_3$, $1350-1457 cm^{-1}$, $1273 cm^{-1}$, and $1151-1195 cm^{-1}$, $967-1056 cm^{-1}$, $817-914 cm^{-1}$, and $553-665 cm^{-1}$ were stretching, C-H symmetrical deformation vibrations, CH_2-CH_3 deformation vibrations, C=S stretching, C-N stretching, C-S stretching, S-S dihedral bending, respectively. From Figure 3.18e of the loaded NP exhibited a typical signal characteristic broadband of DSF showing interactions between PLGA and DSF with distinct shift band of PLGA compared to the DSF, and physically mixed standards spectra (Figure 3.18c and d). While the unloaded PLGA NP (blank) formulation exhibited no DSF melting point of chemical interactions (Figure 3.18f). Therefore, the DSF absorption band of the loaded NP confirmed the presence of DSF crystalline state (Figure 3.18e); this was also confirmed by the DSC thermogram in Figure 3.17e. Appendix-A of Figure 3.25 and 27 showed DSF absorption band of developed PLGA NPs by the SE method (reduced particle size by the HPH and PS techniques), which indicates the crystalline state. Appendix-A of Figure 3.26 and 3.28 presents FTIR spectroscopic analysis of PLGA blanks with no DSF absorption band.
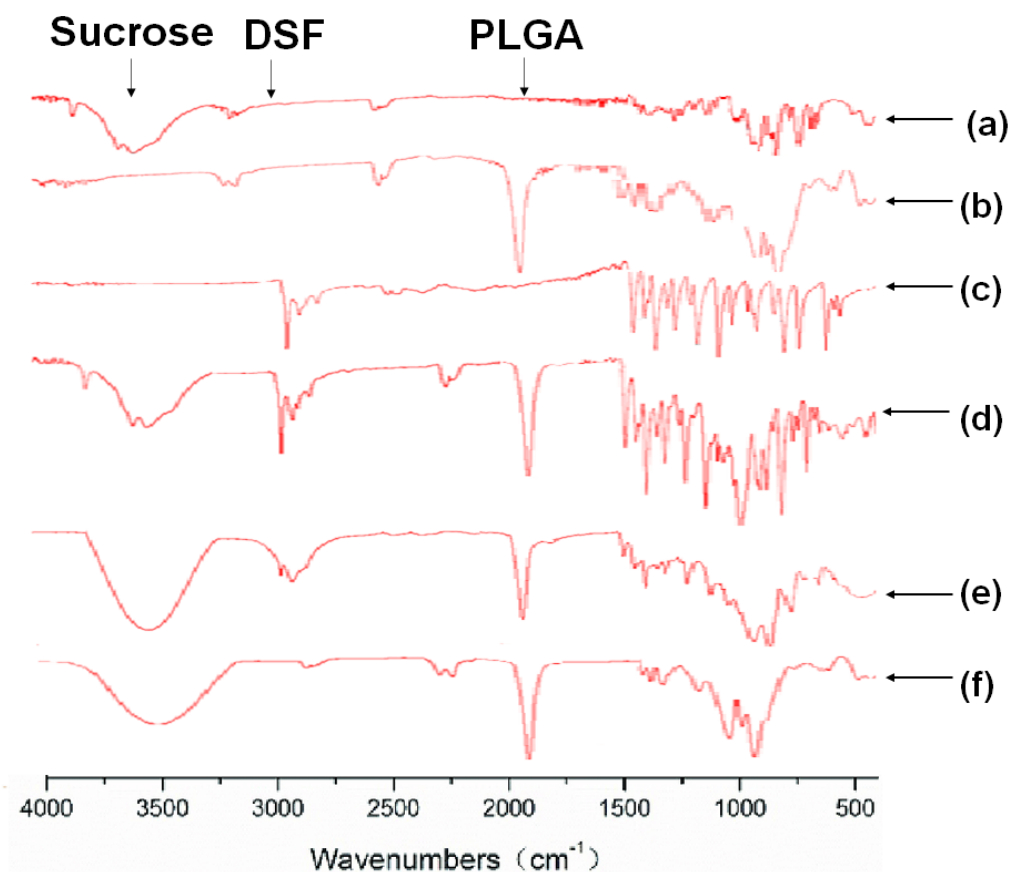
Figure 3.18. A representative of FTIR analysis of (a) sucrose standard, (b) PLGA standard, (c) disulfiram (DSF) standard, (d) physically mixed standards of raw DSF, PLGA, and sucrose, (e) DSF-loaded PLGA nanoparticle (NP), and (f) blank PLGA NP formulations. All NPs formulations were prepared as a drug/polymer 1:9 ratio, and this was applied to the physically mixed standards.

3.4.6 Encapsulation efficiency of DSF-loaded PLGA nanoparticles

As described in chapter 2, a reliable and an efficient method for drug encapsulation efficiency of loaded PLGA NPs has been effectively developed to separate the free DSF (un-encapsulated drug) from the loaded drug (encapsulated NPs).The HPLC method was used to determine the drug contents of the DSF-loaded NPs. However, there are many methods reported to quantify the loaded portion of DSF in NPs (Fasehee, et al., 2016; Song, et al., 2016; Najlah, et al., 2017). Nevertheless, there has been not much detail about the efficiency of these methods in separating the DSF un-encapsulated from the encapsulated DSF NPs. For example, Fasehee, et al., (2016), quantify the encapsulated DSF content by dissolving the loaded NPs in PBS solution with a small amount of the NPs suspension extracted in DMSO to release the

113

encapsulated DSF then adding methanol to precipitate the PLGA polymer. Also, Najlah, et al., (2017) measured percentage encapsulation efficiency by dissolving the loaded NPs in DCM to release DSF and dilute with ethanol to analyze DSF loading efficiency. Therefore, this study has contributed to knowledge by developing a repeatability and reproducibility method that separates the un-encapsulated DSF from the encapsulated DSF-loaded PLGA NPs. Also, this study confirms that the method is effective in separating the DSF un-capsulated from the DSF-loaded PLGA NPs and SLNs. The phenomenon of this efficient method is due to the NPs/SLNs insoluble in cold methanol (PLGA NPs and SLNs are easily precipitates in cold methanol) and allowing un-encapsulated DSF to dissolve in cold methanol freely. This method provided a simple separation for DSF-loaded PLGA NPs samples to be washed gently by ice-cold methanol to remove the un-encapsulated DSF.

The loading efficiency of DSF NPS prepared by the D-Nano-Pr method demonstrated a significantly ($p < 0.05$) increased drug loading effect and was considered superior compared to the SE method followed by particle size reduction using the HPH and PS techniques (Figure 3.19). While the particle size reduction by the HPH and PS techniques showed no significant ($p > 0.05$) change in percentage drug encapsulation efficiency from each other. The mechanical force used for particle size reduction may have caused reduce percentage encapsulation efficiency. As ascribed in Figure 3.19, the energy force applied to reduce particle size causes the drug to diffuse out during sonication/shear forces (O'Donnell and McGinity, 1997).
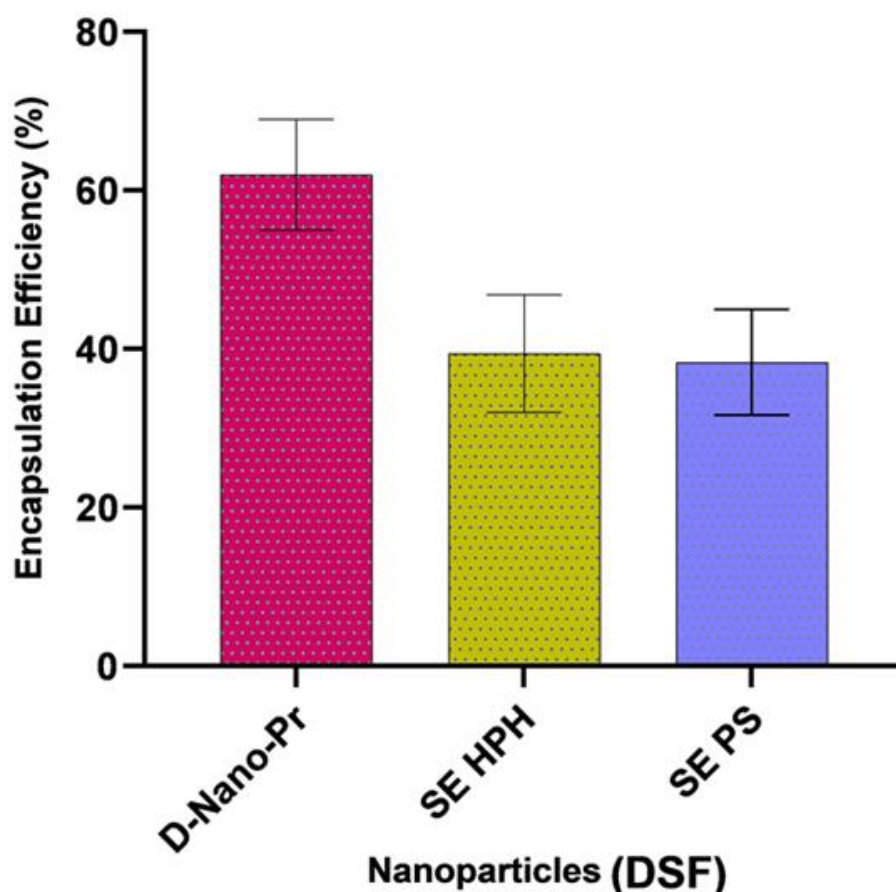
Figure 3.19. Demonstrating mean percentage encapsulation efficiency for DSF-loaded PLGA NPs prepared by using the D-Nano-Pr and SE methods (particle size reduced by the HPH and PS techniques) (Mean ± SD, n=3).

3.4.7 Cumulative release of DSF from DSF-loaded PLGA nanoparticles

The *in vitro* release study was performed using a dialysis bag to compare the cumulative release of free DSF and DSF-loaded PLGA NPs (Figure 3.20). As shown in Figure 3.20, the experimental results of the DSF release were compared to the free DSF solution. The incubated *in vitro* DSF release was determined by measuring the cumulative release of DSF solution under PBS (phosphate buffer solution, pH 7.4) with 1% Tween80 at 37 °C for 24 hours. The percentage encapsulation efficiency values for loaded PLGA NPs formulations were used to calculate the cumulative percentage release of free DSF and loaded PLGA NPs. As shown in Figure 3.20, the release profiles of the free DSF and DSF-loaded PLGA manufactured by using the SE method then reduced particle size through the HPH technique demonstrated a much faster

115

release than the DSF-loaded PLGA NPs manufactured by the D-Nano-Pr method and SE method of the PS technique. Approximately, 98% of DSF was released from the free DSF after being immersed for 24 hours, which indicates the free DSF is unable to maintain a sustained release. As ascribed in Figure 3.20, NPs manufactured by the D-Nano-Pr method incubation for24 h had 54% of DSF cumulative release. While DSF-loaded PLGA NP formulation manufactured by using the SE method with particle size reduced through the HPH and PS techniques showed increased cumulative release of DSF at 94% and 75%, respectively (Figure 3.22). Loaded PLGA NPs reduced using the SE method followed by particle size reduction through the HPH and PS techniques, demonstrated DSF release at an initial burst within 30 and 60 minutes, respectively. The mechanical force might have affected the loaded PLGA NPs formulation during particle size reduction. As ascribed in Figure 3.19 showing low drug encapsulation for loaded PLGA NPs formulations of the SE method followed by particle size reduction through the HPH and PS techniques can be attributed to the considerable amount of free drug (bounded drug to the surface of the NPs) during preparation and particle size reduction process. As a result, the relatively rapid release of the free drug compared to that of the NPs manufactured by using the D-Nano-Pr method showed more extended drug release, and this is regardless of the unloaded drug bounded to the loaded PLGA NPs. Therefore, the loaded NPs prepared by the D-Nano-Pr method might be able to protect the drug for a more extended period and allow the sustainable release of DSF for 24 hours.
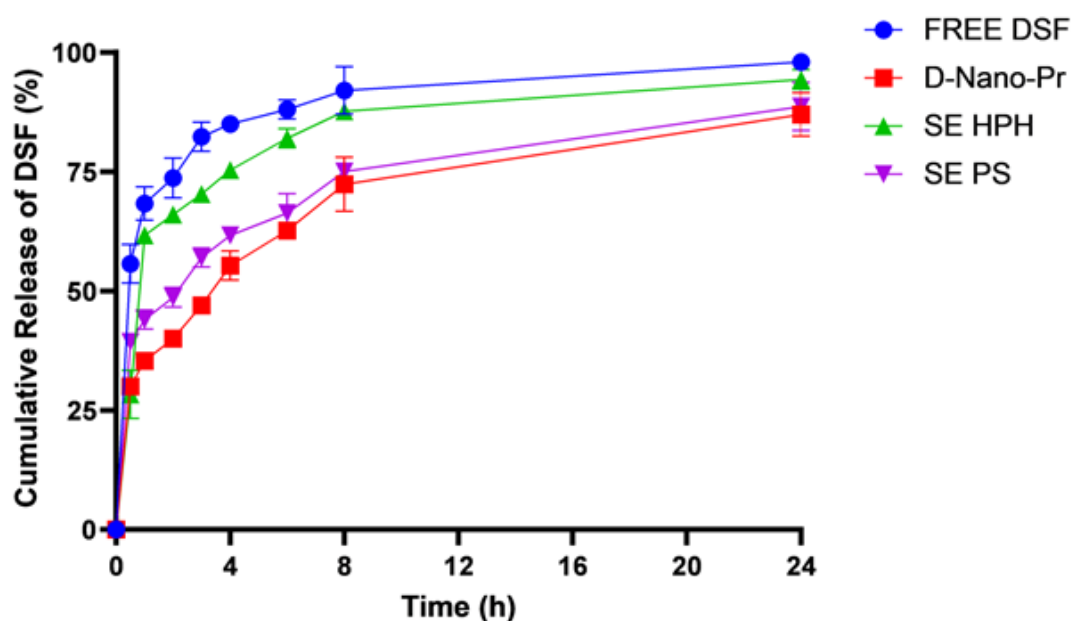
Figure 3.20. Cumulative release of the free DSF and DSF-loaded PLGA NPs re-suspended in PBS with 1% Tween 80 solution using a dialysis membrane. The DSF-loaded NPs were prepared by using the D-Nano-Pr method and SE method followed by particle size reduction through the HPH and PS techniques (Mean ± SD, n=3).

3.5 Conclusion

PLGA-based nano-carrier systems have been widely studied due to their many advantages for drug delivery. This study developed efficient methods used to fabricate unloaded PLGA and DSF-loaded PLGA NPs using different manufacturing methods/techniques. The data obtained after NPs characterization demonstrated that the two water-miscible organic solvents with the right, proportional volume showed superiority. It produces small particle size, uniform particle shape, high charged surface particle, increased encapsulation efficiency and sustainable drug release compared to the SE method followed by particle size reduction through the HPH and PS techniques.

Also, selecting the right choice of hydrolyzed PVA stabilizer effected particle size and zeta potential. However, the low DSF encapsulation efficiency on reduced particle size

117

NPs through the HPH and PS techniques was due to the energy force applied after the development of DSF-loaded NPs formulations by using the SE method. Therefore, this affected the release profile of DSF, causing an early burst of the biodegradable DSF-loaded PLGA NPs. This study confirms for the first time the development of an efficient method that can be used to quantify the amount of un-encapsulated drug bounded to the polymer and the amount of encapsulated drug for all NPs formulations manufactured by the D-Nano-Pr and SE methods.

The D-Nano-Pr method was superior for its production of smaller particle size, narrow PDI, positively charged surface particle, increased drug loading, and sustainable drug release. Finally, due to the lack of mechanical energy force, the PLGA NPs developed by the D-Nano-Pr method potentially prolong DSF half-life, and then improve its stability and enhance bioavailability.

Chapter 4: Development and Characterisation of Disulfiram-Loaded PLGA PEGylated Nanoparticles by the Direct Nanoprecipitation Method, and *In Vitro* Cytotoxicity on Breast Cancer Cells

4.1 Introduction

This study will make use of adjustable ratios of PLGA, PCL, and encapsulated DSF coated with $mPEG_{2k}$-PLGA or DSPE PEG_{2k} NPs fabricated by using the D-Nano-Pr method. Freshly manufactured DSF NPs were characterized to determine particle sizes, PDI, zeta potential, thermal degradation using differential scanning calorimetry (DSC), and functional group confirmation of chemical compounds using Fourier transform infrared spectroscopy (FTIR). The use of HPLC method evaluated the percentage encapsulation efficiency, cumulative drug release and stability studies (in horse serum media) of DSF NPs.

4.2 Aims

To manufacture DSF loaded PLGA NPs using adjustable mixed ratios of biodegradable polymeric materials (PCL and PEG-PLGA) for enhanced drug biostability using D-Nano-Pr method. DSF NPs will be PEGylated using $mPEG_{2k}$-PLGA or DSPE PEG_{2k} to enable DSF long circulation and improve cellular interaction by increasing drug cytotoxicity on cancer cells.

4.3 Experimental Design

The D-Nano-Pr method was adapted from Ford, et al., (2015) as previously mentioned in chapter 3, to prepare the following named NPs, DNP1 (PLGA/DSF), DNP2 ($mPEG_{2k}$-PLGA/PLGA/DSF), DNP3 (DSPE PEG_{2k}/PLGA/DSF), DNP4 ($mPEG_{2k}$-PLGA/PLGA/PCL/DSF), and DNP5 (PLGA/PCL/DSF) which includes the corresponding blank (unloaded DNP1E-DNP5E NPs) NPs, (Table 4.1). The method of preparation was described in section 2.2.1.1. The following PEGs, $mPEG_{2k}$-PLGA or DSPE PEG_{2k} were selected to compare their stability, release profile and *in vitro* long circulation of the encapsulated DSF in cancer cells. Also, to investigate the effect of

120

polymeric and phospholipid PEGs on the surface charge of the nanoparticle or lipid-based nanoparticle.

Table 4.1. Different formulation ratios of disulfiram (DSF) loaded PLGA with polycaprolactone (PCL), and PEGylated nanoparticles were manufactured by the direct nanoprecipitation (D-Nano-Pr) method.

Ingredient (ratio) / Formulation*	PLGA	PCL	mPEG$_{2k}$-PLGA	DSPE PEG2k	DSF	Total
DNP1E	10	-	-	-	-	10
DNP1	9	-	-	-	1	10
DNP2E	9.5	-	0.5	-	-	10
DNP2	8.5	-	0.5	-	1	10
DNP3E	9.5	-	-	0.5	-	10
DNP3	8.5	-	-	0.5	1	10
DNP4E	4.5	4.5	0.5	-	-	10
DNP4	4.25	4.25	0.5	-	1	10
DNP5E	5	5	-	-	-	10
DNP5	4.5	4.5	-	-	1	10

*DNP represented nanoparticles (NPs) of different formulations prepared by using the direct nanoprecipitation (D-Nano-Pr) method. E denotes the empty NPs of different formulations.

Prepared NPs were also characterized by drug encapsulation efficiency, drug release profiles, and drug stability in horse serum. As described in section 2.2.7.2, the *In vitro* cytotoxicity was performed against MCF 7, MDA-MB-231 and MDA-MB-231$_{PTX10}$ breast cancer cells using MTT assay.

4.4 Results and discussion

4.4.1.1 Size, PDI, surface morphology and zeta potential of the PEGylated nanoparticles

Previous results in chapter 3 of the manufactured DSF-loaded PLGA NPs by using the D-Nano-Pr method showed superiority over the SE method, followed by a size reduction of NPs using the HPH and PS techniques. Therefore, in this study, the D-

Nano-Pr method was selected to prepare PEGylated, and non-PEGylated DSF-loaded NPs (Table 4.1).

As ascribed in Figure 4.1, PEGylated and non-PEGylated PLGA NPs were prepared in a binary mixture (acetone/methanol, 3:1) with a drug to polymer ratio 1:9 showed an average particle size ranging from 172.5 ± 12.56 nm to 224.5 ± 25.46 nm. This is similar to the published results for DSF NPs developed by using the D-Nano-Pr method (Fasehee, et al., 2016). The formulation of DNP1 NP showed non-significant ($p > 0.05$) effect on the particle size of DNP2, DNP3, and DNP4 NPs (Figure 4.1). More explicitly, using mPEG$_{2k}$-PLGA for PEGylation in DNP2 NP had a significant ($p < 0.05$) decreased particle size compared to DNP5 NP (Figure 4.1). Previous studies have demonstrated that using PCL enhanced DSF stability, due to slow degradation dependent on the molecular weight (Löbler, et al., 2009). Similar findings of the increased particle size of the combined PLGA and PCL were previously reported (Fasehee, et al., 2016; Najlah, et al., 2017; Wang, et al., 2017).

In addition, DNP1 NP demonstrated significant ($p < 0.05$) decreased particle size than the DNP5 NP (Figure 4.1). Moreover, previous studies have suggested the strategy of coating a surface particle with mPEG$_{2k}$-PLGA, or DSPE-PEG$_{2k}$ forms protection of NPs from opsonization and prevent the initial clearance by the RES and enhanced permeability retention (EPR) effects (Immordino, Dosio and Cattel, 2006). A recent study showed developed PEGylated (mPEG$_{2k}$-PLGA DSF-loaded PLGA NPs) NPs demonstrating passive targeting to trigger potent anticancer effects into tumour-bearing nude mice. It, therefore, enhanced sustainable drug release via the EPR effect (Madala et al., 2018). The use of PEGylated NPs is to overcome opsonization of the hydrophobic negatively charged bared PLGA NPs vulnerable to rapid clearance from blood circulation (Sheng et al., 2009). This shows that PEGylated NPs are capable of

protecting DSF from the rapid removal of bared NPs in the circulatory system, which might affect DSF delivery into cancer cells.

Mostly, loaded NPs were larger than its corresponding blank (DNP1E-5E) NPs, and this might be the effect of the drug embedded within the polymeric matrix and adsorbed on the surface during the nanoprecipitation formulation process. DNP1E NP showed significant ($p < 0.05$) decreased particle size than DNP3E (DSPE PEG$_{2k}$ PLGA NPs) NP, and this is due to the presence of the functionalized DSPE PEG$_{2k,}$ phospholipid coated onto the PEGylated DNP3E NP than being part of the particle structure produces larger particle size. In addition, the bifunctional DSPE-PEG$_{2k}$ with its hydrophobic chain inserted into the lipid membrane and the hydrophilic end extends to the surface in forming a thick hydrogel layer (Dos Santos, et al., 2007; Salvador-Morales, et al., 2009). Also, DNP1E NP demonstrated a significantly (*P < 0.05*) decreased particle size compared to DNP4E NP, which mPEG$_{2k}$-PLGA introduction produces a large particle size. The increased particle size of DNP4E NP shows confirmation of mPEG$_{2k}$-PLGA coating on NP surface (similar PEGylation to that of DNP2E NP). Adding PCL to DNP5E NP formulation showed no significant ($p > 0.05$) change on the particle size for DNP1E NP. On the other hand, DNP2E NP produces no significant ($p > 0.05$) change on particle size over DNP3E NP. PEGylated blanks of DNP2E and DNP3ENPs demonstrated no effect regardless of the different types of PEGs attached to the particle surface (Figure 4.1). However, the DNP2E NP demonstrated a significantly (*P < 0.05*) decreased particle size than the DNP4E NP. The PEGylated blank of DNP2E NP without PCL was expected to maintain decreased particle size than DNP4E NP with PCL present. The non-differences for both DNP2E and DNP4E NPs, therefore, indicate the use of less PLGA (PLGA/PCL, with a 1:1 ratio) of DNP4E NP (Figure 4.1). DNP2E NP had a significant ($p < 0.01$) decreased particle size than DNP5E NP. Also, the interaction between PLGA and mPEG$_{2k}$-PLGA might

123

have caused the decrease in particle size. The non-significant ($p > 0.05$) effect of particle size between DNP1E and DNP2E NPs confirm a similar polymeric interaction of mPEG$_{2k}$-PLGA in both formulations. For this reason, the presence of PCL on DNP4E NP makes no difference in particle size.

DNP3E NP demonstrated a significantly ($P < 0.05$) decreased particle size than DNP4E and DNP5E NPs (Figure 4.1). DNP3E NP decreased particle size might be explained by the interaction between PLGA and DSPE-PEG$_{2k}$. While the DNP4E NP showed a significantly ($P < 0.05$) increased particle size compared to the DNP5E NP (Figure 4.1). Also, the increase in particle size of DNP4E NP is due to the introduction of mPEG$_{2k}$-PLGA as supposed to the absence of mPEG$_{2k}$-PLGA on the DNP5E NP, which causes decreased particle size.
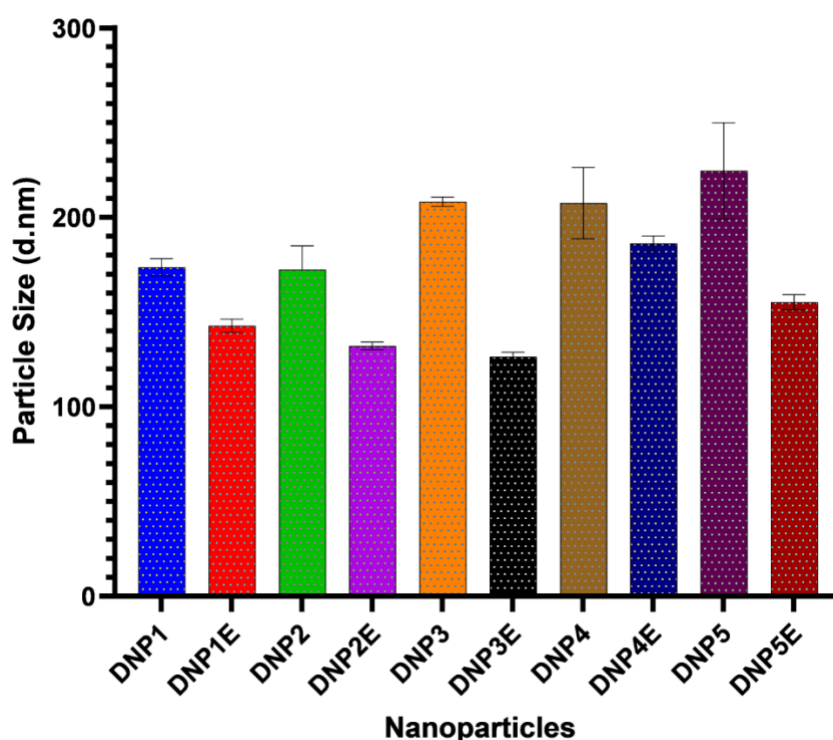
Figure 4.1. Particle sizes of DSF-loaded PLGA (DNP1 to DNP5 NPs) and unloaded PLGA (DNP1E to DNP5E) nanoparticles with a 1:9 drug/polymer ratio were prepared in different organic solvents by using the D-Nano-Pr method (Mean ± SD, n=3).

All DSF NPs showed a narrow size distribution (PDI < 0.3) regardless of drug loading and PEGylationon NPs surface (Figure 4.2). The results obtained are consistent with the published kinds of literature (Song, et al., 2016; Wang, et al., 2017). DNP1 NP had no significant (p > 0.05) change on PDI particle size distribution compared to the DNP2 NP (Figure 4.2). This is different for DNP1 NP, showing a significant (p < 0.05) decreased PDI particle size distribution compared to the DNP3, DNP4, and DNP5 NPs (Figure 4.2). While, the DNP2 NP showed a significantly ($P < 0.05$) decreased PDI particle size distribution compared to DNP3, DNP4, and DNP5 NPs (Figure 4.2). DNP3 NP had no significant (p > 0.05) change on PDI particle size distribution compared to the DNP4 and DNP5 NPs. Similarly, no significant (p > 0.05) difference in PDI observed between DNP4 and DNP5 NPs (Figure 4.2).

In contrast, the PDI blank NPs are significantly lower than loaded NPs, and this is except for the blank, DNP2E NP having no significant effect than the loaded DNP2 NP (Figure 4.2). Adding the drug to the formulation resulted in a high increase PDI which indicates the tendency for NPs to aggregate after drug loading. Nevertheless, the reason is still not very clear, especially when no significant changes observed in zeta potential values after drug loading with exception to DNP4E and DNP4 NPs (Figure 4.3). The zeta potential values had no major changes overall formulations (all below -30 mV) apart from significant, but not effective, drop for DNP4 and DNP4E NPs with zeta potential values of -28.7 mV, and 26.6 -mV, respectively. There is no unambiguous evidence on the impact of different composition, PEGylation, or drug loading (Figure 4.3). The unloaded DNP1E NP, demonstrated non-significant (p > 0.05) change on zeta potential value compared to the DNP2E, DNP3E, and DNP5E NPs. Except for DNP1E NP, which shows a significantly ($P < 0.05$) increased zeta potential value than DNP4E NP. The decrease in zeta potential is due to the addition of the positively charged amphiphilic polymer ($mPEG_{2k}$-PLGA) reducing the negative

charged PLGA (Figure 4.3). No significant ($p > 0.05$) change on zeta potential value observed between DNP2E and DNP3E NPs. The DNP2E NP showed a significantly ($P < 0.05$) increased zeta potential than the DNP4E NP. Also, the DNP3E NP had a significantly ($p < 0.01$) increased zeta potential than the DNP4E NP. While the DNP4E NP had a significantly ($P < 0.05$) decreased zeta potential value than the DNP5E NP. This might be due to the presence of the mPEG$_{2k}$-PLGA polymer used to modify the bared DSF-loaded PLGA/PCL NP.
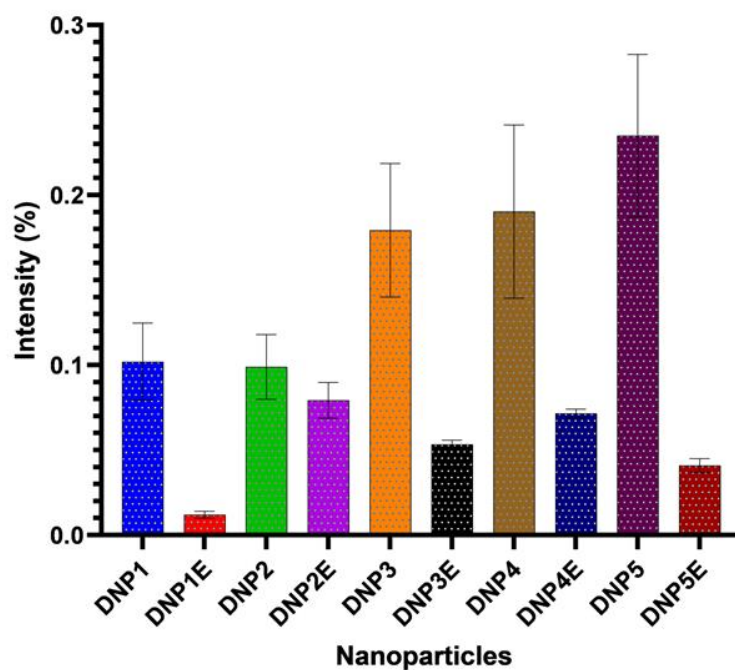
Figure 4.2. Polydispersity index (PDI) of the non-PEGylated and PEGylated blanks and DSF-loaded PLGA NPs with a 1:9 drug/polymer ratio were prepared by using the D-Nano-Pr method (Mean ± SD, n=3).
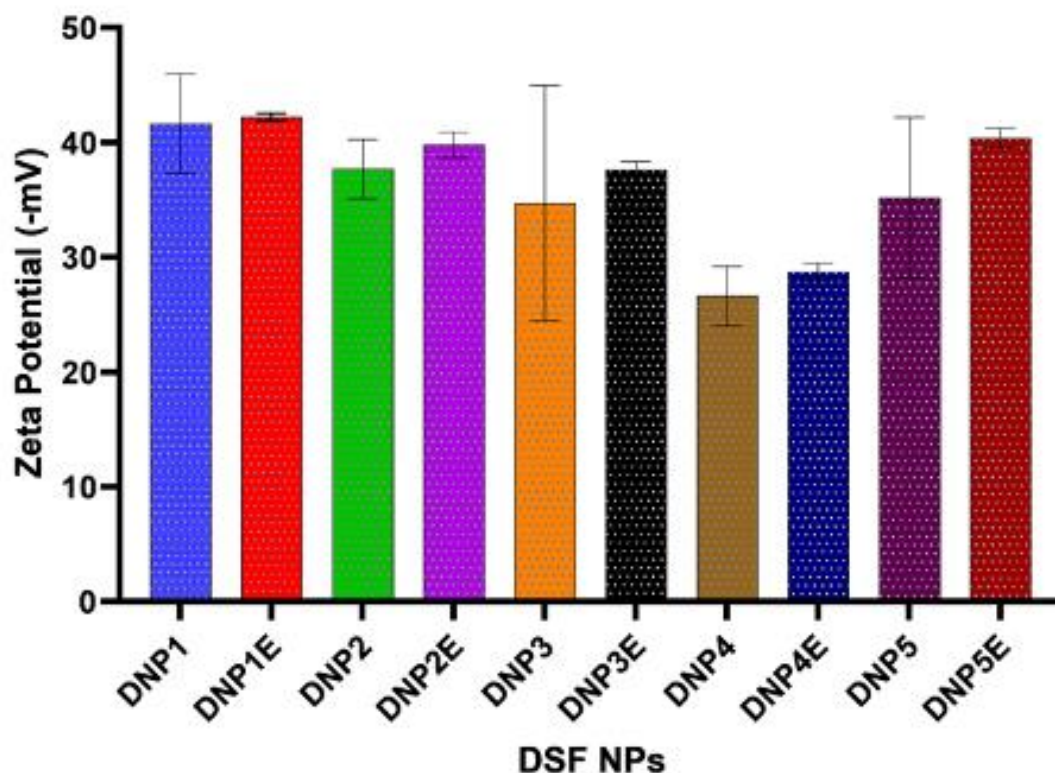
Figure 4.3.The zeta potential of the non-PEGylated and PEGylated blanks and DSF-loaded PLGA NPs with a 1:9 drug/polymer ratio were prepared by using the D-Nano-Pr method (Mean ± SD, n=3).

The morphology of NPs was examined by scanning electron microscopy (SEM) as shown in Figure 4.4-4.9. The SEM images demonstrated DSF-loaded and unloaded NPs have well-defined spherical particles with smooth surface and diameter size ranging from 200 nm to 300 nm. For example, Figure 4.4 shows blank, DNP1E NP of particle sizes mostly at 300 nm compared to the corresponding zeta sizer measurement at 143.5 ± 2.22 nm. The difference in particle sizes between the SEM and zeta sizer based on the particulate estimation of the diameter for a solid NP (dried state) under a high vacuum. Whereas, using the Stokes-Einstein equation, the zeta sizer can be employed to measure the particle size of NPs through the diffusion coefficient of particulate in suspension (Ito, et al., 2004). Figure 4.5-4.8 demonstrated moderately monodispersed particle size distribution with a size of 200 nm for DNP1

NP. SEM images relatively confirm the measured sizes and PDIs of the monodispersed particle size distribution for all NPs. For instance, Figure 4.9 shows a "zoom-out" picture of DNP5 NPs, uniformly size distributed smooth particles that tend to aggregate like clustered sand.
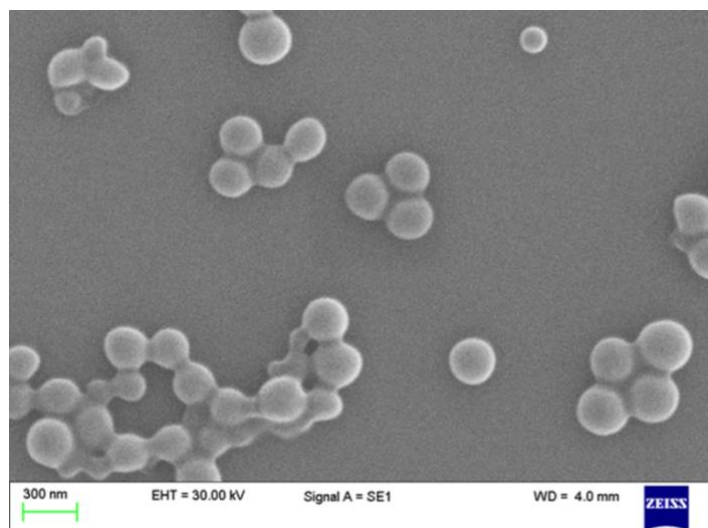
Figure 4.4. Scanning electron microscope (SEM), demonstrating the surface morphological images of DNP1E NP (unloaded PLGA NP) prepared by using the D-Nano-Pr method.
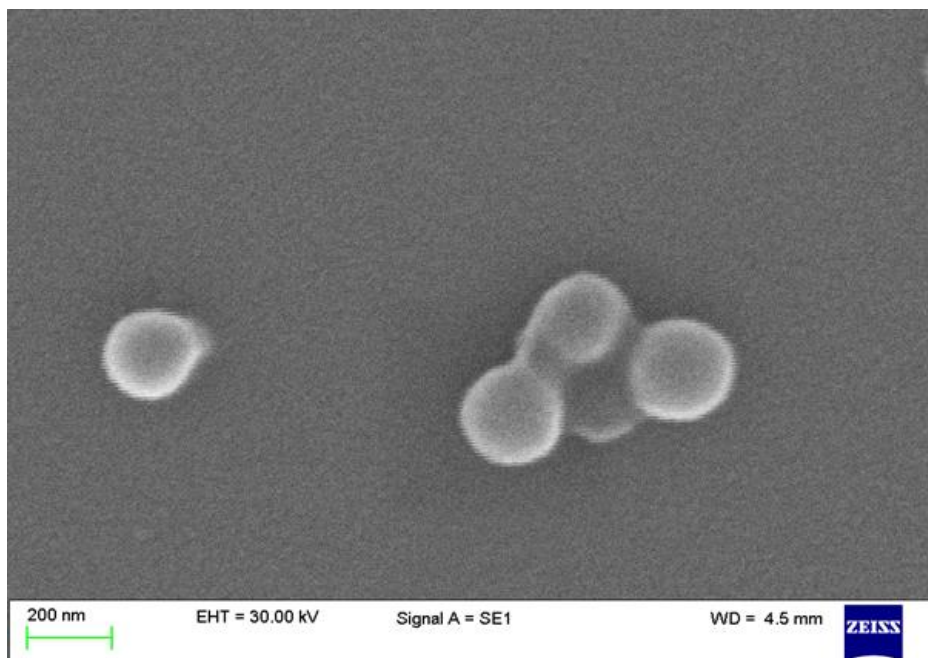
Figure 4.5. Scanning electron microscope (SEM), demonstrating the surface morphological images of DNP1 NP (DSF-loaded PLGA NP) prepared by the D-Nano-Pr method.
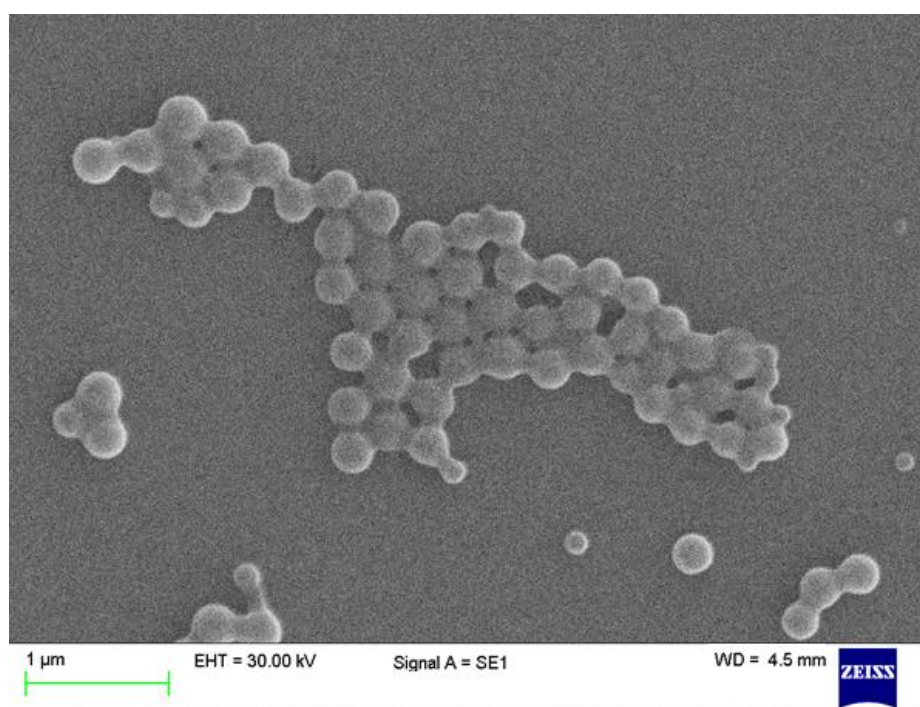
Figure 4.6. Scanning electron microscope (SEM), demonstrating the surface morphological images of DNP2NP prepared by the NPs D-Nano-Pr method.
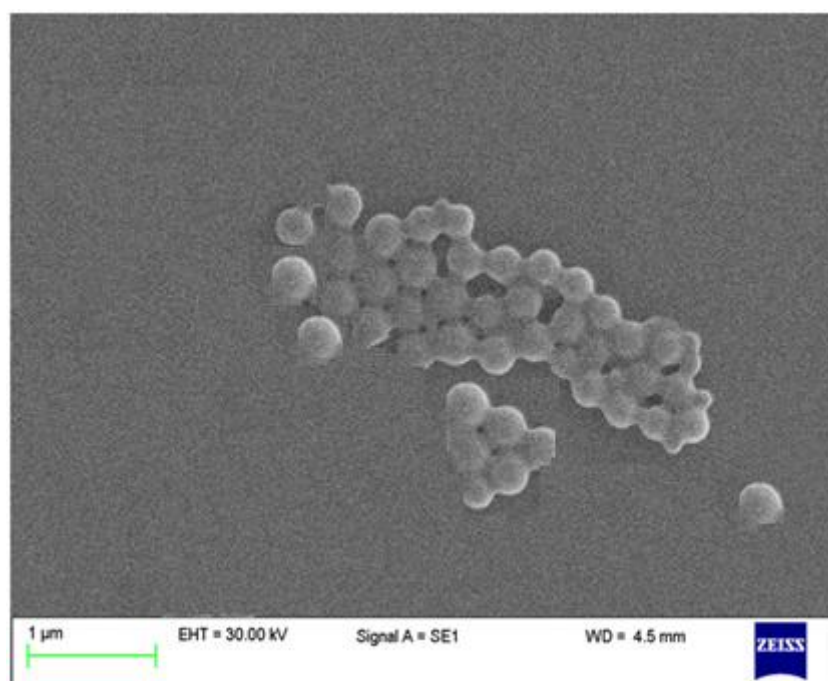
Figure 4.7. Scanning electron microscope (SEM), demonstrating the surface morphological images of DNP3 NP prepared by the D-Nano-Pr method.
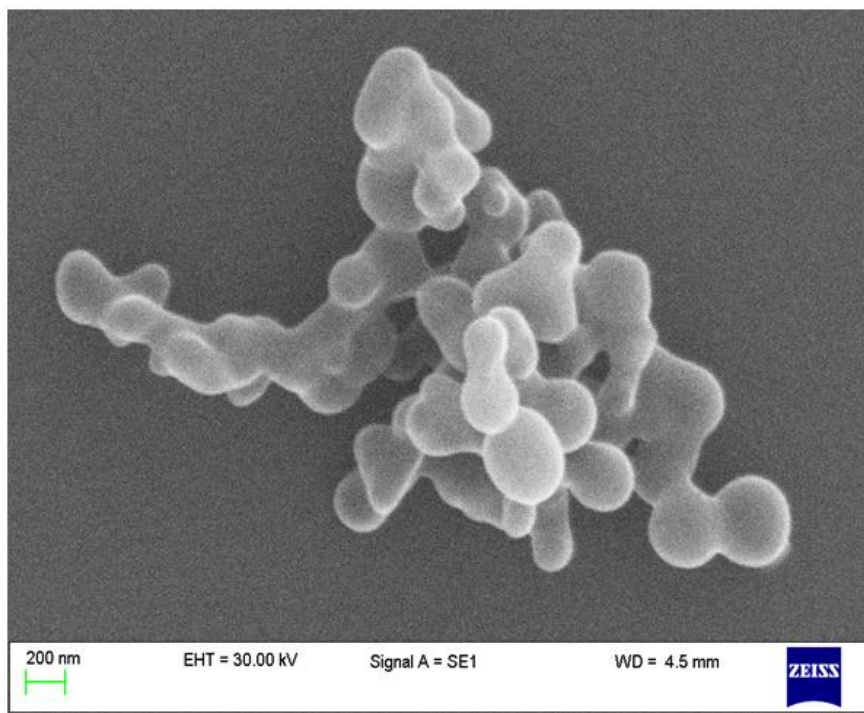
Figure 4.8**.** Scanning electron microscope **(**SEM), demonstrating the surface morphological images of DNP4 NP prepared by the D-Nano-Pr method.
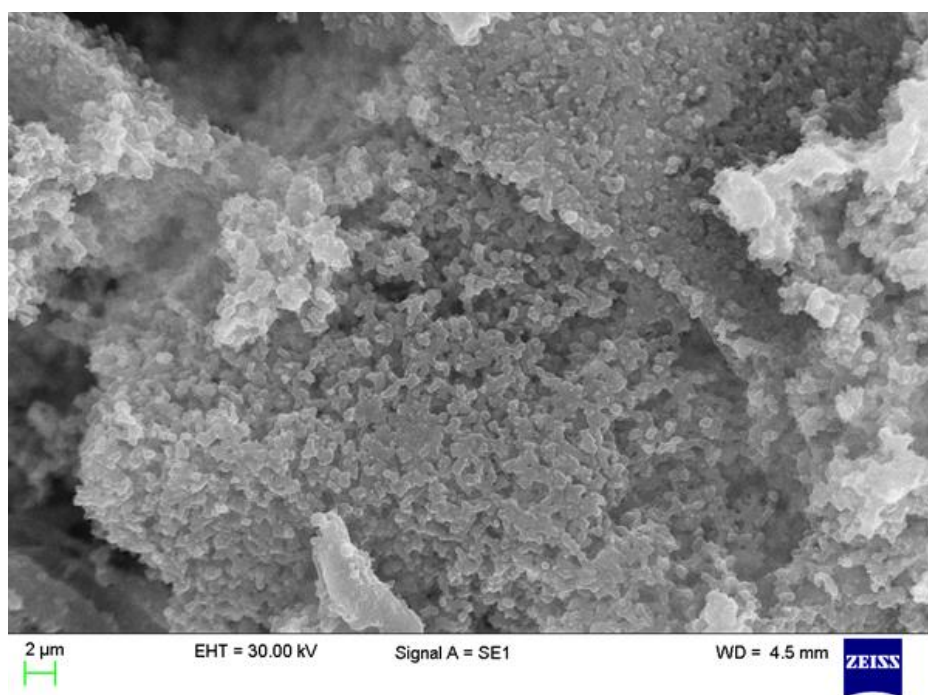
Figure 4.9. Scanning electron microscope (SEM), demonstrating the surface morphological images of DNP5 NP developed by using the D-Nano-Pr method.

4.4.1.2 Differential scanning calorimetry

Differential mechanical strengths of the blanks and loaded DSF NPs formulations were evident from DSC spectra analysis performed to determine the stability of NPs as a crystalline or amorphous state. An equal amount of measurement for standards and NPs were used to define their physical states and detect drug-polymer interactions under consistent heat flow. Representative DSC thermograms of pure DSF, PLGA, PCL, mPEG$_{2k}$-PLGA, DSPE-PEG$_{2k}$, sucrose, physical mixture (DSF, PLGA, PCL, mPEG$_{2k}$-PLGA, DSPE-PEG$_{2k}$, and sucrose) and NPs showed individual endothermic peaks (Figure 4.10). DSC thermograms of PLGA, PCL, mPEG$_{2k}$-PLGA, DSPE-PEG$_{2k}$ and sucrose standards demonstrated endothermic peaks at temperature range tested. The DSF and physical mixture standards exhibited an endothermic peak at 70 ^{o}C used to compare DSC thermograms of the blanks (unloaded NPs) and loaded NPs (Figure 4.10). Loaded NPs showed a small endothermic peak at 70 ^{o}C compared with pure DSF and physical mixture having a typically sharp and long DSF peaks (Figure 4.10). The endothermic peak at 70 ^{o}C confirms DSF crystalline state and its encapsulation to the PLGA polymer indicated a PLGA shift of the loaded NPs formulations which demonstrates DSF interaction with the PLGA polymeric material. Previous studies, showed the DSF endothermic melting peak at 70°C, indicates DSF incorporation in the matrix of the nano-carrier system as a crystalline form (Boyd, et al., 2014). The DSC thermograms of the non-PEGylated and PEGylated DSF-loaded PLGA NPs formulations present a crystalline state in a homogeneous dispersion of the PLGA matrix. Also, Figure 4.10 showed a broad endothermic melting peak of PLGA loaded and unloaded NPs. However, Figure 4.10-i showed thermogram of DNP1E NP without DSF peak when compared to the DSF standard peak (Figure 4.10-c).As shown in appendix-B; DSC thermograms of the loaded DNP3 NP (Figure 4.18), DNP4 NP (Figure 4.20), and DNP5 NP (Figure 4.22) showed a DSF peak at 70 ^{o}C. While the

corresponding unloaded (blanks) DNP3E NP (Figure 4.19), DNP4E NP (Figure 4.21), and DNP5E NP (Figure 4.23) demonstrated non-DSF peak.DSC thermograms suggested the encapsulated DSF nano-carrier systems were in crystalline form as the glass transition temperature was the same as the standard drug (Mainardes, Gremião and Evangelista, 2006; Mello and Ricci-Júnior, 2011).
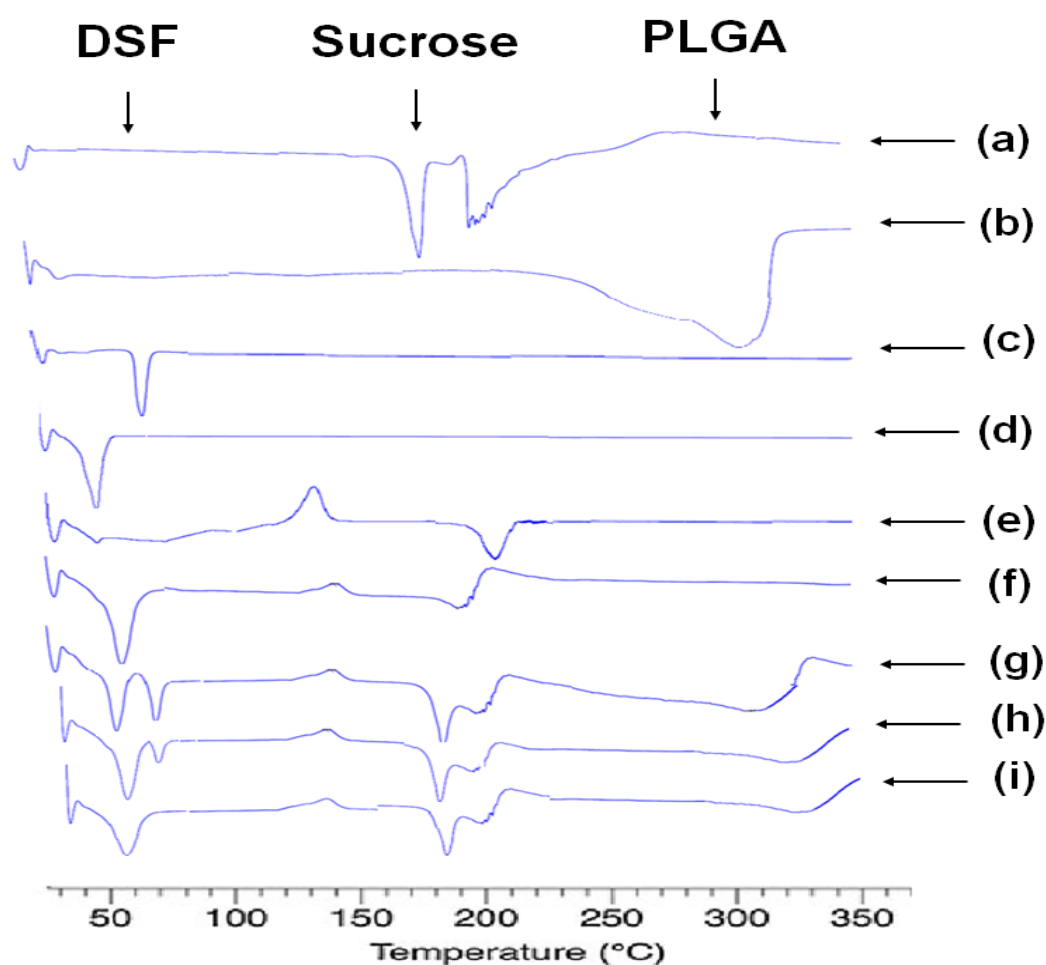
Figure 4.10. A representative of DSC thermal analysis of (a) sucrose standard, (b) PLGA standard, (c) disulfiram (DSF) standard, (d) PCL standard, (e) mPEG$_{2k}$-PLGA standard(f),DSPE PEG$_{2K}$ standard (g) physically mixed standards of raw DSF, PLGA, DSPE PEG$_{2K}$, mPEG$_{2k}$-PLGA, and sucrose, (h) DSF-mPEG$_{2k}$-PLGA loaded PLGA nanoparticle (NP), and (i) blank mPEG$_{2k}$-PLGA PLGA NPs formulations. Both NPs formulations, and physically mixed standards were prepared in a drug/polymer 1:9 ratio by using the D-Nano-Pr method.

4.4.1.3 Fourier transform infrared spectroscopy

FTIR analysis was employed to evaluate the occurrence of any chemical interaction of the loaded NPs between the drug and polymeric materials. FTIR spectrum of the unloaded (DNP2E-i NP) NP shown in Figure 4.11 had no DSF peak. In chapter 3, PLGA was the only polymer used to encapsulate DSF. At the same time, Figure 4.11d-f showed the addition of the following standards, mPEG-PLGA$_{2k}$, DSPE-PEG$_{2k}$, and polycaprolactone (PCL). Therefore, the PEGs and PCL polymer standards were added to compare to the prepared NPs by the D-Nano-Pr method. The DSF-loaded NPs of DNP2 NP in Figure 4.11-h demonstrated a sharp and broad vibrational DSF peak at 2974 cm^{-1} corresponding to the methyl (CH$_3$) stretching vibration compared to the unloaded DSF and mixed standards. This is an indication that DSF appeared in a crystalline form. FTIR spectra of DSF-loaded NPs indicated the incorporation of DSF demonstrated typical methyl stretching broad vibrational peaks of DSF and polymer interaction occurred in the nano-carrier system. Appendix-B showed FTIR spectroscopic analysis of DNP3 NP (Figure 4.24), DNP4 NP (Figure 4.26), and DNP5 NP (Figure 4.28) showed DSF peak at 70 ^{o}C, but the DNP3E NP (Figure 4.25), DNP4E NP (Figure 4.27), and DNP5E NP (Figure 4.29) show no DSF peak.
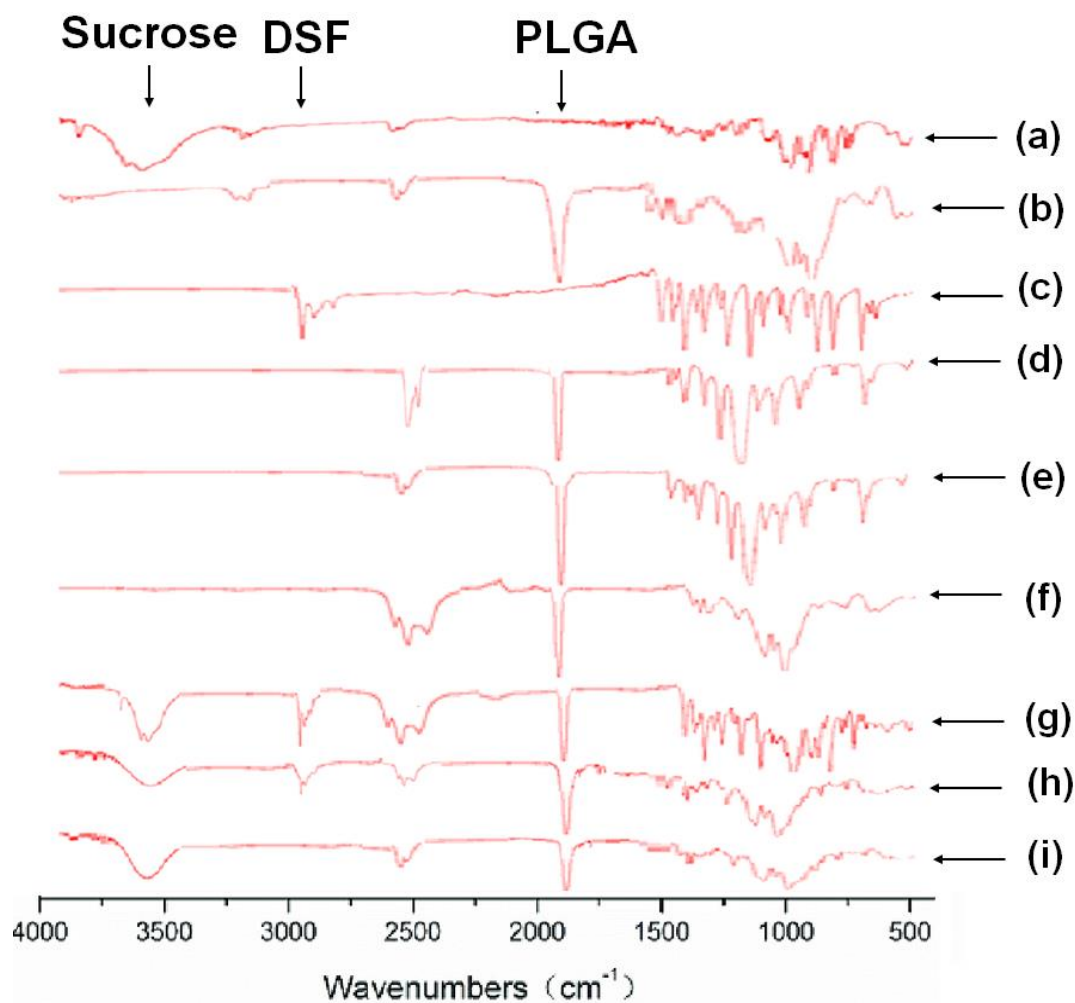
Figure 4.11. A representative of FTIR analysis of (a) sucrose standard, (b) PLGA standard, (c) disulfiram (DSF) standard, (d) PCL standard, (e) mPEG$_{2k}$-PLGA standard,(f) DSPE PEG$_{2K}$ standard, (g) physically mixed standards of raw DSF, PLGA, DSPE PEG$_{2K}$, mPEG$_{2k}$-PLGA, and sucrose, (h) DSF- mPEG$_{2k}$-PLGA loaded PLGA nanoparticle (NP), and (i) blank mPEG$_{2k}$-PLGA PLGA NPs formulations. Both NPs formulations and physically mixed standards were prepared in a drug/polymer 1:9 ratio by using the D-Nano-Pr method.

4.4.1.4 Encapsulation efficiency of DSF-loaded PLGA nanoparticles

Drug percentage encapsulation efficiency plays a vital role in drug delivery of nano-carrier systems as it determines the feasibility of the formulation for clinical application. As shown in Figure 4.20, DNP1 NP had a reasonable percentage encapsulation efficiency of 54% ± 1.41with a significant ($p < 0.05$) decreased drug encapsulation compared to the higher drug encapsulation of the DNP5 NP. Regardless of the method used to determine drug encapsulation. The reported results in the literature show

cytotoxicity effects of manufactured DSF loaded PLGA NPs on breast cancer cells demonstrated drug encapsulation efficiency at 58% (Fasehee et al., 2017), which is slightly higher than DNP1 NP as ascribed in Figure 4.12. Simply, the smaller the particle size, the lower the DSF encapsulation (Halayqa 2014), and this is reflective of particle size shown in Figure 4.1. The DNP1 NP had no significant ($p > 0.05$) effect on drug encapsulation of the DNP2, DNP3, and DNP4 NPs (Figure 4.12). Similarly, DNP2 NP showed no significant ($p > 0.05$) influence in DSF encapsulation compared with the DNP3 and DNP4 NPs. The DNP2 NP showed a significant ($p < 0.01$) decreased drug encapsulation of DSF thanDNP5 NP. However, there is no significant ($p > 0.05$) effect on drug encapsulation between DNP3 and DNP4 NPs. DNP3 NP showed a significant ($p > 0.05$) decreased in drug encapsulation compared to the DNP5 NP. The DNP4 NP had a significant ($p < 0.05$) decreased drug encapsulation of DSF compared to the DNP5 NP (Figure 4.12). Therefore, adding mPEG$_{2k}$-PLGA and PLGA/PCL (1:1) affected DSF loading with increasing drug encapsulation efficiency at 59% and 76%, for DNP4 and DNP5 NPs, respectively (Figure 4.12). DNP4 and DNP5 NPs indicated PCL addition enhances drug loading. Similar results were reported by Song et al. (2016), as they reported that PCL showed a significant effect on the loading efficiency, and this was due to the addition of PCL below 50% ratio. The addition of PCL above 50% ratio suggested decreased encapsulation capability.

DSF-loaded PLGA (DNP1 NP) and PEGylated NPs (DNP2, DNP3, and DNP4 NPs) obtained a satisfactory DSF loading results; all above 50% without significant differences ($p > 0.05$) among all (Figure 4.12). Therefore, the decreased DSF loading of DNP4 NP compared to the DNP5 NP might be due to the inclusion of the mPEG-PLGA polymer with PLGA and PCL core-shell amphiphilic and hydrophilic chain.
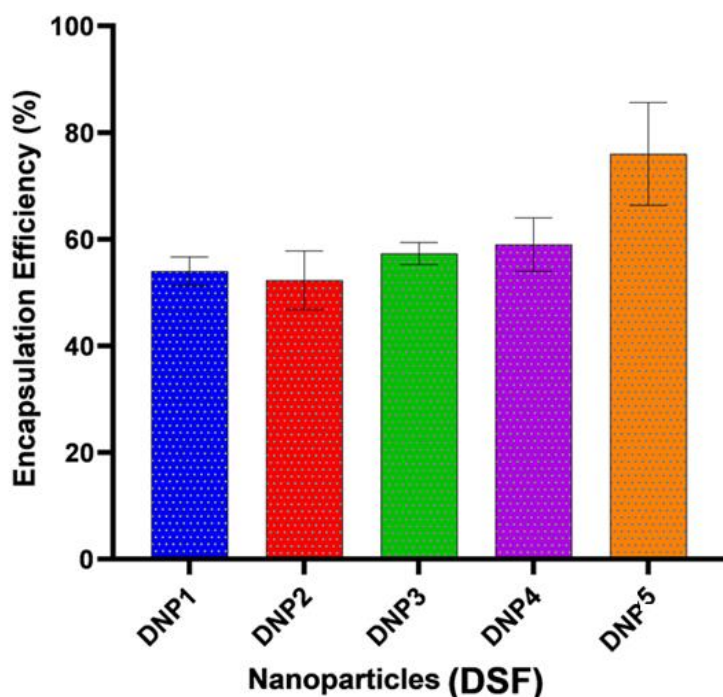
Figure 4.12. The mean percentage encapsulation efficiency of the DSF-loaded PLGA NPs (DNP1 to DNP5 NPs), prepared by using the D-Nano-Pr method, (Mean ± SD, n=3).

4.4.1.5 Cumulative release of DSF-loaded nanoparticles

As previously ascribed in chapter 3 (Figure 3.20), DSF-loaded PLGA NPs with a drug/polymer 1:9 ratio developed by the D-Nano-Pr method shows the ability to the sustainable release of DSF within 24 hours after incubation at pH 7.4. The stability nature exhibited by PLGA polymer/DSF interaction under physiological pH conditions (pH 7.4) may increase intracellular DSF concentration for more than 24 hours incubation. Therefore, the cumulative *in vitro* release behaviour of free DSF and DNP1-5 NPs was performed in PBS containing 1% Tween80 solution for 96 hours. To investigate the cumulative release of DSF under physiological conditions of pH 7.4, at different time intervals measurement was taken to evaluate DSF content. As shown in Figure 4.13, the release behaviour of the free DSF exhibited strong evidence of faster release rate of the drug. The higher release rate of the free DSF compared to the loaded NPs was attributed to the non-encapsulated DSF enhancing its faster cumulative release at 24 hours. The loaded NPs had a satisfactory loading capacity

and sustainable release for 96 hours. Therefore, the polymers have provided thermodynamic stability of DSF within the hydrophobic core-shell without drug leakage (Nishiyama and Kataoka, 2006). As shown in Figure 4.13, DNP1 NP demonstrated the fast release of DSF (26%) owing to possible quick hydrolysis of the naked PLGA within 12 hours in aqueous solution. While DNP2 NP released 15% of DSF within the first 12 hours shows the stable drug release under physiological conditions (Figure 4.13). Adding the PEG chain to DNP2 NP increases the layer (thickness of NPs due to coated PEG), and this slow down the DSF release out to the dissolution media (Zhao J; Feng S 2014). All NPs release profile undergoes two phases; (1) the first 12 hours demonstrated an initial burst release of the DSF at a high amount, and (2) the DSF release profile after 12 hours shows sustained release, especially, DNP1, DNP2 and DNP3 NPs. DNP3 NP cumulative release behaviour of DSF between the PLGA polymer and DSPE-PEG$_{2k}$ matrix showed a biphasic form of slow initial release within the first 24 hours, then continue with a sustainably slower drug release (Figure 4.13).

PLGA is known as a biodegradable polymer. The PLGA copolymer ratio between LA and GA can be manipulated to determine the rate of degradation (Engelberg and Kohn, 1991). In this study, PLGA of 50:50 Mw ratios to LA and GA was used. Therefore, it is expected for the resulting formulations to be hydrolysed or degraded within 96 hours, and this was confirmed by Anderson and Shive, (2012). DNP4 and DNP5 NPs formulations indicated obvious DSF quick self-catalyzed hydrolysis in aqueous solution and demonstrated a significantly faster release than that of DNP1, DNP5 NPs which experienced a high burst within 24 hours and 96 hours of 33% and 57%, respectively (Figure 4.13). Regardless of mPEG$_{2k}$-PLGA and PCL addition, encapsulated DSF cumulative release was facilitated by an early burst of NPs due to the strong interaction of water with mPEG$_{2k}$-PLGA and PCL (Song, et al., 2016). This study shows the modulation of naked NPs with PEG effectively improve DSF release profile. The

chemical properties of PCL showed the advantage of its semi-crystalline, and it provides slow hydrolytic degradation that is suitable for sustainable control release (Sinha, et al., 2004).
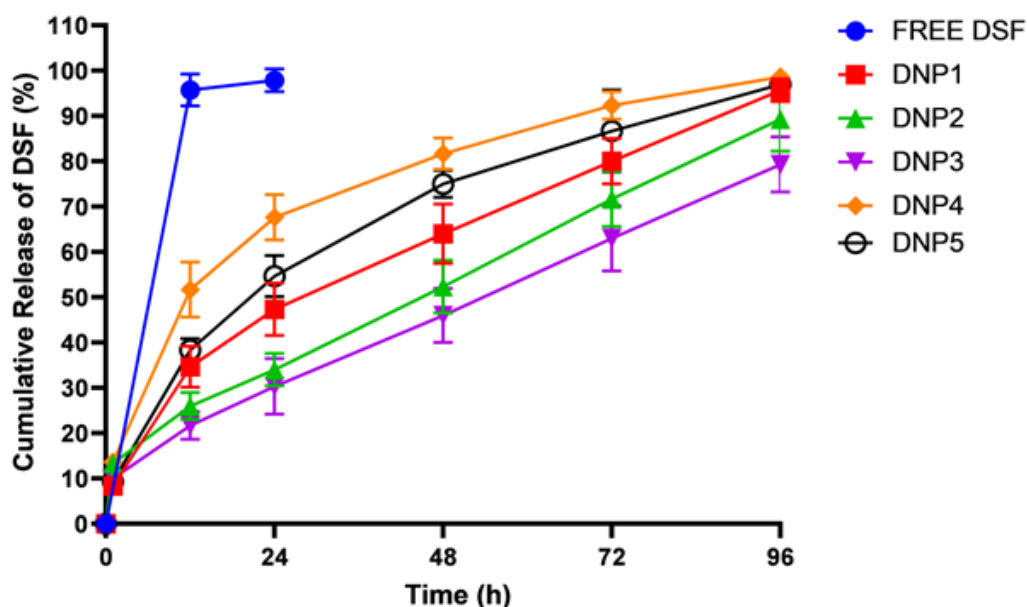
Figure 4.13. DSF Cumulative release of DSF-loaded DNP1 to DNP5 nanoparticles re-suspended in PBS with 1% Tween80 solution using a dialysis membrane, were prepared by using the D-Nano-Pr method(Mean ± SD, n=3).

4.4.1.6 Stability of DSF-loaded nanoparticles and free DSF standard

The establishment method of DSF-loaded PLGA (DNP1 to DNP5 NPs) NPs and free DSF standard stability study performed in serum might be considered a breakthrough, as there is limited information available in most published articles about the techniques used to determine DSF stability. In a recent study, Wang, et al., (2017) investigated the stability of DSF-loaded PLGA NPs and free DSF standard in horse serum at 37 °C. In their report, they demonstrated rapid degradation of the free DSF in horse serum at 30 seconds. In comparison to the stability of the free DSF, this study reported less than

138

half of the free DSF remained intact in the horse serum media at 30 seconds (Figure 4.14).

The manufactured NPs with widely used high molecular weight polyester of PLGA, PCL, and mPEG$_{2k}$-PLGAderived hydrophilic and hydrophobic segment-based core-shell structure nano-carriers suitable for DSF loading showed increased protection of DSF in horse serum media. Entrapped DSF was stable in the PLGA hydrophobic core by protecting against DSF rapid degradation in serum for over three hours compared to the free DSF that was rapidly degraded within the first 30 minutes. This is a confirmation that DSF-loaded PLGA NPs delivery systems in horse serum proved effective for the protection of DSF instability in a physiological environment. For the first time, this study has developed a method that determines *in vitro* stability rate-limiting step of DSF loaded PLGA NPs in serum that may be used as an effective treatment option to circumvent DSF vulnerability in the bloodstream. After 4 hours of incubation in horse serum media, whereby, DNP1 and DNP4 NPs protected DSF up to 69% and 68%, respectively (Figure 4.14). The resultant DNP3 NP provided less protection to the encapsulated DSF (Figure 4.14) after 4 hours of incubation, and only 42% remained intact. This might be temperature-dependent DSF release at 37°C between the PEGylated-phospholipid (DSPE PEG$_{2k}$) and PLGA in formulation gives less robust structure (Zeng, et al., 2012). A study was conducted to test the PEGylated formulation based phosphatidyloligoglycerol (DPPGOG) and phospholipid DSPE PEG$_{2k}$ for *in vitro* experiment that can be used as an alternative clinical approach, and their findings demonstrated DPPGOG was able to prolong the drug than DSPE PEG$_{2k}$ exhibiting fast drug release and instability in serum (Hossann et al., 2007).The release of DSF from DNP3 NP (Figure 4.13) showed the slowest release amongst all NPs and derived as the lowest stability, which contradicts the release study (Figure 4.14). Another explanation, which might be more applicable, is that coating with PEGylated

139

phospholipid is possible to accelerate drug release rate due to increase permeability in serum. This might also explain why DNP1, naked NP, have higher stability than that of PEGylated NPs (DNP2). DNP4 consist of PLGA, PCL, and mPEG2k-PLGA showed a good moderate release profile (Figure 4.14) and the highest stability amongst all NPs ($p < 0.05$). This confirms the importance of using PCL in DSF PLGA NP and highlights the advantages this polymer mentioned in the previous section.
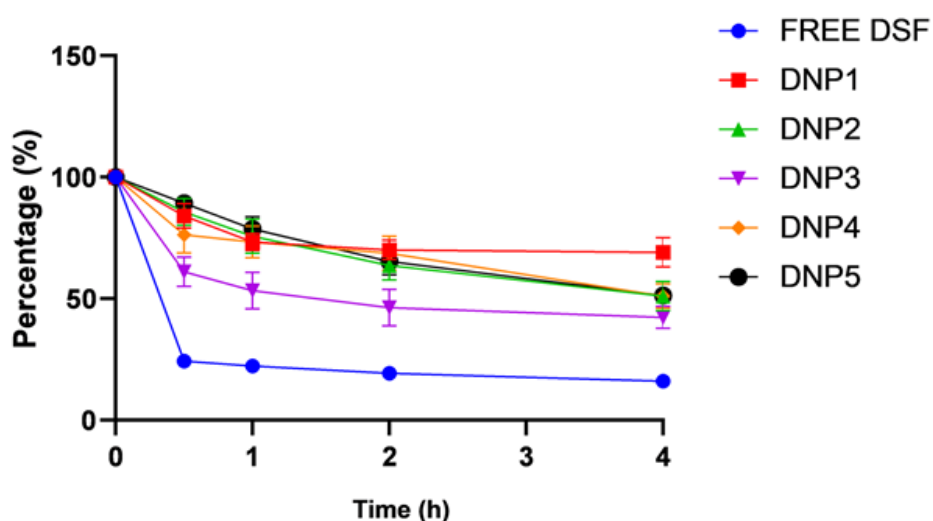
Figure 4.14. DSF stability of the free drug and DSF-loaded PLGA of (DNP1 to DNP5 NPs) nanoparticles produced by using the D-Nano-Pr method, (Mean ± SD, n=3).

4.4.1.7 MTT cytotoxicity assay

Cytotoxicity of the free DSF, DSF/Cu, and DNP1-5 NPs against MCF 7, MDA-MB-231 and MDA-MB-231$_{PTX10}$ cell lines was investigated by using the MTT assay (Figure 4.15-17). The cytotoxicity curves of MTT assay were extrapolated to determine IC$_{50}$ values known as the required concentration to inhibit cell growth by 50% (Table 4.2). DSF/Cu complex was used as a positive control.

The incubated breast cancer cells were treated in different concentrations at 37 °C for 72 h. In a comparison of *in vitro* cytotoxicity by DNP1 NP indicates cytotoxicity against the MCF7 cell line with an IC$_{50}$ value of 48.73 ± 4.32 (Table 4.2), which is highly

140

significant ($P < 0.05$) than the free DSF (Figure 4.15). This is showing that the increased cytotoxicity effect might be attributed to PLGA stability in serum (Figure 4.14) followed by excellent biocompatibility denatured bared PLGA NPs. Also, DNP1 NP showed significant ($p < 0.01$) cytotoxicity effect than DNP3 and DNP5 NPs, but no significant cytotoxicity effect compared to DNP2 NPs, DNP4 NPs, and DSF/Cu. It is indicating that DNP1 NP had a fast release with more than 70% of DSF was released. Based on the results obtained, DNP1 NP is likely to be effective within 48 hours and not beyond 72 hours incubation.

The cytotoxicity effects, of the DNP2 NP against MCF 7had an IC_{50} value of 83.57 ± 5.09 (Table 4.2), with no significant ($p > 0.05$) cytotoxicity effect compared to the free DSF, DSF/Cu, DNP3 NPs and DNP5 NPs. Also, DNP2 NP showed a highly significant ($p < 0.01$) decreased cytotoxicity effect and an increasing IC_{50} than the DNP4 NP. Therefore, the decrease cytotoxicity of DNP2 NP may be attributed to the slow, sustained release of DSF in the physiological condition of pH 7.4 (Figure 4.13). The moderate stability in serum indicates benefit for loaded NPs long circulation. Due to DNP2 NP moderate stability in horse serum, it was demonstrating the ability to impact the cytotoxicity effect for more than 72 hours. Introducing mPEG$_{2k}$-PLGA to DNP2 NP formulation showed the prolonged circulation of DSF release compared to the naked DNP1 NP (Figure 4.13).

The DNP3 NP had a significantly ($P < 0.05$) decreased cytotoxicity effect with an increasing IC_{50}value of 101.35 ± 9.29 (Table 4.2), compared to the DNP4 NP. Similarly, the DNP3 NP demonstrated significant ($p < 0.01$) decreased cytotoxicity effect with an increasing IC_{50} than the DSF/Cu standard. The DNP3 NP had no significant ($p > 0.05$) cytotoxicity effect between the DNP5 NP and free DSF standard (Figure 4.13). The decrease in cytotoxicity of DNP3 NP might be due to slower sustained release of DSF

as DSPE PEG$_{2k}$ exhibits high solubility in the physiological condition of pH 7.4 (Figure 4.13). As shown in Figure 4.14, DNP3 NP demonstrated the least stable in horse serum, and this is because of the phospholipid DSPE PEG$_{2k}$ showing less stable in serum.

The DNP4 NP showed a highly significant ($P < 0.05$) increased cytotoxicity effect with a low IC$_{50}$ value of 28.16 ± 2.56 (Table 4.2) than the DNP5 NP, and this due to the fast release of DSF accompanied by better stability, therefore, increases cell viability at high concentration (Figure 4.15). In addition, the DNP4 NP with mixed formulation ratios of PLGA/PCL (1:1) and 0.5% mPEG$_{2k}$-PLGA demonstrated the ability to exert a therapeutic effect at moderate concentration.

Finally, the free DSF standard showed a significant ($p < 0.01$) decreased cytotoxicity effect against the MCF 7 breast cancer cells with an increasing IC$_{50}$ value of 110.65 ± 14.62 (Table 4.2), compared to the DSF/Cu standard. Under the physiological condition of pH 7.4, the free DSF standard had the fastest release amongst the loaded NPs, and for the first 30 minutes, over 90% of DSF was released (Figure 4.13). Also, more than 50% of DSF was rapidly degraded in serum (Figure 4.14). This study confirms the instability of the free DSF standard in physiological environments which is in support with published kinds of literature. It shows the need for nanotechnology to encapsulate DSF with the ability to enhance higher cytotoxicity and apoptotic effect against cancer cells. The survival curve of cancer cells after being treated by DSF, DSF/Cu confirmed that the cytotoxic effect of DSF is dependent on Cu^{+2} and follows a dose-dependent manner (Figure 4.15 to 4.17). Cu sensitivity in tumour cells is higher compared with normal cells, therefore, treating Cu with DSF-loaded PLGA NPs thus enhance cancer therapy (Navrátilová, et al., 2009; Tisato, et al., 2010).

Table 4.2. Demonstrating IC$_{50}$ of DSF-loaded PLGA (DNP1 to DNP5 NPs) nanoparticles, DSF, and DSF/Cu standards treated against three cancer cell lines, MCF 7, MDA-MB-231 and MDA-MB-231$_{PTX10}$ nM. (Mean ± SD, n=3).

Standards (nM)	MCF 7	MDA-MB-231	MDA-MB-231$_{(PTX\ 10nm)}$
DSF	110.65 ± 14.62	145.18± 29.93	338.25± 22.41
DSF/Cu	53.81± 14.62	97.77± 1.75	79.00± 1.78
DNP1	48.73± 4.32	119.51± 29.55	358.91± 19.72
DNP2	83.57± 5.09	86.23± 10.52	306.71± 64.06
DNP3	101.35± 9.29	114.04± 1.68	183.55± 82.55
DNP4	28.16± 2.56	32.77± 7.05	31.27± 5.31
DNP5	102.00± 23.08	69.56± 31.21	300.84± 17.51
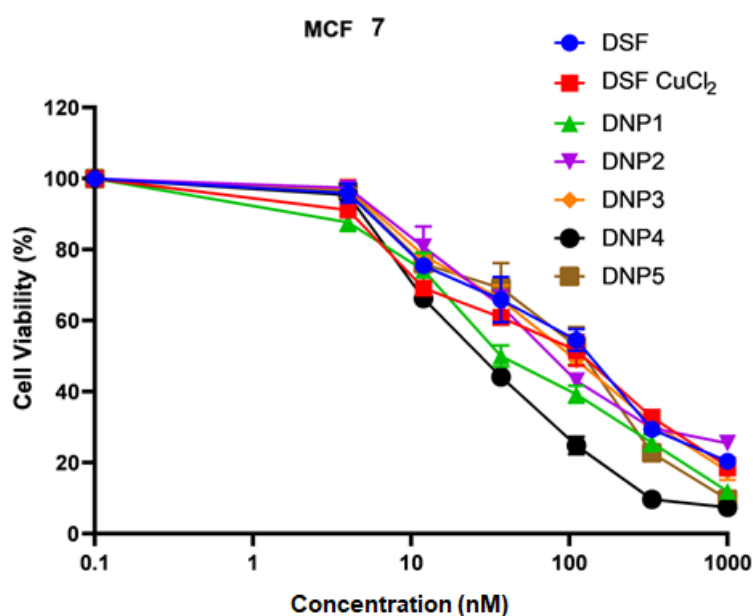
Figure 4.15. MTT assay cytotoxicity of the free DSF, DSF/Cu standards and DSF-loaded PLGA (DNP1 to DNP5) nanoparticles prepared the D-Nano-Pr method were treated against the MCF 7 cancer cells, (Mean ± SD, n=3).

Cytotoxicity effect of the free DSF standard, DSF/Cu standard and loaded NPs treated against the MDA-MB-231cancer cells was investigated by MTT assay, and Figure 4.16 showed the cytotoxicity activity curves after treatment at different concentrations with cells incubated at 37 °C for 72 hours.

As ascribed in Figure 4.16, DNP1 NP had a highly significant ($P < 0.05$) increased cytotoxicity effect with a low IC_{50} value of 119.51 ± 29.55 (Table 4.2) than the free DSF standard. But, DNP1 NP showed a significantly ($p < 0.01$) decreased cytotoxicity effect and an increasing IC_{50} (Table 4.2) than the DNP4 NP. Therefore, it is indicating that DNP1 NP had excellent stability and biocompatibility of denatured PLGA in horse serum (Figure 4.14). In contrast, the cytotoxicity of DNP1 NP showed no significant ($p > 0.05$) effect in cell viability compared to the DNP2 NP, DNP3 NP, DNP5 NP, and DSF/Cu standard (Figure 4.16). This also confirmed that the DNP1 NP might be effective within 48 hours, as more than 70% of DSF was released in physiological conditions of pH 7.4 (Figure 4.13).

DNP2 NP only had a highly significant ($P < 0.05$) increased cytotoxicity effect at a maximum concentration of 1000 nM, and a low IC_{50} value of 86.23 ± 10.52 (Table 4.2) compared to the free DSF (Figure 4.16). In contrast, DNP2 NPs showed no significant ($p > 0.05$) cytotoxicity effect and IC_{50} (Table 4.2) compared to the DNP3 NP, DNP4 NP, DNP5 NP, and DSF/Cu standard (Figure 4.16). As previously stated, DNP2 NP had the ability to impact cytotoxicity beyond 72 hours due to the attached $mPEG_{2k}$-PLGA showing the slower sustainable release of DSF at 96 hours with more than 80% of the drug was released. Therefore, DNP2 NP has the ability to enhance long circulation in cancer therapy.

The DNP3 NP showed a highly significant ($P < 0.05$) increased cytotoxicity effect at a maximum concentration of 1000 nM with a low IC_{50} value of 114.04 ± 1.68 (Table 4.2), compared to the free DSF. In addition, the DNP3 NP also demonstrated a significant ($p < 0.01$) decreased cytotoxicity effect with an increasing IC_{50}, compared to the DNP4 NP. But, the DNP3 NP showed no significant ($p > 0.05$) cytotoxicity effect compared to the DNP4 NP and DSF/Cu standard (Figure 4.16). Adding the PLGA/PCL

144

(1:1) and $mPEG_{2k}$-PLGA in the DNP4 NP exhibits excellent stability by protecting DSF in horse serum with the ability to prolong DSF half-life exerts cytotoxicity beyond 72 hours incubation. This is attributed to the slowest sustainable release of DSF at 96 h with more than 70% of the drug released. The DNP4 NP can also enhance long circulation to target tumour cells.

The DNP4 NP showed a highly significant ($P < 0.05$) increased cytotoxicity effect with a low IC_{50} value of 32.77 ± 7.05 (Table 4.2), than the free DSF standard (Figure 4.16). Mostly, the DNP4 NP demonstrated a significantly increased cytotoxicity effect at moderate concentrations than the DSF/Cu standard (Figure 4.16). In addition, there is no significant ($p < 0.05$) cytotoxicity effect at higher concentrations between DNP4 and DNP5 NPs, as shown in Figure 4.16.

Finally, the free DSF standard showed a highly significant ($P < 0.05$) decreased cytotoxicity effect with an increasing IC_{50} value of 145.18 ± 29.93 (Table 4.2) than the DNP5 NP (Figure 4.16). Interestingly, no significant ($p > 0.05$) cytotoxicity effect observed between the free DSF and DSF/Cu standards (Figure 4.16).
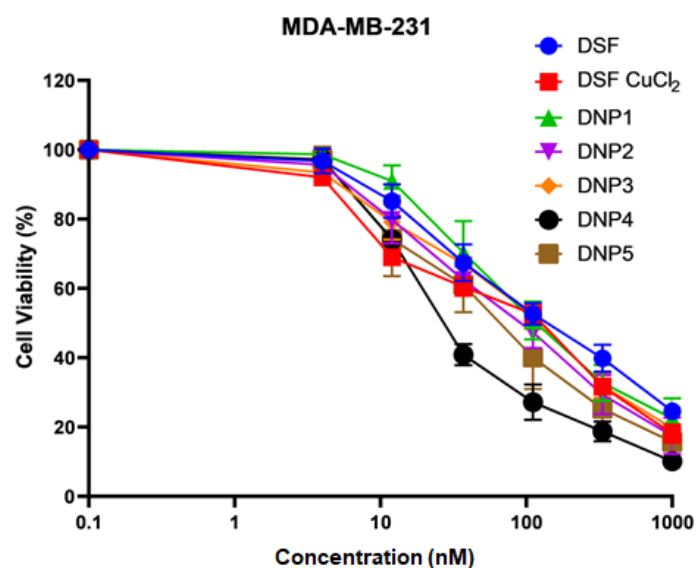
Figure 4.16. MTT assay cytotoxicity of the free DSF, DSF/Cu standards and DSF-loaded PLGA (DNP1 to DNP5) nanoparticles prepared the D-Nano-Pr method were treated against the MDA-MB-231 cancer cells, (Mean ± SD, n=3).

The *in vitro* inhibitory effects of the free DSF standard, DSF/Cu standard, and DNP1-5 NPs against the MDA-MB-231$_{PTX10}$paclitaxel (PTX)-resistant cancer cells was dose-dependent after 72 hours incubation and then exhibited cell viability as shown in Figure 4.17.

As shown in Figure 4.17, DNP1 NP demonstrated no significant ($p > 0.05$) cytotoxicity effect between the DNP2 NP, DNP5 NP, and free DSF standard. After 72 hours of incubation, the dose-dependent manner of DNP1 NP against the MDA-MB-231$_{PTX10}$ showed a highly significant (*P < 0.05*) decreased cytotoxicity effect at low concentrations with an increasingIC$_{50}$ value of 358.91 ± 19.72 (Table 4.2), compared to the DNP4 NP and DSF/Cu standard (Figure 4.17).As revealed in Figure 4.17, DNP1 NP demonstrated a significantly ($p < 0.01$) decreased cytotoxicity effect at lower concentrations, than the DNP3 NP. This is further indicating that DNP1 NP was slowly penetrating the PTX-resistant breast cancer cells compared to the cytotoxicity effect exhibited by the DNP1 NP formulation against the MCF 7 in Figure 4.15.

The DNP2 NP showed no significant ($p > 0.05$) cytotoxicity effect between the free DSF and DNP5 NP (Figure 4.17). As ascribed in Figure 4.17, the DNP2 NP demonstrated a highly significant ($P < 0.05$) decreased cytotoxicity effect at higher concentrations with an increasing IC_{50} value of 306.71 ± 64.06 (Table 4.2), compared to the DSF/Cu standard and DNP4 NP. The DNP2 NP showed significantly ($p < 0.05$) decreased cytotoxicity effect, compared to the DNP3 NP. The $mPEG_{2k}$ -PLGA PEG played a significant role in DNP2 NP to slowly penetrate the PTX-resistantMDA-MB-231_{PTX10} cancer cells (Figure 4.17) than the MDA-MB-231 (non-resistance) indicating less penetration (Figure 4.16). This is a clear indication that DNP2 NP may exhibit high cellular uptake against MDA-MB-231_{PTX10}at above 72 hours incubation.

DNP3 NP showed a significantly ($p < 0.01$) increased inhibitory effect with a low IC_{50} value of 183.55 ± 82.55 (Table 4.2), than the free DSF standard (Figure 4.17). Also, the results of DNP3 NP showed a significantly ($p < 0.01$) decreased cytotoxicity effect than the DNP4 NP. In contrast with the DNP3 NP demonstrated significant ($p < 0.05$) increased cytotoxicity effect than the DNP5 NP. The increased cytotoxicity effect of DNP3 NP formulation is attributed to the PTX-resistant MDA-MB-231_{PTX10} cancer cells, which exhibits slight accumulation of DSF, and this might be the effect of phospholipid DSPE PEG_{2k} increasing cellular uptake that might enhance DSF influence to inhibit P-gp activity by blocking its maturation (Loo et al., 20004). However, there is no significant cytotoxicity effect between the DNP3 NP and DSF/Cu standard.

The DNP4 NP had a highly significant ($P < 0.05$) increased cytotoxicity effect at lower concentrations against the PTX-resistant MDA-MB-231_{PTX10} cancer cells, which consists of a lower IC_{50} value of 31.27 ± 5.31(Table 4.2), compared to the free DSF standard and DNP5 NP (Figure 4.17).

The free DSF standard showed a highly significant ($P < 0.05$) decreased cytotoxicity effect with an increasing IC_{50} value of 338.25 ± 22.41 (Table 4.2), compared to the DSF/Cu standard (Figure 4.17).

In summary, for all three cell cultures, the $IC_{50\%}$ values (Table 4.2) of the DNP1-5 NPs (Table 4.1) demonstrated comparable values with DSF/Cu standard. Therefore, the result mirrors the release profile for NPs that had a slow release. In addition, the DNP1, DNP2, DNP3, and DNP5 NPs demonstrated increased $IC_{50\%}$ against the PTX-resistant MDA-MB-231$_{PTX10}$ cancer cells. But, DNP4 exhibited the strongest ($p < 0.05$) inhibitory activity amongst all NPs due to its sustainable controlled release of DSF as ascribed in Figure 4.13. Most importantly, this was also confirmed by the surviving curves for all three cell cultures (Figure 4.15-17).
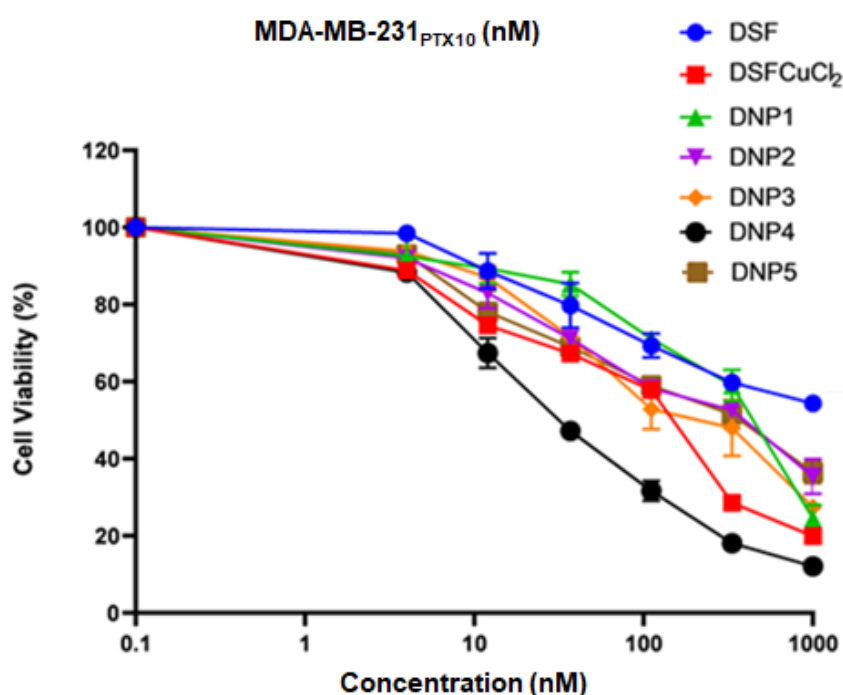
Figure 4.17. MTT assay cytotoxicity of DSF-loaded PLGA (DNP1 to DNP5 NPs) nanoparticles on to the MDA-MB-231$_{PTX10}$cancer cells (Mean ± SD, n=3).

4.5 Conclusion

In this study, we have successfully manufactured nano-carrier delivery systems of DSF-loaded PLGA/PCL coated with mPEG$_{2k}$-PLG and DSPE PEG$_{2k}$ by using the D-Nano-Pr method. The NPs formulations produce increased encapsulation efficiency, sustainable cumulative drug release and DSF stability in horse serum. The DSF-loaded PLGA/PCL coated with mPEG$_{2k}$-PLG produced increased drug entrapment, a prolonged sustainable release, increased DSF protection in horse serum media and high cytotoxicity towards breast cancer cells including those that are resistant to chemotherapy agent (PTX). Production of NPs by the D-Nano-Pr method can be an alternative to solve issues surrounding DSF, such as stability and the ability to enable long circulation of DSF NPs to target cancer cells. Therefore, DSF NPs formulations by the D-Nano-Pr method could be used or introduced into clinical trials and the pharmaceutical industry. The encapsulated DSF-loaded PLGA and coated PEGylated nano-carrier delivery systems can enhance cancer therapy.

Chapter 5 Development and Characterizations of Disulfiram Solid Lipid Nanoparticles

Using the Direct Nanoprecipitation and Single emulsion/solvent evaporation methods

5.1 Introduction

SLNs have been identified as the new generation of novel colloidal drug delivery carrier systems (Wan, et al., 2008). The hot homogenization technique is commonly used in the preparation of SLNs (Al-Haj and Rasedee, 2009). However, depending on the chemical and physical properties of the active ingredient which is sensitive to temperature; therefore, the cold homogenization technique can be utilized as an alternative (Wissing and Müller, 2002).

For over two decades, published articles have reported DSF NPs development against cancer therapy. But, the research field of nanomedicines provides less information about the methods used to fabricate and characterize nano-carrier delivery systems of DSF. Previous studies have shown inconsistency in the determination of percentage encapsulation efficiency of DSF prepared by the SE method then estimated encapsulated DSF using the centrifugation method. Similarly, reported methods for DSF stability in horse serum media lacks clarity (Wang, et al., 2017).This study confirms the new development of standard methods required to determine both encapsulated and un-encapsulated drug contents, and efficient step-by-step procedure to determine DSF stability in horse serum.

In the present study, DSF-loaded SLNs were prepared by using the D-Nano-Pr method and the SE method. Both the D-Nano-Pr and SE methods used the hot homogenizer (HH) technique to develop the SLNs formulations. The particle sizes of SLNs prepared by the SE method were reduced by the mechanical force of the HPH and PS techniques. The newly manufactured SLNs were characterized using the zeta-sizer nano-series to determine particle sizes, polydispersity index (PDI), and zeta potential. Whereas the thermal degradation and functional group confirmation of chemical compounds were analyzed using differential scanning calorimetry (DSC) and Fourier transform infrared spectroscopy (FTIR), respectively. The percentage encapsulation

efficiency, cumulative release, and the stability SLNs in horse serum media were evaluated.

5.2 Aims

Up till the time of submitting this thesis, this is the first attempt for the preparation of DSF-loaded SLNs. Therefore, this study aims to manufacture particulates of un-encapsulated and encapsulated DSF SLNs using the FDA approved biodegradable and biocompatibility phospholipids materials. In addition, previously used methods and techniques as described in section 2.2.1.2 (D-Nano-Pr method), and 2.2.2.3 (SE method) will be employed to determine decreased particle size as described in section 2.2.2.2 (PS technique), and 2.2.2.4 (HPH technique), increased loading efficiency, control drug release and stability of free DSF and loaded NPs in horse serum.

5.3 Experimental Design

5.3.1 Preparation of disulfiram-loaded solid lipid nanoparticles by direct nanoprecipitation method

The D-Nano-Pr method and hot-homogenization (HH) technique was used to manufacture unloaded (DSN1E NP) SLNs and DSF-loaded (DSN1 NP) SLNs nano-carrier delivery systems. As shown in Table 5.1, the total weight of 300 mg between the phospholipids and DSF was dissolved in acetone (6 ml) (lipid phase) as referred to in chapter 2. The aqueous phase consists of ultrapure water (54 ml). DSN1E and DSN1 NPs were prepared at an isothermal temperature under a hot water bath at 80 $^{\circ}$C, as described in section 2.2.1.2.

Table 5.1. The formulation ratios of disulfiram (DSF)-loaded solid lipid nanoparticles were manufactured by direct nanoprecipitation (D-Nano-Pr) method using the high-speed homogenization technique.

Ingredient (ratio) / Formulation*	Preciprol	Compritol	Hydrogenated Phosphatidylcholine from soybean (HPCS)	DSF	Total
DSN1E	6.5	2.5	1	-	10
DSN1	5.5	2.5	1	1	10

*DSN represents solid lipid nanoparticles (SLNs) formulations prepared by the D-Nano-Pr method using high-speed homogenization technique. E denotes the empty SLNs formulation.

5.3.2 Preparation of unloaded solid lipid nanoparticles and disulfiram-loaded solid lipid nanoparticles by single emulsion/solvent evaporation method

To compare the final products prepared by the D-Nano-Pr method (DSN1/DSN1E SLNs), unloaded DPS1E, DPS2E, and DPS3E SLNs and DSF-loaded DPS1, DPS2, and DPS3 SLNs were developed by the SE method using the HH technique as described in section 2.2.2.4. Samples were manufactured in three stages, (i) unloaded DPS1E and DSF-loaded DPS1 SLNs by using the SE method/HH technique (ii) the pre-formulated DPS2E and DSF-loaded DPS2 SLNs by SE method/HH technique then subjected to further particle-size reduction by HPH technique and (iii) unloaded DPS3E and DPS3 SLNs carrier particles were reduced by PS technique. Total weight of 300mg was used to manufacture unloaded and DSF-loaded SLNs using adjustable ratios shown in Table 5.2. Samples were weighed and dissolved in 6 ml of dichloromethane (DCM) (lipid phase), then immersed in a water bath (80 °C) as described in section 2.2.2.5.

Table 5.2. The formulation ratios of the DSF-loaded solid lipid nanoparticles were manufactured by using the single emulsion/solvent evaporation (SE) method. The DPS1E/DPS1 SLNs were prepared without particle size reduction. While, the DPS2E/DPS2 SLNs and DPS3E/DPS3 SLNs were prepared by the SE method with particle size reduction by the PS and HPH techniques, respectively.

Ingredient (ratio) / Formulation*	Preciprol	Compritol	Hydrogenated Phosphatidylcholine from soybean (HPCS)	DSF	Total
DPS1E	6.5	2.5	1	-	10
DPS1	5.5	2.5	1	1	10
DPS2E	6.5	2.5	1	-	10
DPS2	5.5	2.5	1	1	10
DPS3E	6.5	2.5	1	-	10
DPS3	5.5	2.5	1	1	10

*DPS represent solid lipid nanoparticles (SLNs) formulations prepared by the single emulsion/solvent evaporation (SE) method, whereby the particle sizes were reduced using probe sonication (PS) and high-pressure homogenization techniques. E denotes the empty SLN formulation.

5.4 Results and discussion

5.4.1 Particle size, PDI, Morphology of particles, and zeta potential.

To compare the SLNs formulations prepared between the D-Nano-Pr method and SE methods, the characterization of particle size, PDI, and zeta potential was performed immediately after synthesis. Hot homogenization (HH) technique was employed to prepare SLNs dispersion through precipitation in miscible mixed solvent and water (nanoprecipitation), or o/w emulsions (solvent evaporation) (Sjöström and Bergenståhl, 1992). The SLNs carrier systems are mostly produced by the HH technique for poorly water-soluble pharmaceutical drugs (Ugazio, Cavalli and Gasco, 2002). To obtain nano-scale particle size, SLNs were prepared at approximately 5 $^{\circ}$C to 10 $^{\circ}$C above the melting point of the lipid and drug (Liu, et al., 2008).

The mean particle size, PDI and zeta potentials of with or without DSF produce by the D-Nano-Pr, and SE methods were presented in Figures 5.1, 5.2, and 5.8, respectively. The mean diameter of DSN1 NP was 412.0 ± 23.24 nm, had a significantly ($P < 0.05$)

increased particle size compared to the DPS2 and DPS3 SLNs (Figure 5.1), which is due to reduce particle size, therefore, decreased particle sizes were observed as described in Figure 5.1. But, the DSN1 SLN showed no significant ($p > 0.05$) change in particle size compared with the DPS1 SLN, and this is because of DSN1, and DPS1 SLNs prepared by the D-Nano-Pr, and SE methods, respectively, were only homogenized without particle size reduction. However, all SLNs were subjected to hot-homogenization technique, and the only difference after the preparation of DPS2/DPS2E SLNs and DPS3/DPS3E SLNs particulates by the SE method were particle size reduced using the PS and HPH techniques. While the blank (DSN1E SLN) prepared by the D-Nano-Pr method had a mean diameter of 342.7 ± 12.32 nm, and a significantly ($P < 0.05$) increased particle size compared to the DPS1E, DPS2E, and DSL3E SLNs (Figure 5.1).

A similar increase in particle size was observed for DSL1SLN prepared by the SE method, had a mean diameter of 383.0 ± 69.29 nm, which demonstrates a significantly ($P < 0.05$) increased particle size compared to the DPS2, and DPS3 SLNs. As previously stated, that decreased particle sizes of DPS2, and DPS3 SLNs was due to particle size reduction by the, PS and HPH techniques, respectively. Whereas, the DPS1E SLN had a mean diameter of 335.2 ± 8.21 with a significantly ($P < 0.05$) increased particle size compared with DPS2E, and DPS3E SLNs as ascribed in Figure 5.1. Regardless of particle size reduction by the HPH, and PS techniques, no significant ($p > 0.05$) change in particle sizes between DPS2E and DPS3E SLNs (Figure 5.2).

Reduced particle sizes of DPS3 and DPS3E SLNs using the HPH technique produced a mean diameter of 144.9 ± 13.45 nm and 115.1 ± 5.27 nm, respectively (Figure 5.1). The use of HPH technique decreased particle size in the range from 28 to 100 nm

without clogging the valve (Lee, et al., 2009; Kaushik and Singh, 2011). In this technique, SLNs are subjected to turbulence, cavitation and high shear stress to produce reduced mean nano-scale particle diameter (Harris, Martin and Modi, 2001; Silva, et al., 2010).

As ascribed in Figure 5.1, the reduced mean diameter of DPS2 and DPS2E SLNs using the PS technique had the following mean diameters, 139.7 ± 7.44 nm and 124.9 ± 11.45 nm, respectively. The reduced particle sizes by PS technique shown in Figure 5.1 are as per their published results after the particle size of encapsulated SN-38 SLN was reduced by the PS technique (Mosallaei, et al., 2016).

Generally, particles of DSN1/DSN1Eand DSL1/DSL1E SLNs produced by the D-Nano-Pr and SE methods without further size-reduction were significantly larger than the particle size reduction of DPS2/DPS2E and DPS3/DPS3E SLNs (Figure 5.1). Adding the drug, such as DSF in the molten state of the phospholipid at elevated temperature enables DSF incorporation into the hydrophobic core of the phospholipid colloidal particulate and it decreases particle size than the blanks (Mosallaei, et al., and 2016).
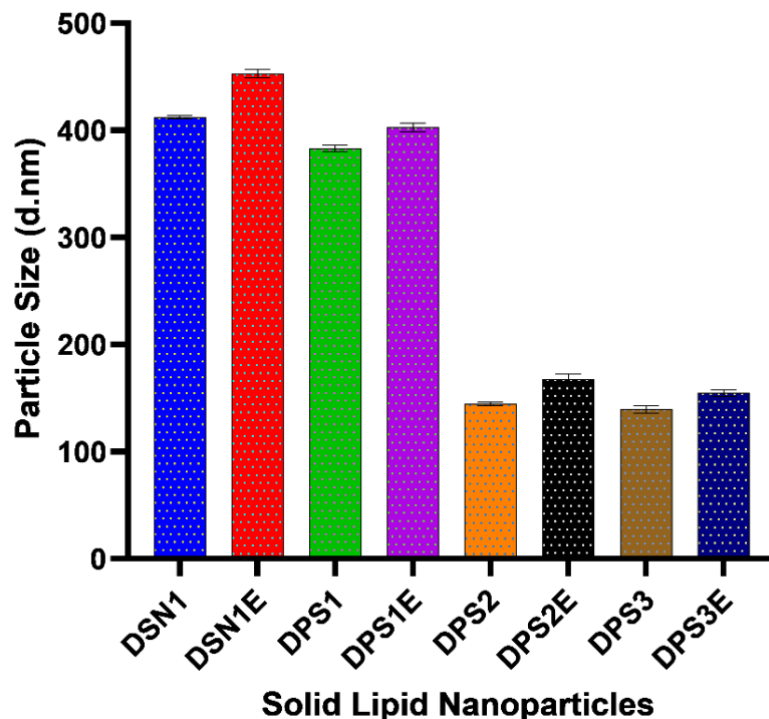
Figure 5.1. Particles sizes of DSF solid lipid nanoparticles, DSN1/DSN1E (D-Nano-Pr method), DPS1/DPS1E (SE method), DPS2/DPS2E (SE method/ PS technique) and DPS3/DPS3E (SE method/ HPH technique) (Mean ± SD, n=3).

As shown in Figure 5.2, all SLNs demonstrated narrowed PDI that is less than 0.6. DSN1 and DSN1E SLNs prepared by the D-Nano-Pr method demonstrated no significant ($p > 0.05$) change in PDI compared to all the SLNs prepared by the SE method.DSN1E SLNs exhibited a significant ($p < 0.05$) increased PDI than DPS2E (Figure 5.2). Also, there are no significant ($p > 0.05$) changes in PDIs between DPS1, and DPS3 SLNs. But, DPS1 SLN showed a significant ($p < 0.05$) change in PDI than the DPS2 SLN. There is no significant ($p > 0.05$) change in PDI between DPS2E and DPS3E SLNs prepared by the SE method and reduce particle sizes using the PS, and HPH techniques, respectively. Using the techniques such as the HPH or PS decreased the sizes of SNLs but increase the PDI, which is due to particle aggregation. This can be proven in Figure 5.2, where DSL3 and DPS2 SLNs have higher PDI compared to DPS1 SLN.

157
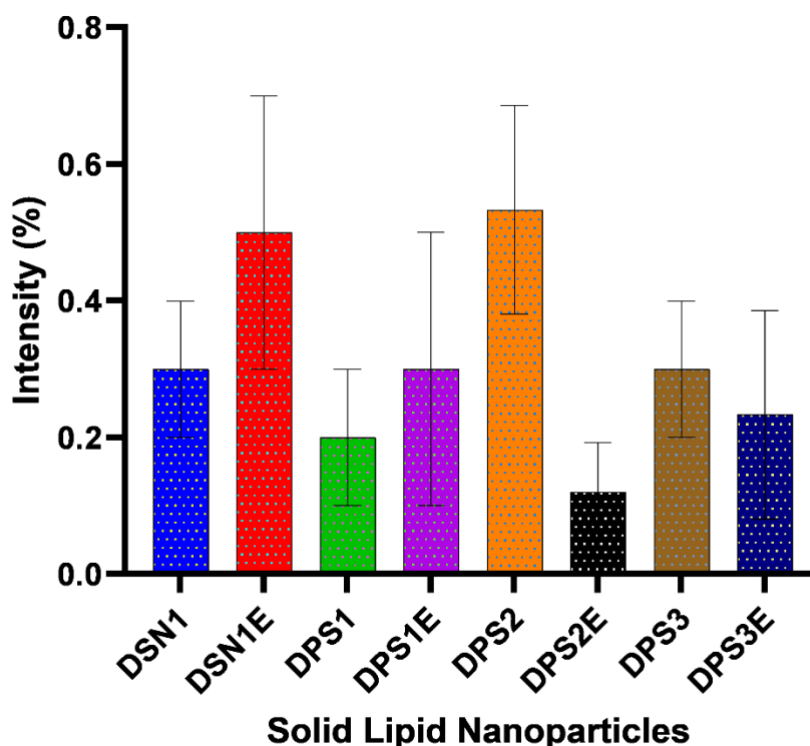
Figure 5.2. Polydispersity index (PDI) of DSF solid lipid nanoparticles, DSN1/DSN1E (D-Nano-Pr method), DPS1/DPS1E (SE method), DPS2/DPS2E (SE method/HPH technique) and DPS3/DPS3E (SE method/PS technique) (SE-PS) (Mean ± SD, n=3).

Figure 5.3 shows the surface morphology of DSF-loaded SLN (DSN1) prepared by the D-Nano-Pr method demonstrated spherical particles with less aggregation. The sizes were approximately 400 nm with narrowed PDIs. The unloaded DSN1E SLN prepared by the D-Nano-Pr method showed few huge lipid SLNs with few particulates of a spherical surface (Figure 5.4). This might explain the large size and relatively high PDI shown by the zeta sizer. This also might highlight the role of DSF as a hydrophobic drug during the construction of the SLNs prepared by the D-Nano-Pr method as the preparation of empty SLNs almost failed without the drug. DPS1 SLN prepared by the SE method demonstrated aggregated oval shape particulates (Figure 5.5). The SEM images confirm the large size SLNs of an approximately 400 nm and the good PDI. However, this aggregation was dispersed to give a smaller particle size (less than 150 nm) but higher PDI after reducing the size by the PS technique (DPS2 SLN), (Figure

158

5.6). The reduced particle size of DPS3 SLN by the HPH technique demonstrated

smooth surfaces and aggregated patched particles (Figure 5.7).
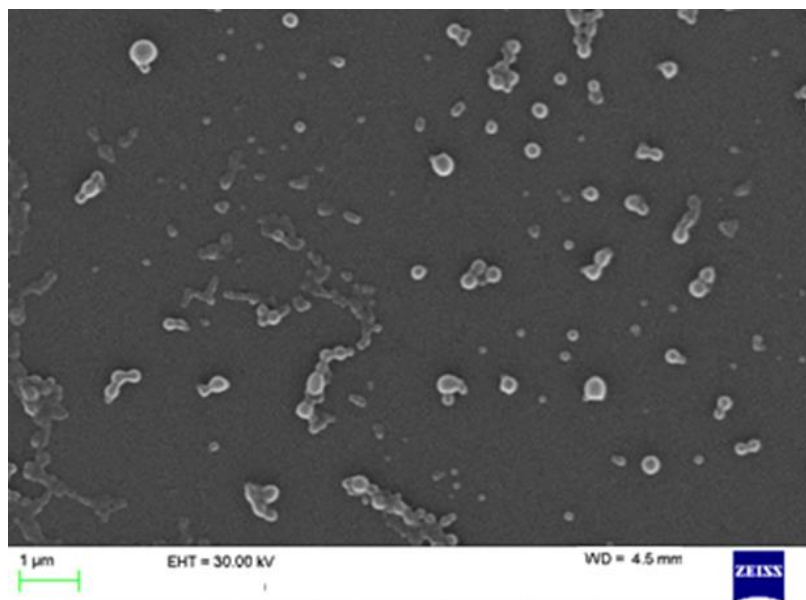
Figure 5.3. Scanning electron microscopy (SEM) surface morphology images of DSF-loaded solid lipid nanoparticles of DSN1 prepared by the D-Nano-Pr method.
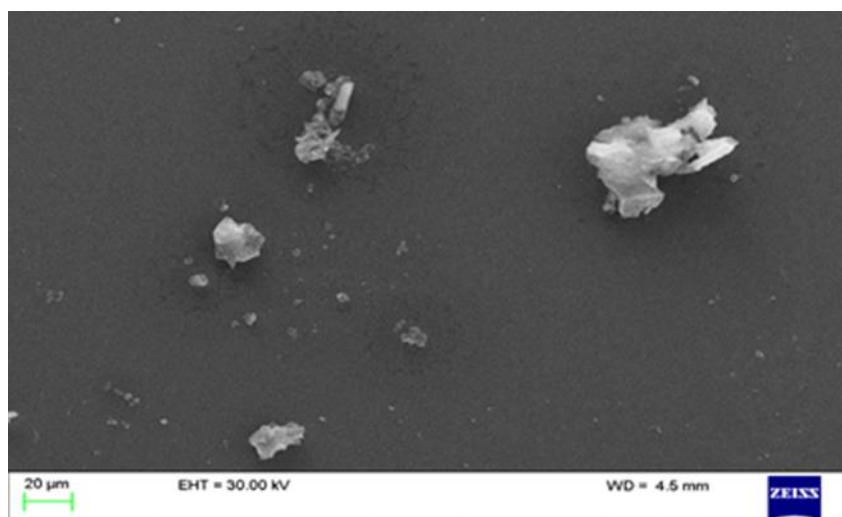
Figure 5.4. Scanning electron microscopy (SEM) surface morphology ofunloaded solid lipid nanoparticles of DSN1E prepared by the D-Nano-Pr method.
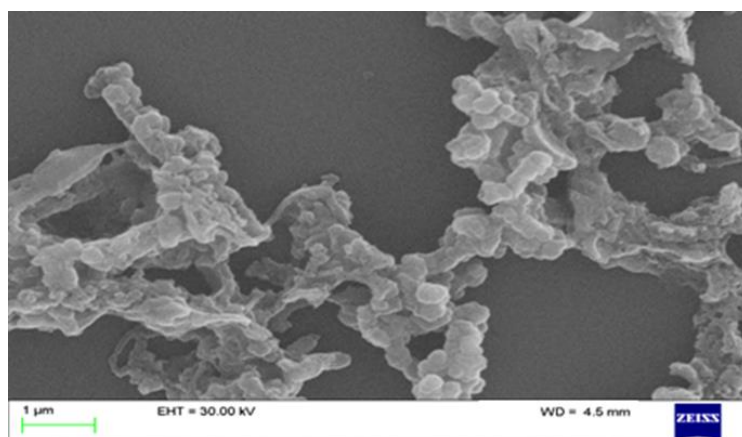
Figure 5.5. Scanning electron microscopy (SEM**)** surface morphology of DSF-loaded solid lipid nanoparticles of DPS1 by SE method and hot homogenization (HH) technique.
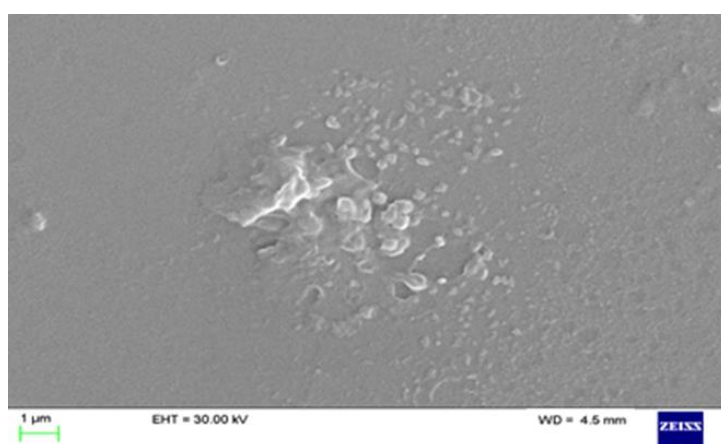
Figure 5.6. Scanning electron microscopy (SEM) surface morphology of DSF-loaded solid lipid nanoparticles of DPS2 prepared by SE method followed by PS.
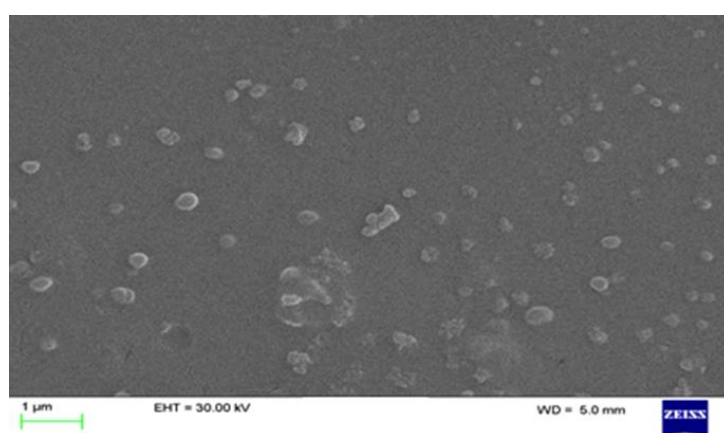
Figure 5.7. Scanning electron microscopy (SEM)surface morphology of DSF-loaded solid lipid nanoparticles of DPS3 prepared by SE method followed by HPH.

The zeta potential is a vital parameter for the stability of particle formulations. Studies have shown that higher values of zeta potential can exhibit high electric charges on the surface of particle by causing strong repellent forces among particulates to prevent aggregation (Harris, Martin, and Modi, 2001). Figure 5.8 demonstrates that all formulations have similar zeta potential values regardless of drug loading, and this including methods of preparations and techniques for size reduction. Nonetheless, zeta potential values for all formulations were below 25 -mV; this may indicate good stability of SLNs in aqueous dispersion (Müller, Mäder and Gohla, 2000). SLNs produced by the D-Nano-Pr and SE method showed no significant ($p > 0.05$) changes of zeta potential (Figure 5.8).
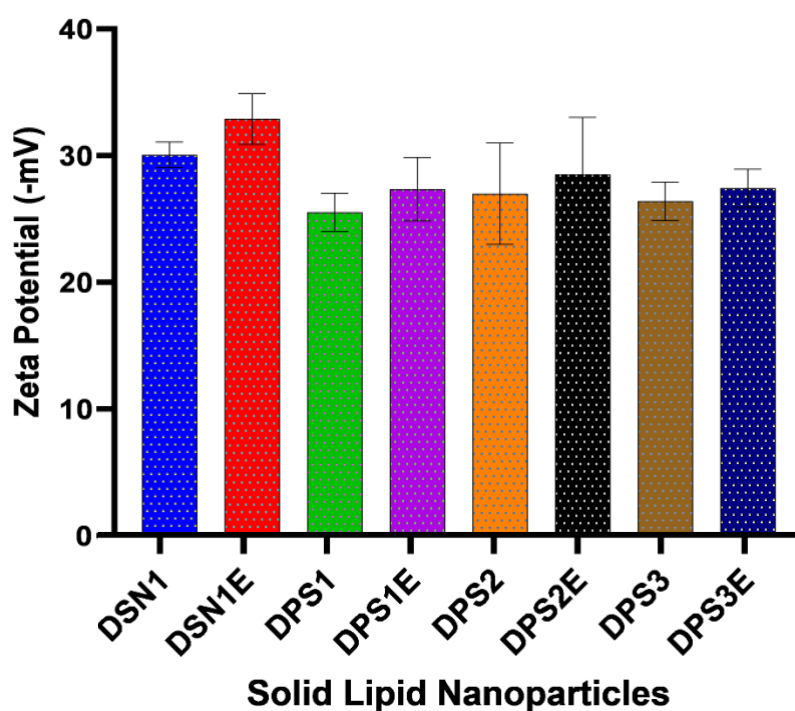
Figure 5.8. Zeta potential of DSN1/DSN1Eprepared by the D-Nano-Pr method, DPS1/DPS1Eprepared by the SE method, DPS2/DPS2E and DPS3/DPS3Ewere prepared by theSE method then particle size reduced by the PS and HPH techniques, respectively. (Mean ± SD, n=3).

5.4.2 Differential scanning calorimetry

DSC studies of SLNs were carried out to investigate the physicochemical state of encapsulated DSF nano-carrier systems. Figure 5.9 demonstrated DSC thermograms of the following standards, DSF, Precirol, Compritol 888 ATO, and sucrose. As shown in Figure 5.9, DSF-loaded SLN (DSN1 SLN) prepared by the D-Nano-Pr method showed no DSF peak, this is indicating DSF amorphous state. The reason for the disappearance of DSF peak in loaded SLNs is due to manufactured loaded SLNs above the melting point of DSF. Also, this is an indication that DSF manufactured above its melting point at 70 $^\circ$C can maintain complete stability when in the amorphous state which allows limited recrystallization (Hancock and Zografi, 1997; Leuner and Dressman, 2000). Figure 5.13 showed no DSF peak of DSN1E SLN. The DSC measurements from a published article using similar phospholipid materials demonstrated no peak of SN38-loaded SLN prepared by using the SE method (Mosallaei, et al., 2016).

In Figure 5.9a-e, the DSC curves of samples indicated by an arrow showed sharp and broad peaks of Precirol, Compritol, DSF, and sucrose standards. Similar peaks were observed from the physical mixtures. Therefore, the DSC spectra heating curves of DSF-loaded DSN1 and unloaded DSN1E SLNs (Figure 5.9 f and g) did not show DSF at 70 $^\circ$C. This effect was attributed to the formulation of the empty or loaded SLNs dissolved at 80 $^\circ$C. The overlapping calorimetric peak of Precirol/Compritol and the broad peak of sucrose are shown in appendix-C (Figure 5.14 – 5.19). The incubation of SLNs formulation at the same temperature of the lipid phase at 80 $^\circ$C induces no DSF peak compared to the physical mixture and DSF standards. Considering the disappearance of the DSF peak from the loaded SLNs indicates complete dissolution in the lipid phase at a temperature (80 $^\circ$C) above the DSF melting point (70 $^\circ$C). The only DSF peak that is constant among the DSC spectra can be observed between the

standards (Figure 5.9 b, and e). The disappearance peak of DSF suggested that the hydrophobic drug was preferentially dissolved in the lipid phase and that DSF was inside the lipid matrix of the SLN. Regardless of the high temperature affecting the SLNs, which constituted aggregates SLNs inside the lipid particles (Figure 5.5 – 5.7), hence produce satisfactory percentage drug encapsulation efficiency.
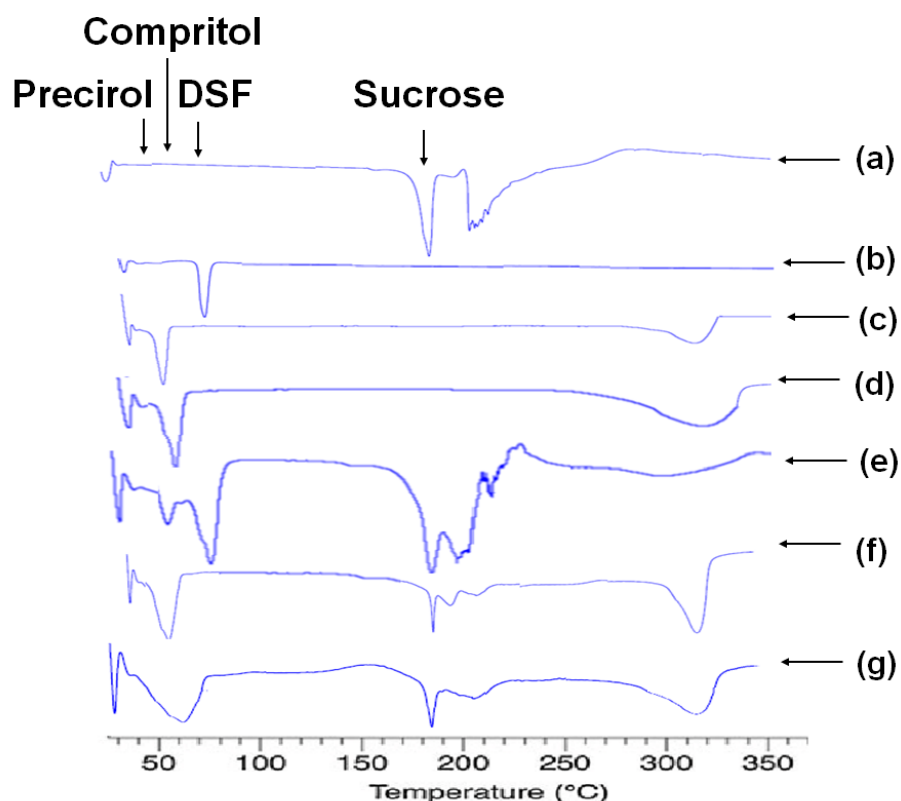
Figure 5.9. A representative of DSC thermograms of (a) sucrose standard, (b) DSF standard, (c) Precirol standard, (d) Compritol standard, (e) physically mixed standards (f), DSF loaded solid lipid nanoparticles (SLNs), and (g) blank SLNs. Both NPs formulations and physically mixed standards were prepared in a drug/polymer 1:9 ratio by SE method followed by HPH technique (particle size reduction).

5.4.3 Fourier transform infrared spectroscopy

The thermal results of SLNs and standards were confirmed by FTIR analyses in Figure 5.10. The SLNs formulations were used to make a comparison in terms of DSF functional groups to the following standards, Precirol ATO-5, Compritol 888 ATO, and mixed (DSF, Precirol AT0-5, Compritol 888 ATO, mPEG-PEG$_{2k}$, DSPE-PEG$_{2k}$, and sucrose). In Figure 5.10, DSF showed no characteristic of CH$_3$ stretching vibrational bands. The FTIR analysis of the blank SLNs showed confirmation of DSF

disappearance vibrational stretches of CH_3 as it was observed from the DSC thermograms. Appendix-C the following Figures 5.20, 5.22, and 5.24 presented no characteristic band for DSF but suggesting DSF encapsulation in the lipid matrix core. Also, in appendix-C of the corresponding blanks in Figure 5.21, 5.23, and 5.25 were like the same FTIR spectra as the DSF-loaded SLNs. The blank SLNs demonstrated that the formulations were not influenced by the phospholipid concentration in the lipid phase. The characteristic band of DSF standard showed a crystalline state than the amorphous state of DSF-loaded SLNs. At high temperature of the lipid phase enabled DSF formation of amorphous state region inside the lipid matrix core.

The FTIR thermograms of the loaded SLNs confirmed DSF encapsulation in the following compatibility excipients, preciprol, and compritol solid lipid matrix core, which enhances the entrapment of DSF. The FTIR spectra of blank (DSN1E) SLNs containing preciprol and compritol excipients showed a different length with a characteristic band of 1,638 cm^{-1} on the C=O stretch vibration, compared to the standards (Figure 5.10g).The FTIR spectra of the unloaded and loaded SLNs matched the published results of SLNs.
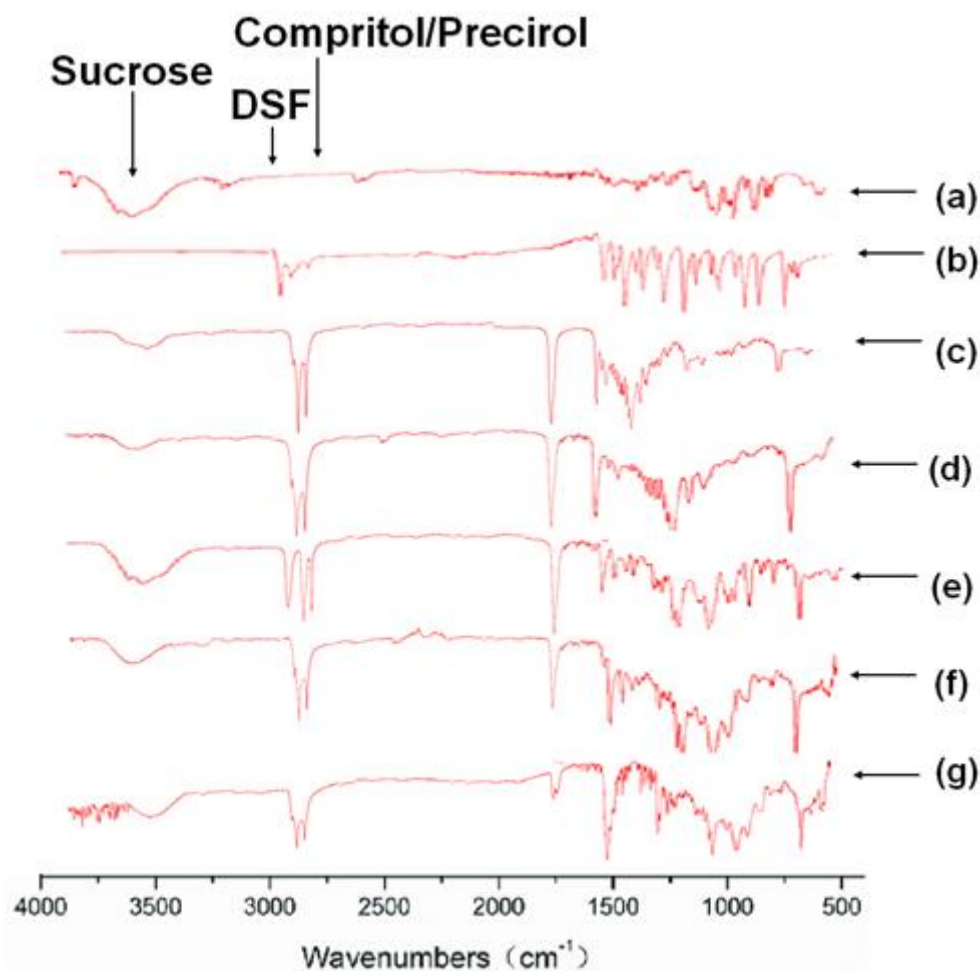
Figure 5.10. A representative of FTIR spectroscopic analysis demonstrated(a) sucrose standard, (b) DSF standard, (c) Precirol standard, (d) Compritol standard, (e) physically mixed standards (f), DSF loaded solid lipid nanoparticles (SLNs), and (g) blank SLNs. Both NPs formulations and physically mixed standards were prepared in a drug/polymer 1:9 ratio by SE method followed by HPH technique (particle size reduction).

5.4.4 Encapsulation efficiency

Irrespective of the different methods employed to prepare DSF-loaded SLNs the encapsulated drug needs to be adequately partitioned into lipid droplets of nano-scaled size so that to achieve increased drug loading efficiency (Mehnert and Mäder, 2012). As shown in Figure 5.11, the encapsulation efficiency of 69% for DSN1 SLN demonstrates a significant increased ($p < 0.05$) drug loading efficiency compared to DPS1 and DPS3 SLNs with an encapsulation efficiency of 57% and 56%, respectively. DPS2 SLN encapsulation efficiency was approximately 65% with no significant

differences ($p > 0.05$) compared to DPS1 and DPS3 SLNs (Figure 5.11). DSN1 SLN showed no significant difference ($p > 0.05$) compared to the DPS2 SLN (Figure 5.11). This means the produced SLNs by the D-Nano-Pr and SE methods demonstrated highest percentage encapsulation efficiency, which indicates that the D-Nano-Pr method hadDPS1 SLN of high percentage encapsulation efficiency, but large particle size (around 400 nm).Irrespective of drug concentration in the lipid phase DSF entrapment increases in the lipid matrix due to DSF amorphous state. The SE method followed by particle size reduction using the PS technique produced high percentage encapsulation efficiency of DSL2 SLN exhibited a smaller size (less than 150 nm) but with a relatively high PDI (around 0.5).
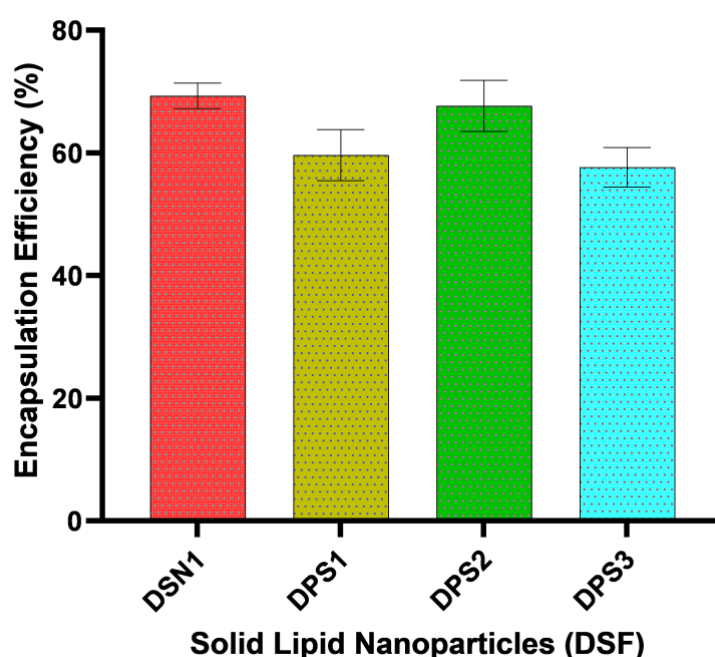
Figure 5.11. The encapsulation efficiency of DSN1 SLN prepared by the D-Nano-Pr method, the DPS1 SLN prepared by the SE method, while the DPS2 and DPS3 SLNs were also prepared by the SE method, then particle sizes reduced using the PS and HPH techniques, respectively.(Mean ± SD, n=3).

5.4.5 Cumulative release

The *in vitro* drug release of thefree DSF standard and DSF-loaded SLNs were performed in PBS (pH 7.4) with 1% Tween80. As shown in Figure 5.12, all SLNs demonstrated a slow control DSF cumulative release at an interval time of three hours obtained percentage release of 13% 16%, 12% and 17%, respectively. Within 24 hours, the free DSF standard showed fast release compared to all SLNs incubated. Overall, the DPS2 SLN had no significant ($P > 0.5$) change, but markedly the slowest release amongst all SLNs. The slow drug release demonstrates the high stability of DSF-loaded SLNs (Zur Mühlen and Mehnert, 1998). This is indicating the preparation of SLNs for controlled delivery of DSF is suitable to enhance the prolonged circulation of DSF for therapeutic effect. At 24 hours time, a slow release of DSN1, DPS1, DPS2, and DPS3 SLNs demonstrated burst release of DSF at 35%, 32%, 25% and 39%, respectively, (Figure 5.12).
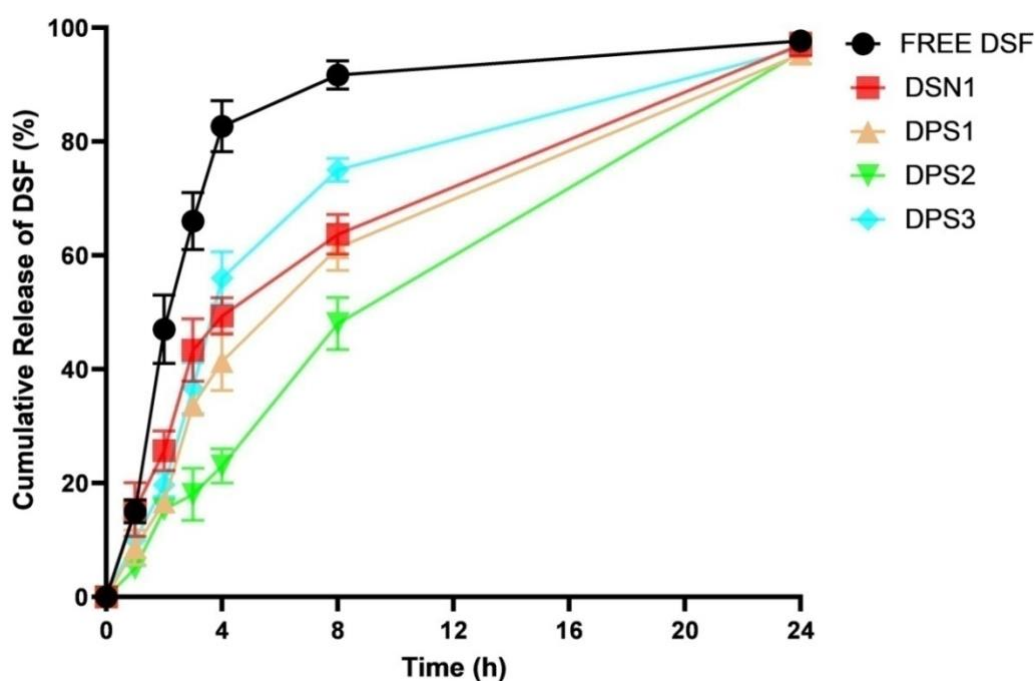
Figure 5.12. Cumulative release of the free DSF standard,DSN1 SLN prepared by the D-Nano-Pr method, the DPS1 SLN prepared by the SE method, while the DPS2 and DPS3 SLNs were also prepared by the SE method, then particle sizes reduced using the PS and HPH techniques, respectively.(Mean ± SD, n=3).

5.4.6 Stability

The stability of DSF-loaded DSN1 and DPS1-3 SLNs prepared by the D-Nano-Pr method and the SE method was evaluated in horse serum after incubation. The incubated DSF-loaded SLNs in serum were taken at different time-period, and DSF peak was detected using the HPLC method. As shown in Figure 5.13, the freeze-dried manufactured samples demonstrated higher stability in horse serum than the free DSF standard. At a time interval of one minute, the stability of free DSF in horse serum was very low with over 50% of DSF is degraded, whereas more than 50% of all SLNs remained intact after 2 hours of incubation. No significant differences in the stability profiles for DPS2 and DPS3 SLNs and both have less stability than DPS1 SLN. This is expected as DPS1 SLN has a larger particle size than both, hence less surface area, and higher stability. Previous studies indicated that 50% of DSF loaded liposomes were degraded within 20 min (Wang et al., 2012). In this study, solid lipid nanoparticles extended this time to more than two hours incubation. This might be because SLNs are more rigid and tolerant than liposomes.
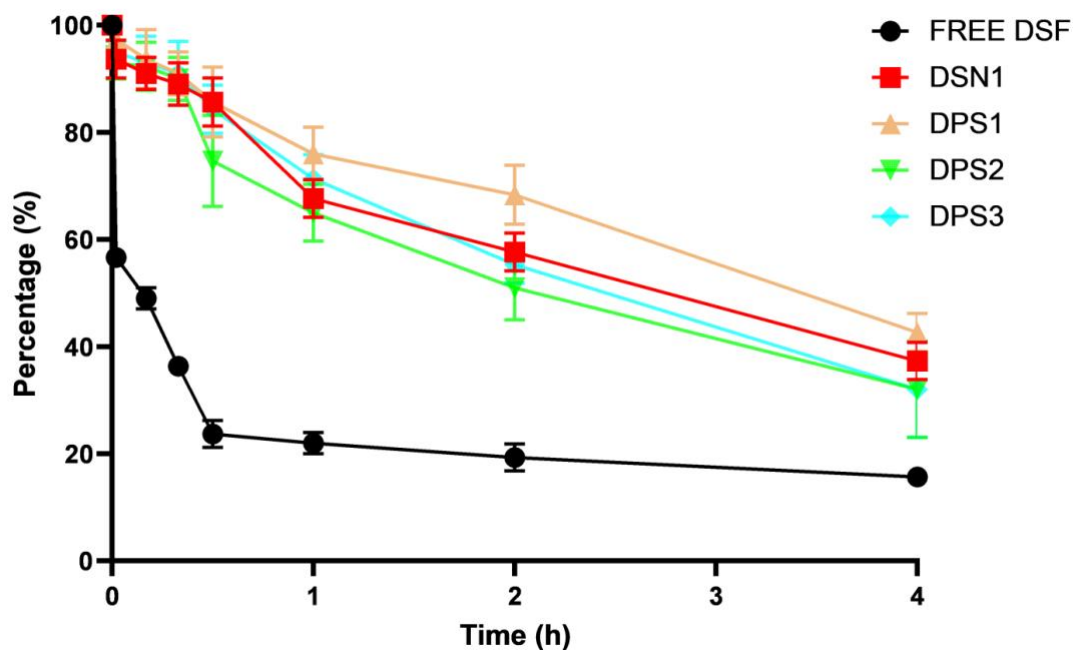
Figure 5.13.Stability of the free DSF standard,DSN1 SLN prepared by the D-Nano-Pr method, the DPS1 SLN prepared by the SE method, while the DPS2 and DPS3 SLNs were also prepared by the SE method, then particle sizes reduced using the PS and HPH techniques, respectively.(Mean ± SD, n=3).

5.6 Conclusion

The D-Nano-Pr and SE methods were used prepared DSF-loaded solid lipid nanoparticles (SLNs) by the hot homogenization (HH) technique at elevated temperature above the melting point of both the phospholipids and DSF. The precirol and compritol excipients were used to manufacture and characterized DSF-loaded and unloaded SLNs. Due to high temperature, the SLNs produced aggregated and collapsed morphology and lipid matrix core-shell structure. The D-Nano-Pr method produced relatively large nanoparticles but with narrow PDI. Also, DPS1 SLN prepared by using the SE method assisted by hot melt mixing without particle size reduction has a larger particle size. The increase in drug concentration may be attributed to the large particle sizes. The reported particle size results from the literature markedly reflected the results obtained after characterization. However, reducing the size of SLNs prepared by the SE method, then particle sizes reduction were performed using the

HPH, and PS techniques produced SLNs with nano-size less than 150 nm with acceptable PDI. A good percentage of drug encapsulation efficiency was achieved irrespective of particle size reduction by the HPH, and PS techniques. Therefore, DSF-loaded SLNs prepared from both methods showed suitability to enhance bioavailability for therapeutic effect towards cancer therapy.

All SLNs had high negative zeta potentials indicating high dispersion stability. All prepared SLNs showed a slow release profile and increased stability in horse serum. SLNs prepare using the SE method followed by particle size reduction using the HPH technique proves superiority over the rest due to its smaller particle size, high encapsulation efficiency, and increased stability in horse serum.

Chapter 6: Development and Characterisation of PEGylated Disulfiram Encapsulated

Solid Lipid Nanoparticles Prepared by the Single Emulsion/Solvent Evaporation

Method and High-Pressure Homogenization Technique

6.1 Introduction

In this study, DSF loaded SLNs, including PEGylated (mPEG-PLGA$_{2k}$ and DSPE-PEG$_{2k}$) and unloaded (blanks) SLNs carrier systems were developed and characterized for DSF delivery against breast cancer cells. Freshly prepared samples were characterized in terms of particle size, zeta potential, percentage encapsulation efficiency, DSC, and FTIR. The cumulative drug release between DSF SLNs and PEGylated SLNs was evaluated. The MTT assay was employed to investigate the anti-cancer effect of free DSF and DSF-loaded SLNs/PEGylated SLNs in MDA-MB-231 cancer cells.

6.2 Aims

To prepare and characterize long circulation nano-carrier delivery systems of DSF loaded PEGylated SLNs prepared by the SE method then particle size reduced using the high-pressure homogenization technique (HPH) technique. This is to investigate the anti-cancer activity of non-PEGylated, and DSF-loaded PEGylated SLNs in cancer cells.

6.3 Experimental Design

6.3.1 Preparation of PEGylated disulfiram-loaded solid lipid nanoparticles

From the previous experiments in chapter 5, the SE method followed by HPH technique was superior to other methods of preparation such as the D-Nano-Pr method. Also, the use of PS technique for particle size reduction procedures reported in the literature suggested the presence of alloy aluminium and titanium dioxide (TiO$_2$) contaminated the NPs/SLNs suspensions from tip erosion during direct sonication. Therefore, unloaded/DSF-loaded SLNs (DSL1E/DSL1 SLN) and unloaded/PEGylated DSF-loaded SLNs (DSL1aE/DSL1a and DSL1bE/DSL1b SLNs) colloidal particulates were prepared by the oil-in-water (O/W) SE method (Najlah, et al., 2017), through the

HH technique (Mehnert and Mäder, 2012). After the preparation of SLNs, particle sizes were reduced by using the HPH technique, as described in section 2.2.2.5. Table 1 shows the ratios of materials used in the preparation of non-PEGylated and PEGylated SLNs.

Table 6.1.Different formulation ratios of disulfiram (DSF) PEGylated loaded solid lipid nanoparticles (SLNs) manufactured by single emulsion/solvent evaporation (SE) method.

Ingredient (ratio) Formulation*	Preciprol	Compritol	HPCS	mPEG$_{2k}$-PLGA	PEG$_{2k}$-DSPE	DSF	Total
DSL1aE	6.5	2.5	1	0.5	-	-	10
DSL1a	5	2.5	1	0.5	-	1	10
DSL1bE	6.5	2.5	1		0.5-	-	10
DSL1b	5	2.5	1	-	0.5	1	10

*DSL(a & b) represent PEGylated solid lipid nanoparticles (PEG-SLNs) formulations prepared by the single emulsion/solvent evaporation (SE) method, then particle sizes were reduced using the high-pressure homogenization (HPH) technique. E denotes the empty SLN formulation.

6.4 Results and discussion

6.4.1 Particle size and PDI

Also, this is the first study to manufactured PEGylated DSF-loaded SLNs using different ratios of phospholipids, DSF, and the two types PEGylation (mPEG$_{2k}$-PLGA and DSPE PEG$_{2k}$) into a molten solution by using the SE method. For all formulations, the blank SLNs had smaller particle sizes than its corresponding loaded ones (Figure 6.1). This might be an initial indicator of an interaction between the drug and the lipid used in the preparation. Such interaction may be a solid in solid solution or dispersion, or simply drug adsorption on the surface. In this context, all loaded SLNs were of size below 250 nm.

After particle size reduction by using the HPH technique, DSL1 SLN had a mean diameter of 144.9 ± 13.45 nm with a significant ($P < 0.05$) decreased particle size than DSL1a SLN. The increased particle size of DSL1a SLN was due to the attached

PEGylation ($mPEG_{2k}$-PLGA). DSL1 SLN had a similar significant ($p < 0.01$) decrease in particle size than DSL1b SLN. Reduced particulates of DSL1a SLN showed a significant ($p < 0.01$) increased particle size than DSL1b SLN when phospholipid DSPE PEG_{2k} diffuses at higher temperature the particle size increases.

The blank DSL1E SLN had a mean diameter of 105.2 ± 2.61 nm with a significantly ($P < 0.05$) decreased particle size than the DSL1aE SLN (Figure 6.1). Similarly, the DSL1E SLN had a significant ($p < 0.01$) decreased particle size than the DSL1bE SLN. The DSL1aE SLN demonstrated significant ($p < 0.05$) increased particle size compared to the DSL1bE SLN (Figure 6.1).

Furthermore, there are significant differences in the sizes among the loaded SLNs in the following order DSL1a > DSL1b > DSL1 SLN. More explicitly, PEGylated SLNs are larger than the naked SLN, which might be due to the PEG grafts expansion in the aqueous solution because of its hydrophilic nature. Unsurprisingly, DSL1a SLN PEGylated by the $mPEG_{2k}$-PLGA polymer was significantly ($p < 0.05$) larger than the DSL1b SLN PEGylated by the $DSPE-PEG_{2k.}$ Also, this might be explained by the difference of DSF interaction with the lipids used to manufacture the SLNs. Besides, the $mPEG_{2k}$-PLGA might have coated the SLNs resulting in larger nanoparticles, while $DSPE-PEG_{2k}$ was of a similar lipid nature and contributed to the particle construction.
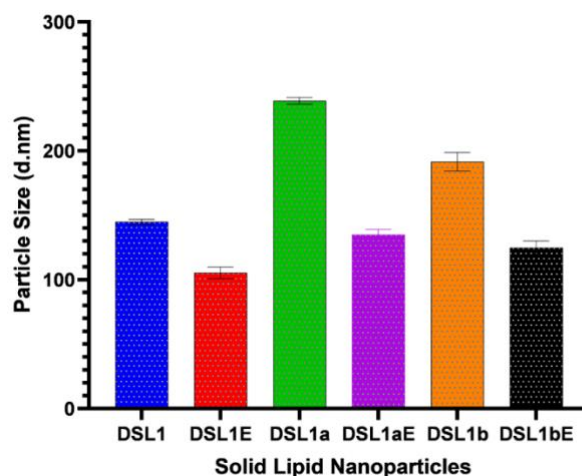
Figure 6.1. Particle sizes of PEGylated DSF solid lipid nanoparticles prepared by SE followed by HPH, (Mean ± SD, n=3).

As shown in Figure 6.2, all SLNs produced PDIs below 0.5 and were considered as narrow particle size distribution. DSL1 SLN showed significant ($p < 0.01$) increased PDI than the DSL1a SLN (Figure 6.2). But, no significant ($p > 0.05$) change in PDI between DSL1 and DSL1b SLNs. In comparison, DSL1a SLN showed significant ($p < 0.01$) increased in PDI compared to the DSL1b SLN.

The blank of DSL1E SLN showed significant ($p < 0.01$) decreased PDI than the DSL1aE SLN. While the DSL1E SLN had a significant ($p < 0.05$) decreased PDI compared to the DSL1bE SLN. But, no significant ($p > 0.05$) change in PDI observed between DSL1aE and DSL1bE.This also might be due to the difference in lipid composition among the three SLNs.
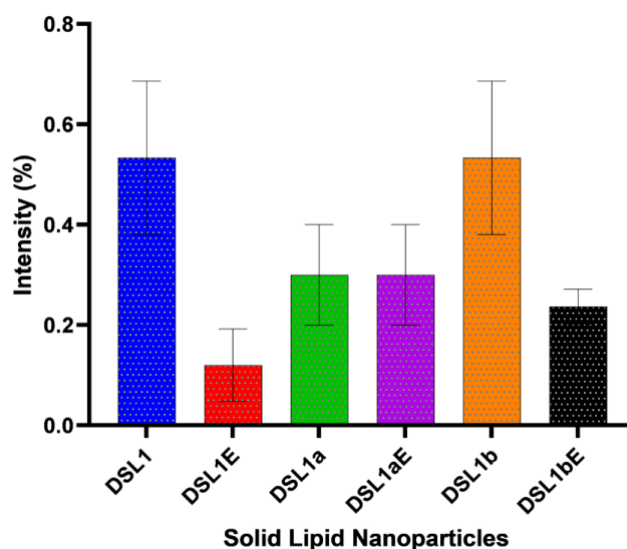
Figure 6.2. Figure 6. 1. Polydispersity index (PDI) of the PEGylated DSF solid lipid nanoparticles prepared by the SE followed by the HPH technique, (Mean ± SD, n=3).

6.4.2 Zeta potential

The Unloaded/DSF-loaded (DSL1/DSL1E) SLNs and unloaded PEGylated/DSF-loaded PEGylated (DSL1b/DSL1bE) SLNs demonstrated satisfactory zeta potential values than unloaded PEGylated/DSF-loaded PEGylated DSL1a/DSL1aE SLNs. No significant difference was found between each blank and its loaded counterpart. This might indicate that the drug is entrapped inside the loaded particles rather than adsorbed on the surface.

As shown in Figure 6.3, DSL1 SLN showed a significant ($p < 0.05$) increased the zeta potential value of 27.0.2 ± 6.27 nm than DSL1a SLN with a zeta potential value of 9.1 ± 1.19 nm. The addition of surface modifiers such as the amphiphilic mPEG$_{2k}$-PLGA on bare solid lipid nanoparticles significantly reduced zeta potential values, and this was due to the hydrophilic polymer chain masking the surface particle (Garcia-Fuentes, Torres and Alonso, 2005). The SLN was modified in DSL1a formulation by using the mPEG$_{2k}$-PLGA copolymer acting as protection towards the naked SLN,

176

therefore, resulted in a reduced charged particle of a lower zeta potential due to the PLA copolymer long-chain masking the carboxyl end groups of the phospholipid surface area (Gombotz et al., 1991). In contrast, the DSPE PEG$_{2k}$ added in DSL1b demonstrated higher charged surface of zeta potential, which indicates the formation of lower ionic force (Gombotz et al., 1991). The masked DSL1a SLN produced a thicker surface area of mPEG$_{2k}$-PLGA coiling around the naked SLN created a barrier that is assumed as efficient steric protection (Gombotz et al., 1991). This resulted in an increase particle size of DSL1a SLN than the naked DSF-loaded SLN formulation (DSL1 SLN) (Figure 6.1). This study showed PEGylated DSL1a/DSL1aE SLNs masked particle surface area of reduced zeta potential are in good agreement with similar results reported on drug-loaded PEGylated SLNs (Pignatello, et al., 2013; Mosallaei, et al., 2016).

There is no significant ($p > 0.05$) change in particle size between DSL1 and DSL1b SLNs.DSL1a SLN had a significant ($p < 0.01$) decreased particle size than the DSL1b SLN with a zeta potential value of 38.4 ± 6.46 nm (Figure 6.3). Adding the phospholipids' PEG, such as DSPE-PEG$_{2k}$ in DSL1b SLN enhances zeta potential value compared to that of the DSL1a and DSL1 SLNs (Figure 6.3). DSPE-PEG is a well-known establish electrostatic, steric stabilizer that increases zeta potential values (Woodle, et al., 1992; Lim and Kim, 2002). Previous studies reported that formulations prepared by the inclusion of DSPE-PEG$_{2k}$ at different ratios had their zeta potential values increased as the DSPE-PEG$_{2k}$ ratio increased (Lim and Kim, 2002). The unloaded DSL1E SLN produced significant ($p < 0.01$) increased zeta potential than the DSL1aE SLN (Figure 6.3). Whereas, the DSL1E SLN showed no significant ($P > 0.05$) change in zeta potential compared to the DSL1bE SLN. Finally, there is a significant ($p < 0.05$) change in zeta potential than the DSL1bE SLN.
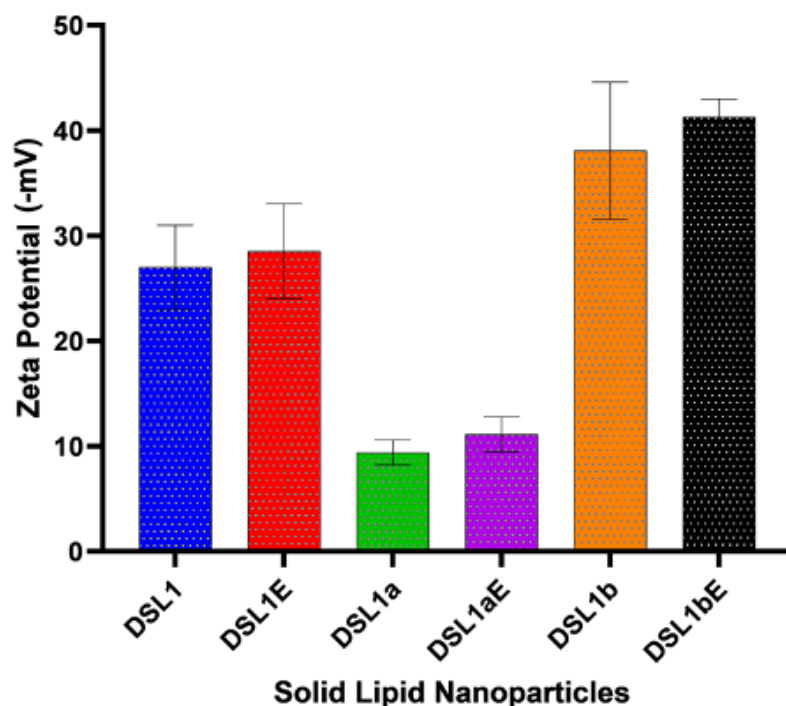
Figure 6.3. Zeta potential of the PEGylated DSF solid lipid nanoparticles prepared by the SE followed by the HPH technique, (Mean ± SD, n=3).

6.4.3 Differential scanning calorimetric

The thermograms of free DSF, preciprol, compritol, mPEG$_{2k}$-PLGA, DSPE PEG$_{2K}$, sucrose, physical mixture, non-PEGylated SLNs, PEGylated and the corresponding blank SLNs are shown in Figure 6.4. Free DSF had a sharp endothermic peak at 70.0 °C melting point of free DSF suggesting its crystalline state. DSC was utilized to determined DSF stability from the loaded PEGylated SLNs shown in Figure 6.4. In contrast, only sucrose, preciprol, compritol, mPEG$_{2k}$-PLGA, DSPE PEG$_{2K}$, and blank SLNs characteristic peaks are detected at different melting points. The DSC thermograms of loaded SLNs demonstrated no endothermic peak of DSF, which indicates an amorphous state. The blank and DSL1a (mPEG$_{2k}$-PLGA) SLN had a broad endothermic peak through 55.0-67.0 °C, and this is suggesting an overlap of precirol and compritol (Figure 6.4). Therefore, sharp endothermic peaks of sucrose

and combine Precirol/Compritol showed sharp melting points at 186.0-189.0 °C, and 289.0-320.0 °C. Appendix-D, showed the DSC thermal analyses of DSL1b SLN (Figure 6.12), and DSL1bE SLN (Figure 6.13) showed no DSF peak for the loaded and unloaded SLNs. The melting endothermic DSC thermograms of freeze-dried DSF-loaded/PEGylated SLNs had no DSF endothermic peak indicating DSF has incorporated amorphously within the matrix of the colloidal particulate system (Figure 6.4). DSC thermograms of SN38-loaded solid lipid nanoparticles demonstrated similar endothermic peak domain (Mosallaei, et al., 2016).
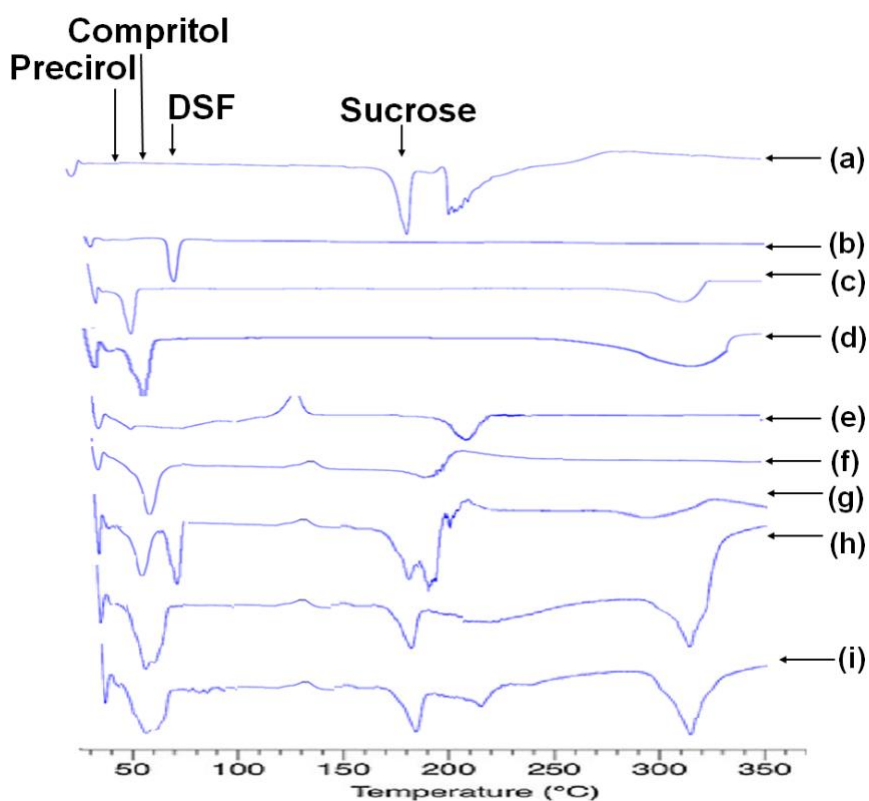
Figure 6.4. A representative of DSC thermograms demonstrating (a) sucrose standard, (b) DSF standard, (c) Precirol standard, (d) Compritol standard, (e) mPEG$_{2k}$-PLGA (f), DSPE PEG$_{2k}$, (g) physically mixed standards, (h) DSF-loaded SLNs (mPEG$_{2k}$-PLGA), and (i) blank SLNs (mPEG$_{2k}$-PLGA). Both NPs formulations, and physically mixed standards were prepared in a drug/polymer 1:9 ratio using SE method followed by HPH (particle size reduction).

6.4.4 Fourier transform infrared spectroscopy

The intermolecular interactions between standards and SLNs were investigated by FTIR as ascribed in Figure 6.5. Typical spectrum in Figure 6.5 demonstrated FTIR

179

analysis of DSF-loaded SLNs with characteristic peaks of O-H stretch (3453 cm^{-1}), C=O stretch (1719 cm^{-1}) from Precirol, Compritol, and PEGs. The corresponding blank SLNs exhibited similar characteristic peaks, as the loaded SLNs. In appendix-D, FTIR spectroscopic analyses of DSL1b SLN (Figure 6.14), and DSL1bE SLN (Figure 6.15) showed no DSF peak for the loaded and unloaded SLNs. The non-appearance of DSF indicates the amorphous state, and this is confirmed by the DSC thermograms of DSF non-melting peak as shown in Figure 6.4. The FTIR spectra of the solid lipid nanoparticles produced similar results compared to the published literature (Mosallaei, et al., 2016; Zeng, et al., 2018). After introducing the mPEG$_{2k}$-PLGA in loaded DSL1a SLN showed a shift of characteristic peaks for C=O at 1758 cm-1 compared with the original standards of precirol, and compritol, which confirmed the successful incorporation of DSF amongst the loaded SLNs. The non-appearance of DSF peak from the loaded DSL1a SLN was found similar to the unloaded DSL1aE SLN, as shown in Figure 5.10.
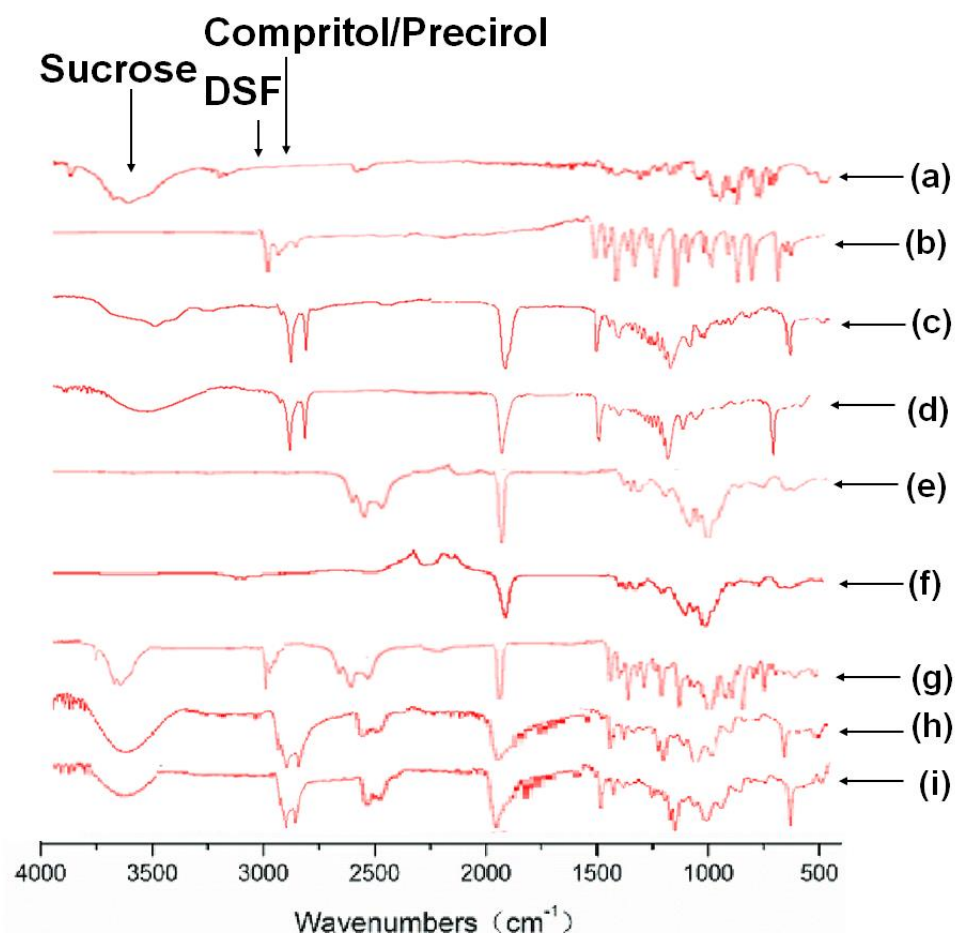
Figure 6.5. A representative of FTIR spectroscopic analysis demonstrating (a) sucrose standard, (b) DSF standard, (c) Precirol standard, (d) Compritol standard, (e) mPEG$_{2k}$-PLGA (f), DSPE PEG$_{2k}$, (g) physically mixed standards, (h) DSF-loaded SLNs (mPEG$_{2k}$-PLGA), and (i) blank SLNs (mPEG$_{2k}$-PLGA). Both NPs formulations, and physically mixed standards were prepared in a drug/polymer 1:9 ratio using SE method followed by HPH (particle size reduction).

6.4.5 Encapsulation efficiency of disulfiram solid lipid nanoparticles

Figure 6.6showed the percentage encapsulation efficiency of DSF incorporated in DSL1a, DSL1b and DSL1 SLNs. As shown in Figure 6.6, the encapsulation efficiency percentages of DSL1 SLN (DSF-loaded SLN), DSL1a SLN (DSF-loaded mPEG$_{2k}$-PLGA SLN), and DSL1b SLN (DSF-loaded DSPE-PEG$_{2k}$ SLN) were 65 ± 5.91%, 59 ± 7.37% and 37 ± 5.13%, respectively.

There is no significant ($p > 0.5$) change in DSF encapsulation efficiency between DSL1 and DSL1a SLNs. But, adding DSPE-PEG into the formulation of DSL1b SLN

demonstrated a significantly ($p < 0.01$) decreased loading efficiency compared to the non-PEGylated DSL1 SLN (Figure 6.6). Similarly, DSL1b SLN showed a significant ($p < 0.05$) decreased in DSF encapsulation efficiency than the DSL1a SLN (Figure 6.6).This phenomenon suggested the obstruction of steric stabilization by decreasing drug incorporation in the innermost solid lipid core; therefore drug loading was decreased (Heiati, et al., 1997; Jenning and Gohla, 2001). Also, decreased DSF loading efficiency by the inclusion of DSPE-PEG$_{2k}$ might be, due to the increased electrostatic stabilization expelling DSF (Woodle, et al., 1992; Jenning and Gohla, 2001). However, naked DSL1 SLN colloidal particulates had a satisfactory drug loading efficiency indicating high drug solubility in lipids (Müller, Mäder and Gohla, 2000). Similar studies reported the low percentage encapsulation efficiency of SN-38 loaded by PEGylated (PEG$_{2k}$-DSPE) SLN (Mosallaei, et al., 2016).
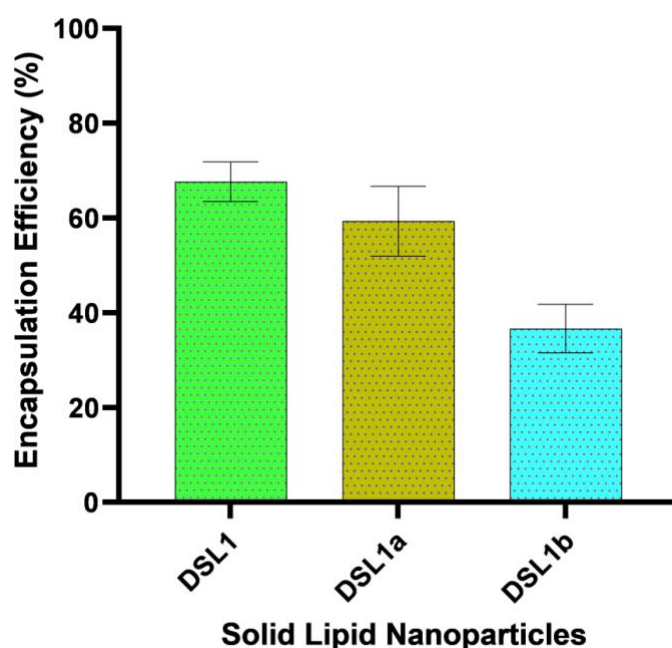
Figure 6.6. The encapsulation efficiency of DSF-loaded SLN, DSF-loaded mPEG$_{2k}$-PLGA SLN and DSF-loaded DSPE-PEG$_{2k}$SLN, (Mean ± SD, n=3).

6.4.6 Cumulative release of disulfiram solid lipid nanoparticles

Figure 6.7 showed cumulative *in vitro* release of free DSF, DSL1a, DSL1b and DSL1 SLNs in PBS (1% Tween80) solution exhibit temporal release of DSF. In the release medium, 1% Tween-80 (v/v %) was added to improve the stable condition of SLNs in PBS solution. Previous research study confirmed the stable release of encapsulated PTX NPs in Tween80 solution (Yang, et al., 2007). The free DSF release showed non-sustainable drug release with high percentage cumulative release compared to DSF encapsulated SLNs. The three formulations demonstrated slow-release if DSF over 24 hours (Figure 6.7). After three hours, DSL1b and DSL1 SLNs showed a similar release percentage of 12%. Whereas, DSL1a SLN demonstrated a significantly increased ($p < 0.01$) DSF release of 24% (Figure 6.7). After 24 hours, DSL1a SLN produced a significantly higher ($P < 0.05$) release of DSF (40%) compared to DSL1b and DSL1 SLNs with DSF release of 23% and 25%, respectively, (Figure 6.7). The DSL1a SLN demonstrated the fastest release of DSF amongst all formulations. This can be explained by the fact that DSL1a SLN has the smallest particle size amongst the three formulations, hence larger surface area allowing faster diffusion. The SLNs indicated the ability to minimize the content of premature drug release by extending drug circulation to target cancer cells within the intracellular compartments of the human body.
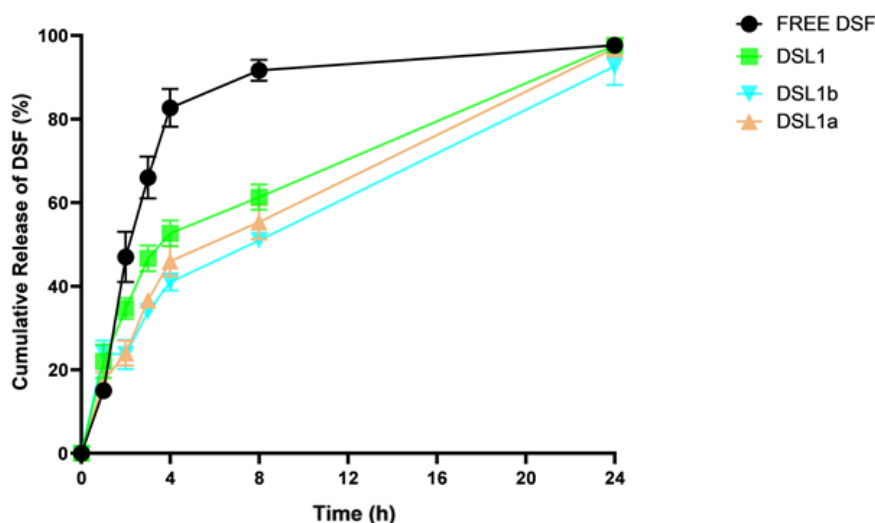
Figure 6.7. The cumulative release of the free DSF standard and PEGylated DSF-loaded SLNs. (Mean ± SD, n=3).

6.4.7 Stability

Stability of naked and PEGylated DSF-loaded SLNs of DSL1, DSN1a, and DSL1b were evaluated in the presence of horse serum by developing methods explained in chapter 2. After 1 min of *in vitro* testing, almost half of the free drug (DSF) (57%) was rapidly reduced in the presence of horse serum (Figure 6.8). Whereas, after 1 min of incubationDSL1a, DSL1b and DSL1 SLNs demonstrated the stability of DSF in the presence of horse serum at around 94%, 90%, and 92%, respectively (Figure 6.8). The zeta potential is an important measure towards the physical stability of particle dispersions in distilled water of very low conductivity to obtain direct surface charge measurements. Regardless of the low amount of zeta potential on the DSL1a SLN ($mPEG_{2k}$-PLGA), the reduced electrostatic repulsion improves stability in horse serum. Whereas, DSL1b SLN (PEGylated DSPE) shows stability in horse serum due to the hydrophilic branches of PEG, and steric repulsion that prevents the SLNs from aggregation or fusion (Nikolova and Jones 1996). As shown in Figure 6.8, the sterically stabilized non-PEGylated and PEGylated SLNs in physiological media are capable of

prolonging SLNs lifetime, which makes them suitable as nano-carrier delivery systems than free DSF. Therefore, non-PEGylated and PEGylated SLNs are capable of the delivery of DSF to enhance therapeutic efficiency.

After four hours, the amount of DSF remaining from DSL1a, DSL1b and DSL1 SLNs produced 26%, 20%, and 32%, respectively (Figure 6.8). While the free DSF quickly degraded with just 3% of the drug remaining (Figure 6.8). Surprisingly, the naked SLNs demonstrated higher stability than both PEGylated SLNs. The hydrophilic PEG chain was supposed to protect DSF from the serum proteins and delay the interaction hence increase the stability. The masked surface charge of DSL1a SLN exhibited efficient steric stabilization by providing a better plasma protein adsorption to protect DSF from rapid degradation in the horse serum. However, the lower stability of PEGylated SLNs might indicate some structural defects and more formulation studies are required to develop PEGylated SLNs with higher stability.
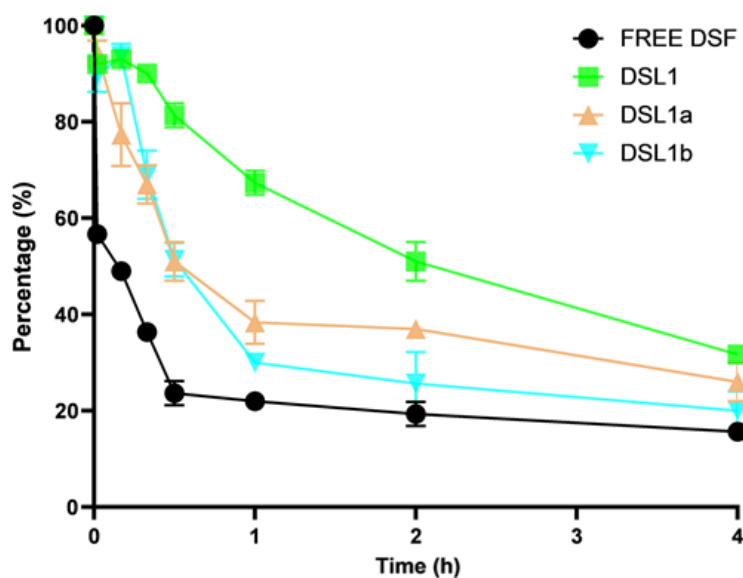
Figure 6.8. The stability of the free DSF, including DSF-loaded non-PEGylated and PEGylated SLNs were incubated in horse serum at 37 $^{\circ}$C for 4 h, (Mean ± SD, n=3).

6.4.8 MTT cytotoxicity assay

The cytotoxicity of the free DSF, DSF/Cu, manufactured DSL1,DSL1a, DSL1b SLNs and the corresponding blanks of the loaded SLNs treated against MCF 7 (Figure 6.9), MDA-MB-231 (Figure 6.10) and MDA-MB-231$_{PTX10}$ (Figure 6.11) cells were investigated using the MTT assay.

The MCF 7 cells, DSL1 SLNs, showed a significantly ($P < 0.05$) decreased toxicity at100 nM, and 1000 nM followed by decreased IC$_{50\%}$ of 152.56± 17.39 than the free DSF standard had an increasingIC$_{50\%}$ of 257.57 ± 52.54 (Table 6.2). As shown in Figure 6.8, the use of lower concentrations of DSL1 SLN indicates decreased cytotoxicity effect than the highest concentration (1000 nM), which indicates an increased inhibitory effect. The toxic effect of DSL1 SLN showed significant ($P < 0.05$) decreased at 37 nM, 100 nM, and 1000 nM concentrations than DSF/Cu with an IC$_{50\%}$ of 46.93 ± 11.41(Table 6.2). Similarly, DSL1 SLN showed a significant ($P < 0.05$) decreased cytotoxicity effect than the DSL1b SLN. But, the DSL1b SLN did not show any significant ($p > 0.05$) inhibitory effect between the DSL1 and DSL1a SLNs. Besides, DSL1 SLN was expected to be more toxic simply because of DSL1 SLN was shown to demonstrates increased percentage encapsulation efficiency (Figure 6.6), fastest drug release within 24 hours (Figure 6.7), also indicating the most stable in horse serum (Figure 6.8) among the PEGylated formulations (DSL1a and DSL1b SLNs).

DSL1 SLN sensitivity towards MCF 7 cells might be attributed to higher surface charged (zeta potential) (Figure 6.3), shown cellular uptake at 100 nM and 1000 nM concentrations indicating lower repulsion with surface charged of SLNs formulation on cell membrane at a different incubation time. The SLNs prepared by hot homogenization with higher melting point lipids showed influence in physical structure

186

as ascribed from the SEM images in chapter 5 (Figure 5.5). Therefore, the HH technique performed above the melting point of lipids temperature might be due to accelerating drug and phospholipid carrier degradation (Lander et al., 2000). This is possible especially during particle size reduction when SLNs are subjected to several passes (like 3-5 passes) through the HPH technique, thus increases the temperature on SLNs (Muller Rainer H 1998).

There is no significant ($p > 0.05$) inhibitory effect among DSF/Cu versus PEGylated formulations and PEGylated SLNs (Figure 6.8). The free DSF standard showed a significantly ($p < 0.05$) decreased inhibitory effect than the DSF/Cu standard (DSF/Cu is 5-fold potent than DSF, as shown in Table 6.2). PEGylated SLNs between 2000-5000 molecular weights are capable of suppressing plasma protein adsorption, slowdown particulates clearance, and improve protection against liver uptake (Chen et al., 2001).

Table 6.2. SLNs and standardsIC$_{50\%}$ on breast cancer cell lines. (Mean ± SD, n=3**).**

Samples (nM)	MCF 7		MDA-MB-231		MDA-MB-231$_{PTX10}$	
DSF	257.57	± 52.54	174.83	± 32.20	182.7	± 17.25
DSF-Cu	46.93	± 11.41	50.35	± 17.29	71.4	± 11.41
DSL1a	88.07	± 25.63	45.02	± 15.02	68.8	± 25.63
DSF1b	42.22	± 6.01	29.78	± 0.94	57.1	± 6.01
DSL1	152.56	± 17.39	109.56	± 28.39	97.6	± 17.39
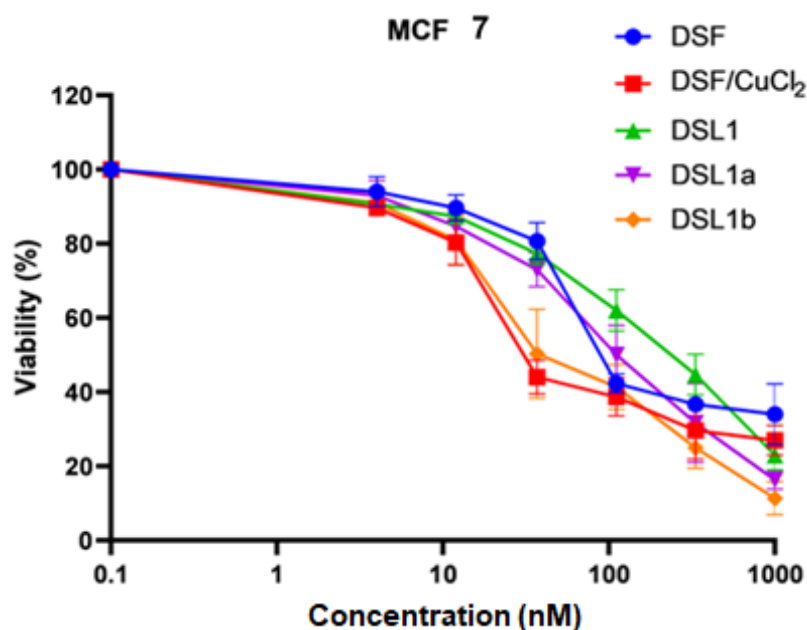
Figure 6.9. MTT cytotoxicity assay of MCF 7 treated with non-PEGylated and PEGylated SLNs (Mean ± SD, n=3).

In MDA-MB-231 cells, the DSL1 SLN showed a significantly ($P < 0.05$) increased inhibitory effect of an $IC_{50\%}$ (109.56 ± 28.39) than the DSF with an increasing $IC_{50\%}$ of 174.83 ± 32.20 (Table 6.2). In contrast, DSL1 SLN treated against MDA-MB-231 cells (Figure 6.9) demonstrated a slight decrease in $IC_{50\%}$, this is indicating a much lesser repulsion of DSL1a SLN on cell membrane enhances drug uptake than MCF 7 cells in Figure 6.8. While the DSL1 SLN showed a significant ($P < 0.05$) decreased inhibitory effect at a higher concentration than the DSF/Cu standard with an $IC_{50\%}$ of 50.35 ± 17.29 (Table 6.2). When compared with the DSL1 SLN to the PEGylated formulations, DSL1 SLN demonstrated a significant ($P < 0.05$) decreased cytotoxicity effect than the DSL1a SLN, and a similar significant ($P < 0.05$) decreased of the DSL1 SLN compared to the DSL1b SLN (Figure 6.9). Also, in Figure 6.9, DSF had significant ($P < 0.05$) decreased inhibitory effect than the DSL1a SLN, and DSL1b SLN ($p < 0.05$). While the

DSF standard showed significant ($P < 0.05$) decreased inhibitory effect than the DSF/Cu standard. But, the DSF/Cu standard versus DSL1a/DSL1b SLNs and PEGylated SLNs showed no significant ($p > 0.05$) inhibitory effect at 72 hours incubation.
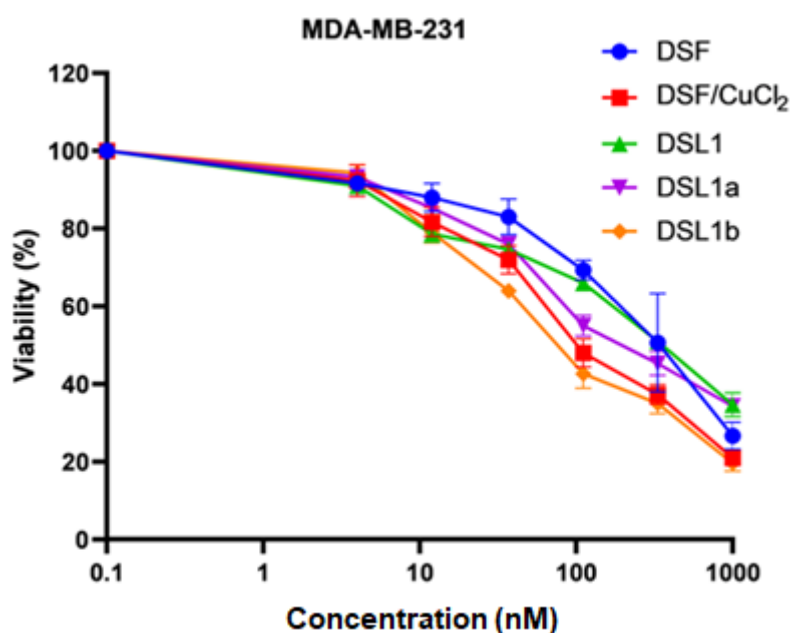
Figure 6.10. MMT cytotoxicity assay of MDA-MB 231 dosed with non-PEGylated and PEGylated SLNs, (Mean ± SD, n=3).

In MDA-MB-231$_{PTX10}$ cells, DSF showed significant ($P < 0.05$) decreased inhibitory effect and IC$_{50\%}$ of 182.7 ± 17.25 than the DSF/Cu standard with an IC$_{50\%}$ of 97.6 ± 17.39 (Table 6.2). The DSF standard showed a significant ($P < 0.05$) decreased inhibitory effect than the DSL1 SLN. Also, the DSF standard showed significant ($p < 0.05$) decreased inhibitory effect than the DSL1a and DSL1b SLNs (Figure 6.10). However, the DSF/Cu standard did not show any inhibitory effect ($p > 0.05$) among the DSL1 SLN and PEGylated formulations of DSL1a and DSL1b SLNs. In contrast, the DSL1b SLN had the lowest IC$_{50}$ (Table 6.2) for all three cell lines compared to the

189

DSL1a and DSL1 SLNs. This is indicative that the presence of DSPE-PEG$_{2k}$ in the lipid matrix enhances the permeability across the cell membrane, hence increases DSF-Cu uptake into cancer cells (Zhao, et al., 2012). The formulation of poorly water-soluble drugs by using the HH technique can improve the drug solubility as the drug will be within the lipid in an amorphous state (Pokharkar, et al., 2006). Thus, the cytotoxicity effect will be increased as a result of enhanced interaction/incorporation with the cellular membrane (Wehbe, et al., 2016). Surprisingly, these results do not align with the release study as the DSL1b SLN showed the slowest release among the three formulations (Figure 6.9), hence it was expected to have the lowest cytotoxicity towards cells. However, the DSL1b SLN was the least stable among all as indicated by the stability study in the horse serum (Figure 6.10); this might support the idea that there is an improved interaction, mediated by DSPE-PEG$_{2k}$, with the biological moieties for such protein or cell membrane. This led to lower stability in horse serum but higher cytotoxicity. Previous studies have demonstrated PEGylated SLNs nano-delivery carrier systems can enable drug long circulation in the bloodstream for effective cancer therapy (Stolnik, Illum and Davis, 1995). The cytotoxicity results confirm the potential use of SLNs delivery systems of DSF in cancer therapy.
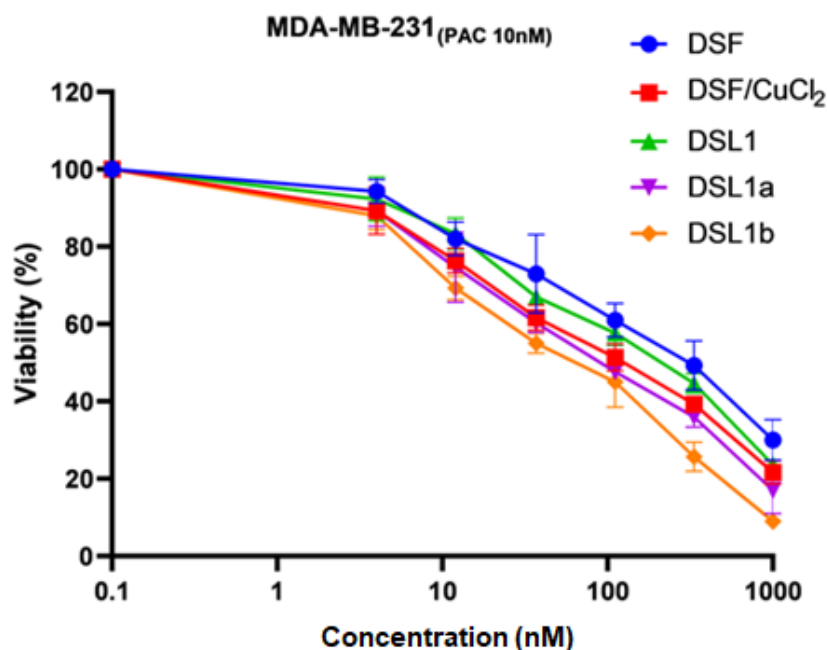
Figure 6.11. MMT cytotoxicity assay of MDA-MB 231$_{PTX10}$ cell line was treated with DSF PEGylated and non-PEGylated SLNs, (Mean ± SD, n=3).

6.5 Conclusion

In this study, non-PEGylated and PEGylated SLNs were developed by the SE method assisted using the HH technique, and after particle size reduction characterized by the DSF delivery into breast cancer cells. Aimed SLNs were reduced using the HPH technique. This technique was preferred due to non-residual contaminant of alloy aluminium and titanium from the tip erosion during direct sonication (nano-titanium dioxide particles in suspension with NPs/SLNs) compared to the PS technique. The PEGylated SLNs were performed either by adding mPEG-PLGA$_{2k}$ or DSPEPEG$_{2k}$. All formulated SLNs were of a satisfactory size, PDI, and Zeta Potential. All the manufactured SLNs confirmed DSF amorphous state by DSC thermograms. The formulations were of percentage encapsulation efficiency ranging from 40% to 65% and demonstrated a sustained release and good stability of DSF in horse serum. The incorporation of DSPEPEG$_{2k}$ resulted in SLNs that might have an ability to penetrate cell membranes; thus, allow DSF-loaded colloidal nano-carriers delivery into breast

cancer cells. PEGylated SLNs have shown the potential for developing a stable nano-carrier delivery system of DSF for cancer treatment.

Chapter 7: General Conclusion and Future Work

7.1 General conclusion

During the early discovery of DSF, it's primarily known as a drug for alcoholism treatment. Presently, research studies have shown evidence of DSF anti-cancer activity as the potential for inhibition of tumour cell growth under *in vitro* and *in vivo* experiments. Such strong evidence of DSF potent anti-cancer activity has been considered for drug repurposing delivery to target haematological malignancy and solid tumours. Therefore, due to extreme instability of DSF in the gastric intestinal tract and bloodstream is critical of DSF rapid degradation in clinical trials. A successful application of DSF delivery into cancer cells is the development of an efficient carrier system.

Moreover, few studies have demonstrated the need to improve DSF encapsulation efficiency and loading stability as it is critical of DSF delivery for cancer therapy. For this reason, this study showed successful incorporation of DSF into naked and PEGylated NPs/SLNs for DSF delivery into breast cancer cells. Besides, this study has developed simple and effective methods used to determine the amount of unloaded and DSF-loaded NPs/SLNs percentage encapsulated efficiency and DSF stability of loaded NPs/SLNs in horse serum.

At the early stage of this study, the initial goal was to established methods that are essential in the development and characterization of unloaded and DSF-loaded NPs/SLNs nano-carrier delivery systems. However, the physicochemical properties of unloaded and DSF-loaded NPs/SLNs such as their particle size, PDI, zeta potential, morphological structure, and the determination of stability and chemical interactions among physical materials play a vital role in achieving efficient nano-carrier drug delivery systems for cancer therapeutic application. The development of successful NPs/SLNs using FDA approved biocompatible and biodegradable

194

polymers/phospholipid materials by the D-Nano-Pr, and SE methods have helped to obtain smaller particle sizes. However, smaller particle sizes have reported gaining access in the intracellular compartments of tumour sites exhibiting higher retention time to overcome the EPR effect compared with normal tissues. Such obstacles occurring during blood vessel, the formation could result in leaky vessels having a gap size at approximately, 220 nm to 1.2 μm at a distance that is adjacent within endothelial cells. Therefore, previous studies have suggested that particle sizes ranging below 220 nm are more likely to gain access to tumour sites. Still, particle sizes lesser than 10 nm are vulnerable towards rapid renal clearance. This study mostly produced NPs/SLNs particle sizes that are above 220 nm with the advantage for higher retention and less likely to pass through the leaky vasculature system of tumours.

Moreover, $mPEG_{2k}$-PLGA and DSPE-PEG_{2k} were used to coat bared DSF-loaded NPs/SLNs to prevent NPs/SLNs clearance from the bloodstream by phagocytic uptake and RES system effect. The drug versus polymer/phospholipid 1:9 ratio was used throughout this study to develop NPs/SLNs by using the D-Nano-Pr and SE methods. Both methods demonstrated best particle sizes and PDIs for DSF delivery into MCF 7, MDA-MB-231, and MDA-MB-231$_{PTX10}$ breast cancer cell lines. The NPs developed by D-Nano-Pr method resulted in a smoothly uniform morphological structure capable of escaping the passage of leaky vessels in the intracellular compartments of tumour sites through the EPR effect. The PEGylated NPs also produced best particle sizes and adding DSF in the formulation makes slight changes to the particle size, but no larger sizes reported. The D-Nano-Pr method produces smaller particle sizes with a satisfactory percentage drug encapsulation efficiency of DSF-loaded NPs/SLNs. The efficient method of D-Nano-Pr had reduced PDI and increased electrically charged surface between NPs/SLNS. The resulted NPs/SLNs are reflective of most published results investigated by various research studies using the D-Nano-Pr method.

195

For the SE method, particulates are reduced to nano-scale using HPH and PS techniques. The non-PEGylated bared and PEGylated DSF-loaded PLGA (50:50 M/W, GA/LA copolymer with a molecular weight of 31k) NPs developed by SE method were characterized to determine particle size, PDI and zeta potential. To start with, finding the appropriate volume of the organic solvent to dissolve the hydrophobic DSF, and polymer/phospholipid materials are critical of the final drug versus polymer/phospholipid concentration in the organic phase, as it is a vital parameter to produce acceptable nanoparticle sizes. Previous studies have indicated the use of low-volume organic solvent demonstrates the best particle size and PDIs than the high-volume organic solvent, which produces larger nanoparticle sizes.

Also, selecting the right type of PVA stabilizers enhances stable particle sizes and increased drug loading depending on the method employed during formulations. This study found the blank PLGA/PVA (31-50K, Mw) 1:1 ratio to produce a relatively smaller monodispersed particle size distribution. It included increase zeta potential after size reduction of 5 minutes sonication. In contrast, the PVA products of 20-30K and 95K molecular weight produces increased particle sizes. Chapter 3 and 4 showed SEM images of PVA 31-50K molecular weight as the most superior. Therefore, it prevents coalescence and agglomerates in the emulsification process of NPs/SLNs formulations.

The SE method followed by the PS particle size reduction technique demonstrated the use of PVA mid-range molecular weights, such as 31-50K could efficiently be absorbed in the interface to avoid coalescence by lowering the interfacial tension and the energy of the surface area. The results are in support of the published articles using less sonication time to obtain reduced particle size. Monodispersed distribution of

NPs/SLNs and increased drug-loading efficiency compared with the high sonication time of 8 minutes.

After method development and characterization of smaller particle sizes with monodispersed PDIs, and increased zeta potential prepared by the D-Nano-Pr, and SE methods, the next phase was to develop unloaded and DSF-loaded PLGA nano-size carrier systems for long circulation. DSF anticancer activity on breast cancer cell lines was evaluated using NPs/SLNs, PLGA/PCL, and phospholipids coated PEGylations to enhance long circulation. D-Nano-Pr and SE methods were compared to select the required method for the production of smaller particle sizes monodispersed PDIs and increased zeta potential. The morphological structure by SEM, thermal analysis by DSC, Chemical interactions between functional groups of substances by FTIR, percentage encapsulation efficiency, and stability of DSF encapsulated NPs in horse serum were evaluated to compare between non-PEGylated and PEGylated PLGA NPs manufactured by the D-Nano-Pr and SE methods. Producing the best particle size can determine the destination of NPs/SLNs in the human body as previous studies have demonstrated size-dependent intracellular uptake of smaller-sized particulates efficiently transfected intracellularly. Moreover, both developing methods showed particle sizes of nano-carrier delivery systems that are above the recommended range of 220 nm for the delivery of DSF into solid tumours.

The D-Nano-Pr method was found superior over the SE method of particle size reduction through HPH, and PS techniques. The manufactured NPs/SLNs by D-Nano-Pr method were within the range of best particle size with the monodispersed distribution. Lower PDI for both NPs and SLNs formulations was observed, and this is regardless of drug-loading, and addition of PEGs. In contrast, particulates prepared

using the SE method followed by reduced particle sizes through HPH, and PS techniques produced increased particle sizes and PDIs. D-Nano-Pr method maintained monodispersed distribution and the SEM images confirmed this.

The D-Nano-Pr method had increased zeta potential than the SE method with reduced particle size by PS and HPH techniques. The reduced particle size of SLNs indicated mechanical energy force which effected on the electrical surface charge of NPs/SLNs particulates. Also, $mPEG_{2k}$-PLGA demonstrated reduced zeta potential, showing the effect of the amphiphilic copolymer conjugates with the anion PLGA/phospholipid. Both DSF non-PEGylated and PEGylated NPs/SLNs demonstrated satisfactory percentage encapsulation efficiency. NPs/SLNs have controlled release properties capable of delivering an increased amount of DSF over an extended period from 24 hours to over 48 hours. The initial fast release of DSF from NPs/SLNs indicates adsorbed drug on the surface of the nano-carrier systems. After the initial burst release of DSF, the NPs/SLNs demonstrated sustainable drug release for the period of 96 h incubation.

Compritol 888 ATO, Precirol ATO-5, and hydrogenated phosphatidylcholine (HPCS) (derived from Soybean) were used to prepared PEGylated and non-PEGylated SLNs. Therefore, the use of phospholipids influences particle size, PDI, and zeta potential. This study successfully developed efficient methods that can be used to produce the smaller particle size of DSF-loaded NPs/SLNs by the D-Nano-Pr method and SE method with a defined molecular weight of the stabilizer and sonication time. In addition, the development methods established to determine DSF stability in horse serum and DSF entrapment efficiency by separating the free drug form encapsulated NPS/SLNs.

This study shows DSF-loaded NPs/SLNs are capable of protecting DSF in horse serum. DSF encapsulated NPs/SLNs showed over 40% of DSF remain stable after

four hours incubation in horse serum. DSF free drug degraded in horse serum rapidly with less than 20% of DSF remains at four hours.

The MTT assays of DSF-loaded NPs/SLNs demonstrated advantage over the free DSF by exhibiting increased cytotoxicity due to high uptake of DSF by breast cancer cells. DNP4 NPs with $mPEG_{2000}$-PLGA shows more apoptosis in all three breast cancer cell lines (MCF 7, MDA-MB-231, and MDA-MB-231$_{PTX10}$). It seems that DSF-loaded NPs PEGylated $mPEG_{2k}$-PLGAdemonstrated increased cytotoxicity in breast cancer cells. The high inhibitory effect of DNP4 NPs can be attributed to$mPEG_{2k}$-PLGA ability to interact with the cell membrane without detection by the phagocytic cells from rapid clearance in the bloodstream. Also, this is apparent that DNP4 NPs can be quickly delivered into cancer cells of the intracellular compartments without the trigger of ROS. Therefore, the MTT assay results demonstrated that DSF-loaded NPs/SLNs have the ability to exert more cytotoxicity effect against breast cancer cells, and this including PTX-resistant MDA-MB-231 cancer cells compared to free DSF and DSF/Cu. This is an indication that $mPEG_{2k}$-PLGAis a potential nano-carrier delivery system for nanomedicine application towards cancer treatment, which is due to the PEGylated NPs (DNP4) internalization of DSF into cancer cells. The use of $mPEG_{2k}$-PLGA is to help circumvent the bared NPs from the effect of P-glycoprotein (P-gp) pumps and increases the inhibitory effect against cancer cells. Another advantage of using $mPEG_{2k}$-PLGA is to act as an intracellular drug depot by facilitating the slow release of the encapsulated DSF for enhancing therapeutic efficacy.

For the fact that DSF is well-tolerated in the human body, the development of DSF-loaded NPs/SLNs could provide drug accumulation into cancer cells. The low price of DSF and its availability in the market can improve clinical cancer therapy.

7.2 Future Work

The next stage of this study might include testing the stability of DSF-loaded NPs/SLNs in an animal model such as rats to confirm the enhanced stability of DSF *in vitro* (in horse serum) by the reported NPs/SLNs. Also, the *in vivo* anticancer activity will be necessary to confirm the feasibility of using both NPs and SLNs as nano-carriers of DSF for anticancer treatment, and mostly confirming the hypothesis that the PEGylating NPs/SLNs will facilitate prolonged circulation in vivo.

This study indicated satisfactory drug entrapment efficiency, but all the experiment was conducted in a ratio of1:9 between the drug and polymer/phospholipid. This will lead eventually to challenges in delivering the dose in vivo as large amount of excipients will be required to deliver an effective dose of the drug. This still considered as of the limitation of the nanomedicine in general; nevertheless, more work to enhance the loading efficiency of polymeric NPs and other nano-drug delivery systems will worth investigating.

List of Conference Abstracts and Prizes

1. Najlah, M., Dumbuya, I., Said Suliman, A., and M. Webster, 2019. Development and evaluation of disulfiram-loaded solid lipid nanoparticles, a proposed nanomedicine for chemo-resistance triple-negative breast cancers. Proceed. APS International PharmSci conference, Greenwich, UK.
2. Najlah, M., Dumbuya, I. 2019. Development, characterisation, and in vitro evaluation of disulfiram loaded PEGylated nanoparticles for breast cancer treatment. Proceed. 13th Edition of International Conference on Nanomedicine and Advanced Drug Delivery, London, UK. (keynote speaker)
3. Dumbuya, I., Webster, M., Tolaymat, I., Najlah, M., 2017. The effect size reducing technique on characteristics of disulfiram loaded lactic-co-glycolic acid nanoparticles. Proceed. UKICRS Symposium, Glasgow, UK. 24.
4. Dumbuya, I., Webster, M., Tolaymat, I., Najlah, M., 2017. Development of disulfiram polymeric-based nano-carriers to enhance cancer therapy. Proceed. UKICRS Symposium, Glasgow, UK. 25.

Prizes

Best poster for the abstract "Development of long circulation nano-enabled drug carriers for cancer treatment", ARU Interdisciplinary Conference, Anglia Ruskin University, Chelmsford, March 2017.

List of References

Adams, C.P. and Brantner, V.V., 2006. Estimating the cost of new drug development: is it really $802 million? *Health affairs,* 25 (2), pp.420-428.

Aitken, R.J. and Roman, S.D., 2008. Antioxidant systems and oxidative stress in the testes. *Oxidative medicine and cellular longevity,* 1 (1), pp.15-24.

Albanese, A., Tang, P.S. and Chan, W.C., 2012. The effect of nanoparticle size, shape, and surface chemistry on biological systems. *Annual Review of Biomedical Engineering,* 14, pp.1-16.

Alexis, F., 2005. Factors affecting the degradation and drug-release mechanism of poly (lactic acid) and poly [(lactic acid)-co-(glycolic acid)]. *Polymer International,* 54 (1), pp.36-46.

Alexis, F., Rhee, J., Richie, J.P., Radovic-Moreno, A.F., Langer, R. and Farokhzad, O.C., eds. 2008. *Urologic Oncology: Seminars and Original Investigations* Elsevier.

Al-Haj, N. and Rasedee, A., 2009. Solid lipid nanoparticles preparation and characterization. *Int J Pharmacol,*1, pp.90-93.

Allison, S.D., Chang, B., Randolph, T.W. and Carpenter, J.F., 1999. Hydrogen bonding between sugar and protein is responsible for inhibition of dehydration-induced protein unfolding. Archives of Biochemistry and Biophysics, 365 (2), pp.289-298.

Al-Jamal, W. and Kostarelos, K., 2007. Liposome–nanoparticle hybrids for multimodal diagnostic and therapeutic applications.

Alves, T.R., Lima, F.R.S., Kahn, S.A., Lobo, D., Dubois, L.G.F., Soletti, R., Borges, H. and Neto, V.M., 2011. Glioblastoma cells: a heterogeneous and fatal tumor interacting with the parenchyma. *Life Sciences,* 89 (15-16), pp.532-539.

Anandharamakrishnan, C., Rielly, C.D. and Stapley, A.G., 2010. Spray-freeze-drying of whey proteins at sub-atmospheric pressures. *Dairy Science & Technology,* 90 (2-3), pp.321-334.

Anderson, J.M. and Shive, M.S., 1997. Biodegradation and biocompatibility of PLA and PLGA microspheres. *Advanced Drug Delivery Reviews,* 28 (1), pp.5-24.

Anderson, J.M. and Shive, M.S., 2012. Biodegradation and biocompatibility of PLA and PLGA microspheres. *Advanced Drug Delivery Reviews,* 64, pp.72-82.

Aragon, C. and Amit, Z., 1993. Differences in ethanol-induced behaviors in normal and acatalasemic mice: systematic examination using a biobehavioral approach. *Pharmacology Biochemistry and Behavior,* 44 (3), pp.547-554.

Ashburn, T.T. and Thor, K.B., 2004. Drug repositioning: identifying and developing new uses for existing drugs. Nature reviews Drug discovery, 3 (8), pp.673-683.

Augustin, M.A. and Sanguansri, P., 2009. Nanostructured materials in the food industry. *Advances in Food and Nutrition Research,* 58, pp.183-213.

Avgoustakis, K., Beletsi, A., Panagi, Z., Klepetsanis, P., Karydas, A.G. and Ithakissios, D.S., 2002. PLGA–mPEG nanoparticles of cisplatin: in vitro nanoparticle degradation, in vitro drug release and in vivo drug residence in blood properties. *Journal of Controlled Release,* 79 (1-3), pp.123-135.

Awad, T.S., Moharram, H.A., Shaltout, O.E., Asker, D. and Youssef, M.M., 2012. Applications of ultrasound in analysis, processing and quality control of food: A review. *Food Research International,* 48 (2), pp.410-427.

Bánfi, B., Molnár, G., Maturana, A., Steger, K., Hegedûs, B., Demaurex, N. and Krause, K., 2001. A Ca2 -activated NADPH oxidase in testis, spleen, and lymph nodes. *Journal of Biological Chemistry,* 276 (40), pp.37594-37601.

Bang, J.H. and Suslick, K.S., 2010. Applications of ultrasound to the synthesis of nanostructured materials. *Advanced Materials,* 22 (10), pp.1039-1059.

Bangham, A.D. and Horne, R.W., 1964. Negative staining of phospholipids and their structural modification by surface-active agents as observed in the electron microscope. *Journal of Molecular Biology,* 8 (5), pp.66-IN10.

Barnes, A.F., Hardy, M.J. and Lever, T.J., 1993. A review of the applications of thermal methods within the pharmaceutical industry. *Journal of Thermal Analysis,* 40 (2), pp.499-509.

Behrend, O., Ax, K. and Schubert, H., 2000. Influence of continuous phase viscosity on emulsification by ultrasound. *Ultrasonics sonochemistry,* 7 (2), pp.77-85.

Benoit, J.P., Couvreur, P., Devissaguet, J.P., Fessi, H., Puisieux, F. and Roblot-Treupel, L., 1988. Les Formes «vectorisées» ou à «distribution modulée», nouveaux systèmesd'administration des médicaments. *Bulletin de la Société de pharmacie de Lille,* 44 (2-3), pp.75-85.

Bhattacharjee, S., Rietjens, I.M., Singh, M.P., Atkins, T.M., Purkait, T.K., Xu, Z., Regli, S., Shukaliak, A., Clark, R.J. and Mitchell, B.S., 2013. Cytotoxicity of surface-functionalized silicon and germanium nanoparticles: the dominant role of surface charges. *Nanoscale,* 5 (11), pp.4870-4883.

Bilensoy, E., Sarisozen, C., Esendağlı, G., Doğan, A.L., Aktaş, Y., Şen, M. and Mungan, N.A., 2009. Intravesical cationic nanoparticles of chitosan and polycaprolactone for the delivery of Mitomycin C to bladder tumors. *International journal of pharmaceutics,* 371 (1-2), pp.170-176.

Blanco, E., Shen, H. and Ferrari, M., 2015. Principles of nanoparticle design for overcoming biological barriers to drug delivery. *Nature biotechnology,* 33 (9), pp.941.

Bleeker, E.A., de Jong, W.H., Geertsma, R.E., Groenewold, M., Heugens, E.H., Koers-Jacquemijns, M., van de Meent, D., Popma, J.R., Rietveld, A.G. and Wijnhoven, S.W., 2013. Considerations on the EU definition of a nanomaterial: science to support policy making. *Regulatory toxicology and pharmacology,* 65 (1), pp.119-125.

Borja-Oliveira, C.R., 2014. Alcohol-medication interactions: the acetaldehyde syndrome. Journal of Pharmacovigilance.

Borst, P., Evers, R., Kool, M. and Wijnholds, J., 2000. A family of drug transporters: the multidrug resistance-associated proteins. *Journal of the National Cancer Institute,* 92 (16), pp.1295-1302.

Bouaouina, H., Desrumaux, A., Loisel, C. and Legrand, J., 2006. Functional properties of whey proteins as affected by dynamic high-pressure treatment. *International Dairy Journal,* 16 (4), pp.275-284.

Bourdélat-Parks, B.N., Anderson, G.M., Donaldson, Z.R., Weiss, J.M., Bonsall, R.W., Emery, M.S., Liles, L.C. and Weinshenker, D., 2005. Effects of dopamine β-hydroxylase genotype and disulfiram inhibition on catecholamine homeostasis in mice. *Psychopharmacology,* 183 (1), pp.72-80.

Boyd, P., Major, I., Wang, W. and McConville, C., 2014. Development of disulfiram-loaded vaginal rings for the localised treatment of cervical cancer. *European Journal of Pharmaceutics and Biopharmaceutics,* 88 (3), pp.945-953.

Bray, F., Ferlay, J., Soerjomataram, I., Siegel, R.L., Torre, L.A. and Jemal, A., 2018. Global cancer statistics 2018: GLOBOCAN estimates of incidence and mortality worldwide for 36 cancers in 185 countries. *CA: a cancer journal for clinicians,* 68 (6), pp.394-424.

Brazier, M. and Fovargue, S., 2006. A brief guide to the Human Tissue Act 2004. *Clinical Ethics,* 1 (1), pp.26-32.

Bregoli, L., Movia, D., Gavigan-Imedio, J.D., Lysaght, J., Reynolds, J. and Prina-Mello, A., 2016. Nanomedicine applied to translational oncology: a future perspective on cancer treatment. *Nanomedicine: Nanotechnology, Biology and Medicine,* 12 (1), pp.81-103.

Brewer, C., 1992. Controlled trials of Antabuse in alcoholism: the importance of supervision and adequate dosage. Acta Psychiatrica Scandinavica, 86 (S369), pp.51-58.

Budhian, A., Siegel, S.J. and Winey, K.I., 2007. Haloperidol-loaded PLGA nanoparticles: systematic study of particle size and drug content. International journal of pharmaceutics, [e-journal] 336 (2), pp.367-375.

Buechter, D.D., 1988. Free radicals and oxygen toxicity. *Pharmaceutical research,* 5 (5), pp.253-260.

Bunjes, H., Koch, M.H. and Westesen, K., 2003. Influence of emulsifiers on the crystallization of solid lipid nanoparticles. *Journal of pharmaceutical sciences* 92 (7), pp.1509-1520.

Bunjes, H., Westesen, K. and Koch, M.H., 1996. Crystallization tendency and polymorphic transitions in triglyceride nanoparticles. *International journal of pharmaceutics,* 129 (1-2), pp.159-173.

Burkitt, M.J., Bishop, H.S., Milne, L., Tsang, S.Y., Provan, G.J., Nobel, C.S.I., Orrenius, S. and Slater, A.F., 1998. Dithiocarbamate toxicity toward thymocytes involves their copper-catalyzed conversion to thiuram disulfides, which oxidize glutathione in a redox cycle without the release of reactive oxygen species. *Archives of Biochemistry and Biophysics,* 353 (1), pp.73-84.

CADDEN, A., 1987. Comparative effects of particle size reduction on physical structure and water binding properties of several plant fibers. *Journal of Food Science,* 52 (6), pp.1595-1599.

Cailleau, R., Olive, M. and Cruciger, Q.V., 1978. Long-term human breast carcinoma cell lines of metastatic origin: preliminary characterization. *In vitro,* 14 (11), pp.911-915.

Carroll, K.M., Fenton, L.R., Ball, S.A., Nich, C., Frankforter, T.L., Shi, J. and Rounsaville, B.J., 2004. Efficacy of Disulfiram and Cognitive Behavior Therapy in Cocaine-DependentOutpatients: A Randomized Placebo-Controlled Trial. *Archives of General Psychiatry,* 61 (3), pp.264-272.

Carroll, K.M., Nich, C., Ball, S.A., McCance, E., Frankforter, T.L. and Rounsaville, B.J., 2000. One-year follow-up of disulfiram and psychotherapy for cocaine-alcohol users: sustained effects of treatment. *Addiction,* 95 (9), pp.1335-1349.

Carroll, K.M., Nich, C., Ball, S.A., McCance, E. and Rounsavile, B.J., 1998. Treatment of cocaine and alcohol dependence with psychotherapy and disulfiram. *Addiction,* 93 (5), pp.713-727.

Carroll, K.M., Rounsaville, B.J. and Bryant, K.J., 1993. Alcoholism in treatment-seeking cocaine abusers: clinical and prognostic significance. *Journal of studies on alcohol,* 54 (2), pp.199-208.

Cavalli, R., Gasco, M.R., Chetoni, P., Burgalassi, S. and Saettone, M.F., 2002. Solid lipid nanoparticles (SLN) as ocular delivery system for tobramycin. *International journal of pharmaceutics,* 238 (1-2), pp.241-245.

Celej, M.S., Montich, G.G. and Fidelio, G.D., 2003. Protein stability induced by ligand binding correlates with changes in protein flexibility. *Protein science,* 12 (7), pp.1496-1506.

Cen, D., Gonzalez, R.I., Buckmeier, J.A., Kahlon, R.S., Tohidian, N.B. and Meyskens, F.L., 2002. Disulfiram induces apoptosis in human melanoma cells: a redox-related process1. *Molecular cancer therapeutics,* 1 (3), pp.197-204.

Chan, J.M., Zhang, L., Yuet, K.P., Liao, G., Rhee, J., Langer, R. and Farokhzad, O.C., 2009. PLGA–lecithin–PEG core–shell nanoparticles for controlled drug delivery. *Biomaterials,* 30 (8), pp.1627-1634.

Chandni, S.V., Viral, S. and Umesh, U., 2011. Solid Lipid Nanoparticles: A Review. *Current Pharma Research,* 1 (4), pp.351.

Chang, G. and Roth, C.B., 2001. Structure of MsbA from E. coli: a homolog of the multidrug resistance ATP binding cassette (ABC) transporters. *Science,* 293 (5536), pp.1793-1800.

Chen, C., Chin, J.E., Ueda, K., Clark, D.P., Pastan, I., Gottesman, M.M. and Roninson, I.B., 1986. Internal duplication and homology with bacterial transport proteins in the mdr1 (P-glycoprotein) gene from multidrug-resistant human cells. *Cell,* 47 (3), pp.381-389.

Chen, D., Cui, Q.C., Yang, H. and Dou, Q.P., 2006. Disulfiram, a clinically used anti-alcoholism drug and copper-binding agent, induces apoptotic cell death in breast cancer cultures and xenografts via inhibition of the proteasome activity. *Cancer research,* 66 (21), pp.10425-10433.

Chen, D. and Dou, Q.P., 2008. New uses for old copper-binding drugs: converting the pro-angiogenic copper to a specific cancer cell death inducer. *Expert opinion on therapeutic targets,* 12 (6), pp.739-748.

Chen, D., Yang, T., Lu, W. and ZHANG, Q., 2001. In vitro and in vivo study of two types of long-circulating solid lipid nanoparticles containing paclitaxel. Chemical and pharmaceutical bulletin, 49 (11), pp.1444-1447.

Chen, L., Remondetto, G.E. and Subirade, M., 2006. Food protein-based materials as nutraceutical delivery systems. *Trends in Food Science & Technology,* 17 (5), pp.272-283.

Chen, X., Arshad, A., Qing, H., Wang, R., Lu, J. and Deng, Y., 2011. Enzymatic condensation of dopamine and acetaldehyde: a salsolinol synthase from rat brain. *Biologia,* 66 (6), pp.1183.

Cheng, J., Teply, B.A., Sherifi, I., Sung, J., Luther, G., Gu, F.X., Levy-Nissenbaum, E., Radovic-Moreno, A.F., Langer, R. and Farokhzad, O.C., 2007. Formulation of functionalized PLGA–PEG nanoparticles for in vivo targeted drug delivery. *Biomaterials,* 28 (5), pp.869-876.

Chiba, T., Suzuki, E., Yuki, K., Zen, Y., Oshima, M., Miyagi, S., Saraya, A., Koide, S., Motoyama, T. and Ogasawara, S., 2014. Disulfiram eradicates tumor-initiating hepatocellular carcinoma cells in ROS-p38 MAPK pathway-dependent and-independent manners. PloS one, 9 (1), pp.e84807.

Chiu, M.H. and Prenner, E.J., 2011. Differential scanning calorimetry: An invaluable tool for a detailed thermodynamic characterization of macromolecules and their interactions. *Journal of Pharmacy and Bioallied Sciences,* 3 (1), pp.39.

Choi, S., Kwon, H., Kim, W. and Kim, J., 2002. Thermodynamic parameters on poly (d, l-lactide-co-glycolide) particle size in emulsification–diffusion process. Colloids and Surfaces A: Physicochemical and Engineering Aspects, 201 (1-3), pp.283-289.

Christensen, J.K., Rønsted, P. and Vaag, U.H., 1984. Side effects after disulfiram: Comparison of disulfiram and placebo in a double-blind multicentre study. *Acta Psychiatrica Scandinavica,* 69 (4), pp.265-273.

Corpe, W.A., 1970. Attachment of marine bacteria to solid surfaces. Edition Place of Publication Academic Press, New York.

Clas, S., Dalton, C.R. and Hancock, B.C., 1999. Differential scanning calorimetry: applications in drug development. *Pharmaceutical science & technology today,* 2 (8), pp.311-320.

Cobby, J., Mayersohn, M. and Selliah, S., 1977. Methyl diethyldithiocarbamate, a metabolite of disulfiram in man. *Life Sciences,* 21 (7), pp.937-941.

Cohen, S., Alonso, M.J. and Langer, R., 1994. Novel approaches to controlled-release antigen delivery. *International Journal of Technology Assessment in Health Care,* 10 (1), pp.121-130.

Coussens, L.M. and Werb, Z., 2002. Inflammation and cancer. *Nature,* 420 (6917), pp.860.

Couvreur, P., 1988. Polyalkylcyanoacrylates as colloidal drug carriers. *Critical reviews in therapeutic drug carrier systems,* 5 (1), pp.1-20.

Couvreur, P., Dubernet, C. and Puisieux, F., 1995. Controlled drug delivery with nanoparticles: current possibilities and future trends. *European journal of pharmaceutics and biopharmaceutics,* 41 (1), pp.2-13.

Cu, Y. and Saltzman, W.M., 2008. Controlled surface modification with poly (ethylene) glycol enhances diffusion of PLGA nanoparticles in human cervical mucus. *Molecular pharmaceutics,* 6 (1), pp.173-181.

Cvek, B., 2011. Targeting malignancies with disulfiram (Antabuse): multidrug resistance, angiogenesis, and proteasome. Current cancer drug targets, 11 (3), pp.332-337.

Dalerba, P., Cho, R.W. and Clarke, M.F., 2007. Cancer stem cells: models and concepts. *Annu.Rev.Med.,* 58, pp.267-284.

Danhier, F., Ansorena, E., Silva, J.M., Coco, R., Le Breton, A. and Prat, V., 2012b. PLGA-based nanoparticles: an overview of biomedical applications. *Journal of Controlled Release,* 161 (2), pp.505-522.

Dechy-Cabaret, O., Martin-Vaca, B. and Bourissou, D., 2004. Controlled ring-opening polymerization of lactide and glycolide. *Chemical reviews,* 104 (12), pp.6147-6176.

DEITRICH, R.A. and ERWIN, V.G., 1971. Mechanism of the inhibition of aldehyde dehydrogenase in vivo by disulfiram and diethyldithiocarbamate. *Molecular pharmacology,* 7 (3), pp.301-307.

De Jaeghere, F., Allémann, E., Leroux, J., Stevels, W., Feijen, J., Doelker, E. and Gurny, R., 1999. Formulation and lyoprotection of poly (lactic acid-co-ethylene oxide) nanoparticles: influence on physical stability and in vitro cell uptake. Pharmaceutical research, 16 (6), pp.859-866.

Delgado, ÁV., González-Caballero, F., Hunter, R.J., Koopal, L.K. and Lyklema, J., 2007. Measurement and interpretation of electrokinetic phenomena. *Journal of colloid and interface science,* 309 (2), pp.194-224.

Demetzos, C., 2008. Differential scanning calorimetry (DSC): a tool to study the thermal behavior of lipid bilayers and liposomal stability. *Journal of Liposome Research,* 18 (3), pp.159-173.

DESAINTBLANQUAT, G., Vidaillac, G., Lindenbaum, A. and Derache, R., 1976. ABSORPTION, DISTRIBUTION AND EXCRETION OF DISULFIRAM IN RAT. *Archives Internationales de Pharmacodynamie et de Therapie,* 223 (2), pp.339-350.

Dingler, A., Blum, R.P., Niehus, H., Muller, R.H. and Gohla, S., 1999. Solid lipid nanoparticles (SLNTM/LipopearlsTM) a pharmaceutical and cosmetic carrier for the application of vitamin E in dermal products. *Journal of microencapsulation,* 16 (6), pp.751-767.

Dos Santos, N., Allen, C., Doppen, A., Anantha, M., Cox, K.A., Gallagher, R.C., Karlsson, G., Edwards, K., Kenner, G. and Samuels, L., 2007. Influence of poly (ethylene glycol) grafting density and polymer length on liposomes: relating plasma circulation lifetimes to protein binding. *Biochimica et Biophysica Acta (BBA)-Biomembranes,* 1768 (6), pp.1367-1377.

Edenberg, H.J., 2007. The genetics of alcohol metabolism: role of alcohol dehydrogenase and aldehyde dehydrogenase variants. *Alcohol Research & Health,* 30 (1), pp.5.

Ekambaram, P., Sathali, A.A.H. and Priyanka, K., 2012. Solid lipid nanoparticles: a review. *Sci Rev Chem Commun,* 2 (1), pp.80-102.

Ekins, S., Williams, A.J., Krasowski, M.D. and Freundlich, J.S., 2011. In silico repositioning of approved drugs for rare and neglected diseases. *Drug discovery today,* 16 (7-8), pp.298-310.

Eldjarn, L., 1950. The metabolism of tetraethyl thiuramdisulphide (Antabus, Aversan) in man, investigated by means of radioactive sulphur. *Scandinavian Journal of Clinical and Laboratory Investigation,* 2 (3), pp.202-208.

Eneanya, D.I., Bianchine, J.R., Duran, D.O. and Andresen, B.D., 1981. The actions and metabolic fate of disulfiram. *Annual Review of Pharmacology and Toxicology,* 21 (1), pp.575-596.

Engelberg, I. and Kohn, J., 1991. Physico-mechanical properties of degradable polymers used in medical applications: a comparative study. *Biomaterials,* 12 (3), pp.292-304.

ErebiáTawari, P. and WaiáTsang, C., 2015. The cytotoxic mechanisms of disulfiram and copper (II) in cancer cells. *Toxicology research,* 4 (6), pp.1439-1442.

Faiman, M.D., Dodd, D.E. and Hanzlik, R.E., 1978. Distribution of S35 disulfiram and metabolites in mice, and metabolism of S35 disulfiram in the dog. *Research communications in chemical pathology and pharmacology,* 21 (3), pp.543.

Faiman, M.D., Kaul, S., Latif, S.A., Williams, T.D. and Lunte, C.E., 2013. S-(N, N-diethylcarbamoyl) glutathione (carbamathione), a disulfiram metabolite and its effect on nucleus accumbens and prefrontal cortex dopamine, GABA, and glutamate: a microdialysis study. *Neuropharmacology,* 75, pp.95-105.

Fang, J., Nakamura, H. and Maeda, H., 2011. The EPR effect: unique features of tumor blood vessels for drug delivery, factors involved, and limitations and augmentation of the effect. Advanced Drug Delivery Reviews, 63 (3), pp.136-151.

Fasehee, H., Dinarvand, R., Ghavamzadeh, A., Esfandyari-Manesh, M., Moradian, H., Faghihi, S. and Ghaffari, S.H., 2016. Delivery of disulfiram into breast cancer cells using folate-receptor-targeted PLGA-PEG nanoparticles: in vitro and in vivo investigations. *Journal of nanobiotechnology,* 14 (1), pp.32.

Fasehee, H., Ghavamzadeh, A., Alimoghaddam, K., Ghaffari, S. and Faghihi, S., 2017. A comparative cytotoxic evaluation of disulfiram encapsulated PLGA nanoparticles on MCF-7 Cells. International Journal of Hematology-Oncology and Stem Cell Research, 11 (2), pp.102.

Fathi, M., Mozafari, M. and Mohebbi, M., 2012. Nanoencapsulation of food ingredients using lipid based delivery systems. *Trends in Food Science & Technology,* 23 (1), pp.13-27.

Fenton, H., 1894. LXXIII.—Oxidation of tartaric acid in presence of iron. Journal of the Chemical Society, Transactions, 65, pp.899-910.

Ferlay, J., Soerjomataram, I., Ervik, M., Dikshit, R., Eser, S., Mathers, C., Rebelo, M., Parkin, D.M., Forman, D. and Bray, F., 2012. Cancer incidence and mortality worldwide: IARC CancerBase. *GLOBOCAN 2012 v10,* 11.

Ferlay, J., Soerjomataram, I., Dikshit, R., Eser, S., Mathers, C., Rebelo, M., Parkin, D.M., Forman, D. and Bray, F., 2015. Cancer incidence and mortality worldwide: sources, methods and major patterns in GLOBOCAN 2012. *International journal of cancer,* 136 (5), pp.E35-E386.

Ferry, D.R., Traunecker, H. and Kerr, D.J., 1996. Clinical trials of P-glycoprotein reversal in solid tumours. *European journal of cancer,* 32 (6), pp.1070-1081.

Ferzoco, R.M. and Ruddy, K.J., 2016. The epidemiology of male breast cancer. *Current oncology reports,* 18 (1), pp.1.

Fessi, H., Puisieux, F., Devissaguet, J.P., Ammoury, N. and Benita, S., 1989. Nanocapsule formation by interfacial polymer deposition following solvent displacement. *International journal of pharmaceutics,* 55 (1), pp.R-R4.

Fonseca, C., Simoes, S. and Gaspar, R., 2002. Paclitaxel-loaded PLGA nanoparticles: preparation, physicochemical characterization and in vitro anti-tumoral activity. *Journal of Controlled Release,* 83 (2), pp.273-286.

Ford, J., Chambon, P., North, J., Hatton, F.L., Giardiello, M., Owen, A. and Rannard, S.P., 2015. Multiple and Co-Nanoprecipitation Studies of Branched Hydrophobic Copolymers and A–B Amphiphilic Block Copolymers, Allowing Rapid Formation of Sterically Stabilized Nanoparticles in Aqueous Media. *Macromolecules,* 48 (6), pp.1883-1893.

Fröhlich, E., 2012. The role of surface charge in cellular uptake and cytotoxicity of medical nanoparticles. *International journal of nanomedicine,* 7, pp.5577.

Fruehauf, J.P. and Meyskens, F.L., 2007. Reactive oxygen species: a breath of life or death? *Clinical Cancer Research,* 13 (3), pp.789-794.

Fuller, R.K. and Gordis, E., 2004. Does disulfiram have a role in alcoholism treatment today? Addiction, 99 (1), pp.21- 24.

Fuller, R.K., Branchey, L., Brightwell, D.R., Derman, R.M., Emrick, C.D., Iber, F.L., James, K.E., Lacoursiere, R.B., Lee, K.K. and Lowenstam, I., 1986. Disulfiram treatment of alcoholism: A Veterans Administration cooperative study. *Jama,* 256 (11), pp.1449-1455.

Garcia, M., Jemal, A., Ward, E.M., Center, M.M., Hao, Y., Siegel, R.L. and Thun, M.J., 2007. Global cancer facts & figures 2007. *Atlanta, GA: American cancer society,* 1 (3), pp.52.

Garcia-Fuentes, M., Torres, D. and Alonso, M.J., 2005. New surface-modified lipid nanoparticles as delivery vehicles for salmon calcitonin. *International journal of pharmaceutics,* 296 (1-2), pp.122-132.

Gentile, P., Chiono, V., Carmagnola, I. and Hatton, P., 2014. An overview of poly (lactic-co-glycolic) acid (PLGA)-based biomaterials for bone tissue engineering. *International journal of molecular sciences,* 15 (3), pp.3640-3659.

George, T.P., Chawarski, M.C., Pakes, J., Carroll, K.M., Kosten, T.R. and Schottenfeld, R.S., 2000. Disulfiram versus placebo for cocaine dependence in buprenorphine-maintained subjects: a preliminary trial. *Biological psychiatry,* 47 (12), pp.1080-1086.

Gerlach, J.H., Endicott, J.A., Juranka, P.F., Henderson, G., Sarangi, F., Deuchars, K.L. and Ling, V., 1986. Homology between P-glycoprotein and a bacterial

haemolysin transport protein suggests a model for multidrug resistance. *Nature,* 324 (6096), pp.485.

Getzoff, E.D., Cabelli, D.E., Fisher, C.L., Parge, H.E., Viezzoli, M.S., Banci, L. and Hallewell, R.A., 1992. Faster superoxide dismutase mutants designed by enhancing electrostatic guidance. *Nature,* 358 (6384), pp.347.

Gey, G., 1952. Tissue culture studies of the proliferative capacity of cervical carcinoma and normal epithelium. *Cancer Res.,*12, pp.264-265.

Gilding, D.K. and Reed, A.M., 1979. Biodegradable polymers for use in surgery—polyglycolic/poly (actic acid) homo-and copolymers: 1. *Polymer,* 20 (12), pp.1459-1464.

Gill, K., Menez, J.F., Lucas, D. and Deitrich, R.A., 1992. Enzymatic production of acetaldehyde from ethanol in rat brain tissue. *Alcoholism: Clinical and Experimental Research,* 16 (5), pp.910-915.

Gillet, J. and Gottesman, M.M., [e-book] 2010. Mechanisms of multidrug resistance in cancer. 2010. *Multi-drug resistance in cancer.* Springer. pp. 47-76.

Goldstein, M., 1966. F. INHIBITION OF NOREPINEPHRINE BIOSYNTHESIS AT THE DOPAMINE-β-HYDROXYLATION STAGE. *Pharmacological reviews,* 18 (1), pp.77-82.

Gombotz, W.R., Guanghui, W., Horbett, T.A. and Hoffman, A.S., 1991. Protein adsorption to poly (ethylene oxide) surfaces. Journal of Biomedical Materials Research, 25 (12), pp.1547-1562.

Gottardis, M.M., Robinson, S.P. and Jordan, V.C., 1988. Estradiol-stimulated growth of MCF-7 tumors implanted in athymic mice: a model to study the tumoristatic action of tamoxifen. *Journal of steroid biochemistry,* 30 (1-6), pp.311-314.

Gottesman, M.M., 2019. P-Glycoprotein-Mediated Multidrug Resistance.

Gottesman, M.M., 1993. How cancer cells evade chemotherapy: sixteenth Richard and Hinda Rosenthal Foundation award lecture. *Cancer research,* 53 (4), pp.747-754.

Gottesman, M.M., Fojo, T. and Bates, S.E., 2002. Multidrug resistance in cancer: role of ATP–dependent transporters. *Nature Reviews Cancer,* 2 (1), pp.48.

Govender, T., Stolnik, S., Garnett, M.C., Illum, L. and Davis, S.S., 1999. PLGA nanoparticles prepared by nanoprecipitation: drug loading and release studies of a water soluble drug. *Journal of Controlled Release,* 57 (2), pp.171-185.

Grady, D., Wenger, N.K., Herrington, D., Khan, S., Furberg, C., Hunninghake, D., Vittinghoff, E. and Hulley, S., 2000. Postmenopausal hormone therapy increases risk for venous thromboembolic disease: the Heart and Estrogen/progestin Replacement Study. *Annals of Internal Medicine,* 132 (9), pp.689-696.

Gref, R., Domb, A., Quellec, P., Blunk, T., Müller, R.H., Verbavatz, J.M. and Langer, R., 2012. The controlled intravenous delivery of drugs using PEG-coated sterically stabilized nanospheres. Advanced Drug Delivery Reviews, 64 Issue , pp.316-326.

Greulich, C., Kittler, S., Epple, M., Muhr, G. and Köller, M., 2009. Studies on the biocompatibility and the interaction of silver nanoparticles with human mesenchymal stem cells (hMSCs). *Langenbeck's Archives of Surgery,* 394 (3), pp.495-502.

Griffiths, P.R. and De Haseth, J.A., 2007. *Fourier transform infrared spectrometry.* John Wiley & Sons.

Gupte, A. and Mumper, R.J., 2009. Elevated copper and oxidative stress in cancer cells as a target for cancer treatment. *Cancer treatment reviews,* 35 (1), pp.32-46.

Haber, F. and Weiss, J., 1934. The catalytic decomposition of hydrogen peroxide by iron salts. Proceedings of the Royal Society of London.Series A-Mathematical and Physical Sciences, 147 (861), pp.332-351.

Halayqa, M. and DomaÅ„ska, U., 2014. PLGA biodegradable nanoparticles containing perphenazine or chlorpromazine hydrochloride: effect of formulation and release. International journal of molecular sciences, 15 (12), pp.23909- 23923.

Hald, J. and Jacobsen, E., 1948. A drug sensitising the organism to ethyl alcohol. *The Lancet,* 252 (6539), pp.1001-1004.

Hamazaki, K., Sato, S., Yunoki, M., Noda, T., Moreira, L.F., Mimura, H. and Orita, K., 1994. Kupffer cell function in chronic liver injury and after partial hepatectomy. Research in Experimental Medicine, 194 (1), pp.237-246.

Han, J., Liu, L., Yue, X., Chang, J., Shi, W. and Hua, Y., 2013. A binuclear complex constituted by diethyldithiocarbamate and copper (I) functions as a proteasome activity inhibitor in pancreatic cancer cultures and xenografts. *Toxicology and applied pharmacology,* 273 (3), pp.477-483.

Hancock, B.C. and Zografi, G., 1997. Characteristics and significance of the amorphous state in pharmaceutical systems. *Journal of pharmaceutical sciences* 86 (1), pp.1-12.

Harris, J.M., Martin, N.E. and Modi, M., 2001. Pegylation. *Clinical pharmacokinetics,* 40 (7), pp.539-551.

Hart, B.W. and Faiman, M.D., 1994. In Vivo Pharmacodynamic Studies of the Disulfiram Metabolite S-Methyl N, N-Diethylthiolcarbamate Sulfoxide: Inhibition of Liver Aldehyde Dehydrogenase. *Alcoholism: Clinical and Experimental Research,*18 (2), pp.340-345.

Hayat, M.A., 1974. Principles and techniques of scanning electron microscopy. Biological applications. Volume 1. *Principles and techniques of scanning electron microscopy.Biologicalapplications.Volume 1*

He, Z., Huang, J., Xu, Y., Zhang, X., Teng, Y., Huang, C., Wu, Y., Zhang, X., Zhang, H. and Sun, W., 2015. Co-delivery of cisplatin and paclitaxel by folic acid conjugated amphiphilic PEG-PLGA copolymer nanoparticles for the treatment of non-small lung cancer. *Oncotarget,* 6 (39), pp.42150.

Heiati, H., Tawashi, R., Shivers, R.R. and Phillips, N.C., 1997. Solid lipid nanoparticles as drug carriers. I. Incorporation and retention of the lipophilic prodrug 3′-azido-3′-deoxythymidine palmitate. *International journal of pharmaceutics,* 146 (1), pp.123-131.

Heurtault, B., Saulnier, P., Pech, B., Proust, J. and Benoit, J., 2002. A novel phase inversion-based process for the preparation of lipid nanocarriers. *Pharmaceutical research,* 19 (6), pp.875-880.

Heurtault, B., Saulnier, P., Pech, B., Proust, J. and Benoit, J., 2003. Physico-chemical stability of colloidal lipid particles. *Biomaterials,* 24 (23), pp.4283-4300.

Hinz, H. and Schwarz, F.P., 2001. Measurement and analysis of results obtained on biological substances with differential scanning calorimetry (IUPAC Technical Report). *Pure and Applied Chemistry,* 73 (4), pp.745-759.

Hoda, M., Pajaniradje, S., Shakya, G., Mohankumar, K. and Rajagopalan, R., 2016. Anti-proliferative and apoptosis-triggering potential of disulfiram and disulfiram-loaded polysorbate 80-stabilized PLGA nanoparticles on hepatocellular carcinoma Hep3B cell line. *Nanomedicine: Nanotechnology, Biology and Medicine,* 12 (6), pp.1641-1650.

Hoda, M., Sufi, S.A., Shakya, G., Kumar, K.M. and Rajagopalan, R., 2015. Influence of stabilizers on the production of disulfiram-loaded poly (lactic-co-glycolic acid) nanoparticles and their anticancer potential. *Therapeutic delivery,* 6 (1), pp.17-25.

Hoda, M., Sufi, S.A., Cavuturu, B. and Rajagopalan, R., 2017. Stabilizers influence drug–polymer interactions and physicochemical properties of disulfiram-loaded poly-lactide-co-glycolide nanoparticles. Future Science OA, 4 (2), pp.FSO263.

Höll, V., Kouba, M., Dietel, M. and Vogt, G., 1992. Stereoisomers of calcium antagonists which differ markedly in their potencies as calcium blockers are equally effective in modulating drug transport by P-glycoprotein. *Biochemical pharmacology,* 43 (12), pp.2601-2608.

Honary, S. and Zahir, F., 2013a. Effect of zeta potential on the properties of nano-drug delivery systems-a review (Part 1). *Tropical Journal of Pharmaceutical Research,* 12 (2), pp.255-264.

Honary, S. and Zahir, F., 2013b. Effect of zeta potential on the properties of nano-drug delivery systems-a review (Part 2). *Tropical Journal of Pharmaceutical Research,* 12 (2), pp.265-273.

Hoskins, C., Wang, L., Cheng, W.P. and Cuschieri, A., 2012. Dilemmas in the reliable estimation of the in-vitro cell viability in magnetic nanoparticle engineering: which tests and what protocols? Nanoscale research letters, 7 (1), pp.77.

Hossann, M., Wiggenhorn, M., Schwerdt, A., Wachholz, K., Teichert, N., Eibl, H., Issels, R.D. and Lindner, L.H., 2007. In vitro stability and content release properties of phosphatidylglyceroglycerol containing thermosensitive liposomes. Biochimica et Biophysica Acta (BBA)-Biomembranes, 1768 (10), pp.2491-2499.

Houchin, M.L. and Topp, E.M., 2008. Chemical degradation of peptides and proteins in PLGA: a review of reactions and mechanisms. *Journal of pharmaceutical sciences,* 97 (7), pp.2395-2404.

Hu, Q., Sun, W., Wang, C. and Gu, Z., 2016. Recent advances of cocktail chemotherapy by combination drug delivery systems. *Advanced Drug Delivery Reviews,* 98, pp.19-34.

Huang, Q., Yu, H. and Ru, Q., 2010. Bioavailability and delivery of nutraceuticals using nanotechnology. *Journal of Food Science,* 75 (1), pp.R5-R57.

Hughes, K.S., Schnaper, L.A., Bellon, J.R., Cirrincione, C.T., Berry, D.A., McCormick, B., Muss, H.B., Smith, B.L., Hudis, C.A. and Winer, E.P., 2013. Lumpectomy plus tamoxifen with or without irradiation in women age 70 years or older with early breast cancer: long-term follow-up of CALGB 9343. *Journal of clinical oncology,* 31 (19), pp.2382.

Hunt, W.A., 1996. Role of acetaldehyde in the actions of ethanol on the brain—a review. *Alcohol,* 13 (2), pp.147-151.

Hunter, D.J., Spiegelman, D., Adami, H., Van Den Brandt, Piet A, Folsom, A.R., Goldbohm, R.A., Graham, S., Howe, G.R., Kushi, L.H. and Marshall, J.R., 1997. Non-dietary factors as risk factors for breast cancer, and as effect modifiers of the association of fat intake and risk of breast cancer. *Cancer Causes & Control,* 8 (1), pp.49-56.

Huynh, N.T., Passirani, C., Saulnier, P. and Benoît, J., 2009. Lipid nanocapsules: a new platform for nanomedicine. *International journal of pharmaceutics,* 379 (2), pp.201-209.

Immordino, M.L., Dosio, F. and Cattel, L., 2006. Stealth liposomes: review of the basic science, rationale, and clinical applications, existing and potential. *International journal of nanomedicine,* 1 (3), pp.297.

Ito, T., Sun, L., Bevan, M.A. and Crooks, R.M., 2004. Comparison of nanoparticle size and electrophoretic mobility measurements using a carbon-nanotube-based coulter counter, dynamic light scattering, transmission electron microscopy, and phase analysis light scattering. *Langmuir,* 20 (16), pp.6940-6945.

Jabr-Milane, L.S., van Vlerken, L.E., Yadav, S. and Amiji, M.M., 2008. Multi-functional nanocarriers to overcome tumor drug resistance. *Cancer treatment reviews,* 34 (7), pp.592-602.

Jain, N.K., 1997. *Controlled and novel drug delivery.* CBS publishers & distributors.

Jain, R.A., 2000. The manufacturing techniques of various drug loaded biodegradable poly (lactide-co-glycolide)(PLGA) devices. *Biomaterials,* 21 (23), pp.2475-2490.

Jalil, R. and Nixon, J.R., 1990. Biodegradable poly (lactic acid) and poly (lactide-co-glycolide) microcapsules: problems associated with preparative techniques and release properties. *Journal of microencapsulation,* 7 (3), pp.297-325.

Jambrak, A.R., Mason, T.J., Lelas, V., Herceg, Z. and Herceg, I.L., 2008. Effect of ultrasound treatment on solubility and foaming properties of whey protein suspensions. *Journal of Food Engineering,* 86 (2), pp.281-287.

Jemal, A., Siegel, R., Ward, E., Hao, Y., Xu, J. and Thun, M.J., 2009. Cancer statistics, 2009. *CA: a cancer journal for clinicians,* 59 (4), pp.225-249.

Jenning, V. and Gohla, S.H., 2001. Encapsulation of retinoids in solid lipid nanoparticles (SLN). *Journal of microencapsulation,* 18 (2), pp.149-158.

Jeon, H., Jeong, Y., Jang, M., Park, Y. and Nah, J., 2000. Effect of solvent on the preparation of surfactant-free poly (DL-lactide-co-glycolide) nanoparticles and norfloxacin release characteristics. *International journal of pharmaceutics,* 207 (1-2), pp.99-108.

Jiao, Y., N Hannafon, B. and Ding, W., 2016. Disulfiram's Anticancer Activity: Evidence and Mechanisms. *Anti-Cancer Agents in Medicinal Chemistry (Formerly Current Medicinal Chemistry-Anti-Cancer Agents),* 16 (11), pp.1378-1384.

Johansson, B., 1992. A review of the pharmacokinetics and pharmacodynamics of disulfiram and its metabolites. *Acta Psychiatrica Scandinavica,* 86 (S369), pp.15-26.

Johansson, B., 1986. Rapid and sensitive on-line precolumn purification and high-performance liquid chromatographic assay for disulfiram and its metabolites. *Journal of Chromatography B: Biomedical Sciences and Applications,* 378, pp.419-429.

Johnson, E.A., 2006. Water in nominally anhydrous crustal minerals: speciation, concentration, and geologic significance. *Reviews in mineralogy and geochemistry,* 62 (1), pp.117-154.

Johnston, C.D., 1953. The in vitro reaction between tetraethylthiuram disulfide (antabuse) and glutathione. *Archives of Biochemistry and Biophysics,* 44 (1), pp.249-251.

Jolivet, J., Froidefond, C., Pottier, A., Chanéac, C., Cassaignon, S., Tronc, E. and Euzen, P., 2004. Size tailoring of oxide nanoparticles by precipitation in aqueous medium. A semi-quantitative modelling. *Journal of Materials Chemistry,* 14 (21), pp.3281-3288.

Jores, K., Haberland, A., Wartewig, S., Mäder, K. and Mehnert, W., 2005. Solid lipid nanoparticles (SLN) and oil-loaded SLN studied by spectrofluorometry and Raman spectroscopy. *Pharmaceutical research,* 22 (11), pp.1887-1897.

Kang, K.W., Chun, M., Kim, O., Subedi, R.K., Ahn, S., Yoon, J. and Choi, H., 2010. Doxorubicin-loaded solid lipid nanoparticles to overcome multidrug resistance in cancer therapy. *Nanomedicine: Nanotechnology, Biology and Medicine,* 6 (2), pp.210-213.

Kao, J., Salari, K., Bocanegra, M., Choi, Y., Girard, L., Gandhi, J., Kwei, K.A., Hernandez-Boussard, T., Wang, P. and Gazdar, A.F., 2009. Molecular profiling of breast cancer cell lines defines relevant tumor models and provides a resource for cancer gene discovery. PloS one, 4 (7).

Kaslander, J., 1963. Formation of an S-glucuronide from tetraethylthiuram disulfide (Antabuse) in man. *Biochimica et biophysica acta,* 71, pp.730-732.

Kasvayee, K.A., 2011. Synthesis of Li-ion battery cathode materials via freeze granulation.

Kaushik, A. and Singh, M., 2011. Isolation and characterization of cellulose nanofibrils from wheat straw using steam explosion coupled with high shear homogenization. *Carbohydrate research,* 346 (1), pp.76-85.

Kelsey, J.L., Gammon, M.D. and John, E.M., 1993. Reproductive factors and breast cancer. *Epidemiologic reviews,* 15 (1), pp.36.

Kesisoglou, F., Panmai, S. and Wu, Y., 2007. Nanosizing—oral formulation development and biopharmaceutical evaluation. *Advanced Drug Delivery Reviews,* 59 (7), pp.631-644.

Key, T.J., 1999. Serum oestradiol and breast cancer risk. *Endocrine-related cancer,* 6 (2), pp.175-180.

Kitson, T.M., 1977. The disulfiram--ethanol reaction: a review. *Journal of studies on alcohol,* 38 (1), pp.96-113.

KLANG, S. and BENITA, S., 1998. FOR INTRAVENOUS ADMINISTRATION. *Submicron emulsions in drug targeting and delivery,* 9, pp.119.

Klibanov, A.L., Maruyama, K., Torchilin, V.P. and Huang, L., 1990. Amphipathic polyethyleneglycols effectively prolong the circulation time of liposomes. FEBS letters, 268 (1), pp.235-237.

Konan, Y.N., Gurny, R. and Allémann, E., 2002. Preparation and characterization of sterile and freeze-dried sub-200 nm nanoparticles. *International journal of pharmaceutics,* 233 (1-2), pp.239-252.

Koppaka, V., Thompson, D.C., Chen, Y., Ellermann, M., Nicolaou, K.C., Juvonen, R.O., Petersen, D., Deitrich, R.A., Hurley, T.D. and Vasiliou, V., 2012. Aldehyde dehydrogenase inhibitors: a comprehensive review of the pharmacology, mechanism of action, substrate specificity, and clinical application. *Pharmacological reviews,* 64 (3), pp.520-539.

Kosten, T.R. and Kleber, H.D., 1992. *Clinician's guide to cocaine addiction: Theory, research, and treatment.* Guilford Press.

Krishna, R. and Mayer, L.D., 2000. Multidrug resistance (MDR) in cancer: mechanisms, reversal using modulators of MDR and the role of MDR modulators in influencing the pharmacokinetics of anticancer drugs. *European Journal of Pharmaceutical Sciences,* 11 (4), pp.265-283.

Kumagai, A., Kodama, H., Kumagai, J., Fukuda, J., Kawamura, K., Tanikawa, H., Sato, N. and Tanaka, T., 2002. Xanthine oxidase inhibitors suppress testicular germ cell apoptosis induced by experimental cryptorchidism. *Molecular human reproduction,* 8 (2), pp.118-123.

Kumar, N., Ravikumar, M.N. and Domb, A.J., 2001. Biodegradable block copolymers. *Advanced Drug Delivery Reviews,* 53 (1), pp.23-44.

Kumar, V. and Yadav, S.K., 2009. Plant-mediated synthesis of silver and gold nanoparticles and their applications. *Journal of Chemical Technology & Biotechnology: International Research in Process, Environmental & Clean Technology,* 84 (2), pp.151-157.

Kumari, A., Yadav, S.K. and Yadav, S.C., 2010. Biodegradable polymeric nanoparticles based drug delivery systems. *Colloids and Surfaces B: Biointerfaces,* 75 (1), pp.1-18.

Labhasetwar, V., Mohan, M.S. and Dorle, A.K., 1994. A study on zeta potential and dielectric constant of liposomes. *Journal of microencapsulation,* 11 (6), pp.663-668.

Lakhani, S.R., Van De Vijver, Marc J, Jacquemier, J., Anderson, T.J., Osin, P.P., McGuffog, L. and Easton, D.F., 2002. The pathology of familial breast cancer: predictive value of immunohistochemical markers estrogen receptor, progesterone receptor, HER-2, and p53 in patients with mutations in BRCA1 and BRCA2. *Journal of clinical oncology,* 20 (9), pp.2310-2318.

Langedijk, J., Mantel-Teeuwisse, A.K., Slijkerman, D.S. and Schutjens, M.D., 2015. Drug repositioning and repurposing: terminology and definitions in literature. *Drug discovery today,* 20 (8), pp.1027-1034.

Lasfargues, E.Y. and Ozzello, L., 1958. Cultivation of human breast carcinomas. *Journal of the National Cancer Institute,* 21 (6), pp.1131-1147.

Lasic, D.D., 1998. Novel applications of liposomes. *Trends in biotechnology,* 16 (7), pp.307-321.

Laverman, P., Carstens, M.G., Boerman, O.C., Dams, E.T.M., Oyen, W.J., van Rooijen, N., Corstens, F.H. and Storm, G., 2001. Factors affecting the accelerated blood clearance of polyethylene glycol-liposomes upon repeated injection. Journal of Pharmacology and Experimental Therapeutics, 298 (2), pp.607-612.

Lee, S., Chun, S., Kang, I. and Park, J., 2009. Preparation of cellulose nanofibrils by high-pressure homogenizer and cellulose-based composite films. *Journal of Industrial and Engineering Chemistry,* 15 (1), pp.50-55.

Leemhuis, M., Van Nostrum, C.F., Kruijtzer, J., Zhong, Z.Y., Ten Breteler, M.R., Dijkstra, P.J., Feijen, J. and Hennink, W.E., 2006. Functionalized poly (α-hydroxy acid) s via ring-opening polymerization: Toward hydrophilic polyesters with pendant hydroxyl groups. *Macromolecules,* 39 (10), pp.3500-3508.

Leemhuis, M., Kruijtzer, J.A., van Nostrum, C.F. and Hennink, W.E., 2007. In vitro hydrolytic degradation of hydroxyl-functionalized poly (α-hydroxy acid) s. *Biomacromolecules,* 8 (9), pp.2943-2949.

León-Rodriguez, L., Leiro-Vidal, J., Blanco-Méndez, J. and Luzardo-Álvarez, A., 2010. Incorporation of PVMMA to PLGA MS enhances lectin grafting and their in vitro activity in macrophages. *International journal of pharmaceutics,* 402 (1-2), pp.165-174.

Leuner, C. and Dressman, J., 2000. Improving drug solubility for oral delivery using solid dispersions. *European journal of Pharmaceutics and Biopharmaceutics,* 50 (1), pp.47-60.

Levenson, A.S. and Jordan, V.C., 1997. MCF-7: the first hormone-responsive breast cancer cell line. *Cancer research,* 57 (15), pp.3071-3078.

Lewis, D.J., Deshmukh, P., Tedstone, A.A., Tuna, F. and O'Brien, P., 2014. On the interaction of copper (II) with disulfiram. *Chemical communications,* 50 (87), pp.13334-13337.

Li, H., Zhao, X., Ma, Y., Zhai, G., Li, L. and Lou, H., 2009. Enhancement of gastrointestinal absorption of quercetin by solid lipid nanoparticles. *Journal of Controlled Release,* 133 (3), pp.238-244.

Li, Y., Pei, Y., Zhang, X., Gu, Z., Zhou, Z., Yuan, W., Zhou, J., Zhu, J. and Gao, X., 2001. PEGylated PLGA nanoparticles as protein carriers: synthesis, preparation and biodistribution in rats. *Journal of Controlled Release,* 71 (2), pp.203-211.

Lim, J., Yeap, S.P., Che, H.X. and Low, S.C., 2013. Characterization of magnetic nanoparticle by dynamic light scattering. *Nanoscale research letters,* 8 (1), pp.381.

Lim, S. and Kim, C., 2002. Formulation parameters determining the physicochemical characteristics of solid lipid nanoparticles loaded with all-trans retinoic acid. *International journal of pharmaceutics,* 243 (1-2), pp.135-146.

Lis, G.P., Mastalerz, M., Schimmelmann, A., Lewan, M.D. and Stankiewicz, B.A., 2005. FTIR absorption indices for thermal maturity in comparison with vitrinite reflectance R0 in type-II kerogens from Devonian black shales. *Organic Geochemistry,* 36 (11), pp.1533-1552.

Liu, K., Sun, J., Wang, Y., He, Y., Gao, K. and He, Z., 2008. Preparation and characterization of 10-hydroxycamptothecin loaded nanostructured lipid carriers. *Drug development and industrial pharmacy,* 34 (5), pp.465-471.

Liu, P., Brown, S., Goktug, T., Channathodiyil, P., Kannappan, V., Hugnot, J.P., Guichet, P.O., Bian, X., Armesilla, A.L. and Darling, J.L., 2012. Cytotoxic effect of disulfiram/copper on human glioblastoma cell lines and ALDH-positive cancer-stem-like cells. *British journal of cancer,* 107 (9), pp.1488-1497.

Liu, Z., Sun, X., Nakayama-Ratchford, N. and Dai, H., 2007. Supramolecular chemistry on water-soluble carbon nanotubes for drug loading and delivery. *ACS nano,* 1 (1), pp.50-56.

Lobatto, M.E., Fuster, V., Fayad, Z.A. and Mulder, W.J., 2011. Perspectives and opportunities for nanomedicine in the management of atherosclerosis. *Nature Reviews Drug Discovery,* 10 (11), pp.835.

Löbler, M., Rohm, H.W., Schmitz, K., Johnston, A.H., Newman, T.A., Ranjan, S., Sood, R. and Kinnunen, P., eds. 2009. *4th European Conference of the International Federation for Medical and Biological Engineering* Springer.

Locatelli, E. and Franchini, M.C., 2012. Biodegradable PLGA-b-PEG polymeric nanoparticles: synthesis, properties, and nanomedical applications as drug delivery system. *Journal of Nanoparticle Research,* 14 (12), pp.1316.

Loo, T.W., Bartlett, M.C. and Clarke, D.M., 2004. Disulfiram metabolites permanently inactivate the human multidrug resistance P-glycoprotein. Molecular pharmaceutics, 1 (6), pp.426-433.

Loo, T.W. and Clarke, D.M., 1999. Molecular dissection of the human multidrug resistance P-glycoprotein. *Biochemistry and cell biology,* 77 (1), pp.11-23.

López-Lázaro, M., 2007. Dual role of hydrogen peroxide in cancer: possible relevance to cancer chemoprevention and therapy. *Cancer letters,* 252 (1), pp.1-8.

Lü, J., Wang, X., Marin-Muller, C., Wang, H., Lin, P.H., Yao, Q. and Chen, C., 2009. Current advances in research and clinical applications of PLGA-based nanotechnology. *Expert review of molecular diagnostics,* 9 (4), pp.325-341.

Lu, Y., Weng, L. and Cao, X., 2006. Morphological, thermal and mechanical properties of ramie crystallites—reinforced plasticized starch biocomposites. *Carbohydrate Polymers,* 63 (2), pp.198-204.

Lundwall, L. and Baekeland, F., 1971. Disulfiram treatment of alcoholism: a review. *Journal of Nervous and mental disease.*

Madala, H.R., Punganuru, S.R., Ali-Osman, F., Zhang, R. and Srivenugopal, K.S., 2018. Brain-and brain tumor-penetrating disulfiram nanoparticles: Sequence of cytotoxic events and efficacy in human glioma cell lines and intracranial xenografts. Oncotarget, 9 (3), pp.3459.

Maeda, H., 2001. The enhanced permeability and retention (EPR) effect in tumor vasculature: the key role of tumor-selective macromolecular drug targeting. Advances in Enzyme Regulation.

Maeda, H. and Matsumura, Y., 2011. EPR effect based drug design and clinical outlook for enhanced cancer chemotherapy. Advanced Drug Delivery Reviews, 63 (3).

Mainardes, R.M., Gremião, M.P.D. and Evangelista, R.C., 2006. Thermoanalytical study of praziquantel-loaded PLGA nanoparticles. *RevistaBrasileira de CiênciasFarmacêuticas,* 42 (4), pp.523-530.

Malcolm, R., Olive, M.F. and Lechner, W., 2008. The safety of disulfiram for the treatment of alcohol and cocaine dependence in randomized clinical trials: guidance for clinical practice. *Expert opinion on drug safety,* 7 (4), pp.459-472.

Mankhetkorn, S., Abedinzadeh, Z. and Houee-Levin, C., 1994. Antioxidant action of sodium diethyldithiocarbamate: reaction with hydrogen peroxide and superoxide radical. Free Radical Biology and Medicine, 17 (6), pp.517-527.

Mao, Y., Daniel, L.N., Knapton, A.D., Shi, X. and Saffiotti, U., 1995. Protective effects of silanol group binding agents on quartz toxicity to rat lung alveolar cells. *Applied Occupational and Environmental Hygiene,* 10 (12), pp.1132-1137.

Marchner, H. and Tottmar, O., 1978. A comparative study on the effects of disulfiram, cyanamide and 1-aminocyclopropanol on the acetaldehyde metabolism in rats. *Acta Pharmacologica et Toxicologica,* 43 (3), pp.219-232. A

Marikovsky, M., Nevo, N., Vadai, E. and Harris-Cerruti, C., 2002. Cu/Zn superoxide dismutase plays a role in angiogenesis. *International journal of cancer,* 97 (1), pp.34-41.

McDonnell, D.P. and Norris, J.D., 2002. Connections and regulation of the human estrogen receptor. *Science,* 296 (5573), pp.1642-1644.

McElroy, S.L., Weiss, R.D., Mendelson, J.H., Teoh, S.K., McAfee, B. and Mello, N.K., 1989. Desipramine treatment for relapse prevention in cocaine dependence. *National Institute on Drug Abuse research monograph series,* 95, pp.57-63.

Mehnert, W. and Mäder, K., 2012. Solid lipid nanoparticles: production, characterization and applications. *Advanced Drug Delivery Reviews,* 64, pp.83-101.

Mello, V.A.d. and Ricci-Júnior, E., 2011. Encapsulation of naproxen in nanostructured system: structural characterization and in vitro release studies. *Quimica Nova,* 34 (6), pp.933-939.

Meot-Ner, M., 2005. The ionic hydrogen bond. *Chemical reviews,* 105 (1), pp.213-284.

Mi, P., Cabral, H. and Kataoka, K., 2020. Ligand‑installed Nanocarriers toward precision therapy. Advanced Materials, 32 (13), pp.1902604.

Miller, R.A., Brady, J.M. and Cutright, D.E., 1977. Degradation rates of oral resorbable implants (polylactates and polyglycolates): rate modification with changes in PLA/PGA copolymer ratios. *Journal of Biomedical Materials Research,* 11 (5), pp.711-719.

Mishra, P.R., Al Shaal, L., Müller, R.H. and Keck, C.M., 2009. Production and characterization of Hesperetin nanosuspensions for dermal delivery. *International journal of pharmaceutics,* 371 (1-2), pp.182-189.

Mller, R.H., Mehnert, W., Lucks, J., Schwarz, C., ZurMhlen, A., Meyhers, H., Freitas, C. and Rhl, D., 1995. Solid lipid nanoparticles (SLN): an alternative colloidal carrier system for controlled drug delivery. *European Journal of Pharmaceutics and Biopharmaceutics,* 41 (1), pp.62-69.

Moinard-Chécot, D., Chevalier, Y., Briançon, S., Beney, L. and Fessi, H., 2008. Mechanism of nanocapsules formation by the emulsion–diffusion process. *Journal of colloid and interface science,* 317 (2), pp.458-468.

Mora-Huertas, C.E., Fessi, H. and Elaissari, A., 2010. Polymer-based nanocapsules for drug delivery. *International journal of pharmaceutics,* 385 (1-2), pp.113-142.

Morrison, B.W., Doudican, N.A., Patel, K.R. and Orlow, S.J., 2010. Disulfiram induces copper-dependent stimulation of reactive oxygen species and activation of the extrinsic apoptotic pathway in melanoma. *Melanoma research,* 20 (1), pp.11-20.

Mosallaei, N., Jaafari, M.R., Hanafi-Bojd, M.Y., Golmohammadzadeh, S. and Malaekeh-Nikouei, B., 2013. Docetaxel-loaded solid lipid nanoparticles: Preparation, characterization, in vitro, and in vivo evaluations. *Journal of pharmaceutical sciences,* 102 (6), pp.1994-2004.

Mosallaei, N., Mahmoudi, A., Ghandehari, H., Yellepeddi, V.K., Jaafari, M.R. and Malaekeh-Nikouei, B., 2016. Solid lipid nanoparticles containing 7-ethyl-10-hydroxycamptothecin (SN38): Preparation, characterization, in vitro, and in vivo evaluations. *European Journal of Pharmaceutics and Biopharmaceutics,* 104, pp.42-50.

Mueser, K.T., Noordsy, D.L., Fox, L. and Wolfe, R., 2003. Disulfiram treatment for alcoholism in severe mental illness. *American Journal on Addictions,* 12 (3), pp.242-252.

Mukhopadhyay, R., 2004. No title. *Product review: portable FTIR spectrometers get moving.*

Mulik, R.S., Mönkkönen, J., Juvonen, R.O., Mahadik, K.R. and Paradkar, A.R., 2010. Transferrin mediated solid lipid nanoparticles containing curcumin: enhanced in vitro anticancer activity by induction of apoptosis. *International journal of pharmaceutics,* 398 (1-2), pp.190-203.

Mullard, A., 2014. No title. *New drugs cost US $2.6 billion to develop.*

Muller, R.H., 1996. Arzneistofftrager aus festen lipidteilchen (Feste Lipidnanospharen (SLN)). *Eur.Patent EP 0605497 B1.*

Müller, R.H., Benita, S. and Bohm, B., 1998. Emulsions and nanosuspensions for the formulation of poorly soluble drugs. Edition w Place of Publication CRC Press.

Müller, R.H., Mäder, K. and Gohla, S., 2000. Solid lipid nanoparticles (SLN) for controlled drug delivery–a review of the state of the art. *European journal of pharmaceutics and biopharmaceutics,* 50 (1), pp.161-177.

Müller, R.H., Rühl, D. and Runge, S.A., 1996. Biodegradation of solid lipid nanoparticles as a function of lipase incubation time. *International journal of pharmaceutics,* 144 (1), pp.115-121.

Murray, C.J. and Lopez, A.D., 1997. Mortality by cause for eight regions of the world: Global Burden of Disease Study. *The lancet,* 349 (9061), pp.1269-1276.

Mutschler, J., Diehl, A. and Kiefer, F., 2008. Pharmacology of disulfiram-an update. *Fortschritte der Neurologie-Psychiatrie,* 76 (4), pp.225-231.

Najlah, M., Ahmed, Z., Iqbal, M., Wang, Z., Tawari, P., Wang, W. and McConville, C., 2017. Development and characterisation of disulfiram-loaded PLGA nanoparticles for the treatment of non-small cell lung cancer. *European Journal of Pharmaceutics and Biopharmaceutics,* 112, pp.224-233.

Narvekar, M., Xue, H.Y., Eoh, J.Y. and Wong, H.L., 2014. Nanocarrier for poorly water-soluble anticancer drugs—barriers of translation and solutions. *AapsPharmscitech,* 15 (4), pp.822-833.

Navrátilová, J., Jungová, P., Vanhara, P., Preisler, J., Kanicky, V. and Smarda, J., 2009. Copper ions regulate cytotoxicity of disulfiram to myeloid leukemia cells. *International journal of molecular medicine,* 24 (5), pp.661-670.

Neve, R.M., Chin, K., Fridlyand, J., Yeh, J., Baehner, F.L., Fevr, T., Clark, L., Bayani, N., Coppe, J. and Tong, F., 2006. A collection of breast cancer cell lines for the study of functionally distinct cancer subtypes. *Cancer cell,* 10 (6), pp.515-527. A

Nicolson, G.L., 1993. Paracrine and autocrine growth mechanisms in tumor metastasis to specific sites with particular emphasis on brain and lung metastasis. *Cancer and metastasis reviews,* 12 (3-4), pp.325-343.

Nikolova, A.N. and Jones, M.N., 1996. Effect of grafted PEG-2000 on the size and permeability of vesicles. Biochimica et Biophysica Acta (BBA)-Lipids and Lipid Metabolism, 1304 (2), pp.120-128.

Nishiyama, N. and Kataoka, K., 2006. Current state, achievements, and future prospects of polymeric micelles as nanocarriers for drug and gene delivery. *Pharmacology & therapeutics,* 112 (3), pp.630-648.

O'Donnell, P.B. and McGinity, J.W., 1997. Preparation of microspheres by the solvent evaporation technique. *Advanced Drug Delivery Reviews,* 28 (1), pp.25-42.

O'Keefe, J.M., Bechtel, A., Christanis, K., Dai, S., DiMichele, W.A., Eble, C.F., Esterle, J.S., Mastalerz, M., Raymond, A.L. and Valentim, B.V., 2013. On the fundamental difference between coal rank and coal type. *International Journal of Coal Geology,* 118, pp.58-87.

Orive, G., Anitua, E., Pedraz, J.L. and Emerich, D.F., 2009. Biomaterials for promoting brain protection, repair and regeneration. *Nature Reviews Neuroscience,* 10 (9), pp.682.

Orts-Gil, G., Natte, K., Drescher, D., Bresch, H., Mantion, A., Kneipp, J. and Österle, W., 2011. Characterisation of silica nanoparticles prior to in vitro studies: from primary particles to agglomerates. *Journal of Nanoparticle Research,* 13 (4), pp.1593-1604.

Osborne, C.K., Hobbs, K. and Clark, G.M., 1985. Effect of estrogens and antiestrogens on growth of human breast cancer cells in athymic nude mice. *Cancer research,* 45 (2), pp.584-590.

Osman, C., Voelker, D.R. and Langer, T., 2011. Making heads or tails of phospholipids in mitochondria. Journal of Cell Biology, 192 (1), pp.7-16.

Pamula, E. and Menaszek, E., 2008. In vitro and in vivo degradation of poly (L-lactide-co-glycolide) films and scaffolds. *Journal of Materials Science: Materials in Medicine,* 19 (5), pp.2063-2070.

Pantziarka, P., Bouche, G., Meheus, L., Sukhatme, V., Sukhatme, V.P. and Vikas, P., 2014. The repurposing drugs in oncology (ReDO) project. *ecancermedicalscience,* 8.

Parikh, S.J. and Chorover, J., 2005. FTIR spectroscopic study of biogenic Mn-oxide formation by Pseudomonas putida GB-1. *Geomicrobiology Journal,* 22 (5), pp.207-218.

Park, G., Kim, S.J., Kim, M.H. and Park, H.S., 2014. Experimental study of the role of nanoparticles in sodium–water reaction. *Nuclear Engineering and Design,* 277, pp.46-54.

Parveen, S. and Sahoo, S.K., 2011. Long circulating chitosan/PEG blended PLGA nanoparticle for tumor drug delivery. *European journal of pharmacology,* 670 (2-3), pp.372-383.

Patil, R.R., Guhagarkar, S.A. and Devarajan, P.V., 2008. Engineered nanocarriers of doxorubicin: a current update. Critical Reviewsâ„¢ in Therapeutic Drug Carrier Systems, 25 (1).

Patravale, V.B. and Ambarkhane, A.V., 2003. Study of solid lipid nanoparticles with respect to particle size distribution and drug loading. *Die Pharmazie-An International Journal of Pharmaceutical Sciences,* 58 (6), pp.392-395.

Pessetto, Z.Y., Ma, Y., Hirst, J.J., von Mehren, M., Weir, S.J. and Godwin, A.K., 2014. Drug repurposing identifies a synergistic combination therapy with imatinib mesylate for gastrointestinal stromal tumor. *Molecular cancer therapeutics,* 13 (10), pp.2276-2287.

Petrakis, I.L., Carroll, K.M., Nich, C., Gordon, L.T., McCance-Katz, E.F., Frankforter, T. and Rounsaville, B.J., 2000. Disulfiram treatment for cocaine dependence in methadone-maintained opioid addicts. *Addiction,* 95 (2), pp.219-228.

Pignatello, R., Leonardi, A., Pellitteri, R., Carbone, C., Caggia, S., Graziano, A.C.E. and Cardile, V., 2013. Evaluation of new amphiphilic PEG derivatives for preparing stealth lipid nanoparticles. *Colloids and Surfaces A: Physicochemical and Engineering Aspects,* 434, pp.136-144.

Pilcer, G. and Amighi, K., 2010. Formulation strategy and use of excipients in pulmonary drug delivery. *International journal of pharmaceutics,* 392 (1-2), pp.1-19.

Pokharkar, V.B., Mandpe, L.P., Padamwar, M.N., Ambike, A.A., Mahadik, K.R. and Paradkar, A., 2006. Development, characterization and stabilization of amorphous form of a low Tg drug. *Powder Technology,* 167 (1), pp.20-25.

Poletto, M., Zattera, A.J. and Santana, R.M., 2012. Structural differences between wood species: evidence from chemical composition, FTIR spectroscopy, and thermogravimetric analysis. *Journal of Applied Polymer Science,* 126 (S1), pp.E337-E344. Available through: google.

Prat, A., Parker, J.S., Karginova, O., Fan, C., Livasy, C., Herschkowitz, J.I., He, X. and Perou, C.M., 2010. Phenotypic and molecular characterization of the claudin-low intrinsic subtype of breast cancer. *Breast cancer research,* 12 (5), pp.R68.

Prato, M., Kostarelos, K. and Bianco, A., 2007. Functionalized carbon nanotubes in drug design and discovery. *Accounts of Chemical Research,* 41 (1), pp.60-68.

Rabinovich-Guilatt, L., Couvreur, P., Lambert, G., Goldstein, D., Benita, S. and Dubernet, C., 2004. Extensive surface studies help to analyse zeta potential data: the case of cationic emulsions. *Chemistry and physics of lipids,* 131 (1), pp.1-13.

Raliya, R. and Tarafdar, J.C., 2013. ZnO nanoparticle biosynthesis and its effect on phosphorous-mobilizing enzyme secretion and gum contents in Clusterbean (Cyamopsistetragonoloba L.). *Agricultural Research,* 2 (1), pp.48-57.

Rao, C. and Biswas, K., 2009. Characterization of nanomaterials by physical methods. *Annual Review of Analytical Chemistry,* [e-journal] 2, pp.435-462.

Rauscher, H., Rasmussen, K. and Sokull-Klüttgen, B., 2017. Regulatory aspects of nanomaterials in the EU. *ChemieIngenieur Technik,* 89 (3), pp.224-231. A

Ravi, P.R., Vats, R., Dalal, V. and Murthy, A.N., 2014. A hybrid design to optimize preparation of lopinavir loaded solid lipid nanoparticles and comparative pharmacokinetic evaluation with marketed lopinavir/ritonavir coformulation. *Journal of Pharmacy and Pharmacology,* 66 (7), pp.912-926.

Reis, C.P., Neufeld, R.J., Ribeiro, A.J. and Veiga, F., 2006. Nanoencapsulation I. Methods for preparation of drug-loaded polymeric nanoparticles. *Nanomedicine: Nanotechnology, Biology and Medicine,* 2 (1), pp.8-21.

Ribeiro, H.S., Chu, B., Ichikawa, S. and Nakajima, M., 2008. Preparation of nanodispersions containing β-carotene by solvent displacement method. *Food Hydrocolloids,* 22 (1), pp.12-17.

Richards, W.T. and Loomis, A.L., 1927. The chemical effects of high frequency sound waves I. A preliminary survey. *Journal of the American Chemical Society,* 49 (12), pp.3086-3100.

Riordan, J.R., Deuchars, K., Kartner, N., Alon, N., Trent, J. and Ling, V., 1985. Amplification of P-glycoprotein genes in multidrug-resistant mammalian cell lines. *Nature,* 316 (6031), pp.817.

Robertson, A.D. and Murphy, K.P., 1997. Protein structure and the energetics of protein stability. *Chemical reviews,* 97 (5), pp.1251-1268.

Robertson, J.F., Osborne, C.K., Howell, A., Jones, S.E., Mauriac, L., Ellis, M., Kleeberg, U.R., Come, S.E., Vergote, I. and Gertler, S., 2003. Fulvestrant versus anastrozole for the treatment of advanced breast carcinoma in postmenopausal women: a prospective combined analysis of two multicenter trials. *Cancer,* 98 (2), pp.229-238.

Royal, S., 2004. Nanoscience and nanotechnologies. *Royal Society, London*.

Saad, M., Garbuzenko, O.B. and Minko, T., 2008. Co-delivery of siRNA and an anticancer drug for treatment of multidrug-resistant cancer.

Saba, T.M., 1970. Physiology and physiopathology of the reticuloendothelial system. Archives of Internal Medicine, 126 (6), pp.1031-1052.

Sahin, A., Esendagli, G., Yerlikaya, F., Caban-Toktas, S., Yoyen-Ermis, D., Horzum, U., Aktas, Y., Khan, M., Couvreur, P. and Capan, Y., 2017. A small variation in average particle size of PLGA nanoparticles prepared by nanoprecipitation leads to considerable change in nanoparticles' characteristics and efficacy of intracellular delivery. Artificial cells, nanomedicine, and biotechnology, 45 (8), pp.1657-1664.

Sahoo, S.K., Dilnawaz, F. and Krishnakumar, S., 2008. Nanotechnology in ocular drug delivery. *Drug discovery today,* 13 (3-4), pp.144-151.

Salvador-Morales, C., Zhang, L., Langer, R. and Farokhzad, O.C., 2009. Immunocompatibility properties of lipid–polymer hybrid nanoparticles with heterogeneous surface functional groups. *Biomaterials,* 30 (12), pp.2231-2240.

Samarasinghe, N., Fernando, S., Lacey, R. and Faulkner, W.B., 2012. Algal cell rupture using high pressure homogenization as a prelude to oil extraction. *Renewable Energy,* 48, pp.300-308.

Samer, C.J. and Schork, F.J., 1999. The role of high shear in continuous miniemulsion polymerization. *Industrial & Engineering Chemistry Research,* 38 (5), pp.1801-1807.

Sanguansri, P. and Augustin, M.A., 2006. Nanoscale materials development–a food industry perspective. *Trends in Food Science & Technology,* 17 (10), pp.547-556.

Sarkola, T., Iles, M.R., Kohlenberg-Mueller, K. and Eriksson, C.P., 2002. Ethanol, acetaldehyde, acetate, and lactate levels after alcohol intake in white men and women: effect of 4-methylpyrazole. *Alcoholism: Clinical and Experimental Research,* 26 (2), pp.239-245.

Schlesinger, K., Kakihana, R. and Bennett, E.L., 1966. Effects of tetraethylthiuramdisulfide (Antabuse) on the metabolism and consumption of ethanol in mice. *Psychosomatic medicine,* 28 (4), pp.514-520.

Schmid, G., 2011. *Nanoparticles: from theory to application.* John Wiley & Sons.

Schubert, S., Delaney Jr, J.T. and Schubert, U.S., 2011. Nanoprecipitation and nanoformulation of polymers: from history to powerful possibilities beyond poly (lactic acid). *Soft Matter,* 7 (5), pp.1581-1588.

Schwarz, C., Mehnert, W., Lucks, J.S. and Müller, R.H., 1994. Solid lipid nanoparticles (SLN) for controlled drug delivery. I. Production, characterization and sterilization. *Journal of Controlled Release,* 30 (1), pp.83-96.

Sellers, T.A., Kushi, L.H., Cerhan, J.R., Vierkant, R.A., Gapstur, S.M., Vachon, C.M., Olson, J.E., Therneau, T.M. and Folsom, A.R., 2001. Dietary folate intake, alcohol, and risk of breast cancer in a prospective study of postmenopausal women. *Epidemiology,* 12 (4), pp.420-428.

Serpe, L., Catalano, M.G., Cavalli, R., Ugazio, E., Bosco, O., Canaparo, R., Muntoni, E., Frairia, R., Gasco, M.R. and Eandi, M., 2004. Cytotoxicity of anticancer drugs incorporated in solid lipid nanoparticles on HT-29 colorectal cancer cell line. *European Journal of Pharmaceutics and Biopharmaceutics,* 58 (3), pp.673-680.

Shao, X., Wei, X., Song, X., Hao, L., Cai, X., Zhang, Z., Peng, Q. and Lin, Y., 2015. Independent effect of polymeric nanoparticle zeta potential/surface charge, on their cytotoxicity and affinity to cells. *Cell proliferation,* 48 (4), pp.465-474.

Shapiro, S., Venet, W., Strax, P., Venet, L. and Roeser, R., 1982. Ten-to fourteen-year effect of screening on breast cancer mortality. *Journal of the National Cancer Institute,* 69 (2), pp.349-355.

Sharma, S., Sahni, J.K., Ali, J. and Baboota, S., 2015. Effect of high-pressure homogenization on formulation of TPGS loaded nanoemulsion of rutin–pharmacodynamic and antioxidant studies. *Drug delivery,* 22 (4), pp.541-551.

Shegokar, R. and Müller, R.H., 2010. Nanocrystals: industrially feasible multifunctional formulation technology for poorly soluble actives. *International journal of pharmaceutics,* 399 (1-2), pp.129-139.

Shehzad, A., Ul-Islam, M., Wahid, F. and Lee, Y.S., 2014. Multifunctional polymeric nanocurcumin for cancer therapy. *Journal of nanoscience and nanotechnology,* 14 (1), pp.803-814.

Shen, D.W., Fojo, A., Chin, J.E., Roninson, I.B., Richert, N., Pastan, I. and Gottesman, M.M., 1986. Human multidrug-resistant cell lines: increased mdr1 expression can precede gene amplification. *Science,* 232 (4750), pp.643-645.

Sheng, Y., Yuan, Y., Liu, C., Tao, X., Shan, X. and Xu, F., 2009. In vitro macrophage uptake and in vivo biodistribution of PLA– PEG nanoparticles loaded with hemoglobin as blood substitutes: effect of PEG content. Journal of Materials Science: Materials in Medicine, 20 (9), pp.1881-1891.

Shieh, Y., Twu, Y., Su, C., Lin, R. and Liu, G., 2010. Crystallization kinetics study of poly (L-lactic acid)/carbon nanotubes nanocomposites. *Journal of Polymer Science Part B: Polymer Physics,* 48 (9), pp.983-989.

Shirgaonkar, I.Z., Lothe, R.R. and Pandit, A.B., 1998. Comments on the mechanism of microbial cell disruption in high-pressure and high-speed devices. *Biotechnology progress,* 14 (4), pp.657-660.

Siegel, R.L., Miller, K.D. and Jemal, A., 2019. Cancer statistics, 2019. *CA: a cancer journal for clinicians,* 69 (1), pp.7-34.

Sies, H., 1997. Oxidative stress: oxidants and antioxidants. *Experimental Physiology: Translation and Integration,* 82 (2), pp.291-295.

Silva, H.D., Cerqueira, M.A., Souza, B.W., Ribeiro, C., Avides, M.C., Quintas, M.A., Coimbra, J.S., Carneiro-da-Cunha, M.G. and Vicente, A.A., 2011. Nanoemulsions of β-carotene using a high-energy emulsification–evaporation technique. *Journal of Food Engineering,* 102 (2), pp.130-135.

Silva, V.M., Sato, A.C.K., Barbosa, G., Dacanal, G., Ciro-Velásquez, H.J. and Cunha, R.L., 2010. The effect of homogenisation on the stability of pineapple pulp. *International Journal of Food Science & Technology,* 45 (10), pp.2127-2133.

Singh, R.P. and Heldman, D.R., 2001. *Introduction to food engineering.* Gulf Professional Publishing.

Sinha, R., Kim, G.J., Nie, S. and Shin, D.M., 2006. Nanotechnology in cancer therapeutics: bioconjugated nanoparticles for drug delivery. *Molecular cancer therapeutics,* 5 (8), pp.1909-1917.

Sinha, V.R., Singla, A.K., Wadhawan, S., Kaushik, R., Kumria, R., Bansal, K. and Dhawan, S., 2004. Chitosan microspheres as a potential carrier for drugs. *International journal of pharmaceutics,* 274 (1), pp.1-33.

Sjöström, B. and Bergenståhl, B., 1992. Preparation of submicron drug particles in lecithin-stabilized o/w emulsions I. Model studies of the precipitation of cholesteryl acetate. *International journal of pharmaceutics,* 88 (1-3), pp.53-62.

Slomberg, D.L. and Schoenfisch, M.H., 2012. Silica nanoparticle phytotoxicity to Arabidopsis thaliana. *Environmental science & technology,* 46 (18), pp.10247-10254.

Smith, A., 1986. Evaluation of poly (lactic acid) as a biodegradable drug delivery system for parenteral administration. *International journal of pharmaceutics,* 30 (2-3), pp.215-220.

Smith, B.C., 2011. *Fundamentals of Fourier transform infrared spectroscopy.* CRC press.

SMITH, B.R., ARAGON, C.M. and AMIT, Z., 1997. Catalase and the production of brain acetaldehyde: a possible mediator of the psychopharmacological effects of ethanol. *Addiction Biology,* 2 (3), pp.277-290.

Soerjomataram, I., Lortet-Tieulent, J., Parkin, D.M., Ferlay, J., Mathers, C., Forman, D. and Bray, F., 2012. Global burden of cancer in 2008: a systematic analysis of disability-adjusted life-years in 12 world regions. *The Lancet,* 380 (9856), pp.1840-1850.

Song, W., Tang, Z., Lei, T., Wen, X., Wang, G., Zhang, D., Deng, M., Tang, X. and Chen, X., 2016a. Stable loading and delivery of disulfiram with mPEG-PLGA/PCL mixed nanoparticles for tumor therapy. *Nanomedicine: Nanotechnology, Biology and Medicine,* 12 (2), pp.377-386.

Soppimath, K.S., Aminabhavi, T.M., Kulkarni, A.R. and Rudzinski, W.E., 2001. Biodegradable polymeric nanoparticles as drug delivery devices. *Journal of Controlled Release,* 70 (1-2), pp.1-20.

Soule, H.D., Vazquez, J., Long, A., Albert, S. and Brennan, M., 1973. A human cell line from a pleural effusion derived from a breast carcinoma. *Journal of the National Cancer Institute,* 51 (5), pp.1409-1416.

Soyka, M., 2014. Nalmefene for the treatment of alcohol dependence: a current update. *International Journal of Neuropsychopharmacology,* 17 (4), pp.675-684.

Stainmesse, S., Orecchioni, A.M. and Nakache, E., 1992. Modelling of an original process to obtain biocompatible polymeric nanospheres. Proc.Sixth Congr.Int.Technol.Pharm, 1, pp.89-97.

Stayshich, R.M. and Meyer, T.Y., 2010. New insights into poly (lactic-co-glycolic acid) microstructure: using repeating sequence copolymers to decipher complex NMR and thermal behavior. *Journal of the American Chemical Society,* 32 (31), pp.10920-10934.

Steichen, S.D., Caldorera-Moore, M. and Peppas, N.A., 2013. A review of current nanoparticle and targeting moieties for the delivery of cancer therapeutics. *European journal of pharmaceutical sciences,* 48 (3), pp.416-427.

Stewart, B. and Wild, C.P., 2014. World cancer report 2014.

Stolnik, S., Davies, M.C., Illum, L., Davis, S.S., Boustta, M. and Vert, M., 1994. The preparation of sub-200 nm biodegradable colloidal particles from poly (β-malic acid-co-benzyl malate) copolymers and their surface modification with Poloxamer and Poloxamine surfactants. Journal of Controlled Release, 30 (1), pp.57-67.

Stolnik, S., Illum, L. and Davis, S.S., 1995. Long circulating microparticulate drug carriers. *Advanced Drug Delivery Reviews,* 16 (2-3), pp.195-214.

Strömme, J.H., 1965. Interactions of disulfiram and diethyldithiocarbamate with serum proteins studied by means of a gel-filtration technique. *Biochemical pharmacology,* 14 (4), pp.381-391.

Stylianopoulos, T., Poh, M., Insin, N., Bawendi, M.G., Fukumura, D., Munn, L.L. and Jain, R.K., 2010. Diffusion of particles in the extracellular matrix: the effect of repulsive electrostatic interactions. *Biophysical journal,* 99 (5), pp.1342-1349.

Suh, J.J., Pettinati, H.M., Kampman, K.M. and O'Brien, C.P., 2006. The status of disulfiram: a half of a century later. *Journal of clinical psychopharmacology,* 26 (3), pp.290-302.

Sun, Q., Radosz, M. and Shen, Y., 2012. Challenges in design of translational nanocarriers. *Journal of Controlled Release,* 164 (2), pp.156-169.

Suslick, K.S. and Price, G.J., 1999. Applications of ultrasound to materials chemistry. *Annual Review of Materials Science,* 29 (1), pp.295-326.

Tan, Y.S., Ooi, K.K., Ang, K.P., Akim, A.M., Cheah, Y., Halim, S.N.A., Seng, H. and Tiekink, E.R., 2015. Molecular mechanisms of apoptosis and cell selectivity of zinc dithiocarbamates functionalized with hydroxyethyl substituents. Journal of inorganic biochemistry, 150, pp.48-62.

Teo, A., Lee, S.J., Goh, K.K. and Wolber, F.M., 2017. Kinetic stability and cellular uptake of lutein in WPI-stabilised nanoemulsions and emulsions prepared by emulsification and solvent evaporation method. *Food Chemistry,* 221, pp.1269-1276.

Tice, T., Gilley, R., Mason, D., Ferrell, T., Staas, J., Love, D., McRae, A., DahlstroKm, A., Ling, E. and Jacob, E., eds. 1996. *Proceedings of the International Conference on Advances in Controlled Delivery, Baltimore, MD.*

Tisato, F., Marzano, C., Porchia, M., Pellei, M. and Santini, C., 2010. Copper in diseases and treatments, and copper-based anticancer strategies. *Medicinal research reviews,* 30 (4), pp.708-749.

Tomita, Y., Rikimaru-Kaneko, A., Hashiguchi, K. and Shirotake, S., 2011. Effect of anionic and cationic n-butylcyanoacrylate nanoparticles on NO and cytokine production in Raw264. 7 cells. Immunopharmacology and immunotoxicology, 33 (4), pp.730-737.

Treuel, L., Eslahian, K.A., Docter, D., Lang, T., Zellner, R., Nienhaus, K., Nienhaus, G.U., Stauber, R.H. and Maskos, M., 2014. Physicochemical characterization of

nanoparticles and their behavior in the biological environment. *Physical Chemistry Chemical Physics,* 16 (29), pp.15053-15067.

Trichopoulos, D., MacMahon, B. and Cole, P., 1972. Menopause and breast cancer risk. *Journal of the National Cancer Institute,* 48 (3), pp.605-613.

Truitt, E.B. and Walsh, M.J., 1971. The role of acetaldehyde in the actions of ethanol. 1971. *The biology of alcoholism.* Springer. pp.161-195.

Truong, N.P., Whittaker, M.R., Mak, C.W. and Davis, T.P., 2015. The importance of nanoparticle shape in cancer drug delivery. *Expert opinion on drug delivery,* 12 (1), pp.129-142.

Tsuruo, T., Iida, H., Tsukagoshi, S. and Sakurai, Y., 1981. Overcoming of vincristine resistance in P388 leukemia in vivo and in vitro through enhanced cytotoxicity of vincristine and vinblastine by verapamil. *Cancer research,* 41 (5), pp.1967-1972.

Turi, E., 2012. *Thermal characterization of polymeric materials.* Elsevier.

Ugazio, E., Cavalli, R. and Gasco, M.R., 2002. Incorporation of cyclosporin A in solid lipid nanoparticles (SLN). *International journal of pharmaceutics,* 241 (2), pp.341-344.

Vaisberg, C.N., Jelezarsky, L.V., Dishlianova, B. and Chaushev, T.A., 2005. Activity, substrate detection and immunolocalization of glutathione peroxidase (GPx) in bovine reproductive organs and semen. *Theriogenology,* 64 (2), pp.416-428.

Van Eerdenbrugh, B., Froyen, L., Martens, J.A., Blaton, N., Augustijns, P., Brewster, M. and Van den Mooter, G., 2007. Characterization of physico-chemical properties and pharmaceutical performance of sucrose co-freeze–dried solid nanoparticulate powders of the anti-HIV agent loviride prepared by media milling. *International journal of pharmaceutics,* 338 (1-2), pp.198-206.

van Ieperen, L., 1984. Sudden death during disulfiram-ethanol reaction. *South African medical journal= Suid-Afrikaansetydskrifvirgeneeskunde,* 66 (5), pp.165.

van Beek, H.L., Beyer, N., Janssen, D.B. and Fraaije, M.W., 2015. Lyophilization conditions for the storage of monooxygenases. Journal of Biotechnology, 203 Issue , pp.41-44.

Vandervoort, J. and Ludwig, A., 2002a. Biocompatible stabilizers in the preparation of PLGA nanoparticles: a factorial design study. *International journal of pharmaceutics,* 238 (1-2), pp.77-92.

Vandervoort, J. and Ludwig, A., 2002b. Biocompatible stabilizers in the preparation of PLGA nanoparticles: a factorial design study. *International journal of pharmaceutics,* 238 (1-2), pp.77-92.

Victoriano, L.I., 2000. The reactivity of metal species towards thiuram sulfides: an alternative route to the syntheses of metal dithiocarbamates. Coordination Chemistry Reviews, 196 (1), pp.383-398.

Vitez, I.M., Newman, A.W., Craig, D. and Reading, M., 2007. Thermal microscopy. *Thermal Analysis of Pharmaceuticals,* 6000, pp.226-262.

Vogus, D.R., Krishnan, V. and Mitragotri, S., 2017. A review on engineering polymer drug conjugates to improve combination chemotherapy. *Current opinion in colloid & interface science,* 31, pp.75-85.

Wan, F., You, J., Sun, Y., Zhang, X., Cui, F., Du, Y., Yuan, H. and Hu, F., 2008. Studies on PEG-modified SLNs loading vinorelbine bitartrate (I): preparation and evaluation in vitro. *International journal of pharmaceutics,* 359 (1-2), pp.104-110.

Wang, C., Yang, J., Han, H., Chen, J., Wang, Y., Li, Q. and Wang, Y., 2017a. Disulfiram-loaded porous PLGA microparticle for inhibiting the proliferation and migration of non-small-cell lung cancer. *International journal of nanomedicine,* 12, pp.827.

Wang, J.M., Deng, X., Gong, W. and Su, S., 1998. Chemokines and their role in tumor growth and metastasis. *Journal of immunological methods,* 220 (1-2), pp.1-17.

Wang, T.D., Triadafilopoulos, G., Crawford, J.M., Dixon, L.R., Bhandari, T., Sahbaie, P., Friedland, S., Soetikno, R. and Contag, C.H., 2007. Detection of endogenous biomolecules in Barrett's esophagus by Fourier transform infrared spectroscopy. *Proceedings of the National Academy of Sciences,* 104 (40), pp.15864-15869.

Wang, W., McLeod, H.L. and Cassidy, J., 2003. Disulfiram-mediated inhibition of NF-κB activity enhances cytotoxicity of 5-fluorouracil in human colorectal cancer cell lines. *International journal of cancer,* 104 (4), pp.504-511.

Wang, W., Wang, Z. and Xiu-Wu, B., 2018. No title. *Disulfiram formulation.*

Wang, X., Jiang, Y., Wang, Y., Huang, M., Ho, C. and Huang, Q., 2008. Enhancing anti-inflammation activity of curcumin through O/W nanoemulsions. *Food Chemistry,* 108 (2), pp.419-424.

Wang, Z., Tan, J., McConville, C., Kannappan, V., Tawari, P.E., Brown, J., Ding, J., Armesilla, A.L., Irache, J.M. and Mei, Q., 2017b. Poly lactic-co-glycolic acid controlled delivery of disulfiram to target liver cancer stem-like cells. *Nanomedicine: Nanotechnology, Biology and Medicine,* 13 (2), pp.641-657.

Warren, B.E., 1969. X-Ray Diffraction. sl.

Wehbe, M., Anantha, M., Backstrom, I., Leung, A., Chen, K., Malhotra, A., Edwards, K. and Bally, M.B., 2016. Nanoscale reaction vessels designed for synthesis of copper-drug complexes suitable for preclinical development. *PloS one,* 11 (4), pp.e0153416.

Wendlandt, W.W., 1986. The development of thermal analysis instrumentation 1955–1985. *Thermochimica acta,* 100 (1), pp.1-22.

Whitesides, G.M., 2003. The'right'size in nanobiotechnology. *Nature biotechnology,* 21 (10), pp.1161.

Wicki, A., Witzigmann, D., Balasubramanian, V. and Huwyler, J., 2015. Nanomedicine in cancer therapy: challenges, opportunities, and clinical applications. *Journal of Controlled Release,* 200, pp.138-157.

Wickström, M., Danielsson, K., Rickardson, L., Gullbo, J., Nygren, P., Isaksson, A., Larsson, R. and Lövborg, H., 2007. Pharmacological profiling of disulfiram using human tumor cell lines and human tumor cells from patients. *Biochemical pharmacology,* 73 (1), pp.25-33.

Williams, E.E., 1937. Effects of alcohol on workers with carbon disulfide. *JAMA,* 109 (109), pp.1472-1473.

Wise, D.L., Trantolo, D.J., Lewandrowski, K., Gresser, J.D., Cattaneo, M.V. and Yaszemski, M.J., 2000. Biomaterials engineering and devices: human applications.

Wissing, S.A. and Müller, R.H., 2002. Solid lipid nanoparticles as carrier for sunscreens: in vitro release and in vivo skin penetration. *Journal of Controlled Release,* 81 (3), pp.225-233.

Wong, H.L., Bendayan, R., Rauth, A.M., Li, Y. and Wu, X.Y., 2007. Chemotherapy with anticancer drugs encapsulated in solid lipid nanoparticles. *Advanced Drug Delivery Reviews,* 59 (6), pp.491-504.

Woodle, M.C., Collins, L.R., Sponsler, E., Kossovsky, N., Papahadjopoulos, D. and Martin, F.J., 1992. Sterically stabilized liposomes. Reduction in electrophoretic mobility but not electrostatic surface potential. *Biophysical journal,* 61 (4), pp.902-910.

Wu, X.S. and Wang, N., 2001. Synthesis, characterization, biodegradation, and drug delivery application of biodegradable lactic/glycolic acid polymers. Part II: biodegradation. *Journal of Biomaterials Science, Polymer Edition,* 12 (1), pp.21-34.

Wuerth, R., Thellung, S., Bajetto, A., Mazzanti, M., Florio, T. and Barbieri, F., 2016. Drug-repositioning opportunities for cancer therapy: novel molecular targets for known compounds. *Drug discovery today,* 21 (1), pp.190-199.

Wunderlich, B., Okazaki, I., Ishikiriyama, K. and Boller, A., 1998. Melting by temperature-modulated calorimetry. *Thermochimica acta,* 324 (1-2), pp.77-85.

Xu, P., Wang, R., Li, J., Ouyang, J. and Chen, B., 2015. PEG–PLGA–PLL nanoparticles in combination with gambogic acid for reversing multidrug resistance of K562/A02 cells to daunorubicin. *RSC Advances,* 5 (75), pp.61051-61059.

Yallapu, M.M., Gupta, B.K., Jaggi, M. and Chauhan, S.C., 2010. Fabrication of curcumin encapsulated PLGA nanoparticles for improved therapeutic effects in metastatic cancer cells. *Journal of colloid and interface science,* 351 (1), pp.19-29.

Yang, T., Cui, F., Choi, M., Cho, J., Chung, S., Shim, C. and Kim, D., 2007. Enhanced solubility and stability of PEGylated liposomal paclitaxel: in vitro and in vivo evaluation. *International journal of pharmaceutics,* 338 (1-2), pp.317-326.

Yip, N.C., Fombon, I.S., Liu, P., Brown, S., Kannappan, V., Armesilla, A.L., Xu, B., Cassidy, J., Darling, J.L. and Wang, W., 2011. Disulfiram modulated ROS–MAPK and NFκB pathways and targeted breast cancer cells with cancer stem cell-like properties. *British journal of cancer,* 104 (10), pp.1564.

Yoshioka, T., Kawazoe, N., Tateishi, T. and Chen, G., 2008. In vitro evaluation of biodegradation of poly (lactic-co-glycolic acid) sponges. *Biomaterials,* 29 (24-25), pp.3438-3443.

Yuan, Y., Gao, Y., Zhao, J. and Mao, L., 2008. Characterization and stability evaluation of β-carotene nanoemulsions prepared by high pressure homogenization under various emulsifying conditions. *Food Research International,* 41 (1), pp.61-68.

Yurgel, V., Collares, T. and Seixas, F., 2013. Developments in the use of nanocapsules in oncology. *Brazilian Journal of Medical and Biological Research,* 46 (6), pp.486-501.

Zahr, A.S., Davis, C.A. and Pishko, M.V., 2006. Macrophage uptake of coreâˆ' shell nanoparticles surface modified with poly (ethylene glycol). Langmuir, 22 (19), pp.8178-8185.

Zamboni, W.C., Torchilin, V., Patri, A.K., Hrkach, J., Stern, S., Lee, R., Nel, A., Panaro, N.J. and Grodzinski, P., 2012. Best practices in cancer nanotechnology: perspective from NCI nanotechnology alliance. *Clinical cancer research,* 18 (12), pp.3229-3241.

Zangar, R.C., Davydov, D.R. and Verma, S., 2004. Mechanisms that regulate production of reactive oxygen species by cytochrome P450. *Toxicology and applied pharmacology,* 199 (3), pp.316-331.

Zembko, I., Ahmed, I., Farooq, A., Dail, J., Tawari, P., Wang, W. and Mcconville, C., 2015. Development of Disulfiram-Loaded Poly (Lactic-co-Glycolic Acid) Wafers for the Localised Treatment of Glioblastoma Multiforme: A Comparison of Manufacturing Techniques. *Journal of pharmaceutical sciences,* 104 (3), pp.1076-1086.

Zeng, L., Liu, Y.Q., Chang, W., Zhang, L., Ding, Z., Wang, W.J. and Huang, H.M., 2018. No title. *Compressible thermal interface materials.*

Zeng, N., Hu, Q., Liu, Z., Gao, X., Hu, R., Song, Q., Gu, G., Xia, H., Yao, L. and Pang, Z., 2012. Preparation and characterization of paclitaxel-loaded DSPE-PEG-liquid crystalline nanoparticles (LCNPs) for improved bioavailability. *International journal of pharmaceutics,* 424 (1-2), pp.58-66.

Zhang, L., Gu, F.X., Chan, J.M., Wang, A.Z., Langer, R.S. and Farokhzad, O.C., 2008. Nanoparticles in medicine: therapeutic applications and developments. Clinical pharmacology & therapeutics, 83 (5), pp.761-769.

Zhang, P., Ma, Y., Zhang, Z., He, X., Li, Y., Zhang, J., Zheng, L. and Zhao, Y., 2015. Species-specific toxity of ceria nanoparticles to Lactuca plants. *Nanotoxicology,* 9 (1), pp.1-8.

Zhao, J. and Feng, S., 2014. Effects of PEG tethering chain length of vitamin E TPGS with a Herceptin-functionalized nanoparticle formulation for targeted delivery of anticancer drugs. Biomaterials, 35 (10), pp.3340-3347.

Zhao, Y., Wang, L., Yan, M., Ma, Y., Zang, G., She, Z. and Deng, Y., 2012. Repeated injection of PEGylated solid lipid nanoparticles induces accelerated blood clearance in mice and beagles. *International journal of nanomedicine,* 7, pp.2891.

Zhou, J., Patel, T.R., Sirianni, R.W., Strohbehn, G., Zheng, M., Duong, N., Schafbauer, T., Huttner, A.J., Huang, Y. and Carson, R.E., 2013. Highly penetrative, drug-loaded nanocarriers improve treatment of glioblastoma. *Proceedings of the National Academy of sciences,* 110 (29), pp.11751-11756.

ZurMühlen, A. and Mehnert, W., 1998. Drug release and release mechanism of prednisolone loaded solid lipid nanoparticles. *Pharmazie,* 53 (8), pp.552-555.

Appendix A (Chapter 3 supplementary data)

DSC thermograms of PLGA NPs by SE method/PS technique
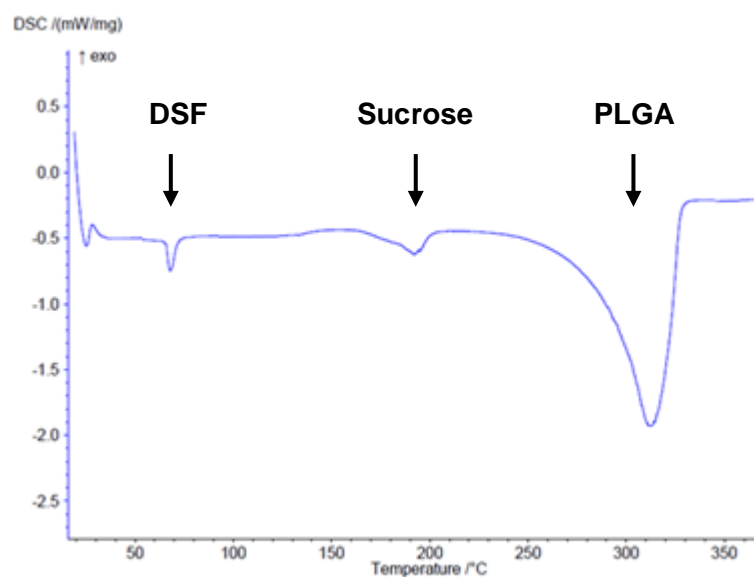
Figure 3.21. DSF-loaded PLGA NPs prepared by solvent evaporation method and reduced particle size through probe sonication technique.
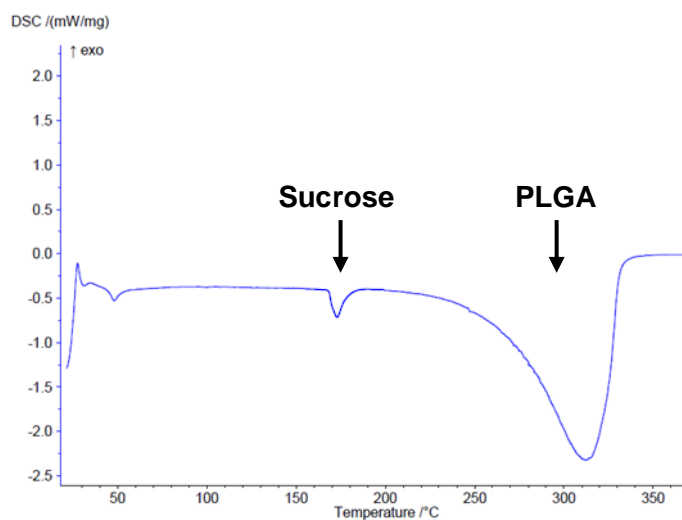
Figure 3.22. Blank PLGA NPs prepared by solvent evaporation method and reduced particle size through probe sonication technique.

DSC thermograms of PLGA NPs by SE method/HPH technique
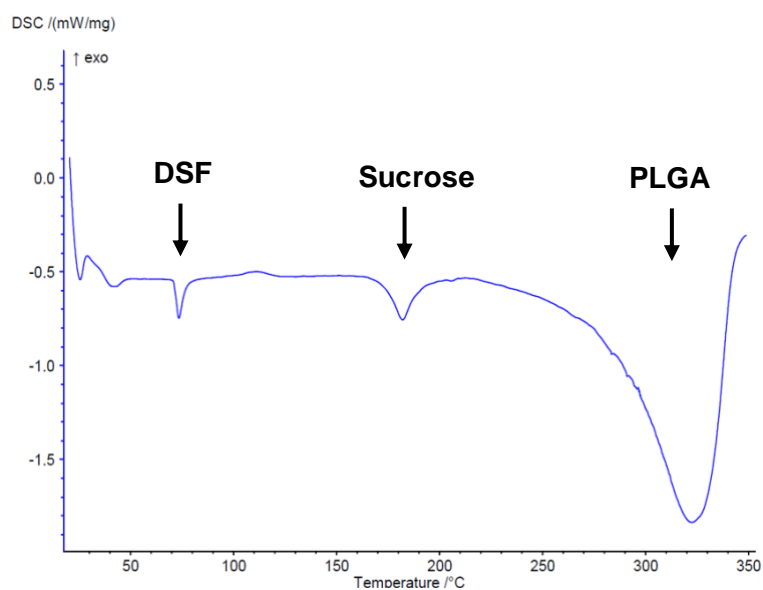
Figure 3.23. DSF-loaded PLGA NPs prepared by solvent evaporation method and reduced particle size through high-pressure homogenization technique.
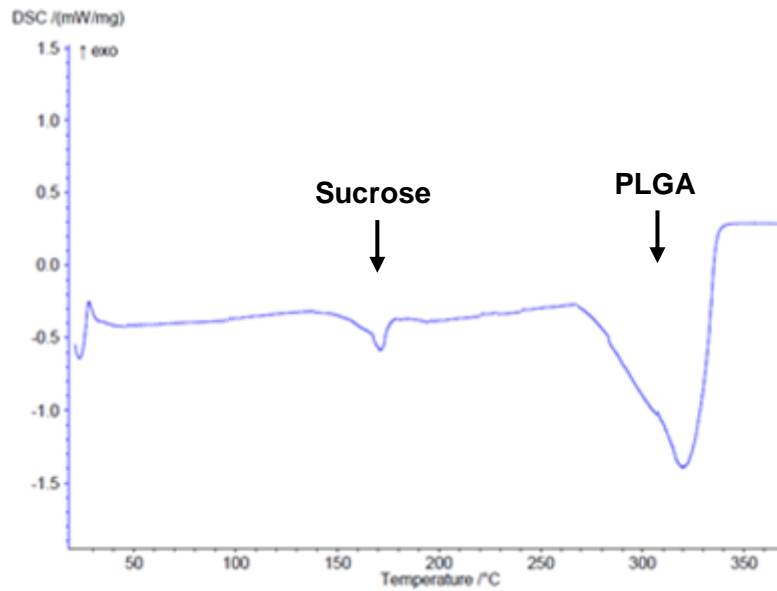
Figure 3.24. Blank PLGA NPs prepared by solvent evaporation method and reduced particle size through high-pressure homogenization technique.
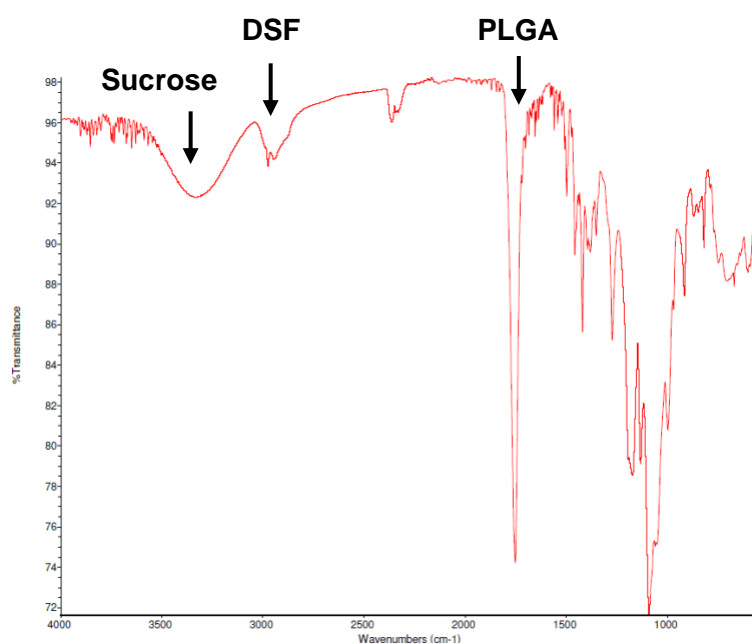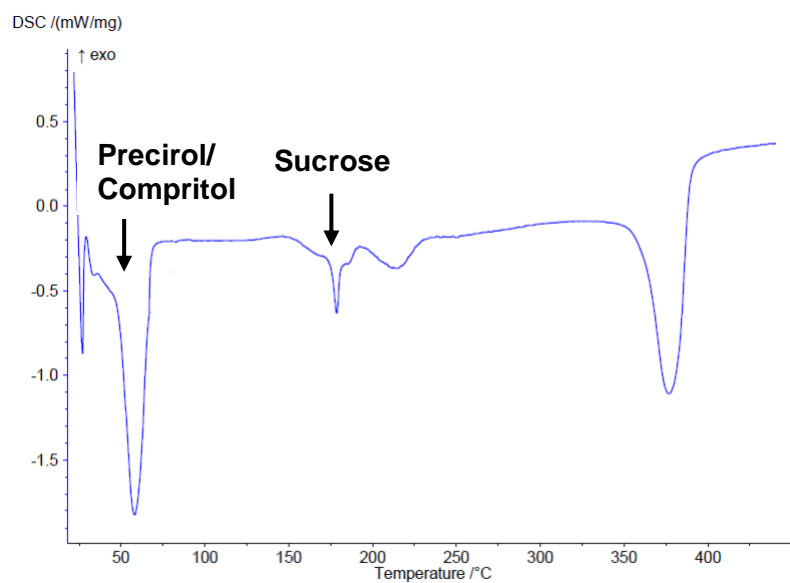
Figure 3.25. DSF-loaded PLGA NPs prepared by solvent evaporation method and reduced particle size through probe sonication technique.
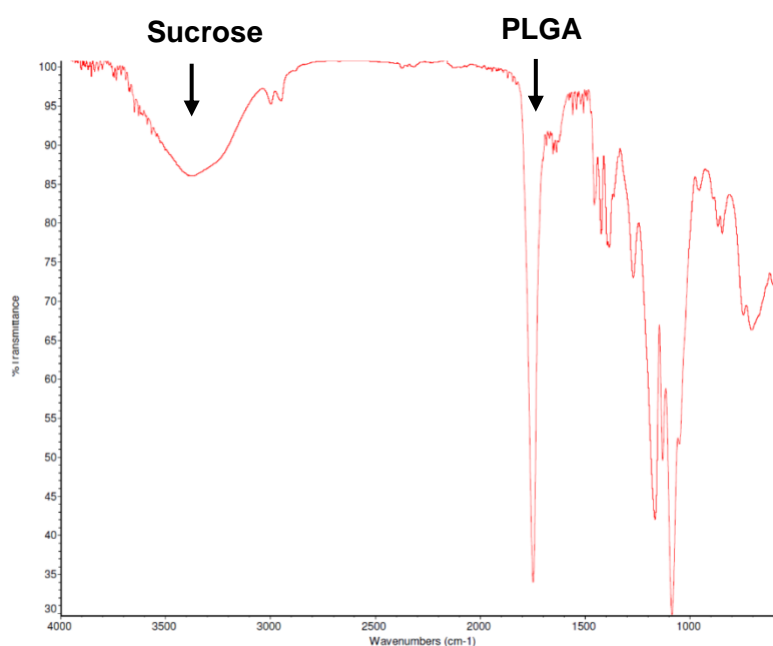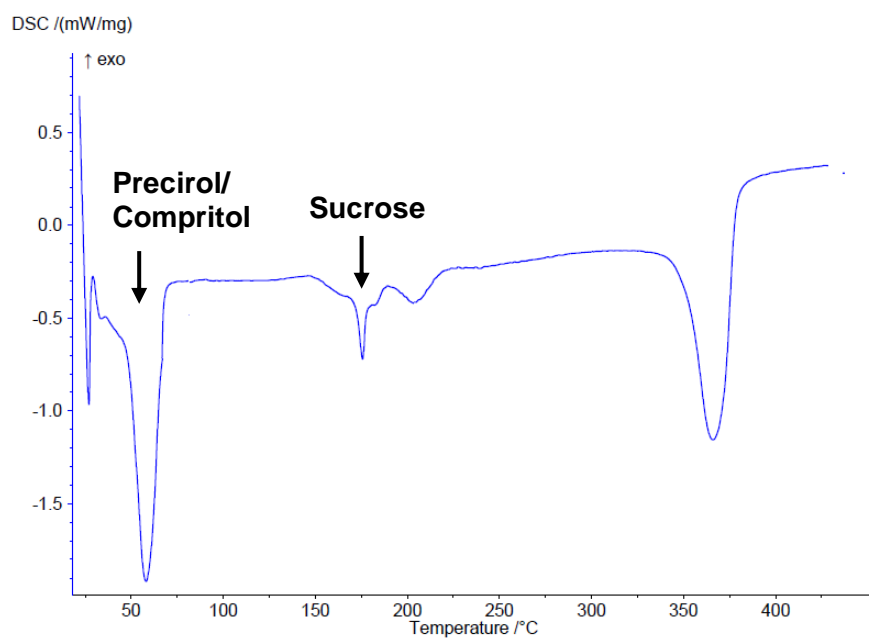

Figure 3.26. Blank PLGA NPs prepared by solvent evaporation method and reduced particle size through probe sonication technique.
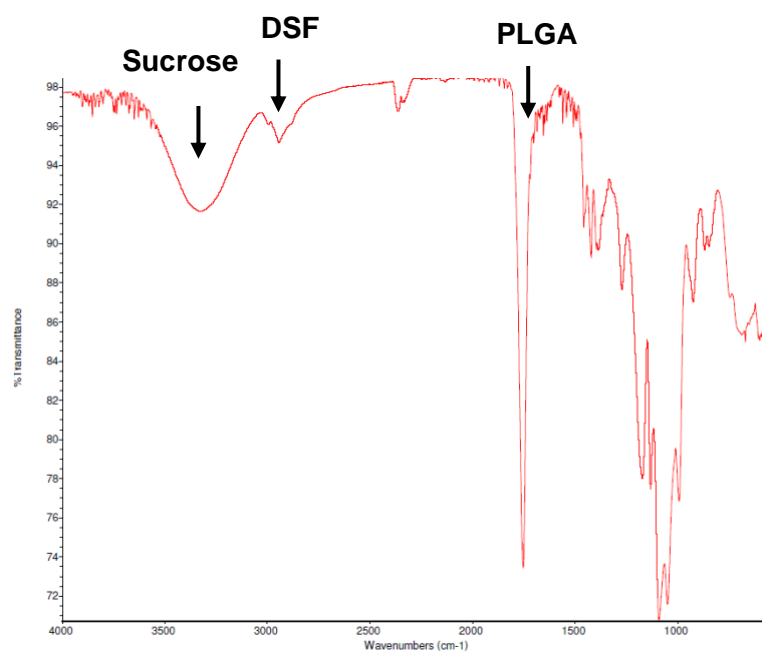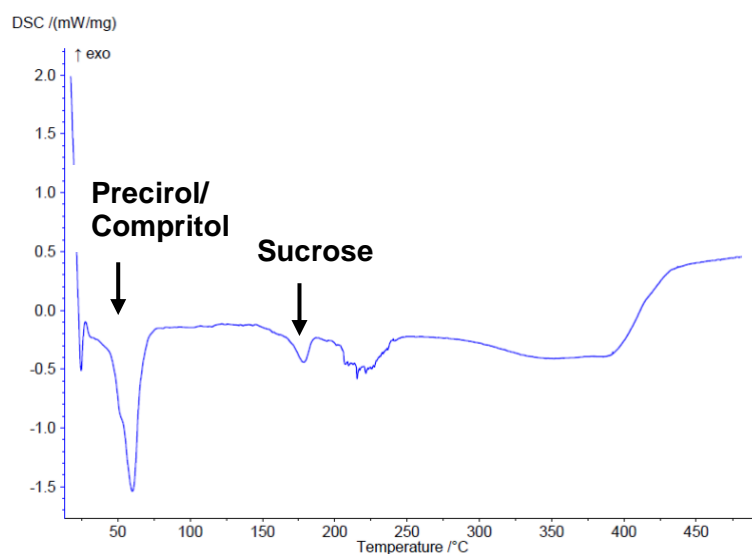
Figure 3.27. DSF-loaded PLGA NPs prepared by solvent evaporation method and reduced particle size through high-pressure homogenization technique.
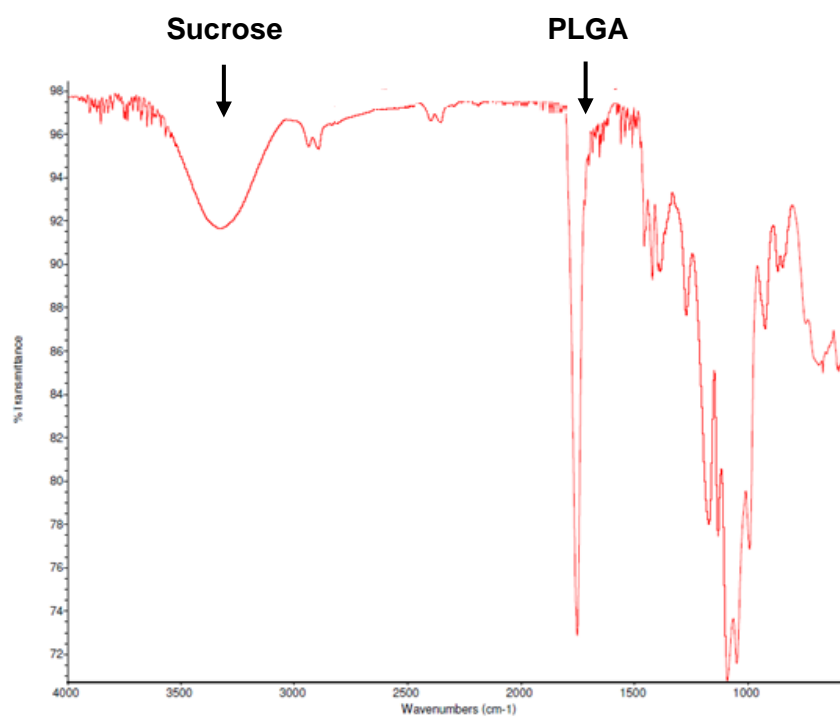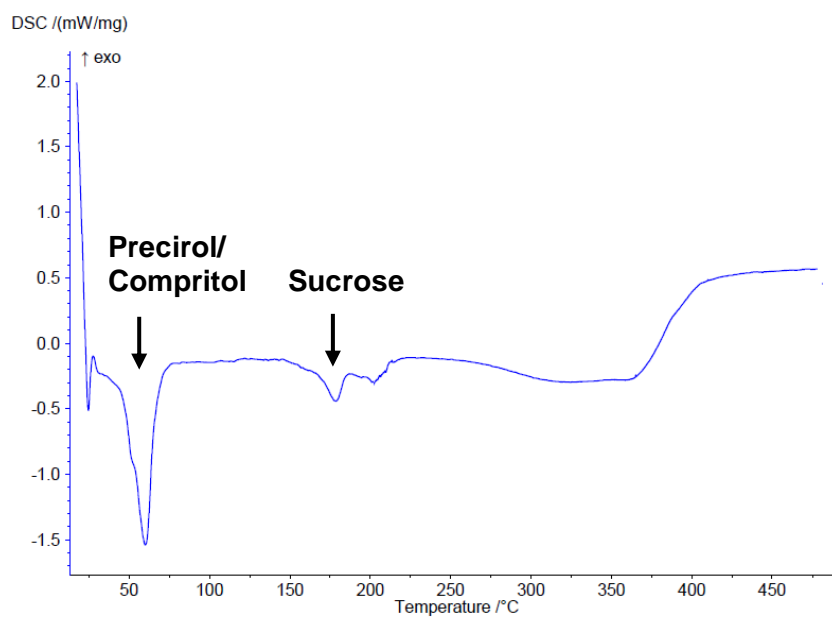

Figure 3.28. Blank PLGA NPs prepared by solvent evaporation method and reduced particle size through high-pressure homogenization technique.

238

Appendix B (Chapter 4 supplementary data)

DSC thermograms of PEGylated and non-PEGylated PLGA NPs by D-Nano-Pr method
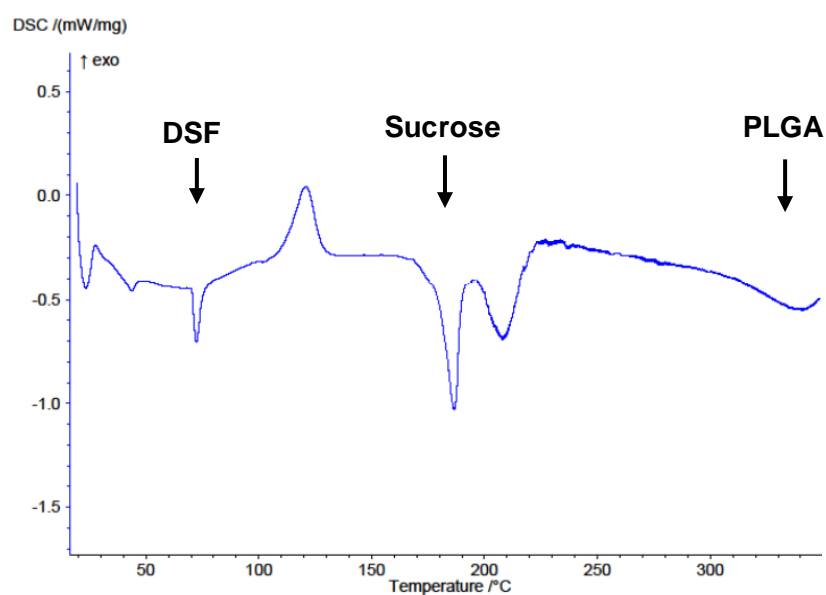
Figure 4.18. DSF-loaded PLGA/DSPE-PEG (DNP3) NPs prepared by D-Nano-Pr method.
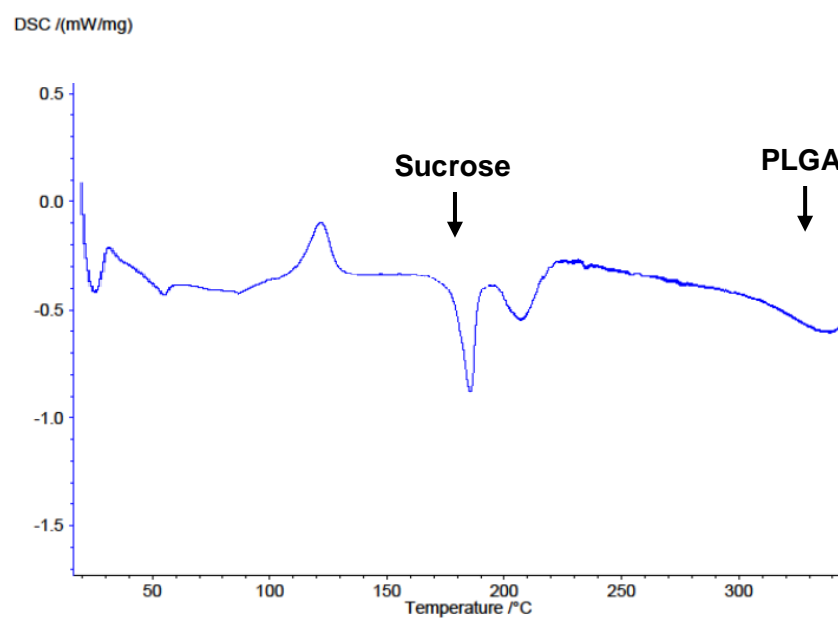
Figure 4.19. Blank PLGA/DSPE-PEG (DNP03) NPs prepared by D-Nano-Pr method.
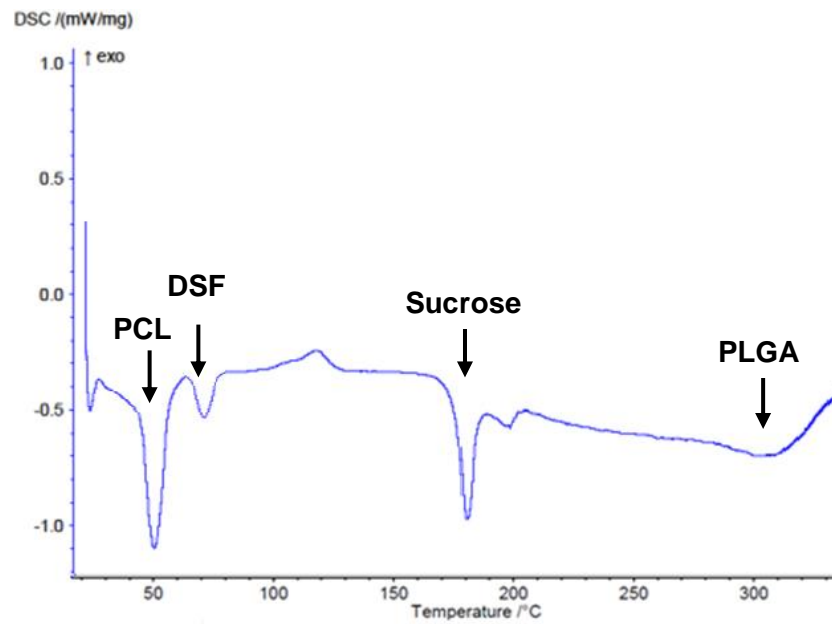
Figure 4.20. DSF-loaded PLGA/PCL/mPEG-PLGA (DNP4) NPs prepared by D-Nano-Pr method.
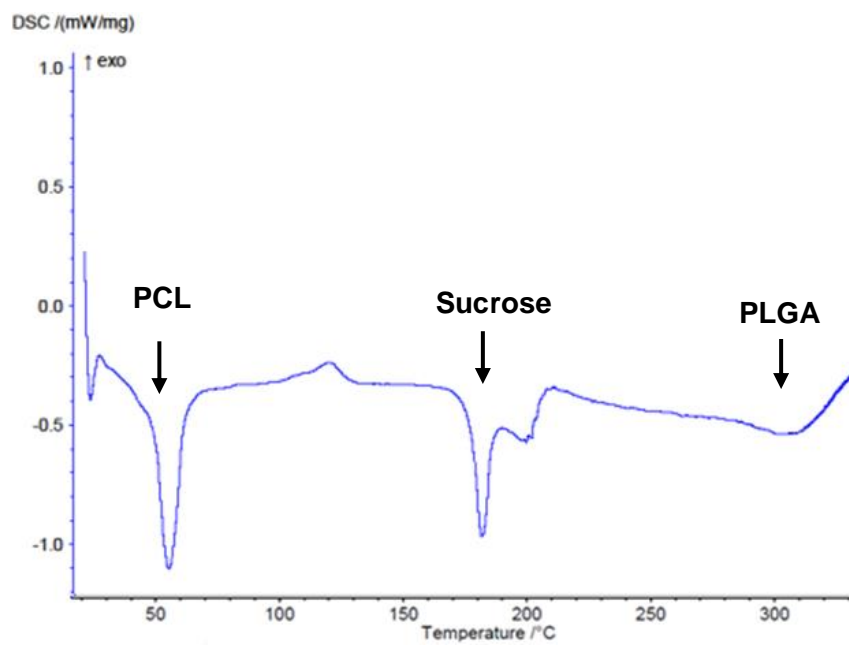
Figure 4.21. Blank PLGA/PCL/mPEG-PLGA (DNP04) NPs prepared by D-Nano-Pr method.
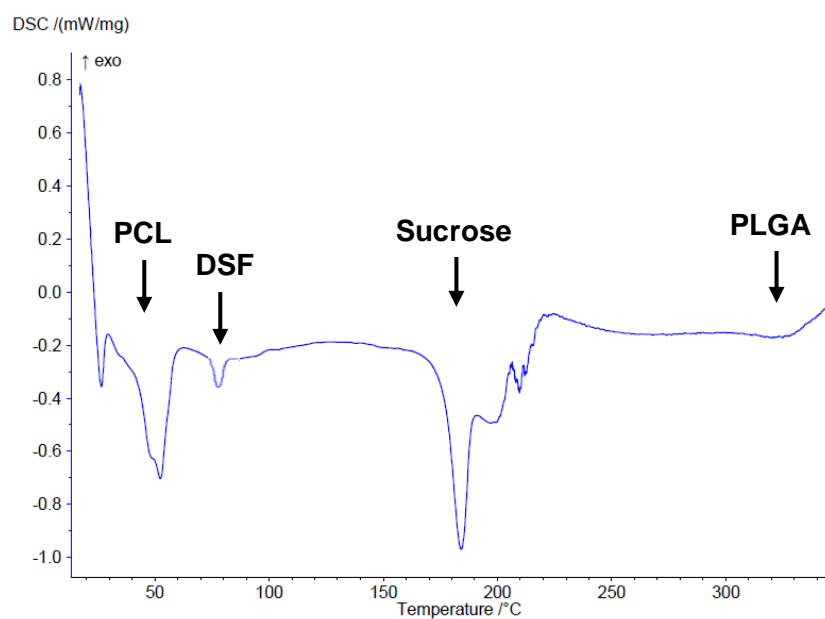
Figure 4.22. DSF-loaded PLGA/PCL (DNP5) NPs prepared by D-Nano-Pr method.
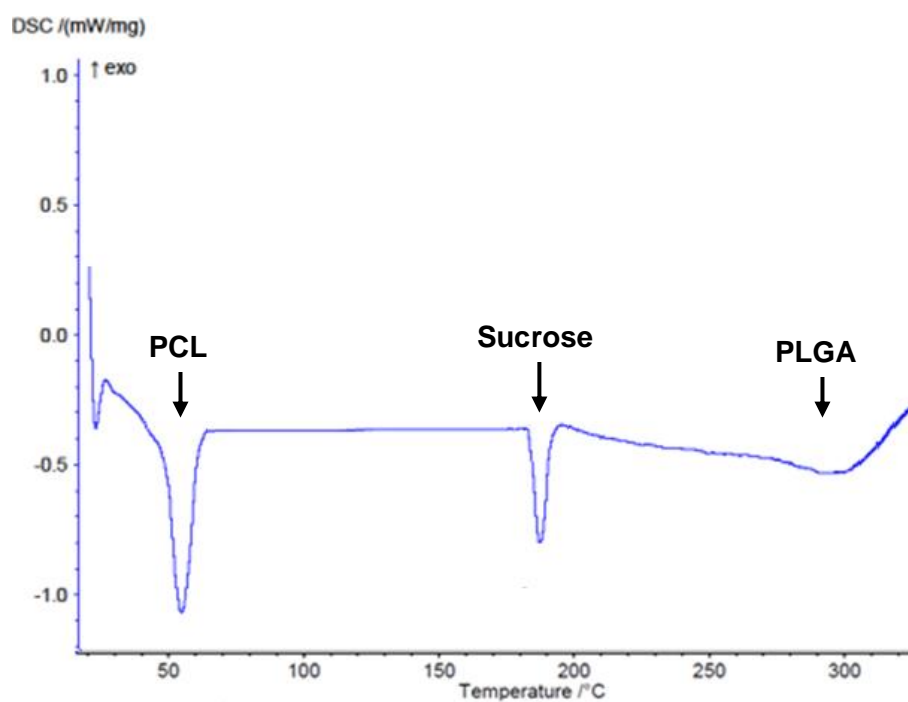
Figure 4.23. Blank PLGA/PCL (DNP05) NPs prepared by D-Nano-Pr method.
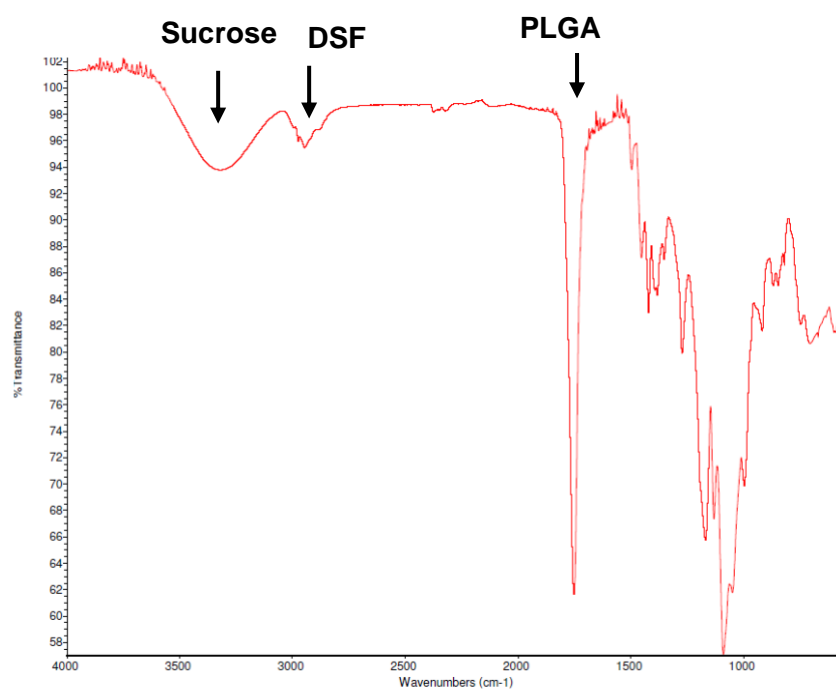
Figure 4.24. DSF-loaded PLGA/DSPE-PEG (DNP3) NPs prepared by D-Nano-Pr method.
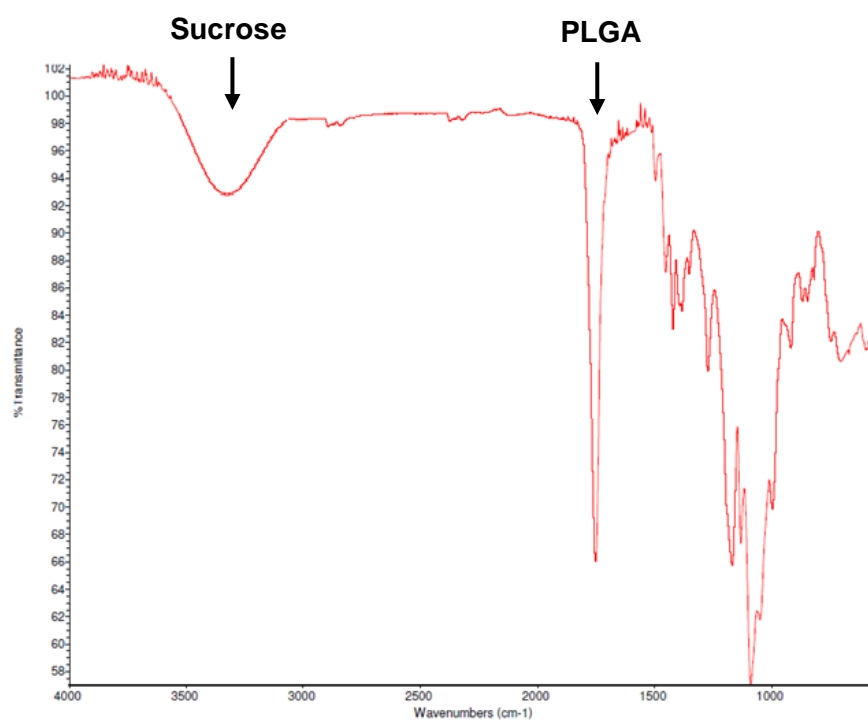
Figure 4.25. Blank PLGA/DSPE-PEG (DNP03) NPs prepared by D-Nano-Pr method.

242
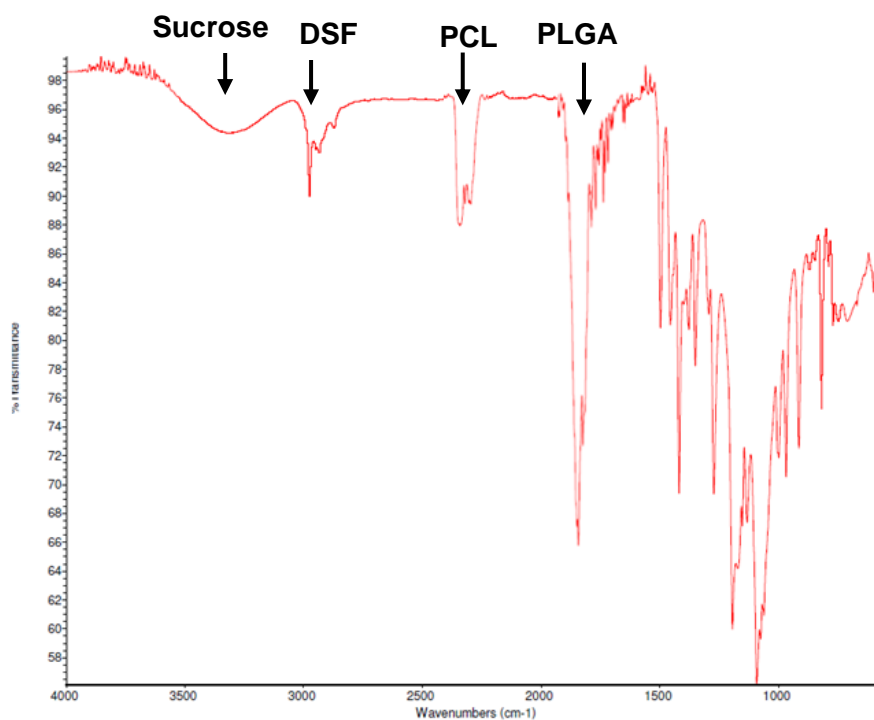
Figure 4.26. DSF-loaded PLGA/PCL/mPEG-PLGA (DNP4) NPs prepared by D-Nano-Pr method.
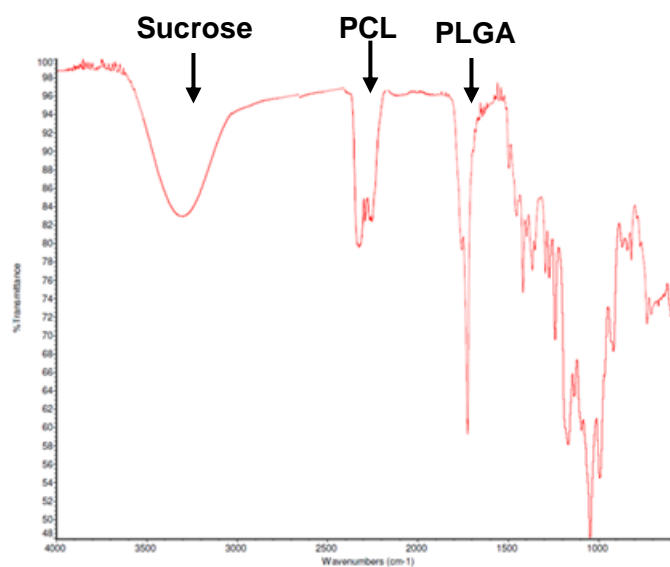
Figure 4.27. Blank PLGA/PCL/mPEG-PLGA (DNP4) NPs prepared by D-Nano-Pr method.
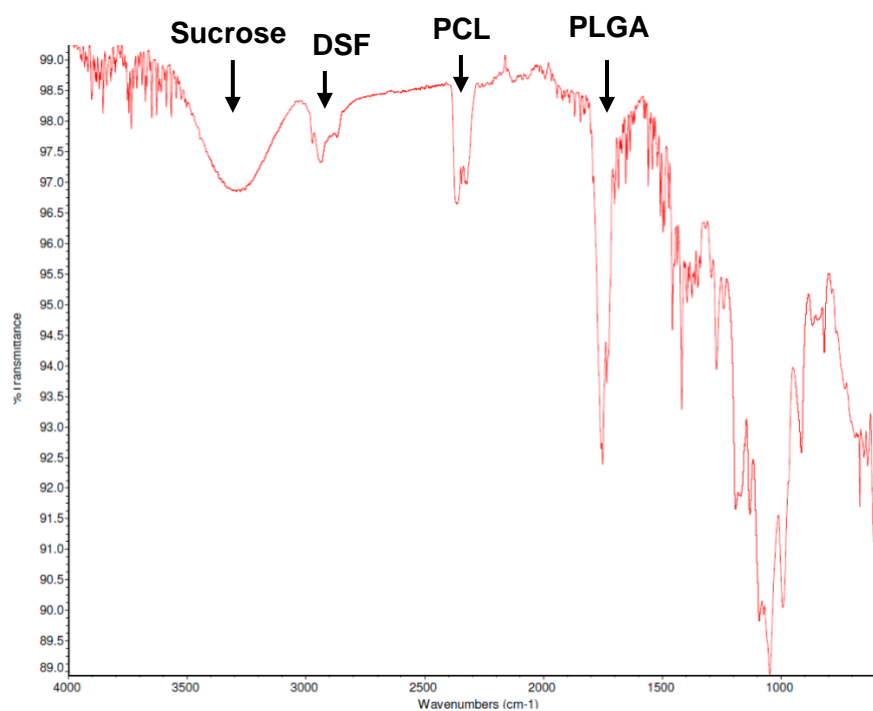
Figure 4.28. DSF-loaded PLGA/PCL (DNP5) NPs prepared by D-Nano-Pr method.
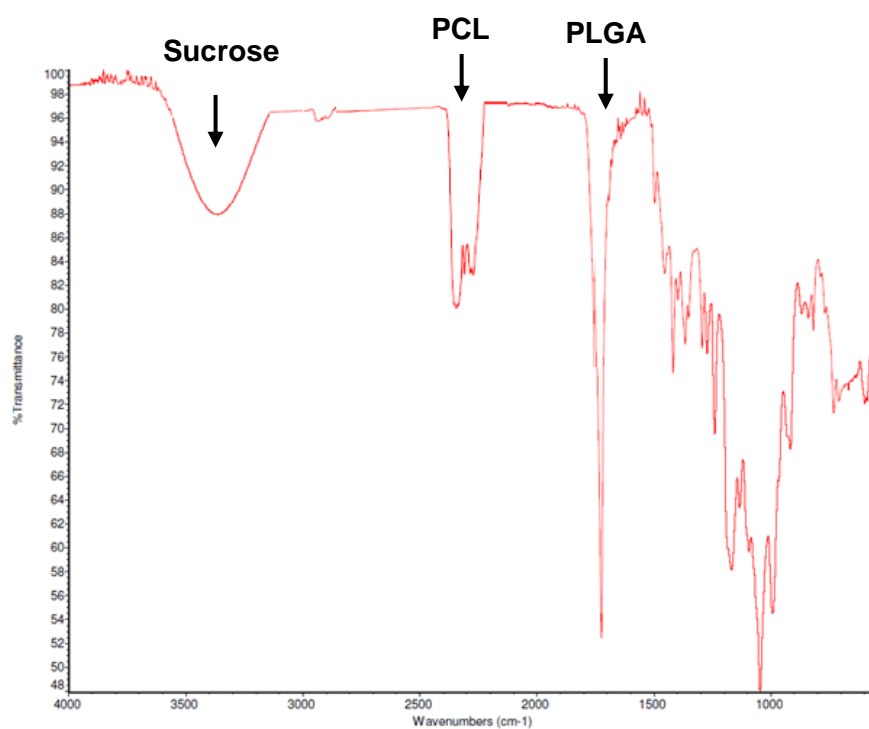
Figure 4.29, Blank PLGA/PCL (DNP05) NPs prepared by D-Nano-Pr method.

244

Appendix C (Chapter 5 supplementary data)

DSC thermograms of SLNs by SE method followed by hot homogenization technique
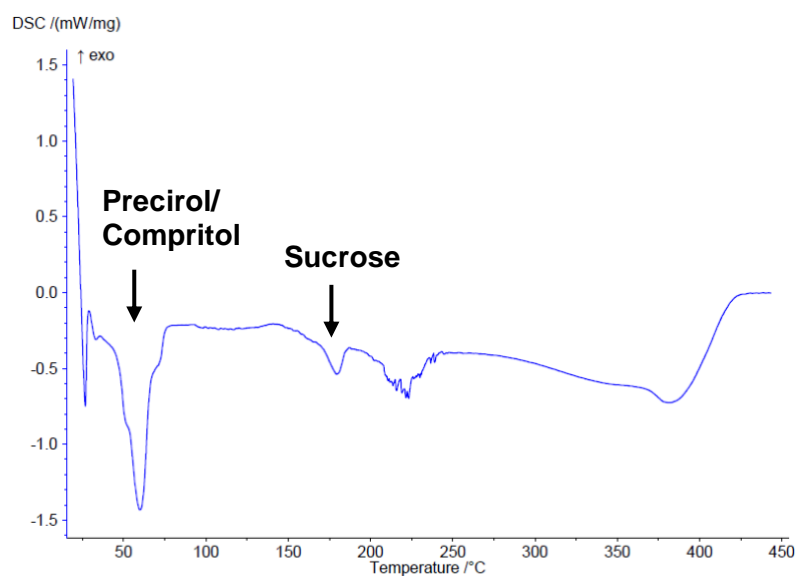
Figure 5.14. DSF-loaded SLNs prepared by solvent evaporation method.
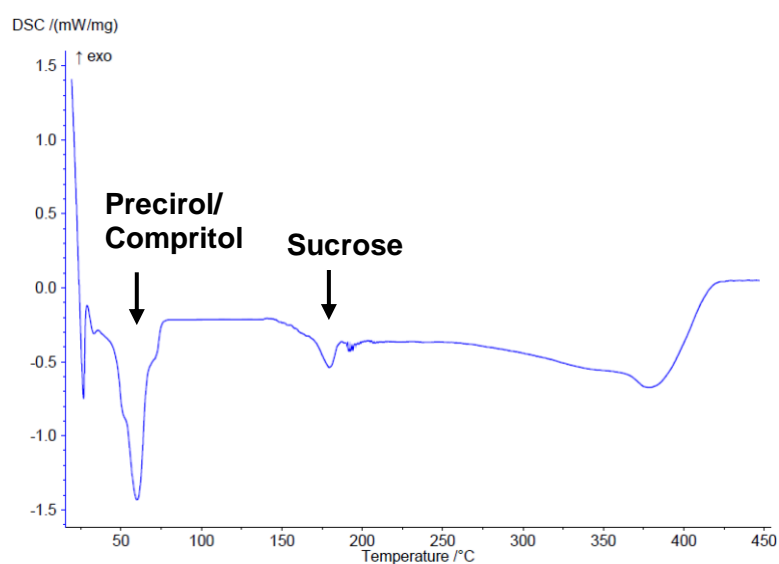
Figure 5.15. Blank SLNs prepared by solvent evaporation method.
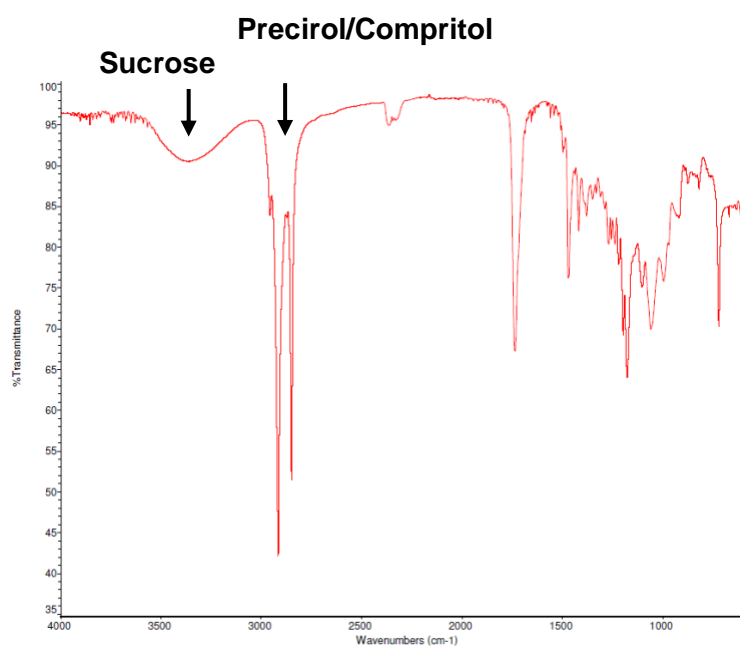
Figure 5.16. DSF-loaded SLNs prepared by solvent evaporation method and reduced particle size through probe sonication technique.

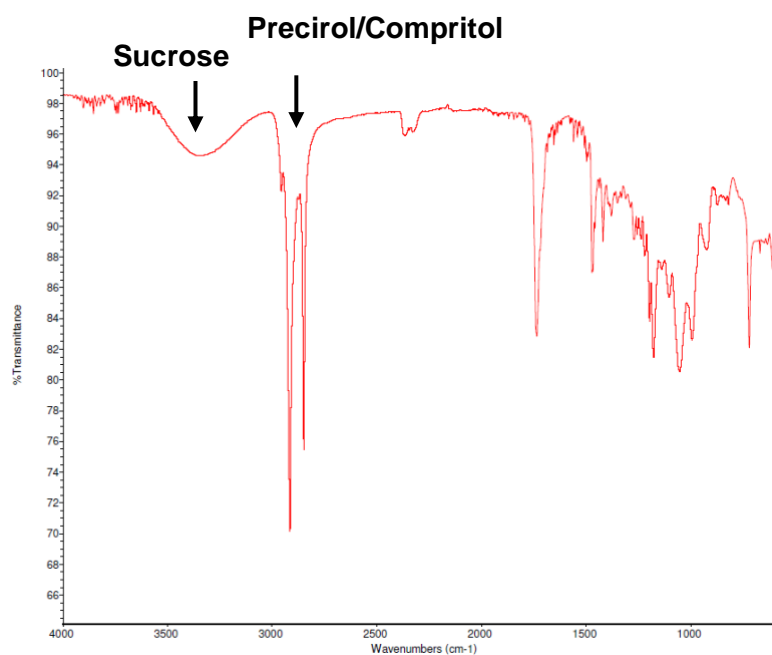Figure 5.17. Blank SLNs prepared by solvent evaporation method and reduced particle size through probe sonication technique.
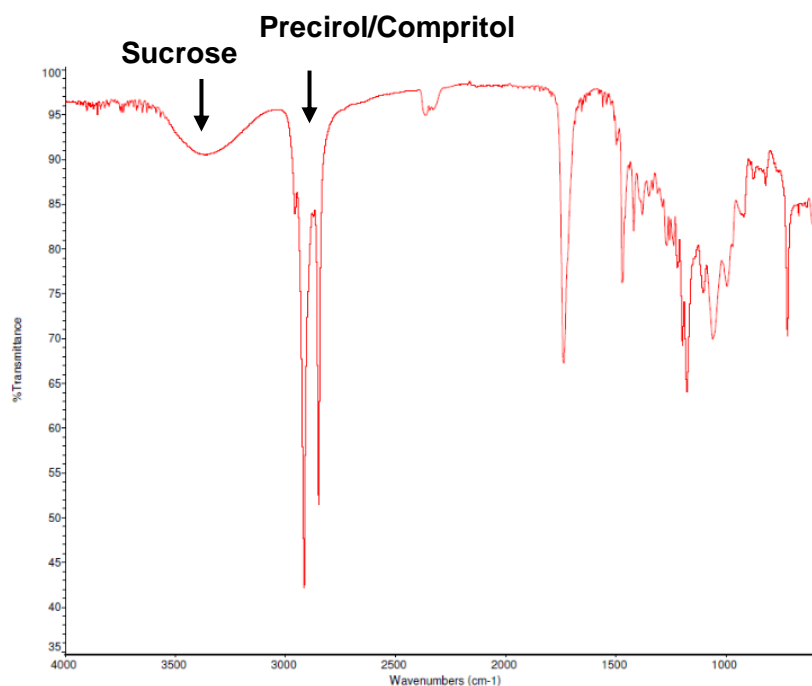
DSC thermograms of SLNs by SE method/HPH technique

Figure 5.18. DSF-loaded SLNs prepared by solvent evaporation method and reduced particle size through high-pressure homogenization technique.
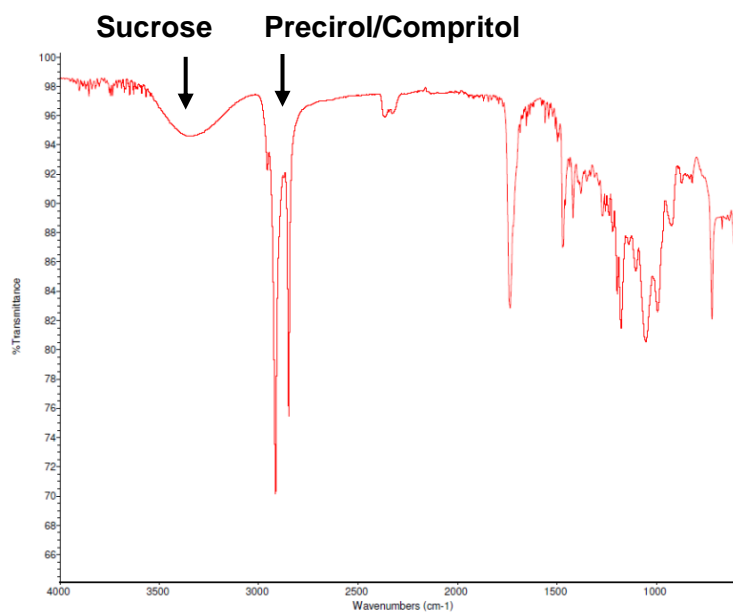

Figure 5.19. Blank SLNs prepared by solvent evaporation method and reduced particle size through high-pressure homogenization technique.
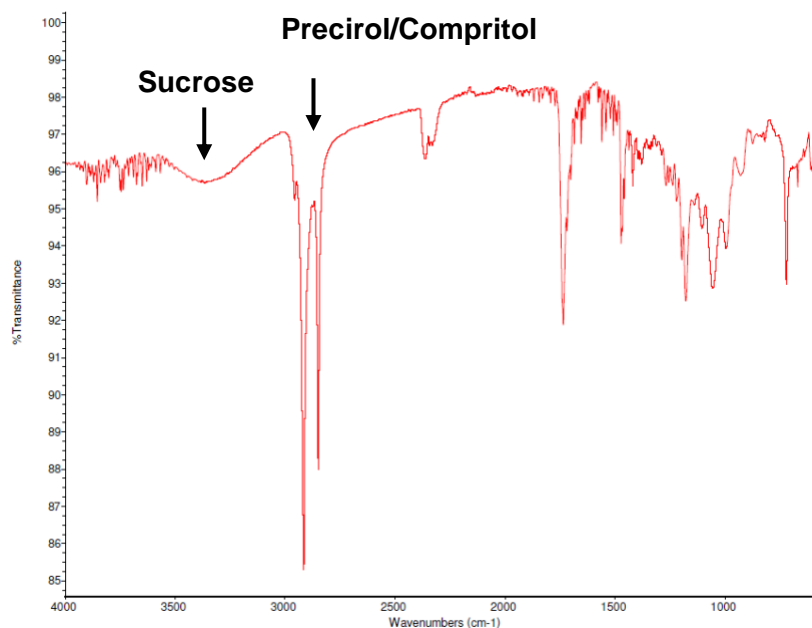
Figure 5.20. DSF-loaded SLNs prepared by solvent evaporation method.
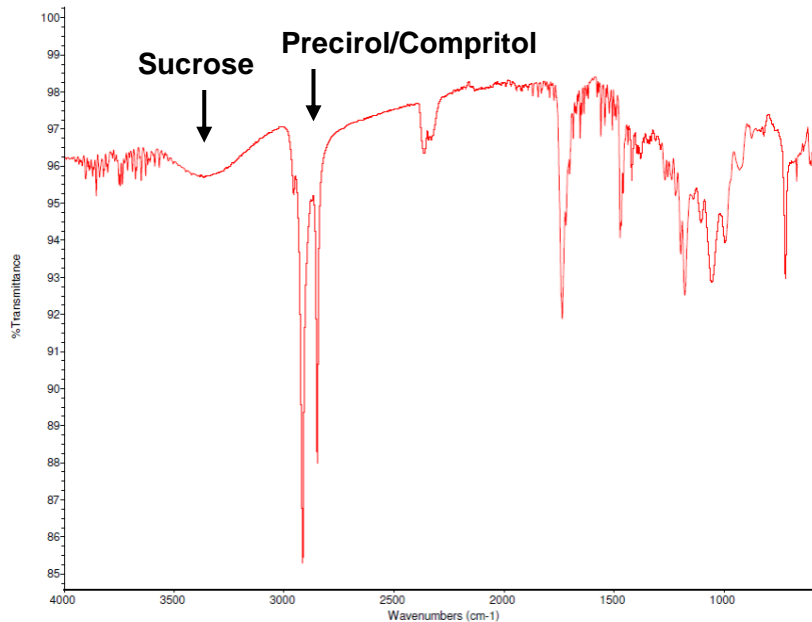
Figure 5.21. Blank SLNs prepared by solvent evaporation method.

Figure 5.22. DSF-loaded SLNs prepared by solvent evaporation method and reduced particle size through probe sonication technique.

Figure 5.23. Blank SLNs prepared by solvent evaporation method and reduced particle size through probe sonication technique.

Figure 5.24. DSF-loading SLNs prepared by solvent evaporation method and reduced particle size through high-pressure homogenization technique.

Figure 5.25. Blank SLNs prepared by solvent evaporation method and reduced particle size through high-pressure homogenization technique.

Appendix D (Chapter 6 supplementary data)

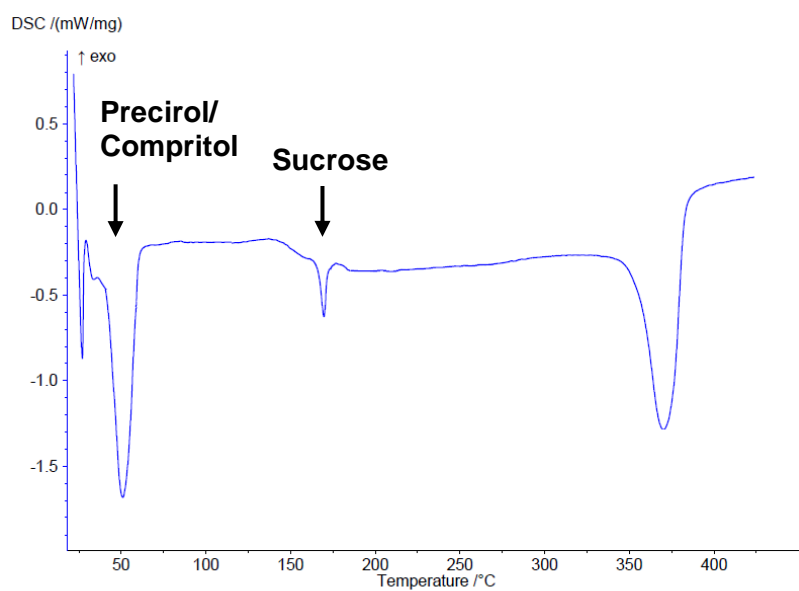## DSC thermograms of DSPE-PEG SLNs by SE method/HPH technique

Figure 6.12.DSF-loaded DSPE-PEG SLNs prepared by solvent evaporation method and reduced particle size through high-pressure homogenization technique.
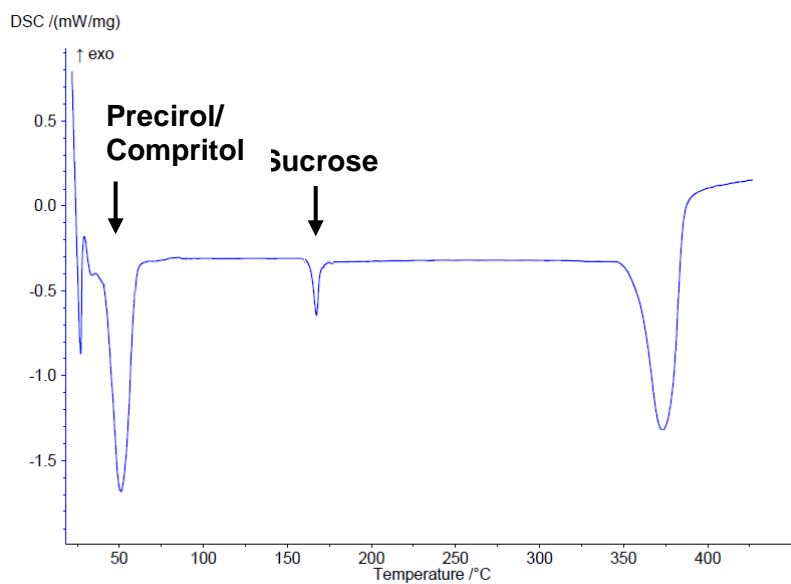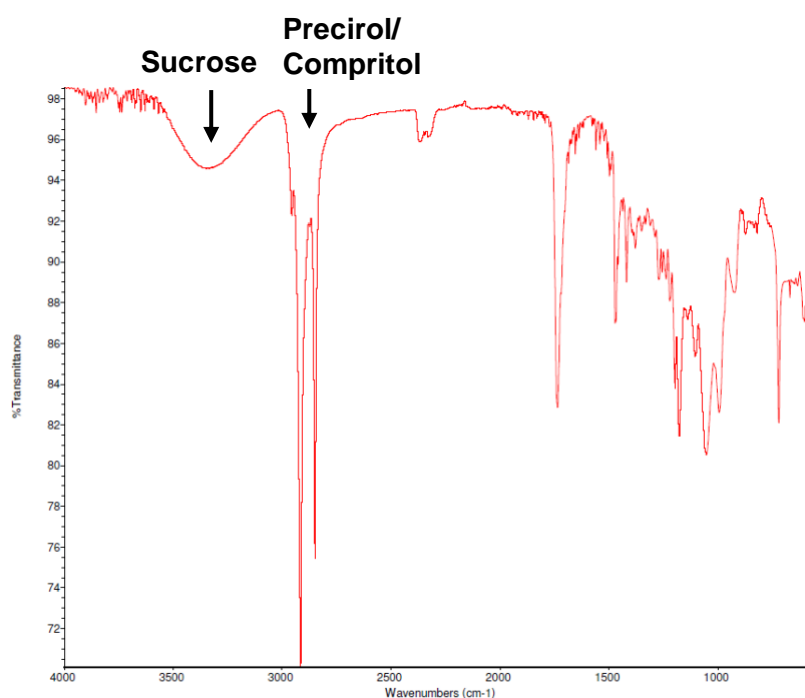

Figure 6.13. Blank DSPE-PEG SLNs prepared by solvent evaporation method and reduced particle size through high-pressure homogenization technique.

Figure 6.14. DSF-loaded DSPE-PEG SLNs prepared by solvent evaporation method and reduced particle size through high-pressure homogenization technique.
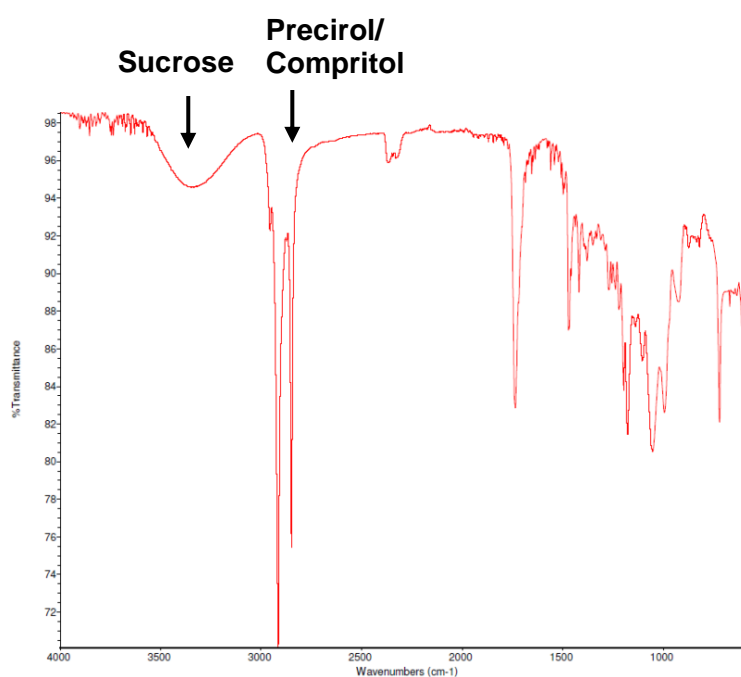

Figure 6.15. Blank DSPE-PEG SLNs prepared by solvent evaporation method and reduced particle size through high-pressure homogenization technique.